DOCTOR OF PHILOSOPHY

Network Inference And Graph Learning in Characterising Alzheimer's Disease

Klepl, Dominik

Award date:
2024

Awarding institution:
Coventry University

Coventry University
Centre for Computational Science and Mathematical Modelling

Network Inference And Graph Learning in Characterising Alzheimer's Disease

Dominik Klepl

Director of Studies: Dr Fei He

Supervisor: Dr Min Wu

A thesis submitted in partial fulfilment of the University's requirements for the degree of Doctor of Philosophy

May 1, 2024

To Mum, Dad, Brother Daniel and my beloved Ivana.

Declaration

All sentences or passages quoted in this document from other people's work have been specifically acknowledged by clear cross-referencing to author, work and page(s). Any illustrations that are not the work of the author of this report have been used with the explicit permission of the originator and are specifically acknowledged. I understand that failure to do this amounts to plagiarism and will be considered grounds for failure.

Certificate of Ethical Approval

Applicant:	Dominik Klepl
Project Title:	Network inference and graph theory: Applications for Characterising Neurodegenerative Diseases from EEG

This is to certify that the above named applicant has completed the Coventry University Ethical Approval process and their project has been confirmed and approved as Medium Risk

Date of approval:	09 Jun 2021
Project Reference Number:	P121994

Acknowledgement

To everyone who has been a part of this challenging yet rewarding experience, I appreciate you all so much. Each of you has contributed to the completion of this thesis in your unique way, and I am truly grateful for your support.

I want to thank my supervisors, Dr Fei He and Dr Min Wu, whose guidance and support have been invaluable throughout my PhD journey. Their expertise and encouragement have played a significant role during these years.

I also want to thank my friends at CSM: Shruti, Tereso, Raj, Ibnu, and Rashid. Your friendship and encouragement have added joy to this academic pursuit. You have made this journey truly memorable.

I am deeply thankful to my loving family for their unwavering support and understanding during the ups and downs of this academic endeavour. Special thanks to my fantastic wife, Ivana, for her endless patience, encouragement, and belief in my abilities.

Abstract

Alzheimer's disease (AD), the predominant cause of dementia, presents a growing global challenge as the number of patients continues to rise. This neurodegenerative condition is characterised by disruptions in brain function and a progressive decline in cognitive abilities. Research shows that it can be identified before the onset of symptoms, providing an opportunity for early intervention. However, current diagnostic approaches are expensive and inaccessible, highlighting the necessity for a cheap and fast alternative.

Electroencephalography (EEG) might offer a viable solution to this need due to its affordability and portability. Although EEG has lower spatial resolution than functional magnetic resonance imaging (fMRI), its excellent temporal resolution in milliseconds makes it a suitable candidate for early detection.

This thesis aims to contribute to the characterisation of AD from a graph perspective. This thesis uses graph theory to model EEG signals as graphs, capturing complex interactions between brain regions through functional connectivity (FC) to identify disruptions in brain networks and generate explainable predictions.

The first contribution introduces cross-bispectrum, a higher-order spectral analysis method, to reconstruct EEG-based FC graphs. This method can quantify both within-frequency coupling and cross-frequency coupling. A novel multilayer graph modelling approach integrates information from both coupling types. The analysis reveals significant cross-frequency differences, particularly increased FC in AD cases' δ-θ coupling. Graph-theoretic analysis proves crucial in understanding the structure and function of cross-frequency brain networks, with vulnerability analysis providing insights into integration and segregation properties.

The second contribution explores various FC measures for creating graph-based biomarkers for AD diagnosis using EEG. Graph neural networks (GNNs) are employed to compare the performance of eight FC measures. The study demonstrates that GNN models outperform baseline models and that using FC measures to estimate brain-

graphs improves the overall performance of GNN. However, no single FC measure consistently outperforms others, highlighting the importance of considering multiple measures for a comprehensive analysis.

The third contribution introduces a novel Adaptive gated graph convolutional network (AGGCN), providing explainable predictions for AD diagnosis. AGGCN combines convolution-based node feature enhancement with a correlation-based power spectral density similarity measure. The gated graph convolution dynamically weighs the contribution of various spatial scales, enhancing the model's interpretability. The proposed AGGCN achieves high accuracy under different conditions and generates consistent explanations of its predictions, offering valuable insights into AD-related alterations of brain networks.

In conclusion, this thesis advances our understanding of AD by leveraging EEG and graph theory. The novel contributions, including cross-bispectrum analysis, exploration of various FC measures, and the development of AGGCN, collectively enhance our ability to characterise and diagnose AD from a graph perspective.

Contents

List of Figures

List of Tables

List of Abbreviations

AD	Alzheimer's-disease-
HC	healthy-control-
NW	network-neuroscience-
MCI	mild-cognitive-impairment-
EC	eyes-closed-
EO	eyes-open-
GNN	graph-neural-network-
RNN	recurrent-neural-network-
NFP	node-feature-pre-processing-module-
FC	functional-connectivity-
EEG	electroencephalography-
MEG	magnetoencephalography-
MRI	magnetic-resonance-imaging-
CT	computerised-tomography-
BCI	brain-computer-interface-
fMRI	functional-magnetic-resonance-imaging-
PET	positron-emission-tomography-
CBS	cross-bispectrum-
CS	cross-spectrum-
PSD	power-spectral-density-
CFC	cross-frequency-coupling-
WFC	within-frequency-coupling-

AUC	area-under-curve-
ML	machine-learning-
DL	deep-learning-
SVM	support-vector-machine-
KNN	k-nearest-neighbours-
SC	structural-connectivity-
EC	effective-connectivity-
GRU	gated-recurrent-unit-
AGGCN	adaptive-gated-graph-convolutional-network-
GCN	graph-convolutional-network-
CNN	convolutional-neural-network-
LSTM	long-short-term-memory-
MLP	multilayer-perceptron-
ND	node-degree-
NS	node-strength-
E_G	global-efficiency-
E_L	local-efficiency-
FFT	fast-Fourier-transform-
BW	betweenness-centrality-
CBW	coupling-betweenness-centrality-
v_G	global-vulnerability-
v_L	local-vulnerability-
PCC	Pearson's-correlation-coefficient-
COH	coherence-
iCOH	imaginary-part-of-coherency-
PLI	phase-lagged-index-
wPLI	weighted-phase-lagged-index-
PLV	phase-locking-value-

AEC amplitude-envelope-correlation-

WCOH wavelet-coherence-

MI mutual-Information-

MST minimum-spanning-tree-

OMST orthogonal-MST-

ChebConv Chebyshev-graph-convolution-

DropEdge edge-dropout-layer-

AM adjacency-matrix-

ASAP adaptive-structure-aware-pooling-

GGCN gated-graph-convolutional-neural-network-

MMSE Mini-Mental-State-Examination-

STGCN spatio-temporal-graph-convolutional-network-

GAT graph-attention-network-

Chapter 1

Introduction

1.1 Background

Alzheimer's disease (AD) is the leading cause of dementia among older individuals, posing a growing challenge to healthcare systems and economies. There are approximately 47 million patients worldwide diagnosed with AD, a figure projected to triple by 2050 [82]. The increase of patients diagnosed with AD is likely related to the average age increasing globally because the prevalence of AD increases rapidly with age. AD is a progressive neurological disorder characterised by the buildup of amyloid plaques and neurofibrillary tangles [211, 259, 252]. This pathology leads to neuronal cell death, loss of neural pathways and consecutively widespread disruptions in brain function [211]. Cognitively, it manifests through a gradual deterioration in memory, executive function, decision-making, and other cognitive abilities, ultimately leading to a stage wherein the patients cannot function independently in their daily lives [88]. These issues affect the families of AD patients in significant ways as well.

Despite ongoing research, the exact causes of AD remain largely unknown; it is estimated that about 79% of the cases of late-onset AD are hereditary and are often linked to specific genes [15], while only around 1% of early-onset cases are familial [111]. Additionally, alterations in brain cortical activity have been observed preceding the onset of cognitive symptoms [67, 14], suggesting the potential for early detection. Although there is currently no cure for AD, an early diagnosis might be crucial to initialise procedures to mitigate the symptom severity and potentially delay or even prevent the progression to later AD stages.

However, the current process for diagnosing AD is expensive, time-consuming and may be inaccessible due to the need for specialised equipment and trained clinicians.

This process entails various neuroimaging scans such as magnetic resonance imaging (MRI), computerised tomography (CT), positron emission tomography (PET) and cerebrospinal fluid analysis, as well as a battery of cognitive tests assessing abilities such as short-term memory, attention and spatial orientation [64, 110, 13]. Therefore, there is an urgent need for a reliable, economical, portable and automated alternative diagnostic method. Despite the desirability of an automated method, it is crucial to provide accurate and easy-to-understand explanations so that experts can validate the automated predictions.

Electroencephalography (EEG) is a suitable candidate for addressing this need. EEG is a non-invasive neuroimaging technique that measures the sum of electrical potentials generated by neuronal populations within the brain. Specifically, EEG functions by placing electrodes on the subject's scalp. Compared to other neuroimaging methods capable of capturing brain dynamics, such as functional magnetic resonance imaging (fMRI) and magnetoencephalography (MEG), EEG is portable and relatively affordable. However, because of recording at the scalp level with a limited number of electrodes, the spatial resolution of EEG is low compared to fMRI. Thus, signals from the brain cortex are predominantly detected. On the other hand, EEG has excellent temporal resolution at the scale of milliseconds [14, 13]. While EEG can be measured at rest and during a task, this thesis focuses only on resting state EEG. Recording EEG data during a resting state presents advantages in investigating AD patients due to its low demand for active engagement and non-intrusive nature, thereby mitigating stress that might be otherwise induced by performing a task.

Although EEG is not currently used in a clinical setting for AD diagnosis, it has been widely used for studying changes induced by neurodegenerative diseases [13, 14]. There is evidence of alterations of brain oscillatory patterns in early AD when compared to age-matched healthy control (HC) prior to observing any structural changes such as signal slowing and complexity reduction [14, 67]. Additionally, EEG has been successfully used to measure brain connectivity, i.e. relationships between pairs of brain regions. As the pathology of AD causes widespread disconnections between brain areas, it can be considered a network disorder (i.e. graph). Thus, studying the connectivity from a graph perspective is crucial for accurately characterising AD [76, 36, 260].

For these reasons, the research presented in this thesis focuses on examining the disruptions in connectivity induced by AD. Specifically, the aim is to examine novel ways to design a graph-based approach to characterise the complex changes in the brain due to AD and utilise these characteristics to generate accurate and interpretable

predictions.

1.2 Motivation

It is well known that the brain is a complex network of neural units interacting across multiple spatial and temporal scales [21]. The patterns of brain oscillations acquired from multiple EEG electrodes have traditionally been analysed in isolation, grand-averaged across electrodes or their pairwise interactions. However, using such an approach, it is not possible to quantify the function of the entire brain [23]. Network neuroscience (NW) is an emerging approach in neuroscience which aims to address this issue. Unlike other neuroscience approaches, NW studies the brain from an integrative perspective [27, 22]. This means that NW assumes that the function of the brain is distributed and cannot be studied by looking at single units. This core assumption is then conceptualised as a graph. In most NW literature, the graph nodes are brain areas, and edges signify some relationship exists between the nodes [27, 196, 40].

Networks on various scales of the brain can be defined from molecular and cellular levels up to macro-regions of the brain [23]. The research presented in this thesis is positioned at the far end of this dimension as EEG provides only a coarse spatial resolution, i.e. electrical potentials measured on the level of macro-regions [204, 14]. Specifically, the nodes are modelled at the electrode level such that each node corresponds to an EEG electrode.

The edges connecting brain regions can be defined in multiple ways. Structural connectivity (SC) edges represent the physical connections between regions retrieved from methods such as MRI or CT [40, 22]. However, information about SC is unavailable in electrophysiological signals such as EEG. In contrast, edges modelled as functional connectivity (FC) and effective connectivity (EC) represent a statistical dependency and causal relationship between regions, respectively [27, 40, 22]. This thesis focuses on FC-based methods to reconstruct brain graphs from EEG recordings.

FC measures can aim to quantify various types of dependencies between pairs of signals. There are linear and nonlinear approaches [224], time and frequency domain approaches [3], and phase and amplitude approaches [35]. Additionally, FC can be computed on full frequency signals (approximately between $0.5Hz$ and $100Hz$) or specific frequency bands. Studies show that AD-related changes can be observed mainly in δ $(0.5 - 4Hz)$, θ $(4 - 7Hz)$ and β $(15 - 31Hz)$ bands [13]. Studies have shown that AD affects distributed brain networks, alters FC and disrupts information processing

across multiple scales [207, 150, 76, 128].

Besides this type of within-frequency coupling (WFC), there is a growing amount of evidence that cross-frequency coupling (CFC) serve a crucial role in the brain [45, 42]. CFC quantifies FC between signals with different frequencies. It is hypothesised that CFC plays a role in synchronising local and global processes and relates to the information integration across distributed systems [135]. Specifically, various types of CFC have been detected in the brain [126], such as amplitude to amplitude [126, 73, 39, 135], phase to phase [126, 42, 251, 135] and phase to amplitude [126, 59, 257, 135]. However, CFC has been predominantly studied to measure pairwise interactions. A comprehensive analysis of CFC from a graph perspective that would elucidate the roles of different frequency components is thus required. CFC brain graphs might be effectively modelled using multilayer graphs where each frequency component is represented by a layer and with inter-layer edges encoding CFC interactions. This is one of the aims of this thesis. Additionally, the utility of accounting for nonlinear interactions in addition to linear is examined in this thesis.

After a brain graph is reconstructed from EEG, the next challenge is to design an effective model to deliver accurate predictions about the graphs. Feature-based machine learning (ML) is one of the available approaches. Graph theory can be leveraged to engineer features describing various brain graph properties manually [40]. Such features can be nodal, i.e. defined for each node of a graph, or global, i.e. an index describing the graph as a whole [3, 27]. Nodal features are commonly used to identify influential nodes in the graph. In the context of AD, node degree [197], and clustering coefficient [273, 172, 52, 84] have been successfully used to determine brain regions important for characterisation and prediction of AD. While ML models can be efficient and offer relatively simple interpretability, the need for manual feature engineering poses a crucial limitation of such an approach. Feature engineering requires expert domain knowledge and is generally time-consuming [50].

Deep learning (DL) models offer an alternative approach with automatic feature extraction, although they require the selection of a large number of hyperparameters compared to ML. However, most traditional DL architectures are ill-suited for graph-structured inputs [37]. Models such as multilayer perceptrons (MLPs), convolutional neural networks (CNNs), and recurrent neural networks (RNNs) were designed for Euclidian inputs such as time series and images. Graph neural networks (GNNs) have been proposed to address this limitation and offer an efficient extension of the convolutional mechanism of CNN to graphs [312]. However, the applications of GNN-

for EEG tasks are relatively limited without a clear set of guidelines for designing such models. Thus, another aim of this thesis is to systematically review this emerging subfield of NW and propose categorisation of the various approaches experimented within the literature.

As discussed above, various FC measures are utilised in the literature. However, selecting an appropriate measure of FC for subsequent graph analysis and classification remains ambiguous. To our knowledge, this is true for both ML and DL approaches. This thesis aims to fill this gap by proposing an empirical evaluation of the effect an FC measure has on the performance of various ML and DL models, including GNNs in the AD diagnosis task.

A crucial area for improvement of the modelling approaches mentioned previously is their explicit lack of explainability, i.e. it is usually possible to generate some explanations via post-hoc analysis. For a model to be successfully deployed in a real-world clinical setting, it is vital to produce consistent and detailed explanations of its predictions that medical experts can validate. For AD prediction task, such explanations need to be generated for multiple spatial scales as AD-related disruptions are well known to present on both local and global levels [6]. GNNs are an ideal architecture for such a purpose due to the inherent nature of the graph convolutional mechanism of graph convolutional network (GCN) family of GNNs [312, 285]. Briefly, GCNs learn via recursive information aggregation across gradually increasing receptive fields. The recursive property of GCNs might be leveraged to quantify patterns across various spatial levels, going from highly localised to coarse-grained whole-brain levels.

Unlike other DL models, the input to GNNs forms the computational graph simultaneously, i.e. graph structure is leveraged both for learning and information propagation [285]. Whether the input graph structure is the optimal computational graph has been a central point of interest in GNN literature [31]. A popular approach has been to decouple the computational graph from the input with methods such as graph rewiring [256, 137], graph lifting to higher dimensional topological spaces [31] and transformer-based methods [152, 292]. However, preserving the FC-based graph structure is essential for brain graph prediction tasks to retain the ability to generate model predictions, which would be lost if the computational graph is fully decoupled from the input. This thesis explores a hybrid strategy where the model learns the graph structure. This offers two advantages: (1) the dilemma of FC measure selection is effectively circumvented, and (2) the model is free to adapt the graph structure to strike a balance between producing an optimal computational graph and recovering

the underlying brain-graph structure.

1.3 Aims and Objectives

Generally speaking, the main aim of this research thesis is to model high-dimensional EEG signals from a graph perspective in order to quantify the changes in the brain connectivity caused by neurodegenerative diseases and to develop novel biomarkers for diagnosis and characterisation of neurodegenerative diseases. Such results can potentially improve the diagnostic process of AD due to the accessibility, ease-of-use and low cost of EEG. This main objective is concisely captured within the following research question:

How can reconstructed complex brain graphs from EEG signals be used for diagnosing and characterising neurodegenerative diseases?

In order to provide a detailed answer to the research question, multiple objectives were identified, highlighting the key elements and potential for novel contributions of this research project. The objectives listed below aim to research the brain structure and function changes induced by neurodegenerative disease. This aim is not explicitly formulated in the objectives to avoid repetition. Although there are other types of neurodegenerative diseases, this research project is going to focus on AD as this disease affects the largest portion of the human population.

1. Assess the predictive power of nonlinear and cross-frequency brain connectivity compared to linear and within-frequency alternatives.

2. Develop methods for analysing cross-frequency coupling from a graph perspective using a multilayer graph analysis framework.

3. Investigate the use of graph representation learning algorithms and graph neural networks to study neurodegenerative diseases and facilitate the diagnostic process.

   (a) Systematically review graph neural networks for EEG classification in order to facilitate a current overview of the field and aid in innovation.

   (b) Examine the usability of common functional connectivity methods to constructing input EEG brain graphs to graph neural networks.

4. Assess the potential of graph neural networks for automatically reconstructing brain graph structures.

5. Develop graph neural network architecture for explainable prediction of neurodegenerative diseases.

1.4 Overview of the Thesis

This thesis is organised into seven chapters and covers the following content:

- **Chapter 2** examines prior research connected to this thesis. It begins by exploring different methods for reconstructing brain graphs from EEG. It then delves into understanding established changes in AD, focusing on graph-level alterations. Lastly, it critically assesses the utilisation of GNNs in analysing EEG. Overall, this chapter pinpoints several research gaps this thesis intends to address.

- **Chapter 3** describes the details of the EEG dataset that is subsequently utilised in chapters 4, 5 and 6.

- **Chapter 4** presents work on utilising the higher-order nonlinear bispectrum to reconstruct multilayer brain graphs incorporating information about both WFC and CFC interactions. It evaluates the benefits of this approach against a single-layer linear alternative in terms of statistical characterisation and ML-based prediction of AD.

- **Chapter 5** presents the practical assessment of the influences of different FC measure on the performance of multiple ML and DL algorithms in AD diagnosis task.

- **Chapter 6** introduces adaptive gated graph convolutional network (AGGCN), a novel GNN architecture designed for AD classification. Unlike traditional graph-based approaches dependent on specific FC measures, this architecture employs a data-driven approach for reconstructing brain graphs. Demonstrating outstanding performance in contrast to several state-of-the-art methods, it generates diverse prediction explanations at graph, node, and edge levels.

- **Chapter 7** summarises the presented contributions and outlines potential future research directions.

1.5 Contributions and Research Outputs

This thesis introduces original contributions focused on utilising machine learning, deep learning, and graph theory methods to characterise AD from graph perspective. This research aims to contribute to developing a data-driven framework for analysing and understanding neurodegenerative diseases.

1. **Chapter 2** reviews previous research on graph approach to reconstruct and classify brain graphs of AD cases from EEG signals. The main contribution of this chapter is a survey of applications of GNNs for EEG classification.

   Based on parts of this work, a review paper has been published:

   - Dominik Klepl, Min Wu, and Fei He. Graph Neural Network-Based EEG Classification: A Survey. *IEEE Transactions on Neural Systems and Rehabilitation Engineering*, 32:493–503, 2024. ISSN 1558-0210. doi: 10.1109/TNSRE.2024.3355750

2. **Chapter 4** introduces novel multilayer graph analysis to elucidate the roles of various brain rhythms in enabling information integration and segregation within the brain and how these roles are disrupted due to AD. This information is then used for ML-based prediction of AD.

   Based on this work, a journal paper and a conference paper have been published:

   - Dominik Klepl, Fei He, Min Wu, Daniel J. Blackburn, and Ptolemaios G. Sarrigiannis. Cross-Frequency Multilayer Network Analysis with Bispectrum-based Functional Connectivity: A Study of Alzheimer's Disease. *Neuroscience*, 521:77–88, June 2023. ISSN 0306-4522. doi: 10.1016/j.neuroscience.2023.04.008
   - Dominik Klepl, Fei He, Wu Min, Daniel Blackburn, and Ptolemaios Sarrigiannis. Bispectrum-based Cross-frequency Functional Connectivity: Classification of Alzheimer's disease. In *2022 44th Annual International Conference of the IEEE Engineering in Medicine & Biology Society (EMBC)*, pages 305–308, July 2022. doi: 10.1109/EMBC48229.2022.9871366

3. **Chapter 5** reports the effect of commonly used FC measures on the performance of ML and DL models in AD classification task. The main focus is on GNNs.

   Based on this work, a journal paper has been published:

- Dominik Klepl, Fei He, Min Wu, Daniel J. Blackburn, and Ptolemaios Sarrigiannis. EEG-Based Graph Neural Network Classification of Alzheimer's Disease: An Empirical Evaluation of Functional Connectivity Methods. *IEEE Transactions on Neural Systems and Rehabilitation Engineering*, 30:2651–2660, 2022. ISSN 1558-0210. doi: 10.1109/TNSRE.2022.3204913

4. **Chapter 6** introduces a novel GNN architecture with a learnable graph structure, thus avoiding the issue of FC measure selection. The focus is on acquiring explainable predictions.

   Based on this work, a journal paper has been published:

   - Dominik Klepl, Fei He, Min Wu, Daniel J. Blackburn, and Ptolemaios Sarrigiannis. Adaptive Gated Graph Convolutional Network for Explainable Diagnosis of Alzheimer's Disease Using EEG Data. *IEEE Transactions on Neural Systems and Rehabilitation Engineering*, 31:3978–3987, 2023. ISSN 1558-0210. doi: 10.1109/TNSRE.2023.3321634

Moreover, additional research outputs have been published during this PhD project:

- Dominik Klepl, Fei He, Min Wu, Matteo De Marco, Daniel J. Blackburn, and Ptolemaios G. Sarrigiannis. Characterising Alzheimer's Disease With EEG-Based Energy Landscape Analysis. *IEEE Journal of Biomedical and Health Informatics*, 26(3):992–1000, March 2022. ISSN 2168-2208. doi: 10.1109/JBHI.2021.3105397

- Sivasharmini Ganeshamoorthy, Laura Roden, Dominik Klepl, and Fei He. Gene Regulatory Network Inference through Link Prediction using Graph Neural Network. In *2022 IEEE Signal Processing in Medicine and Biology Symposium (SPMB)*, pages 1–5, December 2022. doi: 10.1109/SPMB55497.2022.10014835

Chapter 2

Literature Review

Although EEG is currently not used as part of the diagnostic process of neurodegenerative diseases such as AD, its potential for characterisation and diagnosis has recently gained attention in research [19]. In contrast to other neuroimaging methods such as CT, fMRI and PET, EEG offers an excellent temporal resolution (on the scale of milliseconds) but suffers from relatively low spatial resolution. An alternative to EEG is MEG, which maintains a comparable temporal resolution and allows for higher spatial resolution. However, EEG is considerably cheaper and more portable than MEG, making it an ideal candidate for developing an economical and accessible tool for the diagnosis of AD.

EEG records the gross sum of electrical potentials generated by neural assemblies in cortical and sub-cortical areas [204]. However, the positioning of EEG electrodes on a subject's scalp will likely emphasise the contribution of cortical regions to the signals measured by EEG. EEG signals are typically further decomposed into several frequency bands corresponding to different brain rhythms. Namely these are δ, θ, α, β and γ bands. Different processes in the brain generate each frequency band. Generally, high frequencies are related to local communication, while low frequencies support communication between distant regions [266, 231].

Various alterations of these brain rhythms have been reported in AD using electrode-level methods [114, 9, 139, 221, 222, 227, 200]. This category of EEG analysis typically quantifies the alterations on a single electrode level without considering pairwise interactions. These patterns of brain oscillatory rhythms are reviewed in section 2.1.

Network neuroscience extends the analysis of brain oscillations to quantify interactions between brain regions. Such interactions can be reconstructed from neuroimaging data using connectivity analysis. Specifically, three types of connectivity can be typi-

cally reconstructed: functional (FC), structural (SC) and effective (EC). FC measures statistical dependency between pairs of signals indicating functional interaction and is the main focus of this thesis [231]. SC quantifies the physical connection between neuronal populations and brain regions. However, EEG signals do not contain any information about brain structure; thus, SC is not applicable. Finally, EC, considered a subcategory of FC, measures the causality or flow of information between regions.

Upon selecting an appropriate connectivity measure, a brain graph can be reconstructed from EEG by computing the connectivity between all pairwise combinations of available electrodes. In section 2.2, a typical pipeline for reconstructing brain graphs from EEG is reviewed with a focus on common FC measures, brain graph preprocessing and graph measures.

Then, graph-level patterns related to AD are reviewed in section 2.3 together with various ML and DL methods for utilising graph information for automated diagnosis of AD. Among these classification methods, GNNs emerge as a powerful method for learning on graph-structured objects such as EEG-based brain graphs. Thus, GNNs models proposed for various EEG classification tasks are reviewed in section 2.4.

2.1 Brain Oscillation Changes in Alzheimer's disease

This section reviews the findings on brain oscillation changes induced by AD. Brain oscillations influence the timing of individual neuronal firing on a microscopic level while coordinating the interaction among widely dispersed cortical networks on a macroscopic scale [302]. Signals recorded by EEG can then be characterised in the time or frequency domains to study the oscillatory activity.

Identification of oscillations in EEG measurements is typically computed across different EEG channels, i.e. electrodes, either in isolation or by obtaining a grand-averaged signal of the whole brain or a particular region of interest. These oscillatory patterns are typically analysed in frequency bands, thus allowing the study of the processes linked to low-frequency and high-frequency oscillations in isolation. Five canonical frequency bands are defined for EEG signals: δ $(0.5-4Hz)$, θ $(4-7Hz)$, $\alpha(7-15Hz)$ and β $(15-31Hz)$. It has been shown that each band supports various cognitive functions, although some functions do not fit the canonical definition of frequency bands.

Generally, low-frequency oscillations enable long-range global neural communication, while high-frequency oscillations support local communication [231, 266]. For instance, δ rhythm becomes dominant during sleep and θ oscillations in the frontal region are linked to inhibitory regulation of other regions, memory and executive function [117]. α band is related to memory and temporal attention [105], β is linked to motor planning, imagery and execution [199], and γ is related to conscious information processing [232] and active memory [109].

Healthy ageing is characterised by progressive changes in brain wave frequency, power, and distribution during rest [121]. In particular, healthy ageing is associated with an increase of power in δ and θ bands [222] and slowing down of dominant activity of α band [121]. Cognitive decline related to neurodegeneration further enhances the alterations of brain oscillatory activity [193]. The hallmark EEG-based biomarker of AD is the slowing down of brain signals. This is manifested by the reduction of the power of high-frequency rhythms and an increase in the power of low-frequency components [114, 9, 139, 221, 222, 227].

A global δ power increase has been observed in AD [49, 11, 46] whereas θ power increase is limited to central and occipital regions [47, 140]. Reduced α power has been observed in occipital, parietal and temporal regions [11, 179, 157, 140]. Similarly, reduced β power has been detected in central, frontal and occipital regions [140]. Findings related to γ band changes, such as power and synchronisation, are considered controversial due to their inconsistency [101], with some studies reporting a decrease [148, 239]. In contrast, others report an increase of γ [20, 275, 221]. Interestingly, an increase in γ CFC in AD has been suggested to be linked with a compensatory mechanism for the increased need for resources due to network disruptions [275].

Slowing down of EEG signals has also been shown to be a potential indicator of conversion from mild cognitive impairment (MCI) stage to AD [102]. The ratio of θ and γ correlates with AD conversion and decreased memory test scores [219, 192]. Changes in power also correlate with several biomarkers of AD and cortical neurodegeneration. There is a correlation between cerebrospinal-fluid-based biomarkers such as Aβ, p-tau and t-tau, and global power of δ, θ, α and β frequency bands [233]. Studies also report a link between volumetric neurodegeneration [10, 193], with occipital α power correlating with occipital grey matter density [12, 87].

Based on these oscillatory patterns of AD cases, multiple attempts to design ML- and DL-based classification models have been published. support vector machine (SVM) classifier has been trained on time-frequency domain [188] and wavelet trans-

form features extracted to distinguish between AD and HC cases [154]. Next, multiple studies on using artificial neural networks have been published.

Raw EEG signal can be used as an input to a neural network to classify AD [62]. In [7], the EEG signal from a single EEG electrode is transformed into a visibility graph and classified using a neural network. Alternatively, a neural network can be trained on features derived from wavelet transform and short-time Fourier transform [218]. Some approaches have been developed to transform EEG signals from multiple electrodes into images to leverage the image-classification advantages of CNNs. power spectral density (PSD) vectors across all electrodes are computed and stacked to form an input matrix, i.e. image, and fed to a CNN [118]. In [115], wavelet-transform matrices of multiple electrodes are used as tiles to create an input image to a CNN by arranging the tiles according to the spatial positions of corresponding electrodes.

A significant limitation of these classification approaches is the lack of incorporating information about relationships between EEG electrodes. Network-based (i.e. graph-based) approaches seek to address this limitation by using connectivity methods to model these interactions.

2.2 Graph-based EEG Analysis

Graph-based approaches for modelling EEG signals aim to utilise the information from all available electrodes by considering the complex pairwise interactions. This section reviews the core steps in the pipeline of graph-based approaches. First, the methods for reconstructing brain graph structure from EEG, i.e. FC measures, are reviewed. Then, the methods for graph preprocessing are reviewed. Finally, we review the most used graph metrics for characterising brain graphs.

2.2.1 Graph Inference via functional connectivity

There is no consensus on how the edges of a brain graph, i.e. connectivity, should be inferred from EEG. In the case of EEG, this connectivity is referred to as FC as the edges capture merely information about statistical dependency between nodes [201]. This is in contrast to structural connectivity, which models the physical connections between brain regions, e.g. white matter fibres [23]. Although FC does not indicate a physical connection between brain regions, it still describes an interesting property of the brain as it has been shown that synchronised EEG oscillations of two distant brain

	Linear	Nonlinear	Time-Domain	Frequency-Domain	Phase	Amplitude	Cross-frequency
Pearson's correlation coefficient (PCC)	✓		✓				
Coherence (COH)	✓			✓	✓		
Wavelet coherence (WCOH)	✓	✓		✓	✓		
Partial Coherence	✓			✓	✓		
Amplitude envelope correlation (AEC)	✓					✓	✓
Imaginary part of coherency (iCOH)	✓			✓	✓		
Phase lagged index (PLI)	✓	✓		✓	✓		
Weighted phase lagged index (wPLI)	✓	✓		✓	✓		
Mutual Information (MI)	✓	✓	✓	✓			
Transfer Entropy	✓	✓	✓				
n:m Phase synchronisation	✓	✓		✓	✓		
Phase locking value (PLV)		✓			✓		✓
Mean Vector Length	✓	✓			✓	✓	✓
Modulation Index	✓	✓			✓	✓	✓
Cross bispectrum (CBS)	✓	✓		✓	✓	✓	✓

Table 2.1: Categorisation of methods for estimating FC

regions indicate a functional interaction [231].

FC can be divided into two categories: directed and undirected [27, 24]. Directed FC is referred to as effective connectivity and models the causal effects that nodes have on each other. On the other hand, undirected FC models the dependencies but not the directionality of information flow. This review focuses on undirected measures of FC.

The simplest method for estimating FC is Pearson's correlation and is often used with different types of neuroimaging [220, 33] including characterising AD [276]. However, EEG signals are typically non-stationary and exhibit complex nonlinear interactions; thus, correlation is not a well-suited method for use with EEG as it captures only linear relationships and assumes stationarity. Thus, other methods are commonly employed to estimate FC, which consider the interactions' complexity. The various FC methods are listed in Table 2.1. The FC methods are categorised based on whether they measure linear or nonlinear dependencies, whether they are computed in the time domain or frequency domain, which property of EEG signal they measure, and whether cross-frequency coupling can be measured.

Although the brain signals are nonlinear, many linear methods based on correlation are a popular choice for FC estimation. An extension of correlation to frequency domain is coherence, measuring phase synchronisation of two signals [4, 69, 248]. Similarly, correlation is extended to measure relationships between amplitudes of the signals, i.e. envelope correlation [60]. Typically, these methods rely on the Hilbert transform to extract the instantaneous phase and amplitude of the EEG signal.

The limitations of coherence can be resolved by using wavelet transform to obtain wavelet coherence, which is sensitive to nonlinear relationships in addition to linear [127]. However, the inferred FC can be a result of an indirect relationship, e.g. two signals are related via a third signal, partial coherence attempts to resolve this issue by

removing linear effects of all other signals [18]. The imaginary part of coherence can also be used as it removes zero-lag dependencies and thus is well suited for sensor-level EEG FC, which can suffer from volume conduction, i.e. spatial information leakage between adjacent EEG electrodes [203].

Similar to coherence, the phase lag index family of FC methods aims to measure phase synchronisation [241], which utilises asymmetries of the probability distribution of differences between phases of two signals and thus can capture nonlinear relationships. Weighted phase lag index incorporates the imaginary part of coherence by using it to weight the phase lags [265], resulting in more robust FC estimates with respect to noise. An interpretation might be difficult as it mixes information about the magnitude and consistency of the phase.

The last common family of methods to infer FC are based on information theory: mutual information [129] and transfer entropy [189]. Mutual information estimates FC as the amount of information about one signal explained by another signal and vice versa, utilising their marginal and joint probability distributions. It has been shown that mutual information can capture both linear and nonlinear dependencies [129, 119].

However, all of the FC methods introduced above share one major limitation: they rely on splitting EEG signals into frequency bands, which are subsequently analysed in isolation. We refer to these types of FC as WFC as the inferred interactions can occur only between signals within the same frequency band. Recently, there has been increasing evidence that brain signals become entangled across frequency bands, giving rise CFC [125]. CFC is hypothesised to be the underlying mechanism of interaction of local and global processes [135], thus facilitating the integration of information, which is one of the essential properties of the brain. Hence, accounting for WFC and CFC is critical when studying brain networks but has been largely ignored in FC and NW literature.

Both WFC and CFC are generally quantified as coupling between two components of EEG signals, such as phase to phase, amplitude to amplitude, and phase to amplitude. Other coupling types were documented but poorly understood and thus omitted in this review, e.g. phase-frequency [125] and amplitude-frequency [282]. Most of the following measures are not FC measures per se but can be easily adopted as such.

Amplitude-amplitude coupling is most commonly studied using amplitude envelope correlation described above [39, 74] and is usually observed between high-frequency rhythms. n:m-phase synchronisation is used for quantifying phase-phase coupling [268, 226, 58] and is the only CFC measure that has, to the best of our knowledge, been

used as FC measure [42].

Phase-amplitude coupling refers to a coupling where the phase of a low-frequency signal is coupled with the amplitude of a high-frequency signal and is possibly the most studied type of CFC as it has been demonstrated to occur frequently both in human and animal brains [194, 258]. Specifically, $\theta - \gamma$ phase-amplitude coupling plays a crucial role in multiple cognitive processes such as perception, learning or computation [125, 44, 45]. Multiple phase-amplitude coupling measures are reported in the literature, such as mean vector length, phase locking value and modulation index [116].

2.2.2 Graph Pre-processing

In order to reconstruct the brain graph structure from EEG, a chosen FC measure is computed for all pairwise combinations of available EEG channels. Since $\mathrm{FC}(x, y) = \mathrm{FC}(y, x)$, given N channels, this results in a fully connected graph with $\frac{N(N-1)}{2}$ edges. However, using a fully connected graph for further analysis can pose several issues: (1) false positive edges and (2) graph-measures calculating unweighted shortest paths are invalid.

The former can stem from multiple reasons, such as signal noise, volume conduction or spurious coupling. These issues can be controlled by appropriate signal preprocessing, selecting a robust FC measure and using false-positive corrections such as surrogate testing. The latter can be addressed only by transforming the fully connected graph to a sparse version of itself, i.e. discarding a certain number of edges. The choice of graph preprocessing method is crucial, especially for unweighted graph analysis, i.e. edges do not have a strength, as it might alter the graph structure significantly. Some studies omit the graph preprocessing step and analyse the fully connected graphs obtained by chosen FC measure [306, 186]. Despite the limitations described previously, an advantage of this method is obtaining the same number of edges for all graphs, thus making group comparisons unbiased.

A simple graph-filtering method is choosing a specific threshold value of connectivity and removing any edges that are below this threshold [273, 262, 172, 225]. Such a method requires a normalised FC measure to establish a meaningful threshold value. However, the resulting graphs can have varying densities, i.e. the number of edges, and become disconnected such that a node cannot be reached from all other nodes. Thus, comparisons of such graphs might be difficult and biased.

Many studies opt instead for a data-driven graph preprocessing method. Edge-density thresholding is a popular and straightforward approach [5, 271, 123, 236, 190, 294, 122, 42]. This approach establishes a certain edge density level for each graph by keeping the top x% strongest edges. It is, however, challenging to determine the optimal edge density value. Typically, the analysis is repeated with multiple edge densities to prove that the results are independent of the edge density value. Alternatively, the median FC value can be used [295]. A drawback of the edge density threshold is that the actual minimum FC value will differ between graphs. Additionally, this method does not prevent graph disconnection, especially at low edge densities. The number of edges remains fixed across all graphs, provided they have the same number of nodes, thus making comparisons unbiased.

Minimum spanning tree (MST) addresses the limitations of edge density thresholding [294, 122, 297, 180, 65, 208]. MST is an algorithm for extracting the "backbone" of a graph by producing a tree which minimises the sum of edge weights (provided edge weight represents a distance). Thus, for FC graphs, a maximum spanning tree is typically used instead. Specifically, an MST of a graph with N nodes contains $N - 1$ edges. MST-based graph thresholding has been proven to provide an unbiased method for graph comparisons [253]. However, a potential limitation is the low number of edges preserved in an MST.

The orthogonal MST (OMST) method has been proposed to solve the limited number of edges of MST [78, 79]. OMST is an iterative extension of MST. The first iteration equals an MST, and the selected edges are removed from the candidate set of edges. The MST algorithm is then run again, repeating the step until the desired number of iterations is achieved. Thus, I iterations of OMST yield a graph with $I(N - 1)$ edges. OMST thus combined the advantages of MST and edge density methods, i.e. guarantee of a connected graph and fixed number of edges.

2.2.3 Graph Measures

There are various ways to quantify the properties of a graph. This subsection reviews the measures based on graph theory commonly used in brain graph analyses. Graph measures can be divided into node-level and graph-level. Node-level measures can be computed individually for each node, thus allowing one to evaluate the importance of each node in the context of the entire graph. In contrast, graph-level measures characterise the graph as a whole by a single value. Besides graph-theory-based measures, one

can analyse and compare graphs by summarising the adjacency matrix via descriptive statistics or performing edge-wise comparisons. Such approaches are, however, infeasible with large graphs as the number of comparisons grows too large.

Standard node-level measures used in brain graph literature are node degree (ND), node strength (NS), clustering coefficient and betweenness centrality. ND is defined as the sum of edges of a given node, thus giving a rudimentary measure of node centrality since a more connected node implies more information flows through it [165]. NS is the weighted extension of ND, i.e. the sum of edge weights of a given node, and having a similar interpretation [106, 84].

The clustering coefficient measures the tendency of a node to form clusters with other nodes[273, 172, 52, 84]. The clustering coefficient of node i is computed as follows:

$$C_i = \frac{1}{\mathrm{ND}_i(\mathrm{ND}_i - 1)} \sum_{jk} \mathbf{A}_{ij}\mathbf{A}_{jk}\mathbf{A}_{ki}, \tag{2.1}$$

where $\mathbf{A}$ is the adjacency matrix. The average clustering coefficient can be used to assess the degree of information segregation of a graph, a crucial property of the brain [223].

Finally, betweenness centrality (BW) is a measure of node importance in terms of the influence the node has on information flowing through the graph [122, 42]. BW of node i is computed as follows

$$BW(i) = \sum_{i \neq j \neq k} \frac{d_{jk}(i)}{d_{jk}}, \tag{2.2}$$

where g_{jk} is the total number of shortest paths between nodes j and k, and $d_{jk})(i)$ is the total number of d_{jk} passing through node i.

Commonly used graph-level measures are average path length, local efficiency (E_L), global efficiency (E_G) and small-worldness. Average path length quantifies the efficiency of information transport throughout the graph [273, 262, 156]. It is defined as the average length of all possible paths between all pairs of nodes.

E_G measures the information integration across the entire graph [273, 172, 5, 186, 93]. It is computed as

$$E_G(G) = \frac{1}{N(N-1)} \sum_{i \neq j \in G} \frac{1}{d(ij)}, \tag{2.3}$$

where N is the number of nodes in network G and $d(ij)$ is the shortest path length

between nodes i and j.

E_L measures the information segregation in the graph [273, 5, 123, 42] and is computed as follows:

$$E_L(G) = \frac{1}{N} \sum_i E_G(G_i), \tag{2.4}$$

where G_i is the subgraph containing node i and its neighbours.

A small-world graph is a graph with high clustering and short distances between nodes, i.e., neighbouring nodes tend to connect with similar nodes, and each node can be reached via a relatively short path from any other node. Small-worldness measures how close to a small-world graph the given graph is [273, 180, 42].

A particular case of graph measures are measures of vulnerability. These measures compute the change of a graph-level measure after a node is removed. In other words, vulnerability measures quantify the importance of the removed node to facilitate the given property of a graph. For example, characteristic path length vulnerability has been previously used to characterise brain graphs [273].

Additional measures can be employed to characterise a graph structure, such as various graph complexity measures and alternative node centrality measures. However, the graph measures described in this section are the most commonly used to characterise brain graphs.

2.3 Graph-based Alzheimer's disease patterns

This section reviews AD disruptions from a graph perspective. First, global changes in FC are reviewed. Next, AD disruptions expressed as global-level graph measures are examined. Then, we examine the regional changes in brain graphs of AD cases. The changes related to conversion from MCI stage to AD are also reviewed. Finally, graph MLclassification approaches are summarised.

2.3.1 Global changes in functional connectivity

As discussed in Section 2.1, brain oscillatory changes due to AD are observed as a decrease in high-frequency activity and an increase in low-frequency activity. A similar pattern can be observed in the global average FC strength of AD brain graphs. Average FC strength is reduced in the α frequency band [71, 165, 238, 273, 286, 297] and β frequency band [71, 165, 238, 273, 286]. Moreover, the network structure in α of AD

cases has been reported to disintegrate under eyes-open (EO) [65]. A whole-scalp hypo-connectivity of long-range connections independent of a frequency band has also been reported [236]. In contrast, average FC strength in θ is increased in AD cases [297].

Interestingly, it has been demonstrated that α connectivity, measured by AEC, increases after AD patients have been administered medication to reduce cognitive symptoms [34]. This suggests a plausibility of using FC-based approaches for monitoring and evaluation of AD treatments.

There is also some evidence that whole-scalp CFC is disrupted in AD brain graphs [42, 79]. Mean phase-phase CFC is negatively correlated with mean WFC in AD [42]. However, a detailed examination of combined WFC and WFC brain graphs is necessary to characterise the more complex AD-related disruptions.

2.3.2 Changes in Global-level Graph Metrics

The most studied properties of brain graphs are related to information integration across the entire graph and information segregation, i.e., the presence of specialised and localised information processing units. E_G is one of the measures of information integration. Decrease of E_G values has been reported in AD brain graphs [297, 5, 186, 93]. Moreover, this decreased information integration in α band correlates with verbal fluency test scores [52]. Average path length further supports decreased integration in AD graphs. Its inverse is related to E_G. Thus, an increase in average path length observed in AD graphs translates to lower information integration [186, 156]. An increase in average path length has also been observed in CFC multi-layer graphs where each frequency band is represented as a separate layer [42].

Findings related to information segregation in AD brain graphs are not as clear. However, the evidence seems to accumulate in favour of a decrease [5, 93, 296, 186, 156, 52, 2] rather than an increase [123]. Both E_L and the clustering coefficient can be used to quantify the segregation of a graph. One study reports an increase of E_L [123]. In contrast, multiple studies using various FC measures to reconstruct brain graphs report reduction of E_L [5, 93, 296]. Characterisation of information segregation in AD measured with clustering coefficient is more consistent with all studies indicating decreased values [186, 156, 52, 296, 2]. Specifically, reduced average clustering coefficient can be found in α [52, 296, 2] and β [2] frequency bands. Furthermore, this decrease in α clustering coefficient correlates with Mini-Mental State Examination (MMSE) score [93] and score of verbal fluency [52].

AD brain graphs have also been shown to have reduced modularity [123], which might be in conflict with the clustering coefficient findings. Lower average node degree has also been reported in AD graphs [93]. Overall, it seems that AD graphs are further from optimal small-world graphs, with multiple studies reporting reduced small-world indexes [240, 261, 273, 295, 156]. This pattern seems to reverse, however, when CFC information is included in the reconstructed graph [42].

AD graphs have also been reported to be more homogeneous [295], less robust [66], and more vulnerable than their HC counterparts [261, 273, 2, 5]. Increased vulnerability of AD graphs in α and β frequency bands has been demonstrated by quantifying the effect of node removal on E_G values [5]. However, the differences in vulnerability of CFC graphs remain unclear.

2.3.3 Regional Changes of Brain Graphs

Multiple localised graph disruptions in AD have been reported. An overall loss of network organisation has been observed in parietal and occipital areas [297]. Similarly, the average wPLI strength is reduced in α and β bands in occipital and orbitofrontal regions [165].

Coherence between hemispheres in these frequency bands is reduced as well in frontal, temporal and parietal lobes [91, 90, 147, 310] which reflects the general loss of long-distance connectivity in AD [237]. Intrahemispheric coherence is also disrupted between central and occipital regions in δ band [147, 310]. The strength of edges within the frontal lobe and between left-frontal and right-occipital regions have been shown to be strong predictors of AD [236]. Additionally, the information flow from posterior to anterior regions is reduced in AD [85]. In contrast, central to posterior information flow is increased in AD

2.3.4 Graph Biomarkers of Alzheimer's Disease Progression

A few studies propose methods to automatically classify MCI cases that will, over time, convert to AD [212, 288, 185]. A whole-scalp decrease of functional dissimilarity (can be considered an inverse of FC) in δ and θ frequency bands have been identified as predictors of MCI-AD conversion [185].

Region-specific predictors of MCI-AD conversion have been identified using MI in α frequency band across temporal, parietal and frontal lobes [288]. Furthermore, differences in the parahippocampal cortex have been suggested to be linked to the

degradation of visual memory [288].

Node-level graph metrics also reveal various AD-related alterations. An information hub of a graph located in the frontal lobe is damaged in AD [236]. Reduced hub strength in the central area has also been observed in AD when performing a cognitively demanding task [65].

Furthermore, lower NDs and clustering coefficients across all frequency bands in frontal and orbitofrontal areas show further evidence of damaged hubs in these regions [165]. Reduced clustering coefficients have also been reported in δ-β CFC in parietal, occipital and temporal regions [43].

2.3.5 Graph ML for Alzheimer's Disease Diagnosis

Multiple ML classifiers have been proposed to use features extracted from reconstructed brain graphs to diagnose AD. Classifiers trained using graph measures are a popular choice in the literature with methods such as SVM[225, 123, 295, 236, 1, 43, 43], MLP [225], linear discriminant classifier [5] and fuzzy network classifier [296].

Discriminatory electrodes have been identified predominantly in parietal and occipital regions [225]. The SVM-based approach has even been extended to the 3-way classification of AD, MCI, and HC using node degree features [1].

The predictive utility of multiplex brain graphs has also been tested. Multiplex graphs are constructed such that a layer represents each frequency band, and inter-layer edges are inserted to connect the same electrodes across layers. Using such graph construction method, SVM has been trained with multiplex clustering coefficient as features [43].

Finally, one study has demonstrated the importance of linear and nonlinear FC graphs. Comparisons of k-nearest-neighbour classifiers trained using linear and mixed (linear and nonlinear) FC values show that mixed FC performs significantly better [306]. In this section, GNN-based methods have been omitted since those methods require a detailed review to elucidate how such methods should be utilised for AD classification.

2.4 Graph Neural Networks for EEG Classification

[1]GNNs emerge as a powerful tool for modelling EEG data [167] within the NW framework. GNNs are specifically designed to operate on graph-structured data. They can effectively leverage the spatial structure within EEG data to extract features, uncover patterns, and make predictions based on complex electrode interactions. Designing GNN models for EEG classification will likely improve classification tasks and potentially uncover new insights in neuroscience.

Motivated by the potential of GNNs and an increasing number of recent papers proposing GNN for various EEG classification tasks, there is an urgent need for a comprehensive review of GNN models for EEG classification. The main aims of this section include:

- Identifying emerging trends of GNN models tailored for EEG classification.
- Reviewing popular graph convolutional layers and their applicability to EEG data.
- Providing a unified overview of node feature and brain graph structure definitions in the context of EEG analysis.
- Examining techniques for transforming sets of node feature embeddings into a single graph embedding for graph classification tasks.

This review will provide a comprehensive and in-depth analysis of the application of GNN models for EEG classification by addressing these essential aspects. The findings and insights gained from this review will identify promising future research directions.

2.4.1 Overview of Graph Neural Networks

Graphs are widely used to capture complex relationships and dependencies in various domains, such as social networks, biological networks, and knowledge graphs. The problem of graph classification, which aims to assign a label to an entire graph, has gained attention in recent years. GNNs offer a promising solution to this problem by extending the concept of convolution from Euclidean inputs to graph-structured data.

[1]The content presented in this section has been published in Dominik Klepl, Min Wu, and Fei He. Graph Neural Network-Based EEG Classification: A Survey. *IEEE Transactions on Neural Systems and Rehabilitation Engineering*, 32:493–503, 2024. ISSN 1558-0210. doi: 10.1109/TNSRE.2024.3355750

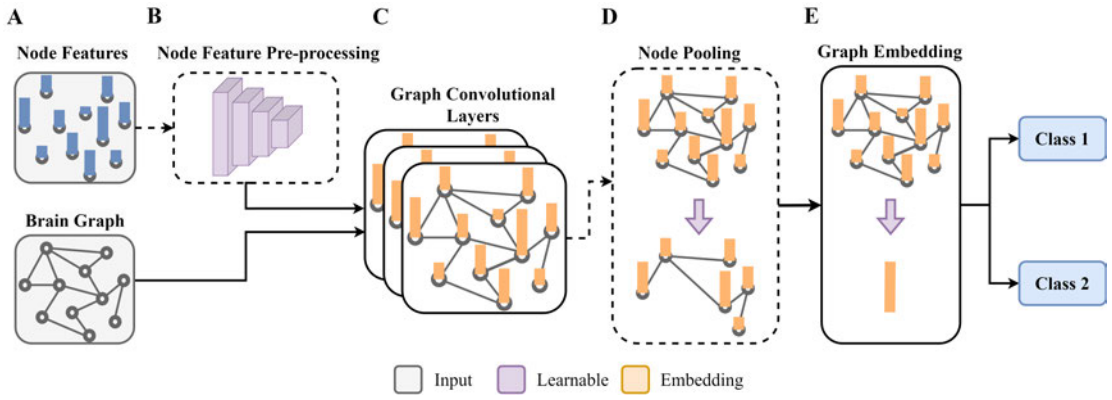

Figure 2.1: The general architecture of a graph neural network model for classification of EEG. (A) The input to the model consists of node features and a possibly learnable brain graph structure. (B) Optionally, the node features can undergo preprocessing via a neural network. (C) Next, the node features are passed to a block of graph convolutional layers, where node embeddings are learned. (D) Then, a node pooling module can be utilised to coarsen the graph. Node pooling may contain learnable parameters as well. (E) Finally, the node embeddings form a graph embedding, which can be used to predict the outcome.

GNNs have been successfully applied in a wide range of fields, such as biology [167], bioinformatics [304], network neuroscience [26], chemistry [280, 216], drug design and discovery [287, 243], natural language processing [184, 283], recommendation systems [95, 284], traffic prediction [134, 182] and finance [274].

In graph classification problems, the input is a set of graphs, each with its own set of nodes, edges, and node features. Let $G = (V, E, H)$ denote a featured graph, where V represents the set of nodes, E represents the set of edges connecting the nodes, and H represents the $V \times D$ matrix of D-dimensional node features. In the case of EEG, the EEG channels are the nodes, and edges represent structural or functional connectivity between pairs of nodes. Each graph G is associated with a label y, indicating its class. The goal is to learn a function $f(G) \rightarrow y$ that can predict the class label y given an input graph G. A general structure of a GNN model for EEG classification is presented in Figure 2.1.

Multiple types of GNNs have been well introduced in [285, 312]. In this survey, we briefly introduce the two main branches of GNNs, namely, spatial and spectral GNNs (Figure 2.2). Other types of GNNs, such as attention GNNs GAT [264], recurrent GNNs [228], and graph transformers [230], can be viewed as special cases of spatial GNNs, and thus we will not provide detailed discussion in this survey. Both spatial-

and spectral GNNs aim to extend the convolution mechanism to graph data. For a detailed review of their similarities and differences, see [55].

Spatial GNNs aggregate information from neighbouring nodes, similar to traditional convolution applied to image data aggregating information from adjacent pixels. Stacking multiple spatial GNN layers leads to information aggregation from various scales going from local to global patterns being captured in early and later layers, respectively. In contrast, spectral GNNs perform information aggregation in the graph frequency domain, with low-frequency and high-frequency components capturing global and local patterns, respectively. However, both approaches learn to capture local and global patterns within the graph, i.e. high and low-frequency information in the spectral domain. The advantage of spectral GNNs is their connection to graph signal processing, allowing for interpretation from the perspective of graph filters. However, spectral GNNs do not generalise well to large graphs since they depend on the eigendecomposition of graph Laplacian. In contrast, spatial GNNs can be applied to large graphs since they perform only local message-passing. On the other hand, spatial GNNs may be challenging to interpret and prone to overfitting because of over-smoothing, where embeddings of all nodes become similar.

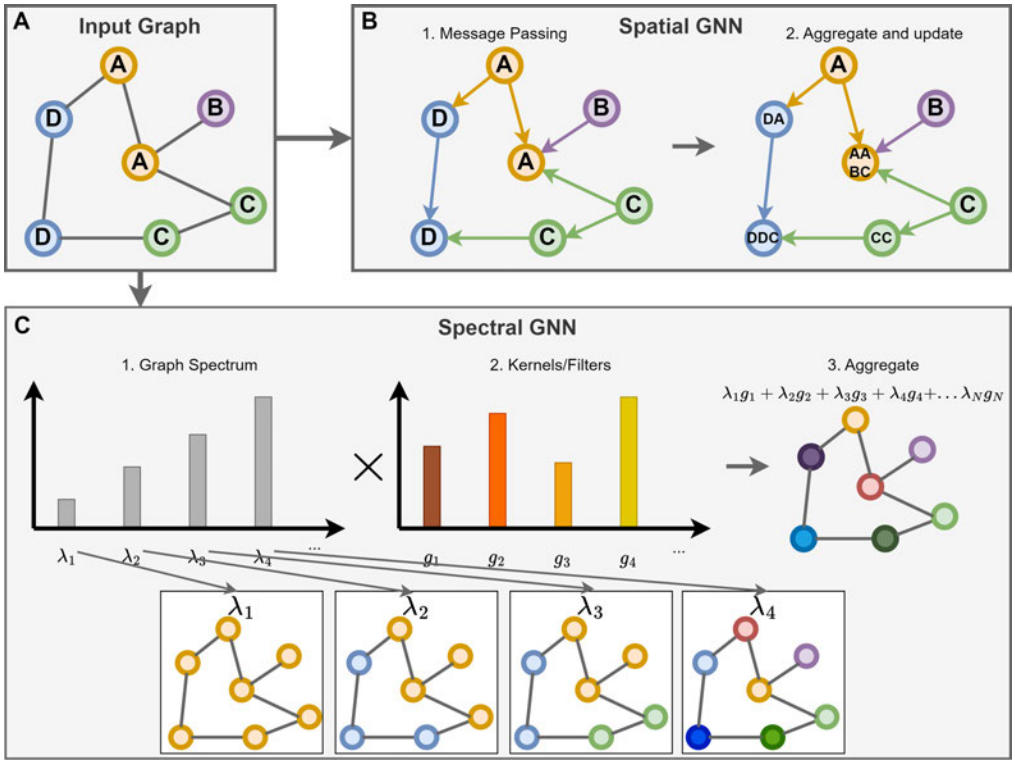

Figure 2.2: Illustration of core mechanisms of spatial and spectral GNNs. A) An undirected featured graph is given as an example input graph with node features. B) Spatial GNNs operate in the graph domain using message passing to update node embeddings. 1) Messages, i.e. transformed node features, are sent along edges. For simplicity, only one direction of the flow of messages is shown. 2) The collected messages at each node are aggregated using a permutation-invariant function and are fused with the original node embedding to form an updated node embedding. Thus, one spatial GNN layer results in node embeddings containing information about the 1-hop neighbourhood of a given node. Thus, L layers are required for node embeddings to access the information from the L-hop neighbourhood. C) In contrast, spectral GNNs operate in the graph spectral domain. 1) Node features are treated as signals on top of a graph and are deconstructed into graph frequencies given by the eigendecomposition of the graph Laplacian. Graph frequency can be interpreted as a variation of the signal. 2) The contribution of each graph frequency is weighted by the set of learnable kernels G, i.e. graph filters. 3) Node embeddings are obtained by aggregating the filtered graph frequencies and projecting them back to the spatial graph domain. Thus, full spectral GNNs can access information from N-hop neighbourhoods where N is the number of nodes of a given graph. However, in practice, approximations such as Chebyshev graph convolution (ChebConv) restrict this to the chosen hop size.

Spatial GNNs

Spatial GNNs directly operate on the graph structure via the adjacency matrix operator. Given a set of nodes and associated features, spatial GNNs perform neighbourhood aggregation to derive node embeddings. This process is referred to as message passing. Intuitively, nodes connected by edges should have similar node embeddings, i.e. local node similarity. Message passing implements this idea by updating node embeddings with aggregated information collected from the node's neighbourhood. Formally, the node update equation in l^{th} layer of spatial GNN with L layers is defined as follows:

$$h_i^{(l+1)} = \sigma\left(W_1^{(l)} h_i^{(l)} + \sum_{j \in \mathcal{N}(v_i)} W_2^{(l)} h_j^{(l)} e_{ji}\right), \tag{2.5}$$

where h_i is the node embedding vector, or when $l = 1$, this is the input node feature vector. σ is the activation function, $\sum$ is the aggregation function, $\mathcal{N}(v_i)$ is the neighbourhood of node v_i, $W \in \mathbb{R}^{d_1 \times d_2}$ is a learnable parameter matrix projecting node embeddings from input dimension d_1 to hidden dimension d_2 and e_{ji} is the edge weight ($e_{ji} = 1$ for unweighted graphs).

A single spatial GNN layer aggregates information from the 1-hop neighbourhood. Thus, to increase the reception field of the model, L spatial GNN layers can be stacked to aggregate information from up to L-hop neighbourhoods. A disadvantage of spatial GNNs is the difficulty of training deep models with many layers. With an increasing number of layers, the node embeddings become increasingly smooth, i.e. variance among embeddings of all nodes decreases. This happens when the messages already contain aggregated information from the whole graph; continual passing of such saturated messages leads to oversmoothing, i.e., all node embeddings becoming essentially identical.

Spectral GNNs

Spectral GNNs can also be applied to EEG classification tasks by leveraging the spectral domain analysis of graph structured data. The EEG graph is transformed into the spectral domain using the Graph Fourier Transform (GFT) and Graph Signal Processing (GSP) techniques. For a detailed review of spectral GNN methods, please refer to [30].

The graph spectrum is defined as the eigendecomposition of the graph Laplacian matrix. The GFT is then defined as $\hat{\mathbf{H}} = \mathbf{U}^T\mathbf{H}$, its inverse as $\mathbf{H} = \mathbf{U}\hat{\mathbf{H}}$, where $\mathbf{U}$

is the orthonormal matrix of eigenvectors of the graph Laplacian $\mathbf{L}$ and $\mathbf{H} \in \mathbf{R}^{N \times D}$ is the matrix of node feature vectors with N and D being the number of nodes and dimensionality of node features, respectively. The graph Laplacian is defined as $\mathbf{L} = \mathbf{D} - \mathbf{A}$, but often the normalized version is preferred: $\hat{\mathbf{L}} = \mathbf{I} - \mathbf{D}^{-1/2}\mathbf{A}\mathbf{D}^{-1/2}$ ($\mathbf{A}$ and $\mathbf{D}$ are the adjacency and degree matrices, respectively).

Spectral-GNN is then typically defined as the convolution ($*$) of a signal defined on graph $\mathbf{H}$ and a spatial kernel g in the spectral domain, thus becoming an element-wise multiplication ($\odot$):

$$\mathbf{H} * g = \mathbf{U}\left(\left(\mathbf{U}^T\mathbf{H}\right) \odot \left(\mathbf{U}^T g\right)\right). \tag{2.6}$$

Generally, $\mathbf{U}^T g$ is defined as a learnable diagonal matrix $\mathbf{G} = diag(g_1, ..., g_V)$ spectral filter [30].

However, the full spectral graph convolution can be computationally expensive. A popular approximation is the ChebConv [75], which performs localised spectral filtering on the graph. The node embedding update equation of a ChebConv is defined as:

$$H * g \approx \sum_{i=1}^{K} \mathbf{\Theta}_i T_i(\hat{\mathbf{L}}'), \tag{2.7}$$

where $\mathbf{\Theta} \in \mathbb{R}^{K \times d \times d}$ are learnable parameters, $T_i(\hat{\mathbf{L}}') = 2T_{i-1}(\hat{\mathbf{L}}') - T_{i-2}(\hat{\mathbf{L}}')$, $T_1(\hat{\mathbf{L}}') = \mathbf{H}$, $T_2(\hat{\mathbf{L}}') = \hat{\mathbf{L}}'\mathbf{H}$, and $\hat{\mathbf{L}}' = \frac{2\hat{\mathbf{L}}}{\lambda_{max}} - \mathbf{I}$ (λ_{max} is the largest eigenvalue of $\hat{\mathbf{L}}$, often approximated as $\lambda_{max} = 2$). The K parameter controls the size of the Chebyshev filter.

However, spectral-GNNs are limited to input graphs with a fixed number of nodes. This is because of the explicit use of the graph Laplacian. This is in contrast to spatial-GNNs, which do not rely on explicitly materialising the adjacency matrix.

2.4.2 Survey Results

This survey is based on a review of 63 articles. These articles were selected by title and abstract screening from a search on Google Scholar and ScienceDirect queried on November 1st, 2022. The search query for collecting the articles was defined as: ("Graph neural network" OR "Graph convolutional network") AND ("Electroencephalography" OR "EEG"). Both peer-reviewed articles and preprints were searched and utilised. All types of EEG classification tasks were included. We summarise the various types of EEG classification tasks identified in the surveyed papers in Fig 2.3. The most common classification tasks are emotion recognition, epilepsy diagnosis and

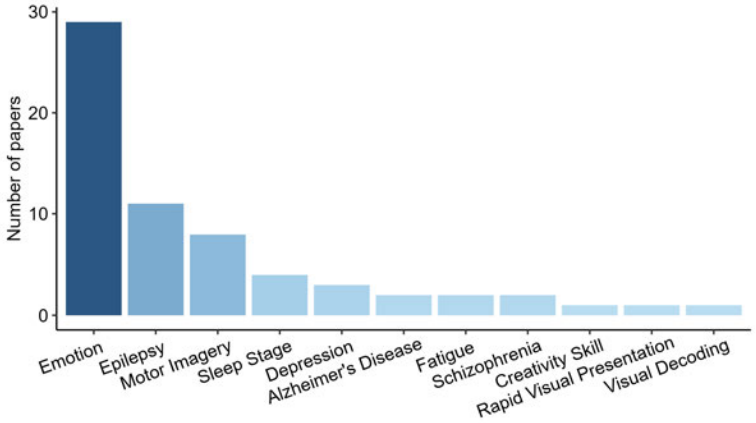

Figure 2.3: Classification tasks presented in the current EEG-GNN literature.

detection and motor imagery. However, the type of classification task should have a relatively minor effect on the GNN architecture design. Thus, we do not analyse and discuss this in detail. Instead, we survey the various GNN-based methods for EEG classification, intending to systematically categorise the types of GNN modules and identify emerging trends in this field independent of the specific classification task.

In the remaining portion of this section, we report the categories of comparisons we identified in the surveyed papers. These are based on the different modules of GNN-based models. Specifically, these are:

- Definition of brain graph structure
- Type of node features
- Type of graph convolutional layer
- Node feature preprocessing
- Node pooling mechanisms
- Formation of graph embedding from the set of node embeddings

2.4.3 Definition of Brain Graph Structure

The first part of the input to a GNN model is the brain graph structure inferred from the EEG data itself (Figure 2.1A). We summarise the methods for defining the

brain graphs in Table 2.2. These methods can be generally categorised as learnable or pre-defined.

An alternative categorisation of the brain graph structures is the functional and the "structural" connectivity. Generally, SC graphs are pre-defined, whereas FC graphs can be both pre-defined and learnable. SC in the classical sense of physical connections between brain regions is not possible to obtain using EEG signals since these are recorded at the scalp surface. Instead, we use the term to describe methods that construct brain graphs based on the physical distance between EEG electrodes. In contrast, FC refers to pairwise statistical relationships between EEG signals.

SC graph is pre-defined such that electrodes are connected by an edge in the following way:

$$e_{ij} = \begin{cases} 1 \text{ or } 1/d_{ij}, & \text{if } d_{ij} \leq t \\ 0, & \text{otherwise} \end{cases}, \tag{2.8}$$

where e_{ij} is the edge weight connecting nodes i and j, d_{ij} is a measure of distance between EEG electrodes, and t is a manually defined threshold controlling the graph sparsity.

Such an approach offers several advantages. First, the SC graph is insensitive to any noise effects of EEG recording since it is independent of the actual signals. Second, all data samples share an identical graph structure, provided the same EEG montage was utilised during the recording. This offers explainability advantages when combined with spectral GNN since the graph frequency components defined by the eigenvectors of graph Laplacian are fixed. On the other hand, the SC graph is limited to short-range relationships. Thus, it might not accurately represent the underlying brain network. Some papers propose to overcome this limitation by manually inserting global [83, 80, 308, 300, 54] or inter-hemispheric edges [311, 161, 289].

In contrast, an FC graph can be obtained from either classical FC measures (FC measure in Table 2.2 or learnable methods (e.g. feature concatenation/distance and attention methods in Table 2.2). We refer to all of these methods as FC because they all measure the degree of interaction between two nodes, thus falling within the traditional definition of FC. Unlike SC, the FC graph is unique for each data sample and can contain both short- and long-range edges. On the other hand, since it is derived directly from EEG signals, it might be noise-sensitive.

Learnable FC based on node feature distance or feature concatenation are generally

Table 2.2: Overview of methods for obtaining the brain graph structure.

Method	Learnable	Pre-defined	Papers
Distance between electrode positions	✗	✓	[311, 177, 77, 214, 249, 291, 242, 83, 289, 124, 80, 308, 300, 130, 210, 131, 54, 164, 133]
Functional connectivity measure	✗	✓	[178, 177, 155, 48, 28, 214, 8, 305, 249, 53, 166, 99, 138, 272, 112, 113, 124, 149, 130, 250, 270, 173, 16, 86, 108, 131, 246, 142, 229]
Manually defined	✗	✓	[311, 161, 83, 289, 308, 300, 54]
Shared learnable mask	✓	✗	[311, 160, 8, 166, 244, 303, 174, 290, 16, 164]
Feature similarity	✓	✗	[162, 161, 166, 80, 290, 164, 181]
Feature distance	✓	✗	[132, 281, 301, 133]
Transformer-style attention	✓	✗	[313, 170]
Concatenation attention	✓	✗	[168, 173]
Dense projection	✓	✗	[234, 235, 176]
LSTM-based	✓	✗	[81]
Multiple/Combined graph definitions	-	-	[250, 177, 48, 161, 214, 8, 166, 235, 83, 289, 308, 290, 300, 130, 250, 173, 16, 131, 54, 164, 133]

computed as:

$$e_{ij} = \theta_1(|h_i - h_j|) \text{ and} \tag{2.9}$$

$$e_{ij} = \theta_2(h_i \parallel h_j), \tag{2.10}$$

respectively, where $\theta_1(\cdot)$ and $\theta_2(\cdot)$ are neural networks with input-output dimensions of $\mathbb{R} : d \rightarrow 1$ and $\mathbb{R} : 2 \times d \rightarrow 1$, respectively; $|\cdot|$ denotes absolute value; $\parallel$ denotes concatenation and h_i is the node feature/embedding of node i. We discuss the attention-based graphs and the types of graph convolutional layers in Section 2.4.5 and thus skip these methods in this section.

Special cases of brain graph definition are the shared-mask methods. These methods defined a matrix of learnable parameters with the same shape as the adjacency matrix of the input graphs that acts as a mask/filter by multiplying it with the adjacency matrix. This learnable matrix is a part of the model. Thus, the same mask is applied

Table 2.3: Overview of methods in defining the input node features

Method	Time-domain	Frequency-domain	Graph-domain	Papers
Differential entropy	✓	✗	✗	[311, 162, 162, 161, 291, 53, 166, 132, 281, 234, 235, 83, 244, 272, 301, 303, 124, 149, 308, 290, 173, 313, 16, 170]
Raw signal	✓	✗	✗	[77, 155, 48, 171, 8, 307, 242, 166, 168, 112, 113, 174, 80, 210, 250, 270, 81, 86, 108, 54, 164, 181, 133, 229]
Fourier Transform	✗	✓	✗	[160, 249, 61]
Power Spectral Density/Band Power	✗	✓	✗	[214, 303, 124, 149, 308, 300, 130, 131, 246, 142]
Graph theory metrics	✗	✗	✓	[178, 99]
Descriptive statistics	✓	✗	✗	[177, 300, 131]

to all input graphs. However, a shared mask limits the size of the input graphs, i.e. the number of nodes must remain fixed so that the adjacency matrix can be multiplied with the shared mask.

In the current stage, the preferred method for brain graph classification tasks remains unclear. Some authors attempt to avoid this issue by combining multiple methods. However, we instead suggest that the researchers carefully consider each of the presented methods in the context of the given classification task, as each method poses its unique set of strengths and weaknesses.

2.4.4 Node Feature Definitions

The second part of the input to a GNN model is the node feature matrix (Figure 2.1A). We summarise the various definitions of node features in Table 2.3. We categorise these definitions based on which domain they are computed, i.e. time, frequency and graph domains.

The time-domain methods are the most commonly used in the current literature. In particular, these are the differential entropy (DE) and raw signal methods. The

Table 2.4: Overview of node feature pre-processing before GNN layers.

Method	Trained separately	Papers
1D-CNN		[77, 162, 307, 168, 83, 210, 81, 181]
Feature-wise attention weighting	✗	[99]
bidirectional-LSTM	✓	[112]
Temporal-CNN	✗	[174, 80, 181]
WaveletCNN	✗	[174]
SincCNN	✗	[210]
MLP	✗	[246]
CNN-Feature-Extractor	✓	[133]

popularity of DE is given by the fact that many of the open EEG datasets include this feature, such as the SEED [309] emotion recognition dataset. DE describes the complexity of a continuous variable and is defined as:

$$DE(X) = -\int_X f(x) log(f(x)) dx \tag{2.11}$$

where X is a random continuous variable and $f(x)$ is the probability density function.

Many papers define the node feature as the raw EEG signal. However, the raw signal can be too long for a GNN to process effectively. Thus, it is often coupled with node feature preprocessing module and spatio-temporal GNNs (See 2.4.4 and 2.4.5 respectively) to either reduce the dimensionality or to extract the temporal patterns contained within the signal effectively. An alternative to the raw signal node feature is descriptive statistics, such as mean, median or standard deviation.

Frequency-domain node features are usually defined as the Fourier frequency components obtained by the Fourier transform or the power spectral density. These methods attempt to quantify the strength of various frequency components within the EEG signal. An advantage of these representations is their relatively low dimensionality compared to the raw signal described previously.

Finally, graph-theoretical features can be utilised to describe the nodes, e.g. mean node weight [178] and betweenness centrality [99, 178]. A severe limitation of this method is that the graph structure needs to be defined prior to node feature extraction. Thus, this node feature type is incompatible with learnable brain graph methods.

Node Feature Preprocessing

An optional next step after node features construction is some kind of node feature pre-processing module (NFP) (Figure 2.1B). We summarise the NFPs types in Table 2.4.

Most of the NFPs are integrated within the GNN architecture, thus allowing the model to be trained in an end-to-end manner. The exceptions are methods that utilise a pre-trained feature extraction neural network implemented as a bidirectional long-short-term-memory (LSTM) [112] or a CNN [133].

The surveyed NFPs are all based on a neural network. In most cases, these are variants of a CNN and MLP. These modules aim to (1) reduce the dimensionality of the node features and (2) enhance the node features, including potentially suppressing noise or redundant information.

2.4.5 Type of Graph Convolutional Layer

A core part of a GNN model are the GCN layers (Figure 2.1C). We summarise the utilised types of GCNs in Table 2.5. We further categorise them based on the type of GNN as introduced in Section 2.4.1, i.e. spatial, spectral. Additionally, we add the temporal category, which is not a type of standalone GCN layer but must be combined with spatial or spectral GCN.

Interestingly, ChebConv is used in the majority of the surveyed papers (counting both ChebConv and spectral spatio-temporal GNN in Table 2.5). Since EEG typically uses 128 electrodes in high-density montages, the size of the brain graphs is relatively small. In such cases, even a full spectral GNN would not be too computationally expensive for EEG classification. Therefore, why many authors opt for the ChebConv approximation of spectral GNN remains unclear. We speculate that the influence of classical signal processing tools in EEG analysis might also serve as a sufficient argument for using spectral GNNs for EEG classification.

On the other hand, the other half of the surveyed papers experiment with a wide range of spatial GNNs. The (simplified) GCN is a popular method amongst these, which is equivalent to a 1st-order ChebConv ($K = 1$). A special case of spatial GNN is the graph attention network (GAT). GAT allows adjusting the graph by re-weighting the edges using an attention mechanism. Generally, the attention mechanism for com-

Table 2.5: Overview of graph convolutional layers.

Method	Spatial	Spectral	Temporal	Papers
Graph Isomorphism Network	✓	✗	✗	[178, 77, 250]
(Simplified) Graph Convolution Network	✓	✗	✗	[311, 305, 307, 166, 83, 244, 272, 289, 80, 300, 86, 131, 142]
Chebyshev Graph Convolution	✗	✓	✗	[155, 48, 214, 8, 291, 53, 138, 301, 112, 303, 113, 124, 149, 308, 130, 270, 81, 16, 170, 246]
Graph Attention Network	✓	✗	✗	[160, 99, 168, 210, 313, 108, 54, 181]
Diffusion recurrent gated	✗	✓	✗	[249]
Spatio-temporal GNN (Spectral)	✗	✓	✓	[242, 61, 173, 229, 132, 281]
Spatio-temporal GNN (Spatial)	✓	✗	✓	[171, 164]
Powers of Adjacency Matrix GNN	✓	✗	✗	[234, 235]
GraphSAGE	✓	✗	✗	[77, 61]
Spectral GNN	✗	✓	✗	[162, 161]
B-Spline Kernel GCN	✓	✗	✗	[177]
Residual GCN	✓	✗	✗	[174]
Multibranch architectures	-	-	-	[168, 301, 290, 300, 270, 164]

puting the new softmax-normalised edge weight e_{ij} is defined as follows:

$$e_{i,j} = \frac{\exp\left(\sigma\left(\mathbf{w}^\top [\mathbf{W}h_i \,\|\, \mathbf{W}h_j]\right)\right)}{\sum_{k\in\mathcal{N}(i)} \exp\left(\sigma\left(\mathbf{w}^\top [\mathbf{W}h_i \,\|\, \mathbf{W}h_k]\right)\right)}, \tag{2.12}$$

where w and W are the learnable parameters of the model, σ is an activation function, h is the node feature vector/embedding, and $N(i)$ is the set of nodes connected to node i. The resulting edge weights can then be passed to Equation 2.5.

Next, the spatio-temporal GNNs were tested for EEG classification in several instances. A spatio-temporal block consists of one GCN layer and one 1D-CNN applied temporally. This structure allows the model to extract both spatial (i.e. graph) and

Table 2.6: Overview of node pooling mechanisms.

Method	Learnable	Papers
TopK	✓	[48, 54]
Hierarchical tree pooling	✓	[178]
SortPool	✓	[77]
EdgePool	✓	[77]
SAGPool	✓	[77, 289]
Set2Set	✓	[77]
Manual Clustering	✗	[234, 235]
Graclus Clustering	✗	[113, 270]

temporal patterns. There are both spatial and spectral variants of spatio-temporal GNN, and there is no indication as to which one should be preferred as no comparative study exists to date.

Finally, several papers adopt multi-branch architectures. These methods utilise multiple GCN layers applied in parallel to allow the model to focus on various aspects (also views) of the input graph. An example of such a model utilises two-branch GNN to learn from both FC- and SC-based brain graph structure [164]. Alternatively, the individual frequency bands of EEG signals can be used to construct various graph views [246].

2.4.6 Node Pooling Mechanisms

In some instances, reducing the number of nodes in the graph might be desirable. This can be achieved with a node pooling module (Figure 2.1D). We summarise the node pooling modules utilised in the surveyed papers in Table 2.6.

There are both learnable and non-learnable node pooling modules in the literature. Please see the corresponding papers for a detailed description of these methods (Table 2.6). Node pooling modules remain a relatively unexplored topic in the EEG-GNN classification models. Node pooling can (1) remove redundant nodes, (2) reduce the size of the graph embedding in a setting where the concatenation of node embeddings forms it, and (3) aid in the explainability of the model by identifying node importance with respect to the classification task.

Table 2.7: Overview of methods for the formation of graph embedding from a set of node embeddings

Method	Learnable	Papers
Sum readout	✗	[178, 311, 16]
Average readout	✗	[214, 166, 289, 61, 131, 54, 246]
Maximum readout	✗	[307, 289, 112, 54, 142]
Concatenate node embeddings	✗	[177, 162, 155, 48, 161, 305, 234, 235, 138, 168, 303, 113, 124, 174, 80, 308, 290, 300, 130, 210, 270, 173, 313, 81, 133, 229]
CNN-like Average/Maximum Pooling	✗	[171, 86]
SortPool	✓	[28]
Attention weighted	✓	[160, 301, 164]
CNN	✓	[8, 242, 149]
LSTM	✓	[291, 170]
Capsule Network	✓	[99]
Transformer	✓	[244]
Bidirectional LSTM	✓	[168, 86, 108]

2.4.7 From Node Embeddings to Graph Embedding

The output of the graph convolutions is a set of learned node embeddings. Node embeddings in this form are suitable for tasks such as node classification and link prediction. However, for graph classification, the set of node features needs to be transformed into a unified graph representation (Figure 2.1E). We summarise the methods for this transformation in Table 2.7.

The most straightforward method to form a graph embedding is to simply concatenate the node features. This approach poses a few limitations. First, the resulting graph embedding grows with the number of nodes. Thus, the classification layer requires a large number of parameters. Second, all input graphs must have the same number of nodes, limiting the model's generalisation to other datasets. Finally, such an approach is likely to include redundant or duplicated information in the graph embedding since GNN produces node embeddings by aggregating information from neighbouring nodes.

A readout function is one of the methods to form a graph embedding that addresses these issues. A readout forms the embedding by passing the node features through a permutation-invariant function. A general definition of a readout to obtain graph

embedding of a graph G_i from a set of V node embeddings $H = [h_1, ..., h_V]$ is given by:

$$G_i = \sum_{k=1}^{V} h_k, \tag{2.13}$$

where $\sum$ can be any permutation-invariant function. In the surveyed papers, these functions were sum, average and maximum. A few papers also experiment with attention-weighted sum to attenuate the role of unimportant nodes within the graph embedding [160]. An interesting alternative is to apply CNN-style average or maximum pooling node-wise [171].

Alternatively, researchers explored various neural network models to obtain graph embeddings, such as CNN [8, 242, 149], (bi-)LSTM [291, 170, 168, 86, 108], Transformer [244] and capsule networks [99]. Additionally, graph pooling methods, such as DiffPool [293], SAGPool [159], iPool [97], TAP [96] and HierCorrPool [279] can be used for this purpose.

2.4.8 Discussion of EEG-GNN Approaches

Despite most of the surveyed papers being relatively recent, a wide range of GNN-based methods have already been proposed to classify EEG signals in a diverse set of tasks, such as emotion recognition, brain-computer interfaces, and psychological and neurodegenerative disorders and diseases (Fig 2.3). This recent rise in popularity of GNN models for EEG might be attributed to (1) the development of new GNN methods and (2) advances in network neuroscience inspired an extension of this framework to deep learning. GNNs offer unique advantages over other deep learning methods. This is mainly the possibility of modelling multivariate time series and interactions among them with a single GNN model, which is not possible with CNN or recurrent networks. Additionally, patterns learned by GNNs can readily be interpreted in the context of network neuroscience, thus enabling a wide range of avenues for model explainability.

This survey categorises the proposed GNN models in terms of their inputs and modules. Specifically, these are brain graph structure, node features and their preprocessing, GCN layers, node pooling mechanisms, and the formation of graph embeddings. This categorisation allows us to provide a quick and simple overview of the different methods presented in the EEG-GNN literature, appreciate the current state of the art in this field and identify promising future directions.

Limitations of Surveyed Papers

Surprisingly, we have identified the least variety and innovation in the category of GCN-layers (Table 2.5). A significant proportion of the surveyed papers utilise either ChebConv or "vanilla" spatial GCN. This might be due to the relative novelty of the EEG-GNN field, and thus, many papers explore other areas of model design, such as node features and brain graph definitions. A few papers seem to successfully experiment with more complex types of GCN-layers [177, 174, 249] and multi-branch architectures [168, 301, 290, 300, 270, 164].

A major limitation of most surveyed papers is the lack of generalisability to external datasets that might use a different number of EEG signals. This is caused by (1) the use of ChebConv and (2) forming graph embedding by node feature concatenation [177, 162, 155, 48, 161, 305, 234, 235, 138, 168, 303, 113, 124, 174, 80, 308, 290, 300, 130, 210, 270, 173, 313, 81, 133, 229]. (1) can be addressed by utilising spatial GCN layers as suggested above, and (2) can be solved by using a readout function or a suitable node pooling mechanism, which coarsens the graph to a fixed number of nodes. Additionally, there is a general lack of transfer learning experiments for EEG-GNN models, which might be a promising direction for future research.

Finally, we have identified an interesting gap in EEG-GNN research: the lack of utilising frequency band information in a more complex way. A few papers train separate models for each frequency band in isolation [178, 311, 177]. Alternatively, they propose concatenating the graph embeddings generated from the frequency-band-GNN branches [161, 234, 242].

Future Directions

Several promising directions can be identified in the rapidly evolving landscape of EEG-GNN research. First, a comprehensive comparison of the various GCN layers (e.g. spatial GNN, ChebConv, GAT and graph transformer) with respect to their influence on classification performance should be carried out to address this crucial design question systematically.

Second, enhancing the generalisability of models by addressing issues related to the varying number of EEG signals/electrodes and exploring transfer learning approaches can open new avenues for research. For instance, pre-trained GNN models on cheap-to-obtain large datasets, such as open databases for emotion recognition or brain-computer interface (BCI) applications, would allow the application of complex GNN architectures

to problems with limited data availability due to the high costs or small populations (e.g. clinical data, rare diseases and disorders). Focusing on these issues would likely improve the generalisability of the models when evaluated on a diverse set of EEG datasets and different classification tasks.

Lastly, the rich frequency information of EEG signals should be explored more. For instance, we suggest a plausible utility of integrating CFC approaches into EEG-GNN models. There is growing evidence in the literature concerning the advanced brain functions (e.g. learning, memory) enabled by CFC [135]. Thus, integrating findings from neuroscience research into the EEG-GNN design promises both performance and explainability gains.

2.5 Chapter Summary

This chapter reviews disruptions of brain activity in AD cases and discusses the methodology for graph-based analysis of EEG. These reviews highlight the need for graph-based approaches to characterise and accurately distinguish AD using EEG multivariate signals. Furthermore, this thesis examines findings on AD from oscillatory and graph perspectives to relate to the explainability capabilities of the research presented in this thesis.

Graph-based methods for EEG analysis are reviewed. First, we focus on brain graph inference, graph preprocessing, and standard graph-theoretical measures to characterise various properties of the brain, such as region importance, information integration, and segregation. Then, the AD disruptions related to FC and graph approach are summarised. The main research gap identified is the need for closer examination of CFC from a graph perspective.

Finally, GNN architectures for EEG classification are reviewed. The surveyed papers were categorised based on model inputs and modules, including brain graph structure inference, definitions of node features, types of GCN layers, node pooling mechanisms, and generation of graph embeddings. Several limitations and areas for improvement were identified. There is a lack of variety and innovation in GCN layers, with many papers utilising ChebConv or "simple" spatial GCN without clear justification. Integration of CFC information and evaluation of methods for brain graph inference are identified as gaps in the literature to enhance the performance and explainability of GNNs.

Chapter 3

Data

This chapter introduces the EEG dataset used in Chapters 4, 5 and 6.

EEG recordings were collected from 20 AD patients and 20 HC participants younger than 70 years. A detailed description of the experimental design and confirmation of the diagnosis is provided in [29]. All the AD participants were recruited from the Sheffield Teaching Hospital memory clinic. AD participants were diagnosed between one month and two years before data collection. All of them were in the mild to moderate stage of the disease at the time of recording, with an average MMSE score of 20.1 (sd = 4). High-resolution structural MRI scans of all AD patients were acquired to eliminate alternative causes of dementia.

Age and gender-matched HC participants with normal neuropsychological tests and structural MRI scans were recruited. This study was approved by the Yorkshire and The Humber (Leeds West) Research Ethics Committee (reference number 14/YH/1070). All participants gave their informed written consent.

All patients underwent examination via high-resolution structural MRI scans to eliminate major underlying causes that could explain their clinical symptoms. None exhibited significant small vessel ischemic disease, as evidenced by FLAIR MRI scans.

Each participant provided consent for a 3 Tesla MRI scanning procedure using a Philips Ingenia scanner, encompassing structural and resting-state functional scans. Additional scans, including diffusion, T2-weighted, and FLAIR acquisitions, confirmed the absence of exclusion criteria. MRI assessments were conducted on average 79 days prior to their inclusion in the study. The purpose of the structural and functional neuroimaging was solely to characterize brain structure and function in these patients, ensuring they were representative of the clinical population under investigation.

Anatomical T1-weighted images were acquired with the following parameters: voxel-

size of 0.94 × 0.94 × 1.00 mm, field of view of 256 mm, matrix size of 256 × 256 × 124, repetition time of 8.2 s, echo delay time of 3.8 ms, and flip angle of 8°. Following a series of dummy scans to achieve electromagnetic equilibrium, a T2*-weighted scan was conducted to assess cerebral hemodynamics at rest. This scan comprised 120 volumes, each containing 35 axial slices acquired in ascending order. Participants were instructed to keep their eyes closed throughout the scan. The scan parameters were set as follows: repetition time of 2.6 s, total acquisition time of 4 minutes and 30 seconds, echo delay time of 35 ms, flip angle of 90°, voxel dimensions of 2.4 × 2.4 × 4.0 mm, and field of view of 230 × 230 × 140 mm.

The cognitive function of AD patients and HC was evaluated using a comprehensive battery of neuropsychological tests designed to detect cognitive impairments typically associated with AD. These tests covered areas such as short and long-term memory (verbal and non-verbal), abstract reasoning, attention and executive function, language comprehension, and fluency in naming, category, and letter retrieval.

EEG data were acquired using an XLTEK 128-channel headbox, Ag/AgCL electrodes with a sampling frequency of 2 kHz using a modified 10-10 overlapping a 10-20 international electrode placement system with a referential montage with a linked ear-lobe reference. The recordings lasted 30 minutes, during which the participants were instructed to rest and not think about anything specific. In case the participants showed signs of drowsiness, they were prompted. Within each recording were five-minute-long epochs during which the participants had their eyes closed, alternating with an equal duration of eyes-open epochs.

All the recordings were reviewed by an experienced neurophysiologist on the XLTEK review station with time-locked video recordings (Optima Medical LTD). For each participant, three 12-second-long artefact-free epochs were isolated. Finally, the following 23 bipolar channels were created: F8–F4, F7–F3, F4–C4, F3–C3, F4–FZ, FZ–CZ, F3–FZ, T4–C4, T3–C3, C4–CZ, C3–CZ, CZ–PZ, C4–P4, C3–P3, T4–T6, T3–T5, P4–PZ, P3–PZ, T6–O2, T5–O1, P4–O2, P3–O1 and O1–O2 [29]. Bipolar montage was selected to limit the volume conduction effects to a certain extent.

As a neurophysiologist confirmed the EEG signal to be artefact-free, we did not further clean the signals. The signals are filtered using a band-pass Butterworth filter to a range of 0.5 Hz and 45 Hz.

The utilisation of a relatively small EEG dataset in the experiments described in this thesis was driven by the absence of larger, open-access data of EEG for AD at the time of performing the experiments. While this dataset undoubtedly posed limitations

in terms of its scope and generalisability, it nonetheless provided a valuable foundation for initial exploration and analysis.

However, since then, an open-access dataset for EEG in AD has been released [191]. This presents an exciting opportunity to enhance the robustness of future research by incorporating such a dataset for external independent validation. By leveraging a more extensive and diverse dataset, researchers can strengthen the reliability and generalisability of their findings.

Chapter 4

Cross-Frequency Multilayer Graph Analysis with Bispectrum-based Functional Connectivity

4.1 Introduction

[1]The main EEG characteristics associated with AD are the slowing of signals, and altered synchronisation [128, 98, 150, 68, 267, 13]. However, these characteristics are typically measured at a single channel or between channel pairs. In contrast, the graph-based analysis considers all EEG channels and reveals AD characteristics such as reduced integration of information [136, 63], and loss of small-worldness [247]. However, these characteristics are often analysed only within specific frequency bands.

This chapter aims to extend the FC beyond WFC, taking the CFC [135] into account. WFC graphs of AD were analysed previously by using coherence (linear) [4] and wavelet coherence (nonlinear) [127]. Only one CFC measure, i.e. phase synchronisation index (PSI), had been used for the graph analysis of CFC graphs in AD [42]. This work extended the findings of reduced integration and loss of small-worldness to CFC multilayer graphs. However, it does not consider the roles of different frequency components in the graphs. The multilayer-graph framework had been used previously for brain graph analysis. Loss of inter-frequency hubs in AD was reported using MEG

[1]The content presented in this chapter has been published in *Dominik Klepl, Fei He, Min Wu, Daniel J. Blackburn, and Ptolemaios G. Sarrigiannis. Cross-Frequency Multilayer Network Analysis with Bispectrum-based Functional Connectivity: A Study of Alzheimer's Disease.* Neuroscience, *521: 77–88, June 2023. ISSN 0306-4522. doi: 10.1016/j.neuroscience.2023.04.008*

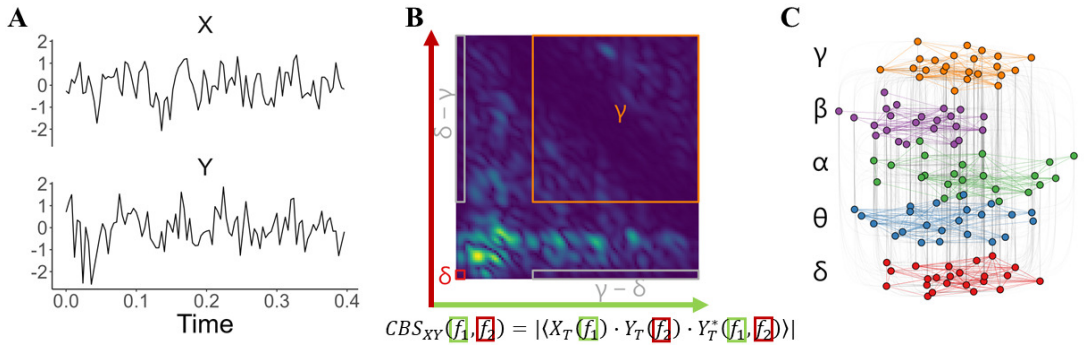

Figure 4.1: A conceptual schematic of implementing the proposed CBS multilayer graph analysis. (A) Each EEG signal is cleaned and scaled. (B) For each pair of EEG electrodes, a cross-bispectrum is estimated. The frequency bands coupling edge weights are given by the average value within the respective CBS window, e.g. δ-δ (red). Note that CBS estimates are directed, e.g. δ-$\gamma \neq \gamma$-δ (both in grey). Thus, from each CBS, 25 edges are inferred. (C) Using the edge weights inferred from CBS, a multilayer graph is constructed with layers representing the frequency bands of EEG. Such a graph has both intra-layer and inter-layer edges, representing within-frequency and cross-frequency coupling, respectively.

multiplex graphs[103, 298], where the inter-layer edges are inserted with fixed weight only between the same nodes across layers. Alterations in multilayer graph hubs have been reported in multimodal graphs in AD [104], and fMRI frequency-band graphs in schizophrenia [70]. Multilayer graphs integrating WFC and CFC have been used to analyse MEG data from healthy [254], and schizophrenic subjects [38]. Tewarie et al. [254] show that frequency-band graph layers interact via CFC, share a certain amount of structure and operate at the edge of independence and interdependence. However, these studies analyse the layer relationships mainly as the correlation of their adjacency matrices or as differences in global average coupling strength.

Bispectrum is a higher-order spectral analysis and quantifies quadratic coupling between two frequency components and their algebraic sum [107]. It has been shown to detect amplitude-amplitude and phase-amplitude CFC in addition to the phase-phase coupling [135, 151]. The bispectral coupling also indicates an increase in non-Gaussianity [278]. Features derived from bispectrum were proposed as biomarkers of epilepsy [183, 32], Parkinson's disease [299], autism [206] and AD [278, 275, 187]. Most of these studies compute (cross-) bispectra of only a few channels or pairs of channels. Although a few studies used bispectrum to compute global graphs from multiple channels [51], these analyses do not use graph theory. Instead, each node

is analysed in isolation [275] or single-channel bispectra are averaged across nodes to derive certain global properties [187]. In contrast, this study computes cross-bispectra between all pairs of EEG channels to estimate the widely distributed FC brain graphs and perform graph-theoretical analysis.

In this chapter, the cross-bispectrum estimates of FC are computed. We aim to investigate the contribution of nonlinear WFC and CFC in differentiating between (AD) and HC in comparison to the equivalent linear WFC measured with cross-spectrum (CS) (Figure 4.1). We report a multilayer graph-based analysis to elucidate the roles of the traditional EEG frequency bands and their CFC in the sensor-level EEG graphs of HC and AD. Moreover, we use the reconstructed brain graphs to classify AD using an SVM classifier.

4.2 Methods

4.2.1 EEG pre-processing

EEG signals were confirmed to be artifact-free. Thus, no additional artefact removal was undertaken. The signals were band-pass filtered to be between 0.1 and 100 Hz using a zero-phase 5^{th} order Butterworth filter; 50 Hz relating to the power line noise was removed using a zero-phase 4^{th} order Butterworth stop-band filter, and the data were down-sampled to 250 Hz using an order 8 Chebyshev type I filter. Finally, the signals were normalised (to zero mean and unit standard deviation).

4.2.2 Cross-spectrum and Cross-bispectrum

The spectrum S_X of a signal X is calculated via a smoothed periodogram. Fast Fourier transform (FFT) is used to estimate the periodogram with Daniell smoothers. The periodogram is computed over 256 frequency bins (0.98 Hz bandwidth). CS at frequency f is then computed as: $CS_{XY}(f) = S_X(f) \cdot S_Y(f)$. An absolute value of CS is calculated. A direct FFT-based method is used to estimate the absolute value of CBS:

$$CBS_{XY}(f_1, f_2) = |\langle X_T(f_1) \cdot Y_T(f_2) \cdot Y_T^*(f_1, f_2) \rangle|, \tag{4.1}$$

where $\langle \cdot \rangle$ denotes averaging, $X_T(f)$ is an FFT of signal X over an interval T and Y_T^* is the complex conjugate. 256-point FFT is used. CBS is computed over 1-second long windows with 50% overlap over the whole frequency range (0.5 - 100 Hz). The

window size and overlap were chosen empirically to balance the spectral and temporal resolutions. The estimated CBS is then smoothed in the frequency domain using the Rao-Gabr window (size 5).

CS and CBS were computed for all pairs of EEG channels. Five frequency bands b are considered: δ $(0.5 - 5Hz)$, θ $(5 - 8Hz)$, α $(8 - 16Hz)$, β $(16 - 32Hz)$ and γ $(32 - 100Hz)$.

The connectivity between channels X and Y and frequency bands b_X and b_Y is computed as:

$$FC_{XY}^{CS}(b) = \langle CS_{XY}(f \in b) \rangle, \tag{4.2}$$

$$FC_{XY}^{CBS}(b_X, b_Y) = \langle CBS_{XY}(f_1 \in b_X, f_2 \in b_Y) \rangle, \tag{4.3}$$

for CS and CBS, respectively, where $\langle . \rangle$ denotes averaging. This resulted in five WFC (CS and CBS) and 20 CFC (CBS only) measures per channel pair. It is of note that the CBS is directed.

In order to ensure the reliability of the estimated connectivity, surrogate thresholding was used [255]. For each pair of channels, 200 surrogate signals were generated using the FFT surrogate, which scrambles the phase of the signal, and their CS and CBS are computed. The 95% confidence interval of surrogate values is computed and used as a threshold. Coupling values below the threshold are set to zero. We chose this approach to ensure the reliability of estimated brain graphs. In contrast, Wang et al. [275] used no such thresholding when analysing bicoherence coupling. Alternative approaches exist in the literature. Chella et al. [51] take advantage of the asymmetric property of CBS to ensure robustness against mixing artefacts.

We obtain a set of connectivity matrices for each EEG recording, i.e. $N \times N$ matrices ($N = 23$). For CS and CBS, there are five and 25 connectivity matrices, respectively. A global (averaged per subject) connectivity is computed for each 23×23 matrix and compared between groups using a two-sample t-test if normally distributed and a Mann-Whitney test otherwise.

4.2.3 Graph Measures

To identify the important channels in the graph, we compute a coupling-specific NS [17] for each channel i and different types of frequency couplings c,

$$NS(i, c) = \sum_{j \in \Pi(i,c)} w_{ij}, \tag{4.4}$$

where $\Pi(i, c)$ are the nodes connected to channel i via edge type c and w_{ij} is the edge weight, i.e. CS or CBS connectivity given by ijth entry of the $N \times N$ connectivity matrix. This measure is computed for both CS and CBS, resulting in 5 (5 frequency bands) and 25 (5× 5 frequency bands) values per channel, respectively.

In order to analyse the importance of the different frequency couplings within the global brain graph, we represent them as a multilayer graph. In this graph, nodes are located within layers representing the different frequency bands. WFC represents the edges between nodes within a single layer, i.e. intra-layer, and CFC represents the edges between nodes located in different layers, i.e. inter-layer. In this work, the CS graphs are not analysed as multilayer graphs since such graphs would have no inter-layer edges and thus would not be comparable directly with the CBS graphs. The following measures are computed only for CBS graphs. We obtain graphs with 23 nodes that are replicated over 5 layers ($L \in [\delta, \theta, \alpha, \beta, \gamma]$), resulting effectively in 115 nodes. There are 5 types of intra-layer edges, such as δ-δ, and 20 types of inter-layer edges, such as δ-θ or θ-δ.

We measure the importance of each type of frequency coupling within the multilayer graph by measuring the contribution of each edge to enable the efficient passing of information through the graph. For this purpose, we define coupling betweenness centrality (CBW) centrality based on an adjusted version of edge betweenness [100]:

$$CBW(c) = \frac{1}{E} \sum_{i=1}^{E} BW(e), \tag{4.5}$$

where E is the total number of edges of coupling type c and $BW(e)$ is edge betweenness centrality given by:

$$BW(e) = \sum_{i \neq j} \frac{g_{ij}(e)}{g_{ij}}, \tag{4.6}$$

where g_{ij} is the number of shortest paths between nodes i and j, and $g_{ij}(e)$ is the number of those paths that go through edge e. The shortest path is defined as a path with the least sum of w_{ij}. CBW quantifies the contribution of each coupling type to the information integration [245], i.e. the amount of information flow through edges. Note that the CBW of a weighted and unweighted version of the same graph results in different value of CBW. Therefore, we analyse both weighted and unweighted CBW.

CBW assumes that the essential processes within the graph occur along the shortest paths. However, there might be alternative paths with only minor length differences,

which CBW ignores. In case of a disruption of the graph structure, these alternative paths might enable the recovery of function with negligible differences. We quantify this as the vulnerability of the graph to the removal of one type of frequency coupling. The vulnerability is measured in two ways: the loss of ability to integrate information [158] and the loss of segregation.

The integration property of graph G, i.e. the ability of a graph to communicate information globally, is approximated with global efficiency (E_G) given by:

$$E_G(G) = \frac{1}{N(N-1)} \sum_{i \neq j \in G} \frac{1}{d(ij)}, \tag{4.7}$$

where N is the number of nodes in graph G and $d(ij)$ is the shortest path length between nodes i and j. E_G is related to CBW. CBW measures the information flow on the more detailed edge level while E_G takes the node-level perspective.

The segregation property of graph G, i.e. the presence of densely connected clusters and sparse connections between them, is approximated with a local efficiency given by:

$$E_L(G) = \frac{1}{N} \sum_{i \in G} E_G(G_i), \tag{4.8}$$

where G_i is the neighbourhood of node i, i.e. subgraph of nodes directly connected to i, without node i itself.

In order to measure the vulnerability of the graph and its dependence on different types of frequency coupling, E_G and E_L are computed for the full graph. The two measures are then re-computed for a perturbed graph where one type of frequency coupling (i.e. a set of edges) is removed. The change in E_G and E_L give the global and local vulnerability measures $V_G(G_c) = 1 - (E_G(G_c)/E_G(G))$ and $V_L = 1 - (E_L(G_c)/E_L(G))$, where G is the full graph and G_c is the perturbed graph with the edges of coupling type c removed.

4.2.4 Graph Thresholding and Statistical Analysis

In order to filter out the unimportant edges that might result from a spurious coupling, the weighted multilayer graphs are thresholded through relative quantile-based thresholding. Given a quantile Q, all edges with a weight lower than Q are removed from the graph. There are considerable differences between the weights of each frequency coupling type (e.g. mean of γ-$\beta = 1.627$ compared to the mean of α-$\alpha = 8.975$); thus,

a separate threshold Q is used. As a result, the graphs retain $Q\%$ of the strongest edges. To ensure that the observed differences between the graphs are not due to the choice of threshold Q, all of the graph measures are computed over 20 threshold values ($Q \in [0, 0.95]$ in increments of 0.05), and only significant differences observed over at least ten thresholds are declared significant. The reported plots and numerical results are generated from such threshold levels of Q that the between-group difference is maximised (i.e. largest effect size). However, the effect of choice of this threshold should be minimal as significant differences were observed over multiple thresholds. All p-values are corrected using the Benjamini–Hochberg false discovery rate method [25].

Additionally, to improve the reliability, we perform epoch-wise test-retest experiments. For each participant included in this study, there are three epochs. Thus, we repeat the full analysis reported in this chapter for each epoch separately. Consequently, only significant differences observed consistently across all three epochs are denoted as significant. An analysis of statistical power given our sample size was performed to identify the threshold effect size where 80% is reached (A.1).

Furthermore, we convert the CBS graph from directed to undirected by taking the mean weight for each pair of directed edges, thus collapsing them into a single edge. Such an approach is the most conservative since the potential effect of outliers is minimised compared to the alternative of taking the maximum weight.

NS is log-transformed to reduce skewness. We do not threshold the graphs for NS computation, as this might lead to isolated nodes with no edges. We test whether node strengths are normally distributed separately for each coupling and channel with a Shapiro test. Node strengths that pass the test are then compared with a two-sample t-test, and those that do not pass the test are compared with a Mann-Whitney U-test.

The multilayer graph measures such as CBW, global vulnerability (v_G) and local vulnerability (v_L) aim to analyse the roles of frequency coupling types in terms of the graph's properties. However, whether such multilayer graphs should be weighted or unweighted is unclear. Thus, we examine the patterns in both weighted and unweighted multilayer graphs. The weighted graphs can be converted into unweighted graphs by setting the weights of all edges to 1. Additionally, the selected graph metrics, except for NS, assume edge weights represent the distance between weights. Since functional connectivity is a measure of similarity, we convert the edge weights to distance as follows,

$$\tilde{w_{ij}} = max(W) + min(W) - w_{ij} \tag{4.9}$$

,where $\tilde{w_{ij}}$ is the transformed edge weight connecting nodes i and j, W is the edge-

weight distribution of the graph and $max(\cdot)$ and $min(\cdot)$.

We test whether CBW, v_G and v_L of both weighted and unweighted graphs are normally distributed using the Shapiro-Wilk test for each coupling type separately. A two-sample t-test is used for normally distributed variables and Mann-Whitney U for non-normally-distributed variables to compare between groups. Furthermore, both weighted and unweighted CBW and v_G are log-transformed to reduce skewness.

4.2.5 Graph Classification

Finally, we train classifiers using the graph metrics to evaluate the predictive power of these biomarkers of AD. Three classifiers are trained using the CS, CBS, and combined features, respectively. In other words, the CS classifier is trained using NS, the CBS classifier uses the NS and multilayer graph metrics, and the combined classifier uses all of the previous. Additionally, these features are collected across all filtered graphs.

As this leads to a large feature space, we introduce an effect-size-based forward feature selection. The features are ordered by the absolute value of effect size (Cohen's d [57]) and sequentially added to the feature vector, which is then used to train the classifier. The first 100 features are evaluated in this manner. Note that comparing the CS and CBS classifiers is likely unfair as the CS utilises considerably smaller and less complex features, as the NS is a relatively simple graph measure. Instead, the CS classifier should be viewed as a naive baseline.

SVM classifier with radial basis kernel is used as the classifier. Moreover, features are scaled to zero mean and unit standard deviation. 10-fold cross-validation repeated 100 times is used to train and evaluate the classifier.

Finally, we use the feature sets of CS and CBS classifiers that achieved the best performance and train a combined classifier. We hypothesise that the information captured by CS and CBS graphs is at least partially unique. Thus a classifier trained on the combined feature sets should outperform the classifiers trained on individual graphs, as it can leverage the information from both functional connectivity measures.

4.3 Results and Discussion

We denote a statistical test as significant only if it is consistently detected across at least ten graph thresholds and in all three epochs. Therefore, for simplicity, only results from epoch two are reported in the following sections, except for the classification results,

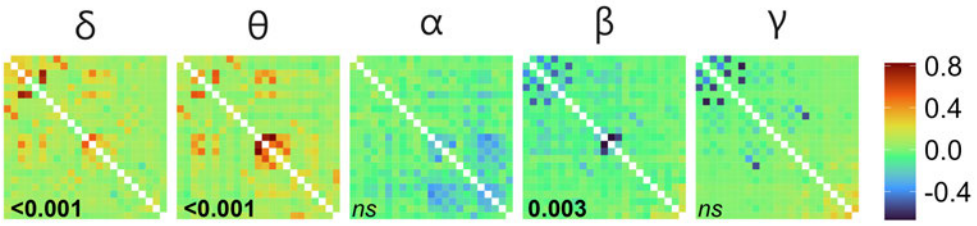

Figure 4.2: The difference between average connectivity matrices (AD − HC) measured with cross-spectrum in epoch 2. For visualisation purposes, the values were min-max normalised. Digits in black denote a p-value (FDR corrected) testing for the difference in global coupling ($p < 0.05$ in bold, in italics otherwise).

where data from all epochs are utilised. Epoch two was selected randomly, which does not affect the reported results as all results were required to be observed across all three epochs. Moreover, for visualisation purposes, we select the graph threshold, where the strongest difference is observed for each comparison separately.

The results and visualisations from epochs 1 and 3 are included in A.2 and A.4, respectively. The numerical results from epoch 2 are included in A.3.

4.3.1 Connectivity Matrices and Average Connectivity

Differences in averaged connectivity matrices (Figure 4.2 and 4.3) indicate that both methods seem to detect variations in the topology of FC graphs. The results of statistical tests are reported in A.3 (Tables A.11 and A.12). By using CS, significant differences in the average connectivity are found in δ and θ bands, where AD cases have increased connectivity. Additionally, CS reveals a decrease in β connectivity of AD cases.

Using CBS, differences can be observed in multiple frequency bands and their couplings. Increased global connectivity is observed in AD cases in θ WFC and θ-δ, δ-θ and δ-α CFC. In contrast, decreased global connectivity in AD cases is found in β WFC and alpha-beta, α-γ, β-α, β-γ, γ-α and γ-β CFC. Overall, AD cases show increased connectivity in low-frequency components and their CFC interactions and decreased connectivity in high-frequency components.

These findings are consistent with the literature reporting increased activity in δ and θ in AD [128, 150]. An increase in δ WFC and low-frequency CFC in AD was also reported using bicoherence [275]. Similarly, Maturana et al. [187] report increased bispectral power in AD in δ and θ and a decrease in α, β_1 and β_2. They also report

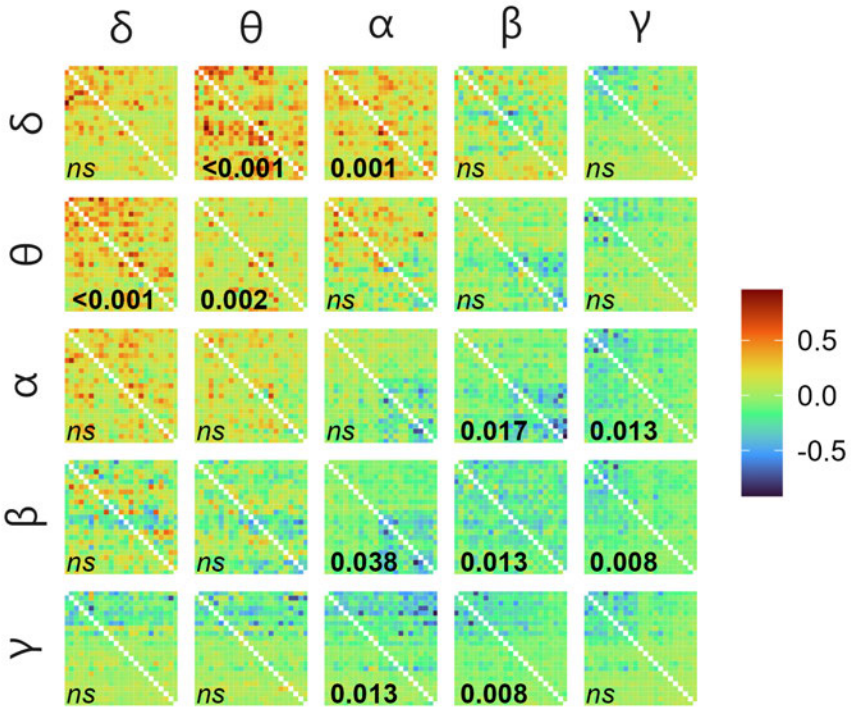

Figure 4.3: The difference between average connectivity matrices (AD − HC) measured with cross-bispectrum in epoch 2 with input frequency on the vertical facets and output frequency on the horizontal. For visualisation purposes, the values were min-max normalised. Digits in black denote a p-value (FDR corrected) testing for the difference in global coupling ($p < 0.05$ in bold, in italics otherwise).

lower bispectral entropy in δ and θ suggesting fewer frequency components interact with these frequency bands. In contrast, Cai et al. [42] report the opposite differences in the same WFC and CFC using PSI, i.e. decrease in δ and θ.

Moreover, the visible structure distortion within multiple frequency bands detected by both CS and CBS suggests connections to the disconnection syndrome and disturbed information processing in AD.

4.3.2 Coupling-wise Node Strength

In order to statistically test the differences in connectivity measured by both CS and CBS and to localise the brain regions which show the most pronounced differences between AD and HC, NS is measured for each channel and coupling type separately. We show the results in Figs. 4.2 and 4.3 for CS and CBS, respectively. The details of these statistical tests are reported in A.3 (Tables A.13 and A.14).

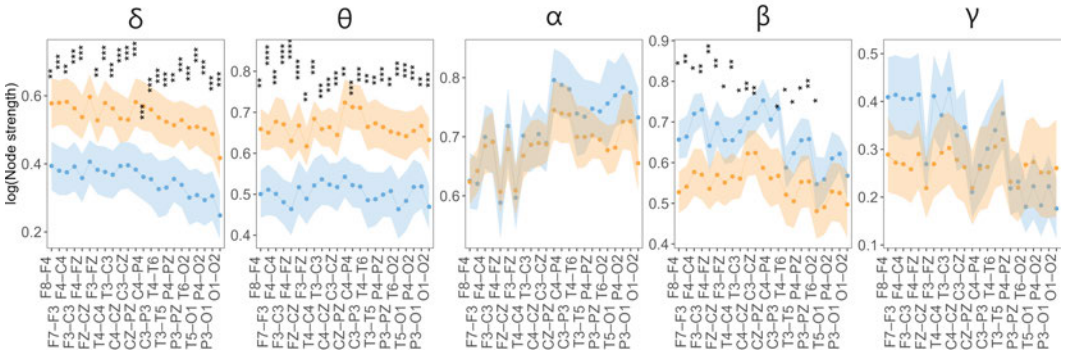

Figure 4.4: NS (min-max normalised) measured with CS of HC (blue) and AD (orange): mean with 95% confidence intervals. Significant differences observed across all epochs are encoded by asterisks. The number of asterisks corresponds to the p-value (FDR corrected), i.e. $p \leq 0.0001$ "****", $p \leq 0.001$ "***", $p \leq 0.01$ "**", and $p \leq 0.05$ "*".

The differences in WFC detected by CS and CBS (Figure 4.4 and diagonal elements in Figure 4.5) are generally similar. Both methods show increased θ NS in AD cases across most channels. Both CS and CBS show decreased β coupling. However, each detects these changes in different regions, i.e. CS across all channels except for occipital, while CBS only in central channels. Interestingly, CBS fails to capture the increased NS in δ in AD cases that can be seen in CS. These differences showcase the importance of assessing both linear and nonlinear coupling in understanding the variations in AD brain graphs.

Multiple differences in the CFC (off-diagonal elements in Figure 4.5) are detected, highlighting the need to analyse the interactions of frequency components in both healthy and AD brain graphs. AD cases show a global increase in δ-θ and θ-δ, and in frontal and temporal areas in δ-α. This is in contrast to the findings in Wang et al. [275], where an increase of δ-θ only in frontal channels is reported. They also report an increase in midline parietal-occipital θ-γ that we do not detect. Furthermore, we observe a frontal, occipital and temporal decrease in α-β and β-α, frontocentral and frontotemporal decrease in α-γ and β-γ, and in frontal, frontocentral and occipital channels in γ-α in AD cases.

Cai et al. [42] report comparable differences using PSI, but in contrast to our results, they show mainly decreased NS in AD cases. This might be because CBS is influenced by the amplitude, while PSI is a pure phase coupling measure. Fraga et al. [92] report an increase of the δ-θ and δ-β amplitude-amplitude CFC in AD cases which is similar to our results. This suggests that CBS indeed measures some mixture

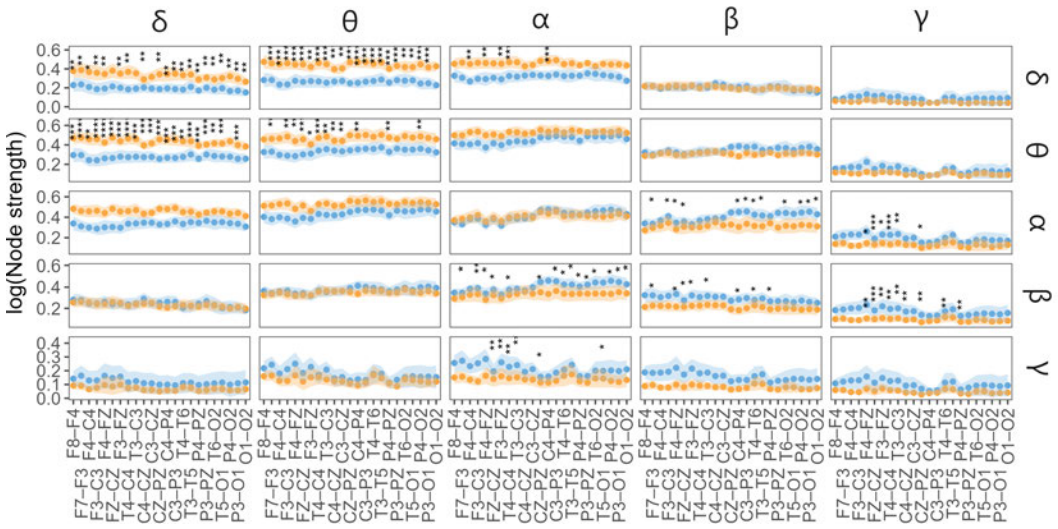

Figure 4.5: NS (min-max normalised) measured with CBS of HC (blue) and AD (orange): mean with 95% confidence intervals. The input frequency is on the vertical facets, and the output frequency is on the horizontal. Significant differences observed across all epochs are encoded by asterisks. The number of asterisks corresponds to the p-value (FDR corrected), i.e. $p \leq 0.0001$ "****", $p \leq 0.001$ "***", $p \leq 0.01$ "**", and $p \leq 0.05$ "*".

of CFC types [135] since our results are partially in line both with phase-phase and amplitude-amplitude CFC studies.

4.3.3 Multilayer Graph Analysis

In order to elucidate the roles of the frequency bands and their coupling, both WFC and CFC, we analyse the CBS graphs as multilayer graphs with five layers representing the traditional frequency bands of EEG. Moreover, both the weighted and unweighted versions of these graphs are analysed.

First, weighted and unweighted CBW are used to assess the importance of each type of coupling for both local and global communications in the graph. Results of statistical tests comparing the unweighted CBW are reported in the appendix (Table A.15) and visualised in Figure 4.6a. Results of statistical tests comparing the weighted CBW are reported in the appendix (Table A.18) and visualised in Figure 4.6b.

The unweighted CBW shows only a decrease in AD cases in the δ-β CFC (Fig 4.6a. In contrast, the weighted CBW shows multiple decreases in AD cases, specifically in α-α and β-β WFC and δ-α, α-δ, α-β, α-γ, β-α and β-γ CFC. As these decreases involve high-frequency components, we speculate that this finding is likely linked to

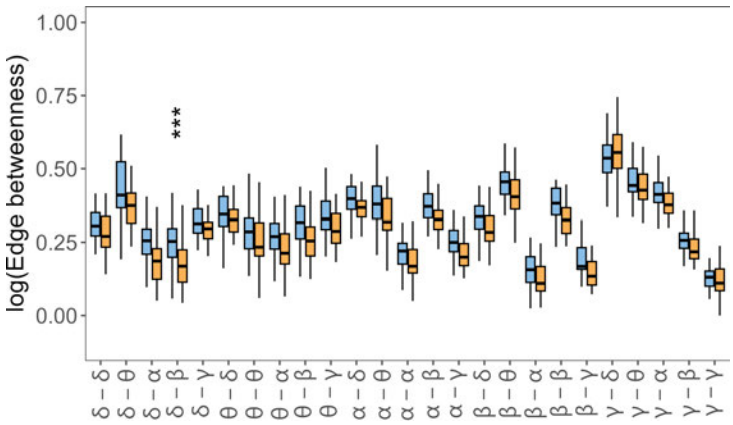

(a) Importance of each type of frequency measured by edge betweenness.

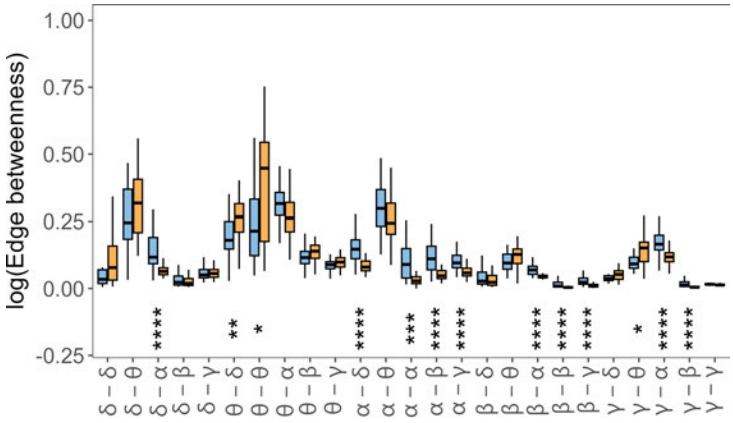

(b) Importance of each type of frequency coupling measured by weighted edge betweenness.

Figure 4.6: Significant differences observed between HC (blue) and AD (orange) in at least ten thresholded graphs and across all epochs are encoded by asterisks. The number of asterisks corresponds to the p-value (FDR corrected), i.e. $p \leq 0.0001$ "****", $p \leq 0.001$ "***", $p \leq 0.01$ "**", and $p \leq 0.05$ "*".

the characteristic slowing down of signals in AD, i.e. a decrease of high-frequency power [128, 98]. On the other hand, we observe an increase of weighted CBW of θ-θ WFC and θ-δ and γ-θ CFC in AD cases. Interestingly, previously, a decrease in γ-θ phase-amplitude coupling was reported to signify progression from mild cognitive impairment to AD [198]. However, our results indicate an opposite pattern.

Then, weighted and unweighted v_G are used to assess the vulnerability of information integration of the graph to the removal of a specific coupling type. Numerical results of comparing unweighted v_G are reported in the Appendix (Table A.16) and visualised in Figure 4.7a. Numerical results of comparing weighted v_G are reported

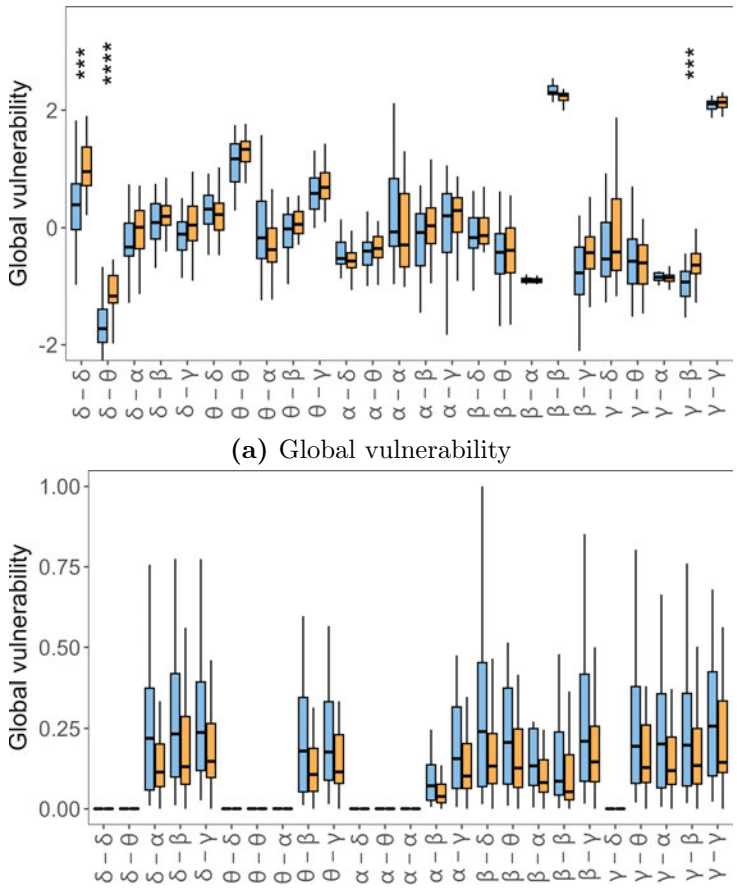

(a) Global vulnerability

(b) Weighted global vulnerability

Figure 4.7: Significant differences observed between HC (blue) and AD (orange) in at least ten thresholded graphs and across all epochs are encoded by asterisks. The number of asterisks corresponds to the p-value (FDR corrected), i.e. $p \leq 0.0001$ "****", $p \leq 0.001$ "***", $p \leq 0.01$ "**", and $p \leq 0.05$ "*".

and visualised in Appendix (Table A.19) and visualised in Figure 4.7b.

The AD brain graphs seem more vulnerable to removing multiple types of couplings. Weighted v_G fails to detect any reliable differences. We speculate this might be caused by edge weight differences across different coupling types, thus biasing the results. v_G is likely more sensitive towards such an issue, as it is a global measure in contrast to the other measures, which consider predominantly local relationships. A significant increase in unweighted v_G in AD cases is observed in δ-δ WFC and δ-θ and γ-β CFC. Interestingly, the removal of WFC generally causes a larger increase in vulnerability compared to CFC (except for α-α, suggesting that while CFC plays a crucial role in the brain graphs, WFC seems dominant in the brain graphs.

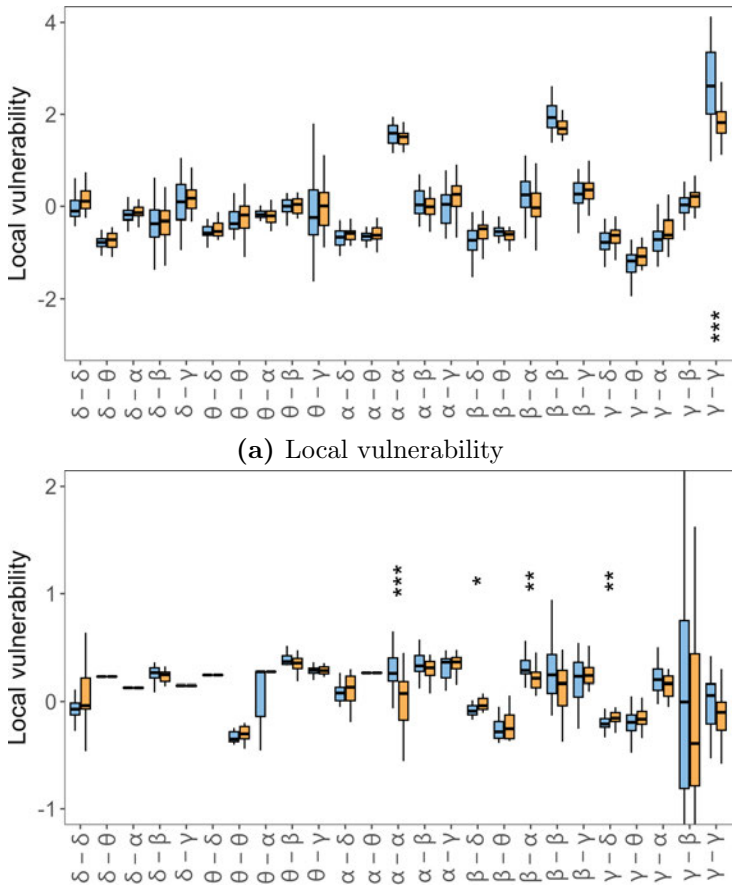

(a) Local vulnerability

(b) Weighted local vulnerability

Figure 4.8: Significant differences observed between HC (blue) and AD (orange) in at least ten thresholded graphs and across all epochs are encoded by asterisks. The number of asterisks corresponds to the p-value (FDR corrected), i.e. $p \leq 0.0001$ "****", $p \leq 0.001$ "***", $p \leq 0.01$ "**", and $p \leq 0.05$ "*".

Finally, weighted and unweighted v_L are used to assess the vulnerability of segregation of the graph to the removal of a particular coupling type. Results of statistical tests comparing unweighted v_L are reported in Appendix (Table A.17) and visualised in Figure 4.8a. Results of statistical tests comparing weighted v_L are reported in Appendix (Table A.20) and visualised in Figure 4.8b.

γ-γ is the most robustly linked to segregation measured with unweighted v_L, which fits well with the evidence of high-frequency oscillations being related to local processing [41]. Moreover, this coupling is significantly more vulnerable in weighted graphs of HC cases, which is likely related to the decreased γ activity in AD [128]. Likely for similar reasons, the removal of α-α WFC and β-α CFC causes a significant increase of

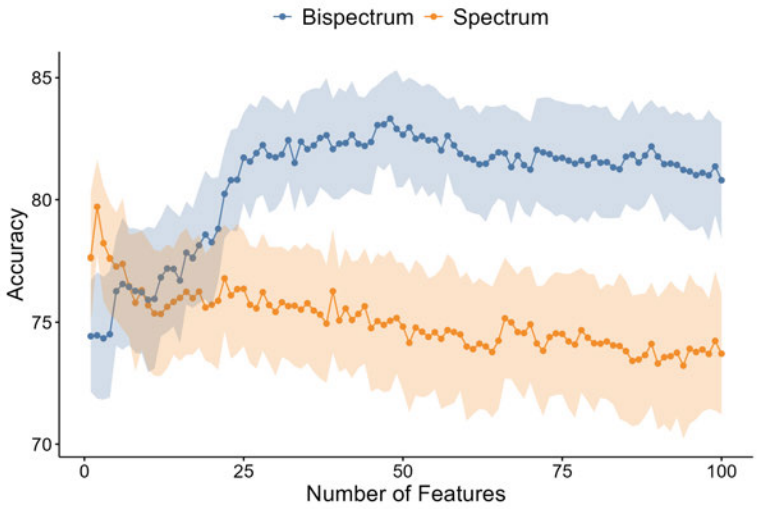

Figure 4.9: Average accuracy (points) with standard deviation (ribbons) of the classifiers trained with graph-theory features using a 10-fold stratified cross-validation repeated 100 times. Specifically, the features considered are NS for cross-spectrum (orange) and NS, CBW, v_G and v_L cross-bispectrum (blue) graphs. The features are sequentially added to the classifier based on their effect size.

weighted-v_L in-HC,-suggesting-the-segregation-function-enabled-by-these-high-frequency-components-is-likely-disrupted-in-AD.- On-the-other-hand,-β-δ and-γ-δ CFC-removal-cause- a- significant- increase- of- weighted- v_L in- AD- cases.- This- suggests- that- in- AD-cases,-the-high-frequency-CFC-takes-over-the-role-of-enabling-graph-segregation-as-the-high-frequency-WFC-is-attenuated.-

4.3.4 Classification Results

SVM-classifiers-were-trained-using-graph-features-extracted-from-CS-and-CBS-separately-to-measure-the-predictive-power-of-CS-and-CBS-based-graphs-and-evaluate-the-multilayer-graph-features-(Figure-4.9).- A-detailed-performance-summary-of-the-best-models-is-reported-in-Table-4.1.-

All-CBS-based-models-outperform-the-CS-based-models,-suggesting-that-information-related-to-nonlinear-and-CFC-coupling-might-be-crucial-for-the-modelling-and-classification-of-AD.- However,-such-a-conclusion-might-be-biased-as-the-CS-based-models-are-trained-using-a-smaller-set-of-features,-i.e.- node-strengths.- Thus,-the-comparison-is-likely-unfair-and-should-be-interpreted-conservatively.-

The-best-CS-based-model-reaches-its-highest-accuracy-of-79.71%-(SD=1.94)-using-

Table 4.1: Performance of the best models trained using graph features identified via forward feature selection. The feature sets contain 2, 48 and 50 features for the spectrum, bispectrum and combined models, respectively.

Model	Accuracy	Sensitivity	Specificity
Spectrum	79.71 % (SD=1.94)	86.42 % (SD=2.95)	74.62 % (SD=4.48)
Bispectrum	83.32 % (SD=1.83)	86.62 % (SD=2.95)	80.71 % (SD=3.9)
Combined	81.39 % (SD=2.09)	85.97 % (SD=2.45)	78.91 % (SD=3.28)

Table 4.2: Features included in the best cross-bispectrum-based classifier. For multilayer graph metrics, the graph thresholds are in parentheses. This is not necessary for the node strengths as these are obtained from the unthresholded graphs.

coupling	Node strength	Multilayer graph metric
α-β	C4P4, CZPZ, P3O1, T5O1	
β-α	C4P4, P3O1	weighted CBW (0.7)
δ-α	F4C4	weighted CBW (0.4, 0.45, 0.5, 0.55, 0.6)
δ-θ	C3P3, C4P4, CZPZ, FZCZ, O1O2	v_G (0.55)
γ-α	F4FZ	weighted CBW (0.4, 0.45, 0.5, 0.55, 0.6, 0.65, 0.7, 0.75, 0.8, 0.85)
θ-δ	CZPZ, FZCZ, P4PZ	
θ-θ	F4C4	
δ-δ		v_G (0.65)
α-δ		weighted CBW (0, 0.05, 0.1, 0.15, 0.2, 0.25)
α-γ		weighted CBW (0.5, 0.55, 0.6, 0.65, 0.7, 0.75, 0.8)

only two features. These features are the node strengths of channels F4-C4 and C3-P3 in the θ frequency band WFC. In contrast, the CBS-based models require considerably more features to achieve the highest accuracy of 83.32% (SD=1.83) with 48 features (Table 4.2). Interestingly, the majority of these features are CFC. Furthermore, the weighted CBW seems to provide the most information to the classifier from the multilayer graph measures introduced in this study, as it is included multiple times in the final feature set. Node strengths from all areas are utilised, but the central-parietal channels are selected repeatedly across multiple frequency couplings. It is worth noting that including the same features across different graph thresholds appears to improve the performance, despite likely strong correlations between such features. If only a single graph threshold was selected (i.e. based on the largest effect size), the accuracy drops by 2%-3%. Interestingly, both CS- and CBS-based models utilise the F4-C4 channel from the θ WFC, suggesting some shared information between these two functional connectivity methods.

Finally, we trained a combined model with the sets of best features concatenated from the CS- and CBS-based models, i.e. using 50 features. However, the accuracy of such a model is only 81.39% (SD=2.09), which is lower than the CBS-based model

suggesting that the addition of CS-based features introduces redundant information into the model.

4.4 Conclusions and Future Work

We have demonstrated that CBS and CS detect similar differences between AD and HC graphs, but CBS has an advantage over CS by including cross-frequency and nonlinear interactions. We report several significant differences in CFC both globally and on a node level, suggesting that including CFC in a graph-theoretic analysis of brain graphs is crucial to obtaining a more detailed insight into their structure and function. Furthermore, we show that multilayer graph analysis provides a simple yet powerful framework for representing and analysing the role of CFC in brain graphs. Using this framework, we present a novel approach to elucidate the roles of different frequency components of EEG signals. Moreover, we show that both CFC and WFC CBS-based graphs can be used to classify AD with high accuracy.

CFC has been suggested to be related to modulatory activity, i.e. slow band modulating the activity of fast oscillations. However, it remains unclear why low-frequency CFC would be increased in AD and requires further in-depth study.

Next, although (cross-)bispectrum was shown to be a powerful tool to detect various types of WFC and CFC, such as phase-phase or phase-amplitude, CBS seems to capture an unknown mixture of these types of couplings. Therefore, a combination of bispectrum with other types of CFC methods might be a plausible direction for future research.

Furthermore, by relying on traditional frequency bands to define the layers of the graphs, our framework might miss some CFC occurring on finer scales, e.g. interaction within one band. However, considering the CFC within only a few bands allows us to construct multilayer graphs with a relatively small number of layers. Thus, we argue that relying on the five bands is necessary to introduce the CFC into graph analysis without increasing the complexity significantly.

The presented multilayer graph analysis focused only on how dependent or vulnerable the graphs are on different types of frequency coupling to enable integration and segregation properties. Although these two properties are hypothesised to be crucial in brain graphs, their analysis is not sufficient to elucidate the functions the frequency couplings might enable across various spatio-temporal scales in normal brains and how these functions disappear or change in AD. Thus, we suggest focusing on other graph-

theoretic measures beyond integration and segregation in future work.

A limitation of our study is the relatively small sample size. This leads to some of the observed significant differences being underpowered. Thus, the small differences we report in this study should be interpreted more conservatively. However, despite this limitation, we identify a set of reliable biomarkers as evidenced by the classification results. In future research, it might also be important and interesting to explore more complex graph-based features that would capture the differences between AD and HC in a lower-dimensional space more efficiently.

4.5 Chapter Summary

This chapter extends the FC graph analysis beyond WFC, incorporating CFC information. This work expands on previously reported graph-based disruptions of brain graphs of AD to multilayer graphs containing both WFC and CFC information. The framework of multilayer graph analysis allows us to consider the different frequency components' roles in enabling well-known brain graph properties such as information integration and information segregation.

Bispectrum analysis has previously been used to quantify EEG interactions on a pairwise level. In contrast, the methodology proposed in this chapter computes cross-bispectra between all pairs of EEG channels to reconstruct a multilayer brain graph with a layer for each frequency band. In such a graph, intra-layer and inter-layer edges denote WFC and CFC interactions, respectively.

By comparing CBS graphs to CS graphs, the linear counterpart of CBS, in terms of node strength and classification performance, the advantages of incorporating nonlinear and CFC information were demonstrated showing a significantly improved prediction.

Statistical analysis of CBS-based graph metrics indicate graph variations of AD and HC cases. AD cases show increased connectivity in low-frequency components and their CFC interactions but decreased connectivity in high-frequency components.

We demonstrate that a graph-theoretic analysis of CFC brain graphs is crucial to obtain a more detailed insight into their structure and function. Vulnerability analysis reveals that different frequency couplings in AD graphs enable the information integration and segregation properties compared to HCs.

In conclusion, the study demonstrates the significance of CBS in capturing nonlinear and CFC interactions, providing insights into AD-related FC alterations. Future research should address limitations like sample size and explore more complex graph-based features to understand AD-related brain graph alterations better.

Chapter 5

EEG-based Graph Neural Network Classification: An Empirical Evaluation of Functional Connectivity Methods

5.1 Introduction

[1]In this chapter, we evaluate a number of commonly used methods to quantify FC from EEG data.

GNN extends the logic of convolution operation to graphs by aggregating information from connected nodes based on the assumption that nodes connected by an edge are similar. However, there is a limited number of GNN applications for EEG brain graph classification. It remains unclear which method should be used to infer the graph structure for the GNN application. A fully connected graph is commonly used in the literature [77]. However, such an approach does not leverage any information encoded by FC brain graphs. A second option is using the distances between spatial positions of EEG electrodes to define the graph structure [77, 269]. Furthermore, Demir et al. [77] utilise distance thresholding and k-nearest-neighbours methods to filter out unimportant edges. Such edge-filtering can be important, as some edges

[1]The content presented in this chapter has been published in *Dominik Klepl, Fei He, Min Wu, Daniel J. Blackburn, and Ptolemaios Sarrigiannis. EEG-Based Graph Neural Network Classification of Alzheimer's Disease: An Empirical Evaluation of Functional Connectivity Methods.* IEEE Transactions on Neural Systems and Rehabilitation Engineering, *30:2651–2660, 2022. ISSN 1558-0210. doi: 10.1109/TNSRE.2022.3204913*

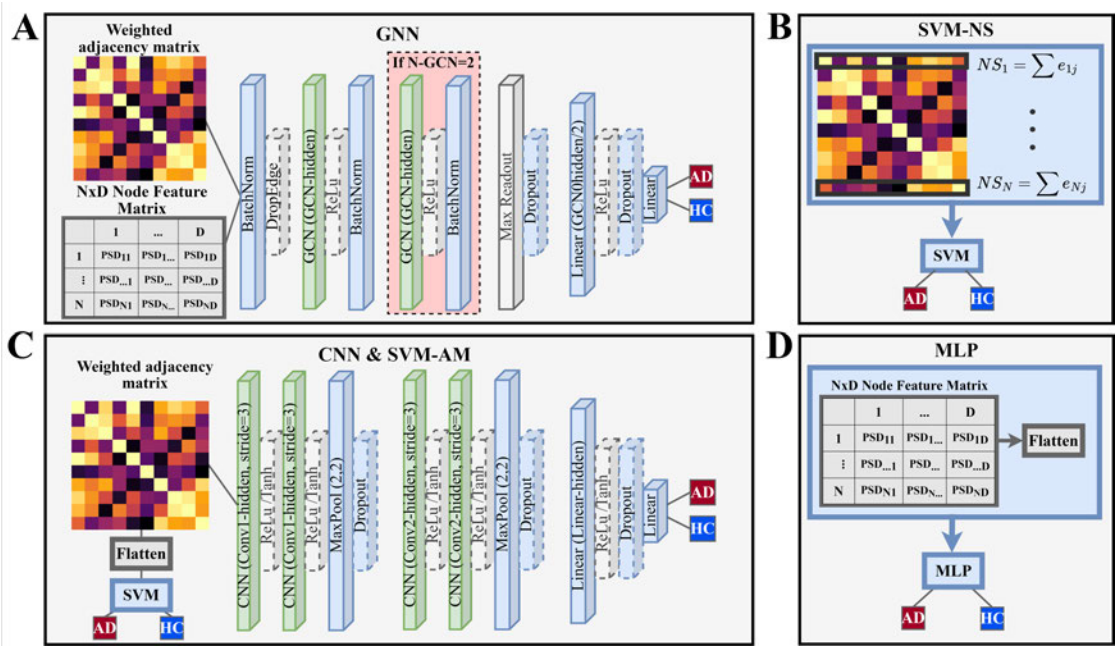

Figure 5.1: Overview of model architectures developed for classification of AD from EEG-FC-based graphs. (A) A GNN takes weighted featured brain graphs with N nodes represented by a weighted adjacency matrix and a node feature matrix ($\mathbb{R}^{N\times D}, D = 100$) where the node features consist of power spectral densities (PSD, $0 - 100Hz$). The N-GCN hyper-parameter controls the number of graph convolutional layers. (B) SVM trained using the node strengths (i.e. the sum of edge weights of neighbouring nodes) as input features (SVM-NS). (C) CNN trained on the brain graphs represented by weighted adjacency matrices. Alternatively, the weighted adjacency matrix is flattened and used as input to a SVM (SVM-adjacency matrix (AM)). (D) Node feature matrix ($\mathbb{R}^{N\times D}$) with power spectral densities across all EEG channels is used to train a MLP.

might be redundant or even introduce additional noise, thus hindering the model from learning the optimal solution. Only a handful of studies use FC measures, such as coherence [269] and wPLI [178]. Additionally, Liu et al. [178] use a MST algorithm to produce sparse brain graphs. This is in contrast to threshold-based edge filtering, as MST can select edges with various edge weights and ensure that the resulting graph is connected. Additionally, Zhong et al. [311] utilise a learnable mask in order to learn the optimal graph structure for a specific classification task without relying on any FC measure.

Other graph-based approaches were successfully used to train machine learning classifiers to diagnose brain disorders using EEG automatically. Manually engineered graph features, such as node strength [202] and vectorised adjacency matrix [197],

could be promising graph-based biomarkers of AD, as both approaches achieve high classification accuracy. Additionally, there were some attempts to utilise deep learning, CNNs, for automatic graph-based feature extraction. Specifically, CNN was trained to classify AD and schizophrenia using adjacency matrices, which are image-like representations of FC graphs [217]. However, an image representation of a graph cannot effectively capture all the properties, as a graph is a non-euclidean object.

In this chapter, we systematically evaluate the effects of using various FC methods to infer EEG brain graphs in training GNN for the classification of AD patients. Two types of edge filtering are used to induce graph sparsity in order to improve the performance of GNN. To compare and evaluate the classification performance of various FC-based GNNs, a GNN-based baseline is trained using a fixed graph structure for all brain graphs, represented by the Euclidean distance between spatial positions of EEG sensors. Three additional baseline models are established: two SVM baselines trained on node strengths (SVM-NS) and vectorised adjacency matrix (SVM-vector), respectively, and a CNN trained on images of adjacency matrices. Figure 5.1 illustrates the model architectures employed for comparative study in this work.

5.2 Methods

5.2.1 EEG Pre-processing

First, a zero-phase 5^{th} order Butterworth filter is employed to remove frequencies below 0.1 Hz and above 100 Hz; a zero-phase 4^{th} order Butterworth stop-band filter is used to remove frequencies between 49 and 51 Hz related to power-noise. The EEG data were then down-sampled to 250 Hz using an 8^{th} order Chebyshev type I filter and scaled to zero mean and unit standard deviation.

In order to increase the sample size and to demonstrate that the classification performance is epoch-independent, the 12-seconds-long epochs were split into 3-second-long non-overlapping segments. Thus, for each subject, there are 12 EEG segments. Finally, frequency bands are created from each EEG segment using a zero-phase 5^{th} order Butterworth filter. Six frequency bands are considered: δ $(0.5-4Hz)$, θ $(4-7Hz)$, α $(7-15Hz)$, β $(15-31Hz)$, γ $(31-100Hz)$ and full $(0.5-100Hz)$.

5.2.2 Functional-Connectivity-based Brain Graph Inference

In this chapter, we selected eight commonly used methods for constructing brain graphs from EEG signals, namely: the absolute value of PCC, spectral COH, iCOH, PLI, wPLI, PLV, MI and AEC.

We estimate FC brain graphs for each EEG segment and frequency band separately. Thus, for each subject, we obtain 72 brain graphs (12 segments $\times$ 6 frequency bands). A brain graph G can be represented by an $N \times N$ adjacency matrix A where $N = 23$. As we consider only FC measures, all edges are undirected, and thus the number of inferred edges can be reduced from N^2 to $[N \times (N-1)/2]$. However, for simplicity, we keep the N^2 edges in the $N \times N$ adjacency matrix A. Thus, each entry of the adjacency matrix A^{FC}_{xy} represents the edge weight between nodes, i.e. the dependency of EEG signals $x \in \mathbb{R}^{\mathbb{T}}$ and $y \in \mathbb{R}^{\mathbb{T}}$ are measured by the connectivity measure FC where T is the signal length. All of the selected measures are normalised to $[0, 1]$ where 0 indicates no coupling and 1 indicates a perfect coupling.

The adjacency matrix using the absolute values of Pearson's correlation coefficients between nodes x and y is given by:

$$A^{PCC}_{xy} = \frac{\sum_t (x(t) - \bar{x})(y(t) - \bar{y})}{\sqrt{\sum_t (x(t) - \bar{x})^2} \sqrt{\sum_t (y(t) - \bar{y})^2}} \ , \tag{5.1}$$

where $x(t)$ is the value of signal x at time t, and $\bar{x}$ is the mean of x. The absolute value is calculated as we are only interested in the coupling magnitude. Next, the adjacency matrix of COH is given by:

$$A^{COH}_{xy}(f) = \frac{|CS_{xy}(f)|^2}{CS_{xx}(f) CS_{yy}(f)}, \tag{5.2}$$

where CS_{xy} and CS_{xx} are cross-spectral and auto-spectral densities respectively at frequency f. The coherence within a frequency band B is then calculated as the mean of $A^{COH}_{xy}(f)$ where $f \in B$.

The iCOH measures phase consistency similar to COH and accounts for volume conduction effects. The adjacency matrix using iCOH is computed as:

$$A^{iCOH}_{xy}(f) = \frac{\Im(CS_{xy}(f))}{\sqrt{CS_{xx}(f) CS_{yy}(f)}}, \tag{5.3}$$

where $\Im$ denotes the imaginary component. The iCOH within a frequency band B is

then calculated as the mean of $A_{xy}^{iCOH}(f)$ where $f \in B$

The phase and amplitude of an EEG signal at time t can be calculated from the analytic representation z of signal x

$$z(t) = x(t) + \mathrm{i}\,\tilde{x}(t), \tag{5.4}$$

where i is the imaginary component and $\tilde{x}(t)$ is the corresponding Hilbert transform. Then the phase and amplitude can be obtained from $z(t)$ as

$$\phi(t) = \arctan\left(\frac{\tilde{x}(t)}{x(t)}\right), \tag{5.5}$$

and

$$amp(t) = \sqrt{[x(t)]^2 + [\tilde{x}(t)]^2}. \tag{5.6}$$

PLI quantifies the asymmetry in phase distributions of two signals and measures only non-zero phase locking [241]. The adjacency matrix using PLI is defined as:

$$A_{xy}^{PLI} = \frac{1}{T}\sum_{t=1}^{T} \operatorname{sign}\sin(\phi_x(t) - \phi_y(t)), \tag{5.7}$$

where ϕ_x is obtained using Eq. 5.5. wPLI is an extension of PLI, which aims to remove the effects of amplitude and volume conduction by maximally weighting the ± 90 deg phase differences and thus omitting uniformly driven differences [265]. The adjacency matrix using wPLI is computed as

$$A_{xy}^{wPLI} = \frac{1}{T}\sum_{t=1}^{T} \frac{|\sin(\phi_x(t) - \phi_y(t))|}{\sin(\phi_x(t) - \phi_y(t))}. \tag{5.8}$$

PLV is another approach to quantify the consistency of phase differences between signals, and its associated adjacency matrix is computed as

$$A_{xy}^{PLV} = \frac{1}{T}\sum_{t=1}^{T} \mathrm{e}^{-\mathrm{i}(\phi_x(t) - \phi_y(t)}. \tag{5.9}$$

AEC aims to quantify the coupling based on the amplitudes of the signals. The adjacency matrix using AEC is computed with Eq. 5.1 where x and y are the amplitudes of respective signals computed using Eq. 5.6.

MI quantifies the amount of known information about a second signal after observ-

ing the first signal. The adjacency matrix using MI is calculated as:

$$A_{xy}^{MI} = \sum_{x_i, y_j} P_{XY}(x_i, y_j) \log\left(\frac{P_{XY}(x_i, y_j)}{P_X(x_i) P_Y(y_j)}\right), \tag{5.10}$$

where P_{XY} and P_X are the joint and marginal probability distributions, respectively.

Edge Filtering Methods

It is worth noting that we did not use any corrections for false positives. Thus, the true brain graph structure might be masked by noise due to spurious coupling. Traditionally, a surrogate threshold might be used to control such spurious edges. However, such a procedure is computationally expensive, as it requires re-computing the connectivity measure on multiple random surrogate versions of the original signals, to estimate a null surrogate distribution. Instead, we implement two edge-filtering methods to select only important edges and thus produce sparse graphs. Compared to the surrogate threshold method, edge-filtering is a fast and efficient, albeit naive method to deal with potentially noisy brain graphs. We also utilise the fully-connected graphs, i.e. without any edge selection, in the classification models in order to test the effect of edge-filtering.

The first edge-filtering method is an FC-strength-based top-k% filter ($k \in \{10, 20, 30\}$), which selects only the top k% strongest edges of the given graph and removes the rest. This approach assumes that edge weight, i.e. the connectivity strength, is directly related to the importance of an edge. However, this assumption might not be valid.

A minimum-spanning-tree-based filter (MST-k), also known as an orthogonal minimum spanning tree [78], addresses this concern as it selects a mix of edge weights and always produces a connected graph, i.e. a path exists among all nodes. Briefly, the MST algorithm [209] aims to extract a backbone of a graph with N nodes by selecting $N - 1$ edges, such that the sum of weights is minimised. We use Prim's algorithm for computing MST [209]. In the case of brain graphs, a stronger edge weight implies a higher degree of coupling; thus, we use an inverted MST algorithm, which maximises the sum of weights instead. When $k = 1$, MST-k is equal to a single iteration of the MST algorithm. For $k > 1$, the edges selected by the previous iterations are removed from the graph, and the MST algorithm is re-run. Thus, the MST-k filter selects $k(N - 1)$ edges.

Table 5.1: Possible values for hyper-parameters of GNN, SVM-NS, SVM-AM, CNN and MLP.

Hyper-parameter	Values	GNN	SVM-NS	SVM-AM	CNN	MLP
Cost	[0,1]		✓	✓		
Batch size	{16, 32, 64, 128, 256}	✓			✓	✓
Learning rate	{0.0001, 0.001, 0.01, 0.1}	✓			✓	✓
GCN_hidden	{256, 516, 1024, 2048, 4096}	✓				
N_GCN	{1,2}	✓				
N_Linear	{1,2,3,4,5}					✓
Conv1_hidden	{16, 32, 64, 128}				✓	
Conv2_hidden	{16, 32, 64, 128}				✓	
Linear_hidden	[32, 64, 96, 160, 256, 516]				✓	✓
Activation	{ReLU, Tanh}				✓	✓
edge dropout layer (DropEdge)	{True, False}	✓				
Dropout_p	{0.1, 0.25, 0.5, 0.75, 0.8, 0.9}	✓			✓	✓
Frequency band	delta, theta, alpha, beta, gamma, full	✓	✓	✓	✓	
Edge filter	full, top-{10,20,30}, MST-{1,2,3}	✓	✓	✓	✓	
Gamma	{0.8, 0.85, 0.9, 0.95}	✓			✓	✓

5.2.3 Graph Neural Network Classification

GNN is an extension of an artificial neural network that is capable of learning on graph-structured data. Specifically, we implement a graph convolutional network (GCN) for a graph classification task (Figure 5.1A).

The input to the GCN classifier is in the form of a graph: $G = \{N, E, F\}$, where N, E, and F are sets of nodes, edges and node features, respectively. The nodes are fixed in our case, as this is the number of EEG electrodes. The set of edges E is given by the adjacency matrix A computed by the FC measures introduced in the previous section. Finally, the node feature matrix F is an $N \times D$ matrix where each row encodes a D-dimensional feature for the corresponding node. Specifically, PSD is computed over 1 Hz increments in an interval between 0 and 100 Hz, forming a 100-dimensional node feature vector (i.e. D=100).

GCN is based on the message passing framework, which assumes that neighbouring nodes should have similar node features. Briefly, a GCN layer updates the node features (i.e. messages) using the optionally transformed messages collected from neighbouring nodes. On a node level, a single GCN layer effectively aggregates information from the 1-hop neighbourhood of each node. Thus, stacking L GCN layers represents ag-

gregation from L-hop neighbourhood. Formally, the GCN layer is implemented on a node-level as follows [195]:

$$x_i^l = \Theta_1 x_i^{l-1} + \Theta_2 \max_{j \in G_i} e_{ij} x_j^{l-1}, \tag{5.11}$$

where x_i^l is the node features of node i at the l^{th} layer, x_i^0 is the i^{th} row of the input node feature matrix F, and Θ is a learnable linear transformation, which maps the node features from shape $[1, D]$ to [1, GCN-hidden]. G_i and e_{ij} are the neighbourhood of node i and the edge weight connecting nodes i and j given by the set of edges E respectively. The GCN-hidden is a tunable hyper-parameter of the GCN architecture. A rectified-linear-unit (ReLU) activation is applied to the output of GCN, and batch normalisation is performed [120]. We refer to the node-wise outputs of GCN as node embeddings.

After L GCN layers are applied, the output is constructed by node embeddings in the form of a $N \times H$ matrix, where H is the hidden size given by GCN-hidden. In order to produce a graph-level embedding, a maximum readout layer is applied, resulting in an H-dimensional graph embedding r for each graph g.

$$r_g = \max_{i=1}^{N} x_i^L, \tag{5.12}$$

where x_i^L is the output of the L^{th} GCN layer for the i^{th} node. Following the readout layer, two linear layers are applied to produce the final classification with output dimensions $H/2$ and 2 (number of classes), respectively. Two linear layers were used to allow for further refining of the graph embedding before outputting the predicted class probabilities.

Additionally, in order to improve the generalisability and reduce the risk of overfitting, dropout layers are utilised (5.1A). Briefly, the dropout layer randomly zeroes elements of the input tensor with p probability drawn from a binomial distribution, where p is a hyper-parameter. A dropout is applied to the graph embeddings, i.e. after the readout layer and after the first linear layer. Furthermore, an edge dropout is implemented, which randomly removes edges from the input graph. The inclusion of the edge dropout in the model is controlled by a hyper-parameter.

In summary, the GNN used in this study has several hyper-parameters, as shown in Table 5.1, which control (1) the model architecture, (2) the form of input data, and (3) the training process to prevent overfitting. In particular, (1) is enabled by

the number of GCN layers (N-GCN) and the inclusion of DropEdge; (2) is enabled by frequency band and edge filter; and finally, (3) is enabled by dropout probability (drop-p), learning rate, gamma and batch size.

5.2.4 Baseline Models

In order to enable a fair assessment of the advantages of using graph-based learning (i.e. the GNN), four baseline classifiers are trained and compared. These baseline models utilise the same graph-structured input data extracted using different FC measures, frequency bands and edge filters, and the same evaluation process. Thus, we argue this to be a fair comparison of models.

The three selected baseline models are based on previously used classifier strategies for learning on FC brain graphs: SVM trained on node strength (SVM-NS) [202], SVM trained on vectorised adjacency matrix (SVM-AM) [197], and CNN trained on image of adjacency matrix [217, 169]. Additionally, we train a MLP on the flattened node feature matrix that was previously used to train the GNN models.

Support Vector Machine Baseline Models

The SVM-NS and SVM-AM are both trained using an SVM classifier. SVM has only one hyper-parameter, namely the cost, as shown in Table 5.1. Additionally, in order to select an appropriate kernel for SVM, we include two kinds of kernels as hyper-parameters: radial and polynomial (up to 3^{rd} order). Both of the SVM-based baseline models are trained on manually extracted features. All features are first normalised to zero mean and unit standard deviation.

The SVM-NS is trained on node strengths (Figure 5.1B). Node strength is defined as the sum of edge weights of one node and can be interpreted as a measure of node importance. Thus, each brain graph is represented by an 23-dimensional feature vector $NS = (ns_1, ns_2, ..., ns_N)$, where N is the number of nodes ($N = 23$).

The SVM-AM is trained on vectorised weighted adjacency matrices (Figure 5.1D). As we use only undirected FC measures, the $N \times N$ adjacency matrix of a brain graph is symmetric. Thus, we can use the upper triangular matrix only and flatten it to form a 253-dimensional feature vector ($N \times (N-1)/2$). Principal component analysis (PCA) is optionally employed for dimensionality reduction with the number of components selected, such that 95% of the variance is captured. A hyper-parameter controls the inclusion of the PCA step.

Convolutional Neural Network

CNN classifiers are trained on the weighted adjacency matrices of the brain graphs. As the adjacency matrix is a square matrix, it is simple to convert it to an image on which a CNN can be trained.

The CNN architecture consists of two convolutional blocks and a final classifier, as shown in Figure 5.1C. Each convolution block contains two convolutional layers (stride = 3), followed by a maximum pooling layer and a dropout layer. The final classifier consists of two linear layers with a dropout between them. We created several hyper-parameters to control the CNN. The number of convolutional filters within each block is controlled by the Conv1 and Conv2 hyper-parameters. Similarly, the hidden size of the linear layers is controlled by the Linear-hidden hyper-parameter. Additionally, there are hyper-parameters controlling the dropout probability, the choice of the activation function (ReLU or Tanh), and the batch size as shown in Table 5.1.

Multilayer Perceptron

MLP classifiers are trained using the flattened node feature matrix $F \in \mathbb{R}^{N \times D}$, where D is the PSD computed over the range 1-100 Hz. Thus the entry F_{ij} corresponds to PSD of the i^{th} node at frequency j. The MLP is thus trained on the input used to train the GNN models, but without leveraging the topological information provided by the FC graph. The MLP architecture is controlled by the following hyper-parameters: N-Linear (number of layers), Linear-hidden (hidden size). Additionally, there are hyper-parameters controlling the dropout probability, the choice of the activation function (ReLU or Tanh), and the batch size as shown in Table 5.1.

5.2.5 Model Evaluation and Implementation

The EEG preprocessing, brain graph construction, and model evaluation are implemented in R 4.1.2 [213] using in-house scripts, and caret [153] for SVM training. The training of CNN and GNN classifiers is implemented using PyTorch 1.10 [205] and PyTorch-Geometric 2.0.2 [89].

The models are trained and evaluated based on repeated 20-fold cross-validation (CV). A 5-times repeated CV is used in order to identify the best combination of hyper-parameters for all models and FC measures. The folds used for CV are created, such that samples from the same subject are kept within a single fold in order to prevent information leakage. We use a smaller number of repetitions in order to reduce the

computational cost of training CNN and GNN models. Hyper-parameter values are selected using random optimisation, where the values of all hyper-parameters are selected randomly. 200 iterations of random optimisation are performed for each combination of FC measure and model type. The hyper-parameters of all three model types and their possible values are summarised in Table 5.1.

The best-performing models are selected using the area under the sensitivity-specificity curve (AUC), i.e. one model per each combination of FC measure and model type. In order to assess the stability of the selected models, 50 times repeated CV is performed. The performance errors are computed using the maximum difference between the mean and 5^{th} and 95^{th} quantiles. This approach does not assume a normal distribution and results in conservative error estimates.

The CNN and GNN models are trained using an Adam optimiser with an exponential learning rate decay (controlled by the gamma hyper-parameter) and cross-entropy loss function. The models are trained for 300 epochs with an early stopping after 15 epochs if the loss stops decreasing.

5.3 Results

Brain graphs were inferred for each 3-second-long EEG segment by using several commonly used FC measures, which aim to quantify both the linear and nonlinear coupling between pairs of brain signals. The brain graphs were then used as an input to train the GNN brain-graph classifier. Moreover, four baseline models were trained on these brain graphs in order to demonstrate which type of classifier performs the best. AUC is used to select the best model.

Table 5.2 reports the AUC values and the 95% confidence intervals of the SVM-NS, SMV-AM and CNN baseline models and GNN across the 8 FC measures. Note that the MLP baseline is not included here, since it does not utilise the FC brain graphs. Additionally, the performance of the baseline GNN using Euclidean distance between spatial positions of EEG (GNN-euclid) is reported in Table 5.2 as well. The hyper-parameter values of the best models from their respective categories are reported in Table 5.4. The averaged sensitivity-specificity curves of these models are shown in Figure 5.2.

All baseline models perform worse than all of the GNN models across all FC measures as shown in Table 5.2. Even the best baseline model, MLP (AUC=0.95), achieves lower performance than the worst GNN model, GNN-euclid (AUC=0.978).

Table 5.2: AUC of GNN, SVM-NS, SVM-AM and CNN models across different FC measures measured by 50-repeated 20-fold cross-validation. The 'euclid' entry refers to the baseline GNN model with a fixed graph structure based on the spatial distance of EEG electrodes.

FC	GNN	SVM-NS	SVM-AM	CNN
AEC	**0.984 ±0.002**	0.75±0.022	0.734±0.01	0.886±0.019
COH	0.982±0.002	0.773±0.007	0.784±0.008	0.901±0.014
PCC	0.982±0.003	0.764±0.008	0.773±0.008	0.887±0.014
euclid	0.978±0.004	✗	✗	✗
iCOH	**0.984 ±0.002**	0.656±0.017	0.648±0.014	0.876±0.01
MI	0.981±0.002	**0.807 ±0.008**	0.779±0.013	**0.924 ±0.015**
PLI	0.982±0.005	0.761±0.057	0.603±0.036	0.893±0.015
PLV	0.982±0.003	0.766±0.008	**0.793 ±0.007**	0.9±0.014
wPLI	**0.984 ±0.003**	0.66±0.069	0.637±0.024	0.869±0.016

Table 5.3: Detailed performance metrics of best-performing models (selected based on AUC) of each model type.

	AUC	Accuracy	Sensitivity	Specificity
GNN (AEC)	0.984±0.002	91.996%±0.41	97.366%±0.941	86.716%±1.013
GNN-euclid	0.978±0.004	91.147%±1.278	93.678%±2.46	88.658%±3.497
CNN (MI)	0.924±0.015	84.689%±2.233	86.212%±3.6	83.192%±4.613
SVM-NS (MI)	0.807±0.008	73.924%±0.852	73.494%±0.926	74.367%±0.934
SVM-AM (PLV)	0.793±0.007	72.929%±0.6	72.123%±0.673	73.799%±1.064
MLP	0.953±0.007	84.97%±1.93	82.77%±2.31	87.13%±2.88

From Table 5.2, we can also see that the GNN models trained using FC-based brain graphs perform better than GNN-euclid, which was trained using a static graph structure.

Furthermore, we report the effect of frequency bands and edge filtering methods on the performance of the trained models in the supplementary materials. Figure S3 and tables S1-S3 report these effects of frequency bands. Figure S4 and Tables S4-S6 report these effects of edge filtering methods.

5.4 Discussion

We trained GNN models over several commonly used FC measures. For comparison, we trained four baseline models. The results suggest that the GNN outperforms all baseline models across all FC measures (Table 5.2). Moreover, neural-network-based models (GNN, CNN and MLP), which perform automatic feature extraction, perform

decisively better than the classical machine learning approaches (SVM-AM and SVM-NS) that rely on manually engineered features.

We argue that the relatively low performance of the machine learning approaches is caused by the inability to remove noise-contaminated information from the input features. This is likely exacerbated by the lack of false positives control during the brain graph inference, which would limit the number of edges caused by spurious coupling. We suggest that the neural network-based models can solve this issue by using weight regularisation and dropout layers, designed to learn generalisable features insensitive to noise.

It could be argued that the GNN models perform better than CNN and MLP because they are trained using two input information sources, i.e. the FC weighted brain graph and the node feature matrix with power spectral density. This is a unique property of GNN as it can aggregate information from both inputs. Moreover, to the best of our knowledge, GNN is the only model architecture that can process these two inputs simultaneously.

The CNN and MLP baseline models offer an interesting comparison to the GNN since each is trained using one of the two input information sources. The CNN and MLP baselines show the individual predictive power of the FC-based brain graph and node feature matrix, respectively. The results suggest that the node feature matrix provides a slightly better source of information in the classification task (Table 5.3). However, GNN performs significantly better, and we argue that the comparison with the CNN and MLP baselines highlights the power of GNN in brain graph classification.

The relatively poor performance of CNN also demonstrates the shortcomings of treating the adjacency matrix of a brain graph as an image. Each pixel of an image has an equal number of neighbouring pixels, and the content of the image depends on the specific spatial ordering of its pixels. Therefore, convolution can be applied to patches of pixels to extract features automatically. This assumption is invalid for a graph where each node can be connected to an arbitrary number of neighbours and no meaningful ordering of nodes exists. In contrast, graph convolution generalises the convolution to solve this issue efficiently by utilising order invariant operations to aggregate information from neighbouring nodes.

Moreover, the hyper-parameter optimisation has identified a GNN model with two graph convolutional layers as the optimal GNN architecture (Table 5.4). This means that the GNN aggregates information not only from the nodes connected by an edge directly (i.e., the 1-hop neighbours) but also from the 2-hop neighbours. This suggests

the importance of global graph properties in diagnosing AD accurately, in addition to the local properties, which could likely be learned with a single layer. This is in line with the reported loss of small-world properties of AD brain graphs [247, 136, 277, 263].

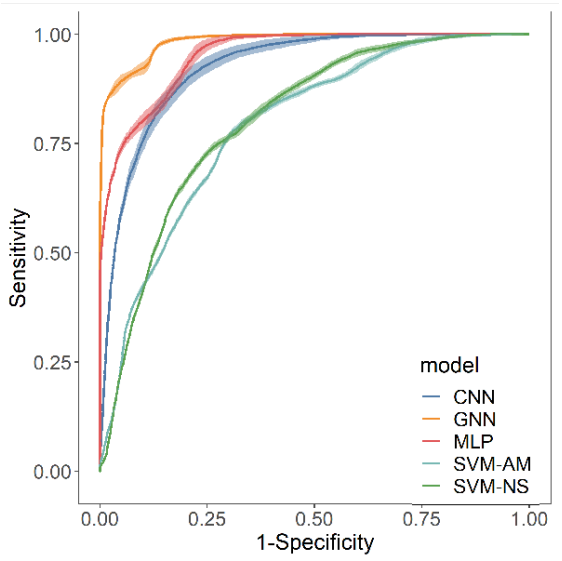

Figure 5.2: Averaged Sensitivity-Specificity curves of the best models of their respective categories with 95% confidence intervals (ribbon).

Next, the results demonstrate that the FC-based GNNs also outperform the GNN-euclid model, which utilises a static graph structure (Table 5.2). This suggests that it is preferable to utilise FC-based brain graphs rather than the distance-based static graphs previously used for EEG-GNN tasks [77, 269]. However, it seems that no FC measure offers clearly superior performance compared to the others. Thus, we suggest that future studies need to carefully consider which FC measure to use based on the type of brain coupling they might wish to focus on. However, we do not claim that the brain graphs inferred from various FC measures are necessarily similar from a graph-theoretic perspective. This is supported by the performance differences of the baseline models where some of the FC measures, such as MI, perform consistently well.

Surprisingly, the GNN-euclid model achieves relatively high accuracy despite utilising a fixed graph structure (Table 5.3). The Euclidean brain graph structure highlights the spatially local relationships between the EEG channels. In contrast, long-range edges have only a low weight. Therefore, we argue that the Euclidean brain graph biases the GNN model to learn local graph features predominantly. On the other hand, the FC-based brain graphs may contain both local and long-range relationships. Previous research suggests that AD-related differences are observed in long-range pathways and global graph properties [13, 247, 277]. In our opinion, the FC-based GNNs outperform GNN-euclid since they can better capture both the local and global differences on the graph level.

To investigate the differences between FC measures on the graph level further, we compute an average adjacency matrix for each FC measure across both groups and frequency bands (Figure S1). In Figure 5.3, we show these matrices for α and θ

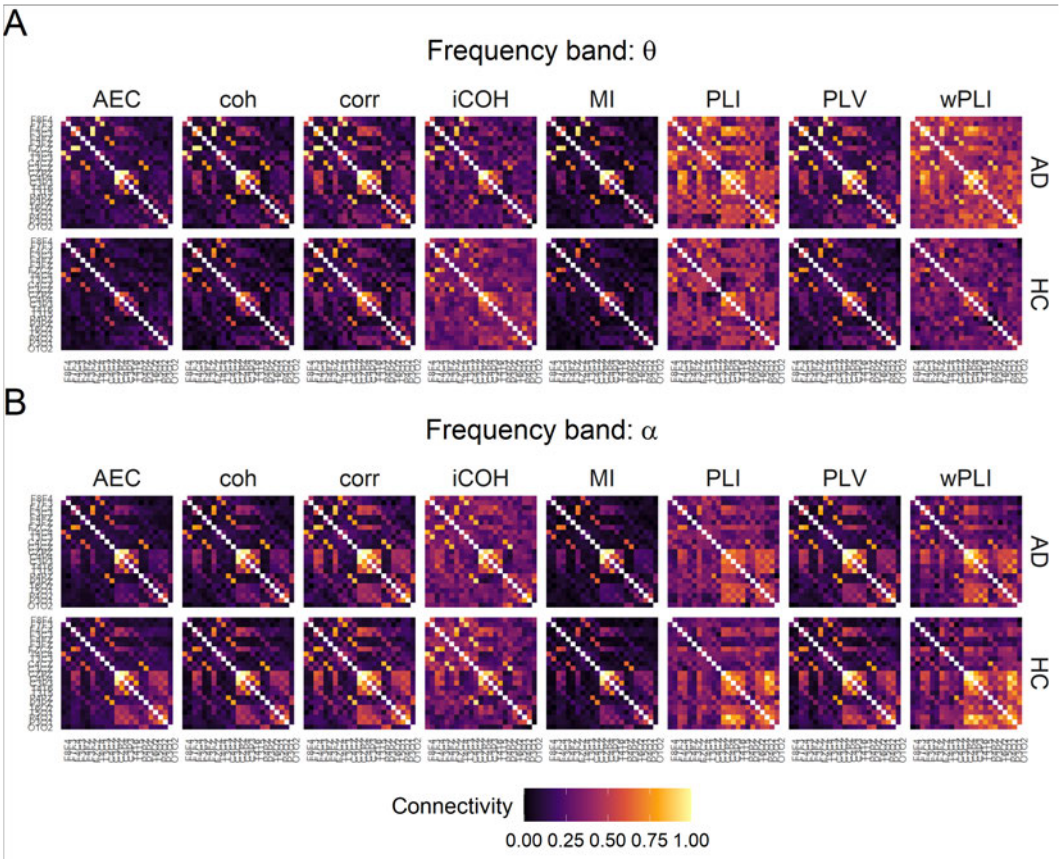

Figure 5.3: Averaged adjacency matrices of AD and HC cases measured with various functional connectivity measures in A) θ (best in CNN, SVM-NS and SVM-AM models), and B) α (best in GNN model) frequency bands.

frequency bands as these are utilised by the best performing models (Table 5.4). The brain graphs are relatively similar across the FC measures. In the θ band, increased connectivity can be observed in AD compared to HC. In contrast, the connectivity seems to be decreased in AD in the α band. These differences are well documented in the literature [68, 267, 13].

Interestingly, all FC measures detect a well-defined cluster containing mostly parietal and occipital EEG channels. The strength of this cluster distinguishes AD from HC consistently across FC measures. We speculate that this cluster contributes most of the predictive information for the classification models. However, since the GNN architecture is a block-box model, it would be difficult to confirm our speculation.

Next, the optimised model architectures suggest that using edge-filtering and filtering the EEG signal within a frequency band improve the model performance. A detailed report of differences between the edge-filtering methods and frequency bands

Table 5.4: Hyper-parameter values of the best performing GNN, SVM-NS, SVM-AM, CNN and MLP measured by AUC.

Hyper-parameter	GNN	SVM-NS	SVM-AM	CNN	MLP
FC measure	AEC	MI	PLV	MI	
Batch size	32			64	32
Learning rate	0.001			0.001	0.01
GCN hidden	1024				
N GCN	2				
N Linear					4
Conv1 hidden				128	
Conv2 hidden				64	
Linear hidden				96	4096
Activation/Kernel		Radial	Poly (1^{st})	ReLU	ReLU
DropEdge	TRUE				
Drop rate	0.9			0.1	0.05
Frequency band	alpha	theta	theta	theta	
Edge filter	Top-20%	MST-3	full	full	
Gamma	0.9			0.9	0.95

across the FC measures and model types is included in the supplements (Figures S3-S4 and Tables S1-S6). Briefly, the best GNN model utilises the α frequency band, and CNN, SVM-AM and SVM-NS utilise the θ frequency band (Table 5.4), suggesting that frequency-centred brain graphs should be preferred over the full-frequency-range brain graphs. The selection of these frequency bands is not surprising, as they are both well-known to be altered in patients with AD [68, 267, 13]. In contrast, the effect of edge-filtering is not so apparent as only the GNN and SVM-NS models use edge-filtering with top-20% and MST-3, respectively. On the other hand, CNN and SVM-AM use unfiltered brain graphs. We expect that a sparse graph is preferable for GNN since there are fewer messages to aggregate while updating the node embeddings. These messages are also less likely to be a product of false-positive brain interaction, thus leading to better node and graph embeddings.

Furthermore, it is worth noting that although GNN accepts two inputs, the relative contribution of each input information is largely unclear. The results suggest that the node feature matrix should contribute slightly more since the MLP baseline outperforms the CNN (Table 5.3). It could be argued that the GNN uses only the topological information provided by the graph structure to enable message-passing, but the FC is not fully reflected in the node embeddings and graph embeddings, by extension. Nev-

ertheless, we believe that the FC information is utilised to some extent by the GNNs since these models perform better than the GNN-euclid, which arguably utilises merely the topological information (Table 5.2). However, the extent to which the information provided by the FC measures is contained within the learned graph embedding remains unclear. One can merely speculate without introducing an additional mechanism into the GNN architecture, which is beyond the scope of this chapter.

Finally, the GNN architecture utilised in this study is relatively simple as one of the simplest GCNs was used, and the readout layer merely computes the maximum of the node embeddings. Previous EEG-GNN applications demonstrated the advantages of using more complex graph convolutional layers and edge pooling mechanisms [77]. We hypothesise that exploiting a learnable edge filtering mechanism akin to that utilised by Zhong et al. [311] might improve the classification compared to the edge filtering methods used in this study.

5.5 Conclusion

GNN is an effective model for learning on graph-structured data, such as FC-EEG brain graphs. However, in the absence of consent about the ideal FC measure for estimating EEG brain graphs, the effect of an FC measure on the performance of GNN classifiers is unclear. In this chapter, we have selected eight common FC measures to investigate this effect.

First, we demonstrated that GNN models are superior to classical machine learning and CNN models for brain graph classification. Unfortunately, the utilised GNN architecture is a black-box model. Thus, future work should focus on implementing interpretable GNN architectures that achieve similar performance but additionally offer interpretability, such as which nodes, i.e. brain regions, drive the prediction. Besides providing an opportunity for experts to validate such models, interpretable predictions might also serve in the development of GNN-informed targeted treatment.

Finally, we showed that utilising FC measures to define the brain graph results in improved performance of GNN models compared to a fixed electrode-distance-based graph structure. While using an FC measure improves the performance, no concrete FC measure can be recommended as the ideal choice. Thus, in future research, the choice of suitable FC measure should be carefully evaluated in the context of the given research question. Alternatively, focusing on fusion methods might lead to developing a novel composite measure of FC.

5.6 Chapter Summary

This chapter systematically evaluates various FC methods in inferring EEG brain graphs for training GNN to classify AD patients. It compares GNNs utilising FC-based brain graphs with baseline models, demonstrating the superior performance of GNN models.

The chapter emphasises that GNN, leveraging information from both FC brain graphs and node feature matrices, outperforms other models, highlighting the unique ability of GNNs to process these inputs simultaneously, unlike other DL and ML models.

The results indicate that FC-based graphs perform better than static distance graphs, suggesting that GNNs can effectively leverage the information about FC to improve predictions. Despite these successes, the choice of FC measure remains ambiguous as none of the testes FC measures perform significantly better than all others.

Additionally, the chapter explores the impact of frequency bands and edge filtering methods on model performance. Frequency-band-specific and sparse brain graphs are consistently favoured over full-frequency range and fully connected graphs.

This chapter focused on relatively simple GNN architectures to highlight the general strengths of GNNs and to fairly test the effect of FC measures. However, the resulting models do not offer any explainability, a crucial property for predictive modelling in health-related settings. Thus, future work needs to emphasise explainability to allow for a clear interpretation of the predicted diagnosis outcome.

Chapter 6

Adaptive Gated Graph Convolutional Network for Explainable Diagnosis

6.1 Introduction

[1]The brain is a complex, densely connected system that operates across multiple spatial and temporal scales. Neurological diseases, such as AD, can alter the connectivity of the brain and thus disrupt brain function [76, 72, 207, 150].

Multiple studies propose GNN-based architectures to process EEG. However, GNN methods for EEG-based diagnosis of AD are limited [142, 229]. GNN-EEG implementations often include several steps: (1) input construction, i.e. graph structure and node features; (2) GNN encoder to learn node embeddings; and (3) aggregation of node embeddings to a graph embedding, which can be used in the final classification step.

There are various approaches to realise the graph construction in step (1). Node features are commonly defined as EEG time-series signal [229, 166, 8, 163], or a statistical summary of the signal in the time domain [214, 249], the frequency domain [142, 244], or the differential entropy [166, 291, 53, 132, 301, 244]. Based on NW literature, many approaches define the brain graph using FC measures [142, 229, 178, 48,

[1]The content presented in this chapter has been published in *Dominik Klepl, Fei He, Min Wu, Daniel J. Blackburn, and Ptolemaios Sarrigiannis. Adaptive Gated Graph Convolutional Network for Explainable Diagnosis of Alzheimer's Disease Using EEG Data.* IEEE Transactions on Neural Systems and Rehabilitation Engineering, *31:3978–3987, 2023. ISSN 1558-0210. doi: 10.1109/TNSRE.2023.3321634*

214, 249, 166, 163]. The graph structure can also be based on the distance between EEG electrodes [249, 291, 53]. However, such an approach largely ignores brain connectivity information. Alternatively, the brain graph can be automatically learned by the model, either as a learnable mask shared across samples [171, 166, 244] or by pairwise node feature distance minimisation regularised by an additional graph loss function [311, 132, 301]. While such approaches are flexible and should converge to an optimal graph structure with respect to a given learning task, the learned brain graph might not be representative of the underlying brain connectivity, i.e. such a graph structure might overestimate the strength of the task-relevant edges compared to the underlying connectivity. In this chapter, an adaptive graph learning mechanism is proposed based on node feature enhancement via CNN and subsequent graph construction. This is achieved using a correlation similarity measure of power spectral density and sparsified via k nearest neighbours (KNN) edge selection. Thus, it combines the strength of the FC-based and automated graph learning methods. Such a combination overcomes the limitations of fully learnable graphs described above since the correlation computation is ultimately detached from the classification task. However, it should be noted that the adaptively learned graph structure reflects brain region similarity rather than a functional relationship assumed by classical FC measures.

The design of GNN encoders in step (2) for EEG applications has been mainly limited to simple architectures, such as the ChebConv [48, 8, 249, 291, 53, 132, 163], and simple GCN [142, 171, 307, 166, 244, 311]. However, we hypothesise that such node embedding updating mechanisms are not optimal for EEG tasks. These graph convolutions update node embeddings by summing the initial embedding and the aggregated messages from the neighbouring nodes. Such updating implies that information from different scales contributes equally to the final node embeddings, hence graph embeddings as well. While brain disruptions caused by AD occur across multiple spatial scales, their predictive power is likely different. Therefore, a gating mechanism is crucial for filtering and weighting the information collected across different scales. We propose to adopt the gated graph convolution [175] to address this issue.

Finally, we implement the aggregation of node embeddings in step (3) by adopting the adaptive structure-aware pooling (ASAP) node pooling mechanism [215] to first learn the most important clusters of nodes, which are in turn concatenated to form the graph embedding. This is in contrast to the previous approaches that do not use any node pooling and form graph embeddings via simple element-wise readout layers [142, 289, 214, 166, 307, 178, 311] or concatenating all nodes of the graph [229, 48].

Other node pooling approaches were tested for EEG applications [77, 289]. In contrast to ASAP pooling, these approaches pool the graph by selecting a specified number of nodes without considering their local context within the graph. Therefore, important information might be lost due to such node pooling.

In this chapter, we propose a novel GNN model for explainable AD classification, which can adaptively enhance node features and dynamically construct brain graph structures as shown in Figure 6.1. The learned brain graphs can then be used for the interpretation of predictions. Moreover, a clustering-based node pooling mechanism is adopted to coarsen the brain graph, thus localising the brain regions that contribute to the predictions. Finally, we conduct extensive ablation and parameter sensitivity experiments to elucidate the importance of the individual blocks within the proposed model architecture.

6.2 Methods

The proposed adaptive gated graph convolutional network (AGGCN) model consists of three blocks: a graph learning module, a GNN encoder and a classifier. The graph learning module receives a node feature matrix as input, enhances it using a 1D-CNN and learns the brain graph structure. The GNN encoder then uses the output of the graph learning module as input, i.e. a featured, weighted, undirected graph. The encoder generates a graph embedding used by the classifier to output the predicted probabilities.

6.2.1 EEG Pre-processing

As a neurophysiologist confirmed the EEG signal to be artefact-free, we did not further clean the signals. The signals are filtered using a band-pass Butterworth filter to a range of 0.5 Hz and 45 Hz and down-sampled to 200 Hz. Finally, 1-second long windows with 50% overlap are created to increase the sample size.

6.2.2 Node Feature and Graph Learning

The node features are defined as power spectral density computed from 1-second long EEG signals with 1 Hz increments from 1 to 45 Hz. Hence, the input is a node feature matrix $\mathbf{X} \in \mathbb{R}^{N \times D_{in}}$, $D_{in} = 45$.

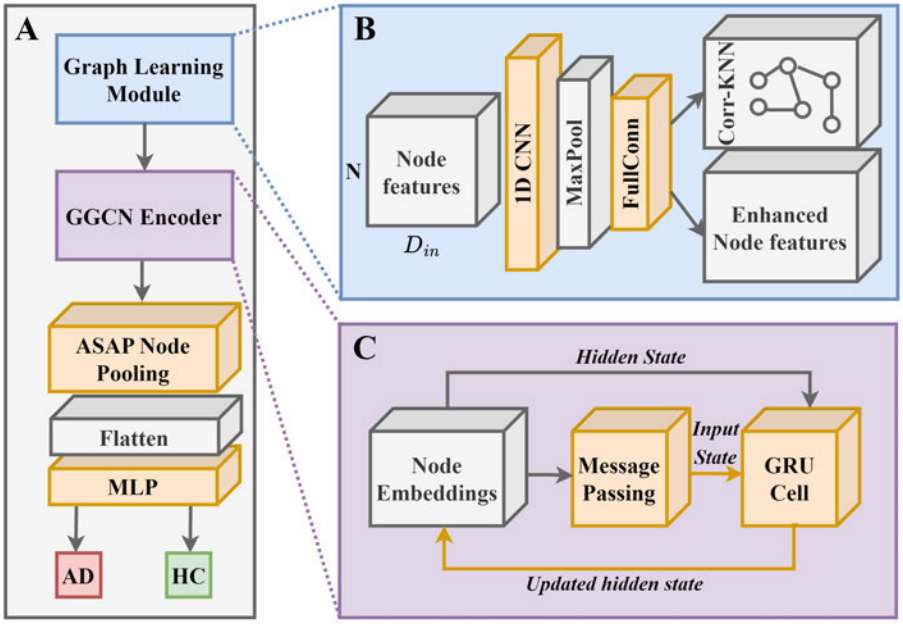

Figure 6.1: The architecture of the proposed adaptive gated graph convolutional network. A) The proposed model consists of a graph learning module, gated graph convolutional neural network (GGCN) encoder, ASAP node pooling module, and a three-layer MLP outputting the predicted probabilities. B) Graph learning module takes a $N \times D_{in}$ node feature matrix as input. Node features are defined as power spectral density from 1 to 45 Hz ($D_{in} = 45$) computed for all N EEG electrodes ($N = 23$). Then, a 1D CNN enhances them. The brain graph structure is then constructed as a correlation graph between the outputs from the 1D CNN and made sparse by a k-nearest-neighbour edge selection (Corr-KNN). C) The enhanced node features and the learned graph structure are then passed to a GGCN encoder. GGCN applies message passing and gated recurrent unit (GRU) recursively over R iterations.

The input is then passed to a CNN with batch normalisation, L_{CNN} 1D convolutional layers and a maximum pooling with kernel size 2 and step size 2. The output is flattened and fed to a fully connected layer with hidden size h_{CNN} and batch normalisation. This neural network outputs a matrix of enhanced node features $\mathbf{X}' \in \mathbb{R}^{N \times D_{h_{CNN}}}$.

A graph structure is then inferred from the enhanced node features by computing the absolute value of Pearson's correlation for each pair of nodes. Thus, a unique graph structure is learned for each input sample and is defined by an adjacency matrix $\mathbf{A} \in \mathbb{R}^{N \times N}$ with $N = 23$ being the number of EEG channels. In order to produce sparse graphs, the k-nearest-neighbours algorithm is utilised. This means that the k strongest edges are preserved for each node.

This proposed graph learning module has multiple hyperparameters that control its architecture. Namely, these are the number of convolutional layers L_{CNN}, the kernel size (which is equal to the step size), the number of filters, the hidden size h_{CNN}, the dropout rate $drop_{CNN}$ and the k_{KNN} parameter that controls the graph sparsity.

6.2.3 Graph Neural Network Encoder and Classifier

A graph convolution extends the classical convolution from the Euclidean domain to the graph domain. The input graph is given by $G = (\mathbf{N}, \mathbf{A}, \mathbf{X}')$ where N is the set of nodes, $\mathbf{A}$ is the learned graph, and $\mathbf{X}'$ is the enhanced node feature matrix. A simple graph convolution is defined by the message passing mechanism wherein the node embedding of node i is learned by aggregating information from its 1-hop neighbourhood, i.e. nodes connected with an edge, as follows:

$$\mathbf{x_i^{l+1}} = \mathbf{x_i^l} + \mathbf{\Theta} \sum_{j \in N(i)} e_{ij} \mathbf{x_j^l}, \tag{6.1}$$

where $\mathbf{x_i^l}$ are the node features of node i at the l^{th} layer, $\mathbf{x_i^0}$ is the i^{th} row of the input node feature matrix $\mathbf{X}$, and $\mathbf{\Theta}$ is a learnable linear transformation. $N(i)$ and e_{ij} are the neighbourhood of node i and the edge weight connecting nodes i and j given by the adjacency matrix $\mathbf{A}$, respectively. Stacking L graph convolutional layers then means aggregating information iteratively from 1-hop to L-hop neighbourhoods, thus gradually going from local to global information about the graph.

Note that the aggregated message is added to the initial node embedding $\mathbf{x_i^l}$. Thus, the entire information collected from each L-hop neighbourhood is always fully integrated into the node embedding. However, information might be distributed unequally across spatial scales in brain graphs. The GGCN [175] addresses this problem by introducing a mechanism to decide what information should be retained at each scale selectively:

$$\mathbf{m_i^{(r+1)}} = \sum_{j \in N(i)} e_{ji} \cdot \mathbf{\Theta^{r+1}} \cdot \mathbf{x_j^{(r)}}, \tag{6.2}$$

$$\mathbf{x_i^{(r+1)}} = \text{GRU}(\mathbf{m_i^{(r+1)}}, \mathbf{x_i^{(r)}}), \tag{6.3}$$

where $\mathbf{m_i}$ are the aggregated messages, $\sum$ is the aggregation function, $\mathbf{\Theta^r}$ is a learnable matrix for iteration r, which maps the node features from shape $[1, D_{h_{CNN}}]$ to $[1, D_{h_{GNN}}]$, and GRU is the gated recurrent unit [56]. Briefly, a GRU is a recurrent

neural network layer with update, reset, and input gates that allow the network to recursively update or forget information about the input. The node embeddings are learned recursively up to R iterations with a shared GRU gate, which is equivalent to stacking R GCN layers.

The node embeddings are then passed through an activation function and a batch normalisation layer. Finally, the node embeddings are passed to the node pooling module. The hyperparameters of the proposed encoder are the number of iterations R, the hidden size h_{GNN}, the activation function, the aggregation function and the dropout rate $drop_{GNN}$ applied after the encoder.

Node Pooling

After learning the node embeddings, the model learns a coarsened graph using the ASAP pooling mechanism [215]. This pooling first learns N clusters, each centred at one node, also named ego-graphs. The membership of node j in the ego-cluster centred at node i is given by the $\mathbf{S_{ij}}$ matrix. Note that this is a soft-cluster assignment matrix; thus, each node can belong to multiple clusters with varying membership strengths. The clusters are learned as follows:

$$S_{ij} = a_{ij}, \tag{6.4}$$

$$a_{ij} = \text{softmax}\left(\theta^{\mathrm{T}}\sigma\left(\mathbf{\Theta}\mathbf{x_i^m} \| \mathbf{x_j}\right)\right), \tag{6.5}$$

$$\mathbf{x_i^m} = \max_{j \in N(i)} \mathbf{x_j}, \tag{6.6}$$

where a_{ij} is the attention score and the membership strength, θ and $\mathbf{\Theta}$ are learnable vector and matrix, respectively. σ is the LeakyReLU activation function, and $\mathbf{x_i^m}$ is the master query representing the initial cluster embedding. The attention scores are also subject to a dropout probability $drop_{pool}$. The final cluster embedding is then calculated as an attention-weighted sum, which is additionally weighted by the cluster score ϕ_i:

$$\mathbf{x_i^c} = \phi_i \sum_{j \in N(i)} a_{ij}\mathbf{x_j}, \tag{6.7}$$

where the cluster score ϕ_i is computed by the local extremum graph convolution [215]:

$$\phi_i = \mathbf{\Theta_1} \cdot \mathbf{x_i} + \sum_{j \in N(i)} e_{ji} \cdot (\mathbf{\Theta_2}\mathbf{x_i} - \mathbf{\Theta_3}\mathbf{x_j}), \tag{6.8}$$

Table 6.1: Performance of the proposed AGGCN in EC, EO and combined (EC+EO) conditions.

Condition	Accuracy	AUC	Sensitivity	Specificity	F1
EC	89.1 ± 1.4	0.895 ± 0.016	92.95 ± 2.59	85.16 ± 2.45	89.7 ± 1.4
EO	85.56 ± 0.96	0.834 ± 0.015	90.88 ± 2.01	79.98 ± 1.47	86.55 ± 0.98
EC+EO	81.79 ± 1.26	0.82 ± 0.016	84.27 ± 2.19	79.22 ± 2.05	82.46 ± 1.27

which is designed to measure the relative importance of each cluster.

The cluster embedding $\mathbf{x_i^c}$ is then used to select the top k scoring clusters, which will be included in the coarsened graph:

$$\bar{i} = Top_k(\mathbf{X^c}), k \in [1, 2, ...N], \qquad \bar{\mathbf{S}} = \mathbf{S}(:, \bar{i}) \tag{6.9}$$

$$\mathbf{A^p} = \bar{\mathbf{S}}^{\mathrm{T}} \cdot \mathbf{A} \cdot \bar{\mathbf{S}}, \qquad \mathbf{X}^{\mathrm{p}} = \mathbf{X^c}(:, \bar{i}) \tag{6.10}$$

where Top_k is a function that returns the indices of clusters $\bar{i}$. $\bar{\mathbf{S}}$ and $\mathbf{X}^{\mathrm{p}}$ are the pruned soft-cluster assignment matrix and the pruned cluster embedding matrix, respectively, and $\mathbf{A^p}$ is the adjacency matrix of the coarsened graph.

The graph pooling module has the following hyperparameters: the size of the pooled graph k_{pool}, the dropout rate $drop_{pool}$ and the negative slope of the LeakyReLU activation.

Multilayer Perceptron Classifier

The cluster embedding matrix $\mathbf{X^p}$ of the coarsened graph returned by the node pooling module is flattened and fed to a MLP classifier. Specifically, a L_{MLP}-layer MLP with hidden size h_{MLP} is utilised with a block of batch normalisation, activation function, and dropout layers utilised between the fully connected layers. The final layer outputs a two-dimensional vector of log probabilities for each class.

The classifier has the following hyperparameters: the number of layers L_{MLP}, hidden size h_{MLP}, activation function and dropout rate $drop_{MLP}$.

6.2.4 Model Implementation and Evaluation

The proposed AGGCN model was implemented using PyTorch 1.10 [205], and PyTorch Geometric 2.0.2 [89] and trained on a laptop with Intel i7 CPU, 16 GB RAM and an NVIDIA RTX 2070 GPU.

The model is trained by minimising the cross-entropy loss. The model performance

is evaluated using repeated (30 times) 10-fold stratified group cross-validation (one-group = subject-identifier) and trained on the dataset collected during the eyes-closed condition. Since all participants have multiple samples, keeping all the samples from the same participant within the same fold is crucial to prevent information leakage. In order to prevent overfitting, another fold is utilised for validation to implement early-stopping and is used to optimise hyperparameters. Thus, in each iteration of the cross-validation, one fold is used as validation, one fold as testing, and the remaining eight folds form the training set.

A stochastic gradient descent optimiser and an exponential learning rate scheduler are used to train the model with a batch size of 128 for 200 epochs. If validation loss does not decrease for 15 epochs, the training is stopped early. Additionally, zero-mean Gaussian noise with standard deviation σ is added to the input during training with probability p_{noise} to improve the generalisability of the model. Eventually, the best-model was identified using the average cross-validated F1-score measured on the validation folds. The selected model was then retrained and tested on the dataset obtained during the eyes-open condition and the combined dataset from both conditions. The final results are then reported using the test folds only. The stability of the performance is assessed by computing the standard deviation of the samples collected over the 30-times repeated cross-validation.

Note that the hyperparameters of the proposed model are optimised using Bayesian optimisation. Ten warm-up random iterations were used to initialise the optimisation, followed by 200 optimisation iterations. The optimisation is evaluated only on the validation sets to prevent overfitting. Moreover, we carry out parameter-sensitivity experiments to verify the influence of a few key hyperparameters of the proposed model architecture. Specifically, these are the number of iterations of the GGCN encoder, the size of the pooled graphs, the sparsity of the learned graph and the choice of aggregation function of the GGCN encoder. Due to the computational cost of running these experiments, we reduce the number of repeats of the cross-validation from 30 to 5. The hyperparameters of the model are reported in Appendix C (Table C.2).

6.3 Results and Discussion

In this section, we report the experimental results of our AGGCN model. As illustrated in Table 6.1, our AGGCN has shown robust performance across all the conditions. Note that the best performance was achieved during the EC condition. This is likely because

with eyes closed, the ocular artefacts are minimised; thus, the underlying dynamics are easier to detect. The performance remains high even in the EO condition, suggesting that the proposed model can detect underlying patterns in both EC and EO conditions. However, the performance decreases significantly on the EC+EO combined dataset. We hypothesise that the patterns learned under the EC and EO conditions share relatively little information; thus, the EC+EO model performs significantly worse. We explore this further in section 6.3.3.

In addition, the hyperparameter values of the optimised model are reported in Appendix C (Table C.1).

6.3.1 Comparison with the Baselines

The proposed model was compared to seven baseline models proposed in the literature across the three conditions. The first baseline is the best-performing model from our previous work [142]. It is a GNN with two spatial graph convolutional layers, maximum readout and brain graph defined using the amplitude-envelope-correlation (AEC-GNN). The second baseline model is the spatio-temporal graph convolutional network (STGCN) that uses temporal convolutions and ChebConv layers and defines the brain graphs using wavelet coherence [229]. Then, two CNN-based models, PSD-CNN [118] and Wavelet-CNN [115], trained on PSD and wavelet transform, respectively, were used. Next, two traditional machine learning approaches were utilised: support vector machine trained on node degree computed from phase lag index graph (NS-SVM) [202], and a logistic regression trained on vectorised adjacency matrices obtained from coherence graphs across seven frequency bands (AM-SVM) [197]. Finally, we use an MLP model where the input is a flattened PSD node feature matrix [142] without using graph-domain information.

Table 6.2 shows the f1 scores of various models across different conditions. Note that all seven models were evaluated under the same setting (e.g. the same 1-second EEG window samples). We can observe that our proposed AGGCN outperforms the baselines across all conditions. Moreover, STGCN was originally evaluated using a cross-validation setup, which mixed samples from the same subject in their original paper.[229]. It is expected that its performance drops significantly when evaluated using stratified group cross-validation in our experiments.

Table 6.2: The F1 score and the number of trainable parameters of the baseline models and the proposed method across conditions. The best-performing model is highlighted in bold.

Model	EC	EO	EC+EO	No. of parameters
AEC-GNN [142]	81.61 ± 3.16	77.91 ± 1.1	76.74 ± 1.87	445,204
MLP [142]	82.01 ± 4.39	76.51 ± 3.34	77.47 ± 4.26	54,628,354
PSD-CNN [118]	88.15 ± 0.77	80.89 ± 1.45	79.51 ± 1.74	3,420,432
STGCN [229]	46.71 ± 8.58	44.34 ± 7.33	38.25 ± 17.16	662,754
Wavelet-CNN [115]	51.35 ± 5.61	57.52 ± 8.02	59.27 ± 6.44	46,755,208
AM-SVM [197]	86.3 ± 1.5	83.8 ± 1.3	80.31 ± 1.3	✘
NS-SVM [202]	55.93 ± 3.04	50.32 ± 3.36	52.9 ± 2.08	✘
Proposed	**89.7 ± 1.4**	**86.55 ± 0.98**	**82.46 ± 1.27**	2,208,861

6.3.2 Model Ablation Study

We perform ablation experiments to determine the contribution of each module of the proposed model. The following seven ablated variants of the proposed model were tested in our experiments.

- **A**: no node pooling;
- **B**: graph learning replaced with a fully connected graph;
- **C**: GGCN replaced with a R^{th}-order ChebConv ($R = 4$);
- **D**: variants A and B combined;
- **E**: variants A and C combined;
- **F**: variants B and C combined;
- **G**: variants A, B and C combined.

The ablation results in Figure 6.2 reveal that each of the proposed modules contributes significantly to the high performance of the proposed architecture. For variant A, we can observe that the contribution of the node pooling module is significant, albeit relatively small. However, this module reduces the number of parameters of the model and helps to produce explainable predictions (Figure 6.7 and Figure 6.8). Without the node pooling, the final MLP classifier would have $N \times h_{GNN} \times h_{MLP}$ parameters ($N = 23$), but node pooling reduces it to $k_{pool} \times h_{GNN} \times h_{MLP}$ ($k_{pool} = 3$). For variant B, it is not surprising that its performance decreases significantly as the graph

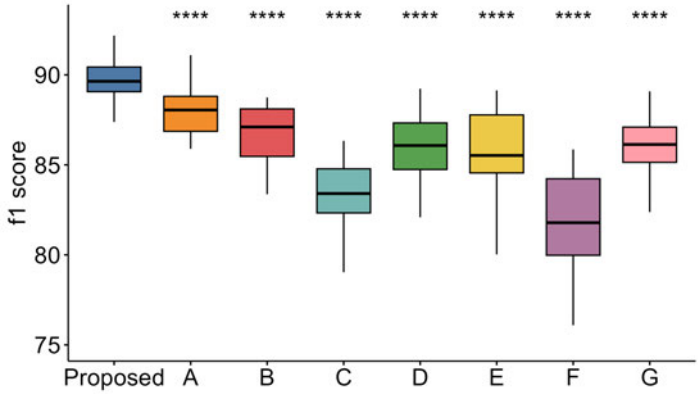

Figure 6.2: F1 scores of model variants. The asterisks report the p-value of a nonparametric Mann-Whitney U test measuring the difference between AGGCN and the ablated variants.

learning module is replaced with a fully connected graph. Thus, it cannot leverage graph-domain information except in the node pooling module.

Next, we demonstrate that the GGCN encoder improves performance significantly compared to a ChebConv encoder according to variant C. A ChebConv layer is similar to a GGCN in its iterative nature, i.e. ChebConv iteratively updates node embeddings by approximating the eigendecomposition of graph Laplacian. However, ChebConv does not have any gating mechanism, which means that information across scales contributes to the final embedding equally. Since all of the major modules of the proposed are shown to contribute to the final performance significantly, it is unsurprising that the rest of the ablated models with more than one of these modules perform significantly worse as well (Variants D-G in Figure 6.2). Note that some of the ablated models maintain a relatively low variance of performance. We speculate this is because the ablated models can still learn robust embeddings, but some of the information within the data remains inaccessible, which would be enabled by the removed module.

The parameter sensitivity experiments also support the optimal values of crucial hyperparameters of the proposed model (Appendix C, Figs C.1, C.2, C.3 and C.4). It is worth noting that the proposed architecture allows training relatively deep models (using up to eleven GGCN iterations) with only a minor performance decrease (Fig C.1). We can also observe that although the optimal values of these hyperparameters result in the best performance, the performance doesn't change much with adjacent values near the optima. This demonstrates that although the proposed model requires a relatively large number of hyperparameters to be determined, its performance remains robust with sub-optimal values, thus suggesting generalisability potential.

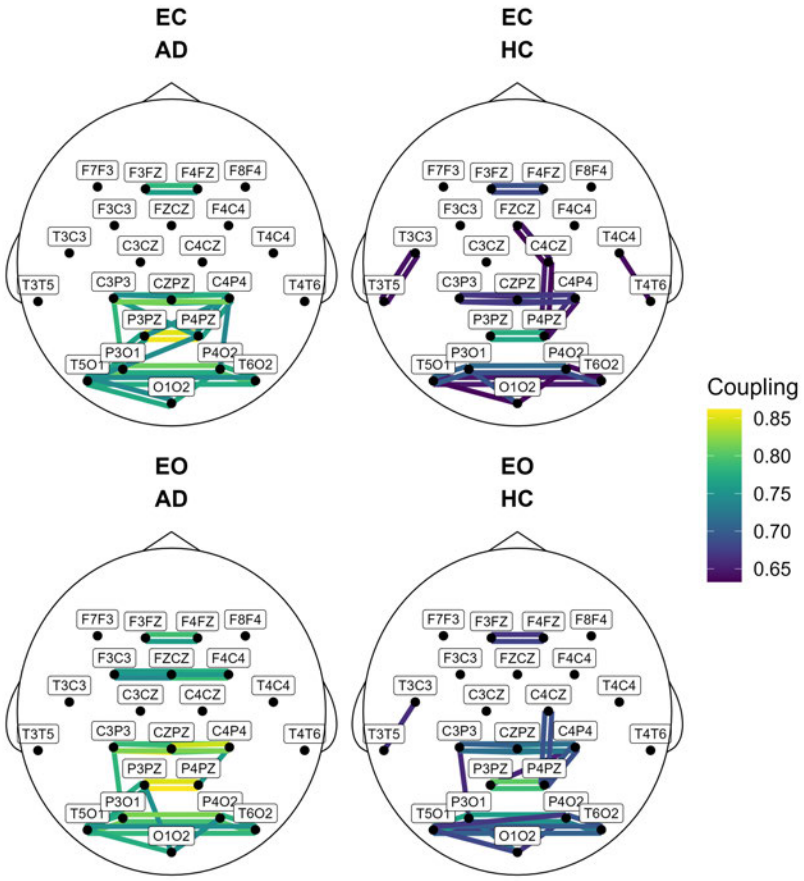

Figure 6.3: Top 30 strongest edges of the AGGCN-learned graphs of AD and HC cases in EC and EO conditions (average of all samples).

6.3.3 Explainability of AGGCN

The proposed model generates plausible and consistent explanations for its predictions. We generate multiple types of prediction explanations. Specifically, these are derived from the following: (1) graph learning, (2) node embedding and GGCN encoder, (3) node pooling, and (4) feature masking. Except for type (4), these explanations could be obtained for individual samples. However, we visualise the diagnosis-averaged explanations to explore the patterns learned by the proposed model.

Graph Learning

The graph learning module learns a clear difference between the AD and HC cases, as shown in Figure 6.3 (alternatively Figure C.5). The learned brain graphs show that AD-

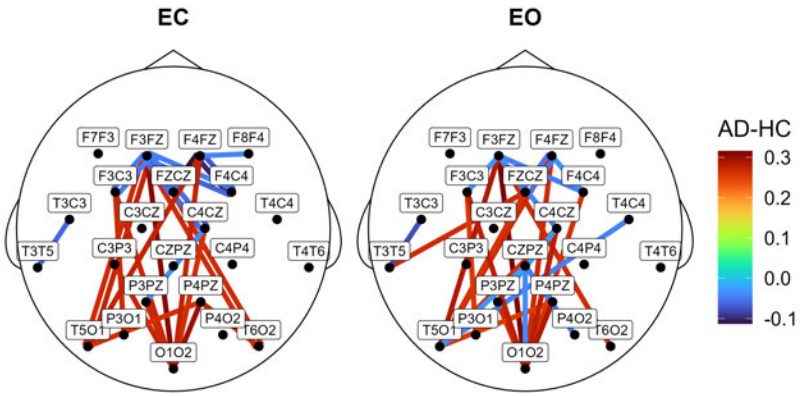

Figure 6.4: The differences between AGGCN-learned graphs for AD and HC cases in EC and EO conditions show the AD-related connectivity disruption. The average of all samples, the top 30 strongest edges were preserved. Values above zero indicate AD increase, while values below zero indicate AD decrease.

cases have increased connectivity overall, while HC graphs seem more sparse with few densely connected regions. A well-defined cluster of densely connected nodes is present in both groups within the centro-parietal and occipital regions and a few strong edges in the frontal and temporal regions. The locations of the strongest edges are consistent across conditions. Figure 6.4 then shows the top 30 edges, where the largest increase/decrease in coupling was observed in AD. AD seems to have increased coupling strength in long-distance edges, particularly between frontal and parietal/occipital regions. These increases are quite consistent between conditions. In contrast, AD cases have decreased coupling strength, mostly in local connections in the frontal (EC) and frontal and centro-parietal (EO) regions.

Additionally, we statistically compared the learned graph structures to determine differences between AD and HC cases across EC and EO conditions (Figure C.6)

Node Embeddings and GGCN

Another prediction explanation can be derived from the node embeddings obtained by the GGCN (Fig 6.5). In particular, we visualise the node embeddings obtained after four iterations of GGCN and compress them to 1D representation using principal component analysis (PCA) and extracting the first principal component. PCA is fitted for each condition separately. The node embeddings do not express a change

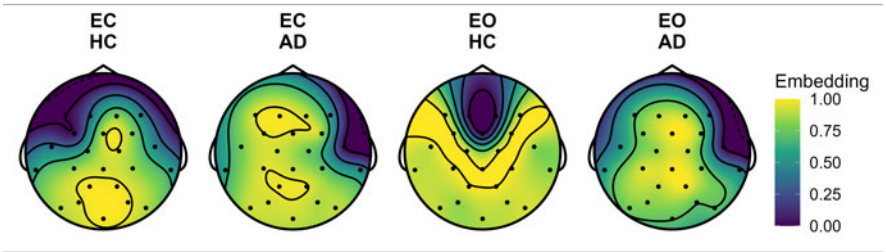

Figure 6.5: Averaged node embeddings across nodes expressed via the first component of PCA for AD and HC cases across EC and EO conditions. Note that embedding value does not suggest increased or decreased activity within a given area but rather the similarity of nodes.

in activity but rather a node similarity. Generally, the node embedding explanations show two large regions of similar embeddings. In EC, these are frontotemporal and centro-parietal regions, and right frontotemporal and the rest of the regions for HC and AD, respectively. The HC similarity region in the EO condition is reduced from frontotemporal to only the frontal region. In contrast, the AD similarity region expands from the right frontotemporal region to the left side. This further highlights the differences in learned patterns under the EC and EO conditions, thus explaining the reduced performance in the combined EC+EO condition.

Next, the role of the gating mechanism is elucidated by analysing the amount of information gathered at each scale, i.e. iteration of GGCN (Figure 6.6). We measure this by computing the average Euclidean distance between the initial and updated node embedding at each iteration, i.e. $\mathbf{x}_i^{(r)}$ and $\mathbf{m}_i^{(r+1)}$ in Eq. 6.3. For instance, a small distance means a small amount of information was gathered at that scale. Local information contributes highly to the node embeddings of the AD cases, and then the degree of contributions linearly decreases with increasing graph scale. The opposite pattern is observed for HC cases, where the later iterations influence the node embeddings. This highlights the degradation of global and distributed information caused by AD since the model can efficiently learn with fewer iterations, i.e. most information is obtained from the first three iterations.

Node Pooling Module

The node pooling mechanism can be exploited to derive two explanations. First, we analyse the frequency with which each node is included in the coarsened graph, i.e. pooling frequency (Figure 6.7). Second, cluster attention scores (i.e. a_{ij} in Eq. 6.5) can

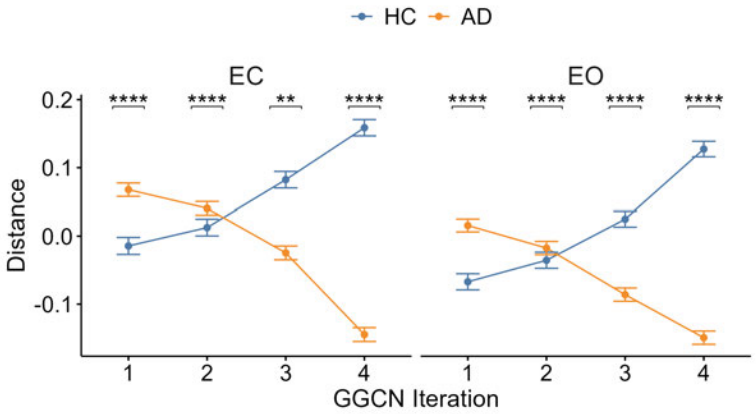

Figure 6.6: The average distance between initial node embedding and updated node embeddings shows the amount of information retained in each iteration of GGCN, i.e. going from local to global information. The asterisks denote the p-value of non-parametric Mann-Whitney U tests comparing the average distance between AD and HC cases and EC and EO conditions.

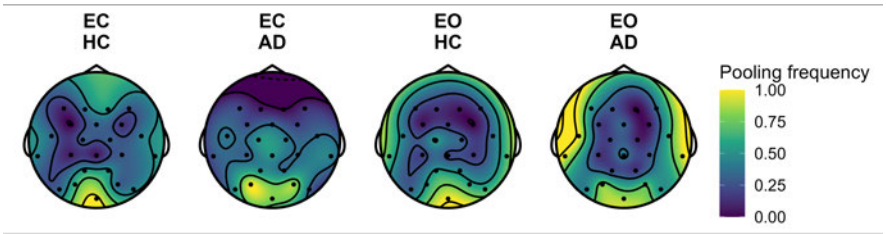

Figure 6.7: The average probability of a node being included in the coarsened graph by the ASAP node pooling module for AD and HC cases across EC and EO conditions. Averaged from all samples and min-max normalised.

be used to identify important hubs that are highly represented in the clusters learned by the node pooling module (Figure 6.8).

The nodes in parieto-occipital regions are consistently selected with high pooling frequency for AD and HC cases across both EC and EO conditions (Figure 6.7). Additionally, in EC condition, HC cases frequently select frontal nodes while AD cases tend to select central nodes. In contrast, in the EO condition, there seems to be more variation in the pooling frequency, with temporal nodes having a high pooling frequency for AD and HC cases.

Note that the nodes of the pooled graphs are, in fact, cluster embeddings, i.e. attention weighted sum of node embeddings (Eq. 6.7). We visualise the nodes with

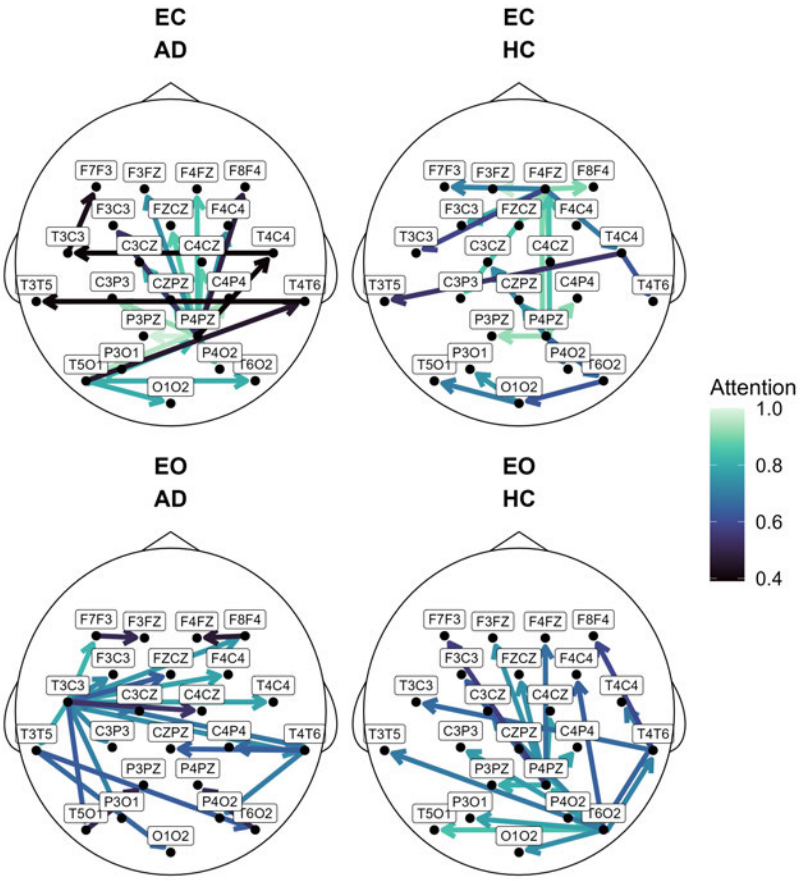

Figure 6.8: Attention scores learned by the node pooling module (a_{ij} in Eq. 6.5), indicating the amount of information transferred from the source node into a cluster centred at the target node. Averaged for all AD and HC cases across EC and EO conditions (single strongest edge preserved for each target cluster node).

the highest attention scores of each cluster to highlight important hubs (Figure 6.8). The attention scores are directed edges from a source node, transferring information to the cluster centred at the target node. Alternatively, these scores can be interpreted as a cluster membership strength. This information transfer should be interpreted as information flow within the model and most likely does not reflect an information flow within the brain.

In EC, AD cases show a large hub at the P4PZ node with strong long-distance and short-distance to various nodes. Additionally, there is a smaller hub at the T5O1. Similarly, in EO, AD cases have a large hub at the T3C3 node and a smaller one at the

T4T6 node. In contrast, HC cases do not have any apparent hubs in the EC condition, with only a small hub at the P4PZ node. The attention links also seem to be rather short-distance. In the EO condition, HC cases show a large hub at the T6O2 node and smaller hubs at the P4PZ and T4T6 nodes.

This variance between EC and EO conditions displayed in the pooling frequency and attention scores suggests a plausible answer to why it is challenging for the model to learn joint representation in the EC+EO combined condition. We speculate this is caused by the additional dynamics introduced by the visual processing during the EO condition.

Feature Masking

We utilise feature masking to elucidate the importance of the frequency components summarised at each node by the node feature vector, i.e. PSD. In this, values at a selected part of the node feature vectors are replaced by zeroes and the model is re-trained on this modified dataset. The relative reduction in f1-scores was then measured and visualised in Fig 6.9 for EC and EO conditions.

In both EC and EO conditions, the frequencies between 6 and 10 Hz are the most important since their masking reduced performance by 4.82% and 9.18%, respectively. This fits well with the well-described increase of power as well as functional connectivity in AD within these frequencies corresponding to θ and low α bands [13, 141]. Similarly, masking of the $[1, 5]$, $[36, 40]$ and $[41, 45]$ frequency ranges results in a significant performance decrease in both EC and EO. Additionally, in EO condition, the $[11, 15]$, $[16, 20]$ and $[26, 30]$ frequency ranges produce a significant performance decrease.

6.3.4 Limitations and Future Work

Although our approach achieves competitive performance, we identify a few drawbacks. First, the relatively small size of our dataset imposes a limit on fitting complex models. We address this issue by segmenting the EEG signals into short windows. The short window length means that the model might not be able to represent information from low-frequency components of the signal.

Next, we do not explore alternative node feature representations beyond PSD in this study. PSD is merely a linear frequency-domain representation of the signal. Including time-domain and nonlinear information in the node features might improve the expressiveness of the model. Similarly, the proposed graph learning mechanism

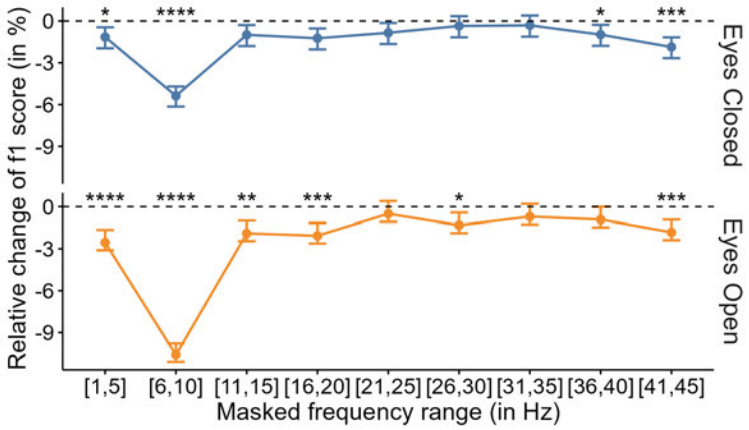

Figure 6.9: Relative change in F1 score when parts of node features are masked, showing the importance of frequency components for the classification task for eyes closed and eyes open conditions. The asterisks denote the p-value of non-parametric Mann-Whitney U tests comparing whether the relative change is significantly different from 0.

is limited to linear coupling patterns because (1) it is inferred from the node features and (2) it is expressed as Pearson's correlation coefficient. Future work should explore other forms of FC that might be integrated into the graph learning mechanism and study ways to include more complex frequency-dependent coupling information.

Finally, the model architecture might be limited by the relatively large number of hyper-parameters that need to be optimised. However, this limitation should be mitigated by utilising a validation set during the optimisation. Moreover, we explore the model stability with respect to some of the important hyperparameters in the parameter sensitivity experiments. These suggest that the performance achieved by the proposed model is not limited purely to the optimal values of the hyperparameters.

6.4 Conclusion

This work proposes a novel graph learning model that performs highly in the AD diagnosis task. We show that the model produces robust and clinically relevant explanations for its predictions via the novel graph structure learning module and the node pooling mechanism. Finally, we highlight the importance of utilising the gating mechanism within a message-passing encoder. This allows the model to represent the multiscale distributed network disruptions accurately.

6.5 Chapter Summary

This chapter introduces a novel GNN model for explainable AD classification. The model dynamically reconstructs brain graph structures and enhances node features adaptively from the data. The resulting brain graphs aid in interpreting predictions. Additionally, we employ a clustering-based node pooling mechanism to localise significant brain regions contributing to predictions.

The experimental results demonstrate the robust performance of our AGGCN model across various conditions. Notably, the model performs best in EC condition but retains high performance in EC condition. However, performance significantly drops in the combined (EC+EO) dataset, indicating the challenge of integrating information from both conditions.

Comparison with seven baseline models shows the superiority of AGGCN across all conditions. Ablation studies further highlight the importance of individual model modules, with each contributing significantly to the performance or explainability.

The explainability of AGGCN is demonstrated by generating prediction explanations across multiple scales. Graph learning reveals distinct brain connectivity patterns between AD and HC cases. Node embeddings and GGCN encoder showcase differences in learned patterns under EC and EO conditions. The node pooling mechanism identifies significant hubs in brain regions contributing to predictions. Feature masking illustrates the importance of frequency components in node feature vectors for AD classification.

While achieving competitive performance, limitations include dataset size constraints and potential enhancements in node feature representations and graph learning mechanisms. Nonetheless, the model demonstrates stability across varying hyperparameter values and provides clinically relevant explanations for AD diagnosis.

In conclusion, the proposed AGGCN model proves effective for AD classification, offering interpretability and insights into brain connectivity patterns relevant to the disease.

Chapter 7

Conclusions

The research presented in this thesis aimed to answer the question of how to leverage graph-based representations to characterise and distinguish AD cases from age-matched HC using multivariate EEG signals. Various FC measures and data-driven methods were utilised to recover functional brain graph structures from EEG. Two approaches to extracting information from brain graphs were tested: (1) feature-based ML and (2) data-driven DL representation learning.

(1) relies on using graph-theory metrics to quantify certain aspects of brain graphs and has been deployed in Chapters 4 and 5 (partially). (2) uses artificial neural networks to extract features useful for prediction automatically and has been deployed in Chapters 5 and 6.

Chapter 4 reports the use of CBS as a novel measure of FC both within and between frequency bands by introducing multilayer graph representations. The reconstructed CBS-based graphs were then used to elucidate the role of frequency bands and their CFC interactions to enable information integration and segregation and how these roles are influenced by AD. This information is subsequently used to train ML model for AD classification.

Chapter 5 then reports an empirical evaluation of commonly used FC measures for training predictive models to enable accurate AD diagnosis. GNN-based models perform significantly better than other tested architectures. Additionally, it has been demonstrated that FC information is crucial for GNN design for EEG classification. However, the choice of optimal FC measure remains ambiguous, as none of the chosen FC measures performs consistently better.

Finally, **Chapter 6** introduces a novel GNN-based architecture for explainable diagnosis of AD. The proposed model implements a data-driven graph learning mechanism,

thus avoiding the issue of selecting an appropriate FC measure. Multiple sample-specific explanations can be derived from the proposed model across various spatial levels, i.e. edge-level, node-level and cluster-level.

7.1 Achieved Research Objectives

7.1.1 Predictive Power of Nonlinear and CFC Connectivity Compared to Linear and WFC Alternatives

Answers to this objective were addressed in Chapters 4 and 5. Specifically, Chapter 4 compares nonlinear FC measure of CFC and WFC (i.e. CBS) with its linear alternative limited to WFC (i.e. CS). Second, Chapter 5 compares several commonly used linear and nonlinear FC measures in terms of predictive performance using four classification approaches.

CBS and CS-based graphs were compared in terms of detecting statistical differences between AD and HC cases and classification performance. As CBS detects comparable differences as CS and even performs significantly better in the classification task, a conclusion can be drawn that the inclusion of nonlinear and CFC information improves AD characterisation and prediction. However, as CBS is not directly comparable to CS, the exact contribution of nonlinear connectivity remains ambiguous.

Next, 5 investigated the classification performance of linear and nonlinear FC measures. GNNs trained on linear and nonlinear FC graphs perform similarly. Thus, there is likely no advantage gained by considering nonlinear information. In contrast, some of the considered nonlinear FC measures such as MI and PLV lead to consistent significant performance gains when using SVM and CNN models.

Overall, this thesis demonstrates several advantages of considering both nonlinear and CFC connectivity in combination with linear and WFC approaches for modelling AD. However, both linear and WFC connectivities are likely dominant in AD and HC EEG signals.

7.1.2 Methods for Analysing Cross-frequency Coupling from a Graph Perspective

The answer to this objective was addressed in Chapter 4. In the literature review chapter (Chapter 2), a research gap has been identified concerning the lack of CFC-

modelling from a graph perspective. This thesis proposed using CBS to reconstruct multilayer brain graphs that incorporate both WFC and CFC information.

The proposed multilayer graph framework was then used to elucidate the roles of frequency components and their CFC interactions. Both WFC and CFC roles of high-frequency components were shown to be disrupted in AD. In contrast, both WFC and CFC roles of low-frequency components seem to be generally increased in AD, thus suggesting a plausible compensatory mechanism for the loss of high-frequency coupling. In conclusion, this thesis demonstrates the utility of modelling both CFC and WFC within a graph-based framework to reveal novel AD-related disruptions.

7.1.3 Graph Learning and Graph Neural Networks to Study Neurodegenerative Diseases and Facilitate Diagnosis

This objective was addressed in Section 2.4 and Chapters 5 and 6. First, applications of GNNs for EEG-based classification were systematically reviewed. The main identified limitations include a lack of experiments with a broader range of GCN layers, limited model explainability and missing integration of CFC information. Moreover, GNN-based diagnosis of AD remains a largely unexplored area.

Therefore, Chapter 5 first investigated the effect of commonly used FC measures on GNN performance for EEG-based classification of AD using relatively simple GNN architecture. Results reported in this chapter demonstrate a clear advantage of GNNs for AD classification compared to baseline models. Additionally, the use of FC-based brain graphs result in superior GNN performance compared to fixed distance-based graphs, indicating the importance of considering FC information when designing GNN architectures. Chapter 6 then introduces a novel GNN architecture for the classification of AD. This model performs significantly better than previously proposed ML and DL approaches, thus further demonstrating the advantages of using GNNs.

7.1.4 Graph Neural Network for Automatically Reconstructing Brain Graph Structures

Multiple FC measures are commonly used in the literature to reconstruct brain graphs from EEG. However, results reported in Chapter 5 show ambiguous results regarding choosing the optimal FC measure. In order to circumvent this issue, data-driven methods can instead be leveraged to reconstruct brain graph structure from the data.

The systematic review of EEG-GNNs (Section 2.4, has identified various data-driven graph learning approaches incorporated within GNN, such as dot-product-based or attention-based methods.

An alternative data-driven graph learning mechanism has been investigated in Chapter 6, utilising a well-known FC measure to produce brain graph structures. The learned graph structures share multiple characteristics with traditional FC graphs and also demonstrate their expressiveness in explaining edge-level differences between AD and HC cases.

7.1.5 Graph Neural Network for Explainable Prediction of Neurodegenerative Diseases

Producing diagnosis explanations is crucial to enable model validation by clinical experts. However, this has often been overlooked in previously proposed DL-based models, including GNNs. Chapter 6, thus, delves into designing a GNN architecture that can produce prediction explanations across multiple spatial scales. The proposed model has been demonstrated to produce consistent explanations.

On the global graph scale, the model leverages more information from local interactions of AD cases compared to HC, suggesting the loss of global information processing due to AD. The model also identified the emergence of a large hub in the parietal region in AD cases that contain both short- and long-range edges. This parietal hub might indicate a compensatory mechanism to counteract the disruption of global information processing. Finally, on the node level, the model shows the importance of parietal and occipital regions for AD classification. These results demonstrate the potential of GNNs models for precise explainable prediction from EEG signals.

7.2 Research Limitations

The research presented in this thesis has a few limitations that could be addressed in future research. First, the reported experiments were all performed on the same dataset. This is mainly due to the cost of obtaining other datasets and with no open access datasets available when these experiments were carried out. The main limitation of the used dataset is its limited size, i.e. 20 AD and 20 HC cases. The small sample size was attempted to circumvent by further splitting the signals into small windows, thus allowing the training of DL models. However, using signal windowing is not applicable

for statistical analysis since there is shared variance between windows from the same participant, thus violating the independence assumption of most statistical tests.

Secondly, the generalisibility of the proposed methods is unclear due to the limited dataset and lack of validation on external datasets. Moreover, there is a risk of hyperparameter overfitting to the used dataset. This limitation could be addressed by utilising nested cross-validation. Due to the high computational cost of such model-validation, we opted for the traditional cross-validation approach commonly used in the literature. We acknowledge the potential risk of such an approach. However, it can be argued that since the AD-related patterns reported in this thesis fit well with the findings reported in the literature, the proposed methods show a potential to generalise well to unseen data. This section outlines the limitations common to the whole thesis. Additionally, each chapter discussed limitations specific to the work presented in the given chapter.

7.3 Future Work

The research objectives set out in this thesis were largely achieved, but several interesting questions remain to be answered by future research. The methods proposed in this thesis were evaluated only in terms of distinguishing AD cases from HC. However, all of the methods are general and flexible enough to potentially (1) generalise to larger AD datasets, (2) be applied to the classification of other neurological diseases and disorders beyond AD and (3) to produce valuable insights about brain function and disease/disorder-related disruptions.

The issue of (1) has already been described in the previous section. Beyond the methodology-related issues brought about by the small sample size, validation on larger, more diverse datasets would be beneficial. Ideally, the dataset should sample data from various countries and ethnically diverse participants to ensure a broad generalisation of the results. (2) would be an exciting extension of the reported work. The proposed methodology does not make any assumptions about the nature of a disorder aside from the assumption of graph disruption. Thus, the methods are likely to perform well in other EEG-based classification tasks such as Parkinson's disease, frontotemporal dementia or epilepsy. Finally, (3) is based on the same assumption of the general nature of the proposed methods. Thus, the multilayer graph analysis and novel GNN model should generate comparable insights to those reported for AD cases.

Another avenue for future research lies in exploring various pre-training techniques

to allow for the training of more complex and plausibly more powerful GNN models, preferably even on small datasets, i.e. datasets on less common diseases. An ideal pre-training population-independent task might be a regression task, i.e. predicting multivariate EEG signals T steps-ahead. Moreover, an accurate multivariate regression GNN model could be further used to simulate additional samples, thus increasing the training set.

A related future research direction would be utilising GNNs combined with unsupervised learning to derive novel data-driven FC measures or even causality measures. Separating graph learning from training a model for a specific classification task might offer significant advantages. This would be in contrast to the AGGCN model (Chapter 6). By learning the graph in isolation (i.e. without optimising the model for classification), the obtained edge weights would be guaranteed to encode brain similarity or causality between brain regions. In contrast, AGGCN-style graph learning might be biased towards edges helpful in solving the classification task.

Although, this thesis demonstrated that incorporating CFC information into reconstructed brain graphs provides novel ways of characterising AD. However, combining GNNs and CFC-based graphs remains unexplored. Generally, only WFC brain graphs have been thus far utilised as input to GNN models. Two ways of leveraging CFC information in GNNs might be of interest in future research. One approach could directly utilise multilayer brain graphs similar to those proposed in Chapter 4 as an input to a GNN model. Alternatively, a single layer CFC graph, e.g. δ-γ graph, would serve as input akin to how WFC graphs have been used in previously proposed approaches.

Finally, while automatically diagnosing AD is crucial, it is merely a first step to deploying automatic diagnostic models in clinical settings. Future research needs to expand the predictive modelling proposed in this thesis to both predict AD in early stages, i.e. conversion from MCI stage, and functional outcomes of the disease, i.e. symptom severity for monitoring and possibly evaluation of treatment effectiveness. Thus, this thesis is a small step in EEG-based diagnosis of AD but a giant leap for this author.

Bibliography

[1] Majd Abazid, Nesma Houmani, Jerome Boudy, Bernadette Dorizzi, Jean Mariani, and Kiyoka Kinugawa. A Comparative Study of Functional Connectivity Measures for Brain Network Analysis in the Context of AD Detection with EEG. *Entropy*, 23(11):1553, November 2021. ISSN 1099-4300. doi: 10.3390/e23111553.

[2] Majd Abazid, Nesma Houmani, Bernadette Dorizzi, Jerome Boudy, Jean Mariani, and Kiyoka Kinugawa. Weighted Brain Network Analysis on Different Stages of Clinical Cognitive Decline. *Bioengineering*, 9(2):62, February 2022. ISSN 2306-5354. doi: 10.3390/bioengineering9020062.

[3] Abdulyekeen T. Adebisi and Kalyana C. Veluvolu. Brain network analysis for the discrimination of dementia disorders using electrophysiology signals: A systematic review. *Frontiers in Aging Neuroscience*, 15, 2023. ISSN 1663-4365. doi: 10.3389/fnagi.2023.1039496.

[4] G Adler, S Brassen, and A Jajcevic. EEG coherence in alzheimer's dementia. *Journal of neural transmission*, 110(9):1051–1058, 2003.

[5] Saeedeh Afshari and Mahdi Jalili. Directed Functional Networks in Alzheimer's Disease: Disruption of Global and Local Connectivity Measures. *IEEE Journal of Biomedical and Health Informatics*, 21(4):949–955, July 2017. ISSN 2168-2208. doi: 10.1109/JBHI.2016.2578954.

[6] Saeedeh Afshari and Mahdi Jalili. Directed Functional Networks in Alzheimer's Disease: Disruption of Global and Local Connectivity Measures. *IEEE Journal of Biomedical and Health Informatics*, 21(4):949–955, July 2017. ISSN 2168-2208. doi: 10.1109/JBHI.2016.2578954.

[7] Mehran Ahmadlou, Hojjat Adeli, and Anahita Adeli. New diagnostic EEG markers of the Alzheimer's disease using visibility graph. *Journal of neu-*

ral transmission, 117(9):1099–1109, September 2010. ISSN 1435-1463. doi: 10.1007/s00702-010-0450-3.

[8] Shiva Asadzadeh, Tohid Yousefi Rezaii, Soosan Beheshti, and Saeed Meshgini. Accurate emotion recognition using Bayesian model based EEG sources as dynamic graph convolutional neural network nodes. *Scientific Reports*, 12(1):1–14, 2022.

[9] C. Babiloni, R. Ferri, D.V. Moretti, A. Strambi, G. Binetti, G. Dal Forno, F. Ferreri, B. Lanuzza, C. Bonato, F. Nobili, G. Rodriguez, S. Salinari, S. Passero, R. Rocchi, C.J. Stam, and P.M. Rossini. Abnormal fronto-parietal coupling of brain rhythms in mild Alzheimer's disease: A multicentric EEG study. *European Journal of Neuroscience*, 19(9):2583–2590, 2004. ISSN 0953-816X. doi: 10.1111/j.0953-816X.2004.03333.x.

[10] Claudio Babiloni, Roberta Lizio, Filippo Carducci, Fabrizio Vecchio, Alberto Redolfi, Silvia Marino, Gioacchino Tedeschi, Patrizia Montella, Antonio Guizzaro, Fabrizio Esposito, Alessandro Bozzao, Franco Giubilei, Francesco Orzi, Carlo C. Quattrocchi, Andrea Soricelli, Elena Salvatore, Annalisa Baglieri, Placido Bramanti, Enrica Cavedo, Raffaele Ferri, Filomena Cosentino, Michelangelo Ferrara, Ciro Mundi, Gianpaolo Grilli, Silvia Pugliese, Gianluca Gerardi, Laura Parisi, Fabrizio Vernieri, Antonio I. Triggiani, Jan T. Pedersen, Hans Göran Hårdemark, Paolo M. Rossini, and Giovanni B. Frisoni. Resting State Cortical Electroencephalographic Rhythms and White Matter Vascular Lesions in Subjects with Alzheimer's Disease: An Italian Multicenter Study. *Journal of Alzheimer's Disease*, 26(2):331–346, January 2011. ISSN 1387-2877. doi: 10.3233/JAD-2011-101710.

[11] Claudio Babiloni, Roberta Lizio, Claudio Del Percio, Nicola Marzano, Andrea Soricelli, Elena Salvatore, Raffaele Ferri, Filomena I. I. Cosentino, Gioacchino Tedeschi, Patrizia Montella, Silvia Marino, Simona De Salvo, Guido Rodriguez, Flavio Nobili, Fabrizio Vernieri, Francesca Ursini, Ciro Mundi, Jill C. Richardson, Giovanni B. Frisoni, and Paolo M. Rossini. Cortical Sources of Resting State EEG Rhythms are Sensitive to the Progression of Early Stage Alzheimer's Disease. *Journal of Alzheimer's Disease*, 34(4):1015–1035, January 2013. ISSN 1387-2877. doi: 10.3233/JAD-121750.

[12] Claudio Babiloni, Claudio Del Percio, Marina Boccardi, Roberta Lizio, Susanna Lopez, Filippo Carducci, Nicola Marzano, Andrea Soricelli, Raffaele Ferri, Antonio Ivano Triggiani, Annapaola Prestia, Serenella Salinari, Paul E. Rasser, Erol Basar, Francesco Famà, Flavio Nobili, Görsev Yener, Derya Durusu Emek-Savaş, Loreto Gesualdo, Ciro Mundi, Paul M. Thompson, Paolo M. Rossini, and Giovanni B. Frisoni. Occipital sources of resting-state alpha rhythms are related to local gray matter density in subjects with amnesic mild cognitive impairment and Alzheimer's disease. *Neurobiology of Aging*, 36(2):556–570, February 2015. ISSN 0197-4580. doi: 10.1016/j.neurobiolaging.2014.09.011.

[13] Claudio Babiloni, Roberta Lizio, Nicola Marzano, Paolo Capotosto, Andrea Soricelli, Antonio Ivano Triggiani, Susanna Cordone, Loreto Gesualdo, and Claudio Del Percio. Brain neural synchronization and functional coupling in Alzheimer's disease as revealed by resting state EEG rhythms. *International Journal of Psychophysiology*, 103:88–102, 2016.

[14] Claudio Babiloni, Katarzyna Blinowska, Laura Bonanni, Andrej Cichocki, Willem De Haan, Claudio Del Percio, Bruno Dubois, Javier Escudero, Alberto Fernández, Giovanni Frisoni, Bahar Guntekin, Mihaly Hajos, Harald Hampel, Emmanuel Ifeachor, Kerry Kilborn, Sanjeev Kumar, Kristinn Johnsen, Magnus Johannsson, Jaeseung Jeong, Fiona LeBeau, Roberta Lizio, Fernando Lopes da Silva, Fernando Maestú, William J. McGeown, Ian McKeith, Davide Vito Moretti, Flavio Nobili, John Olichney, Marco Onofrj, Jorge J. Palop, Michael Rowan, Fabrizio Stocchi, Zbigniew M Struzik, Heikki Tanila, Stefan Teipel, John Paul Taylor, Marco Weiergräber, Gorsev Yener, Tracy Young-Pearse, Wilhelmus H. Drinkenburg, and Fiona Randall. What electrophysiology tells us about Alzheimer's disease: A window into the synchronization and connectivity of brain neurons. *Neurobiology of Aging*, 85:58–73, January 2020. ISSN 0197-4580. doi: 10.1016/j.neurobiolaging.2019.09.008.

[15] Clive Ballard, Serge Gauthier, Anne Corbett, Carol Brayne, Dag Aarsland, and Emma Jones. Alzheimer's disease. *The Lancet*, 377(9770):1019–1031, March 2011. ISSN 0140-6736. doi: 10.1016/S0140-6736(10)61349-9.

[16] Guangcheng Bao, Kai Yang, Li Tong, Jun Shu, Rongkai Zhang, Linyuan Wang, Bin Yan, and Ying Zeng. Linking multi-layer dynamical GCN with style-based re-

calibration-CNN-for-EEG-Based-emotion-recognition.- *Frontiers in Neurorobotics*,- 16:1–12,-2022.-

[17]- Alain- Barrat,- Marc- Barthelemy,- Romualdo- Pastor-Satorras,- and- Alessandro- Vespignani.- The-architecture-of-complex-weighted-networks.- *Proceedings of the national academy of sciences*,-101(11):3747–3752,-2004.-

[18]- Elham-Barzegaran-and-Maria-G-Knyazeva.- Functional-connectivity-analysis-in-eeg-source-space:-the-choice-of-method.- *PloS one*,-12(7):e0181105,-2017.-

[19]- Erol- Başar,- Canan- Başar-Eroğlu,- Bahar- Güntekin,- and- Görsev- Gülmen- Yener.- Chapter- 2- - Brain's- alpha,- beta,- gamma,- delta,- and- theta- oscillations- in-neuropsychiatric- diseases:- Proposal- for- biomarker- strategies.- In- E.- Başar,- C.- Başar-Eroĝlu,- A.- Özerdem,- P.- M.- Rossini,- and- G.- G.- Yener,- editors,- *Supplements to Clinical Neurophysiology*,- volume-62-of-*Application of Brain Oscillations in Neuropsychiatric Diseases*,- pages-19–54.-Elsevier,-January-2013.- doi:-10.1016/B978-0-7020-5307-8.00002-8.-

[20]- Erol- Başar,- Banu- Femir,- Derya- Durusu- Emek-Savaş,- Bahar- Güntekin,- and-Görsev- G.- Yener.- Increased- long- distance- event-related- gamma- band- connectivity-in-Alzheimer's-disease.- *NeuroImage: Clinical*,-14:580–590,-January-2017.-ISSN-2213-1582.- doi:- 10.1016/j.nicl.2017.02.021.-

[21]- Danielle-S.-Bassett-and-Michael-S.-Gazzaniga.- Understanding-complexity-in-the-human- brain.- *Trends in Cognitive Sciences*,- 15(5):200–209,- May- 2011.- ISSN-1364-6613,-1879-307X.- doi:- 10.1016/j.tics.2011.03.006.-

[22]- Danielle-S-Bassett-and-Olaf-Sporns.-Network-neuroscience.- *Nature Neuroscience*,-20(3):353–364,-2017.-

[23]- Danielle-S.-Bassett,-Perry-Zurn,-and-Joshua-I.-Gold.- On-the-nature-and-use-of-models-in-network-neuroscience.- *Nature Reviews Neuroscience*,-19(9):566–578,-September-2018.-ISSN-1471-0048.- doi:- 10.1038/s41583-018-0038-8.-

[24]- André- M- Bastos- and- Jan-Mathijs- Schoffelen.- A- tutorial- review- of- functional-connectivity- analysis- methods- and- their- interpretational- pitfalls.- *Frontiers in systems neuroscience*,-9:175,-2016.-

[25] Yoav Benjamini and Yosef Hochberg. Controlling the false discovery rate: A practical and powerful approach to multiple testing. *Journal of the Royal statistical society: series B (Methodological)*, 57(1):289–300, 1995.

[26] Alaa Bessadok, Mohamed Ali Mahjoub, and Islem Rekik. Graph neural networks in network neuroscience. *IEEE Transactions on Pattern Analysis and Machine Intelligence*, 45(5):5833–5848, May 2023. ISSN 1939-3539. doi: 10.1109/TPAMI.2022.3209686.

[27] Richard F. Betzel. Chapter 2 - Network neuroscience and the connectomics revolution. In Andreas Horn, editor, *Connectomic Deep Brain Stimulation*, pages 25–58. Academic Press, January 2022. ISBN 978-0-12-821861-7. doi: 10.1016/B978-0-12-821861-7.00002-6.

[28] Jinying Bi, Fei Wang, Xin Yan, Jingyu Ping, and Yongzhao Wen. Multi-domain fusion deep graph convolution neural network for EEG emotion recognition. *Neural Computing and Applications*, pages 1–15, 2022.

[29] Daniel J. Blackburn, Yifan Zhao, Matteo De Marco, Simon M. Bell, Fei He, Hua-Liang Wei, Sarah Lawrence, Zoe C. Unwin, Michelle Blyth, and Jenna Angel. A pilot study investigating a novel non-linear measure of eyes open versus eyes closed eeg synchronization in people with Alzheimer's disease and healthy controls. *Brain sciences*, 8(7):1–19, 2018.

[30] Deyu Bo, Xiao Wang, Yang Liu, Yuan Fang, Yawen Li, and Chuan Shi. A survey on spectral graph neural networks, February 2023.

[31] Cristian Bodnar, Fabrizio Frasca, Nina Otter, Yuguang Wang, Pietro Liò, Guido F Montufar, and Michael Bronstein. Weisfeiler and Lehman Go Cellular: CW Networks. In *Advances in Neural Information Processing Systems*, volume 34, pages 2625–2640. Curran Associates, Inc., 2021.

[32] Elie Bou Assi, Laura Gagliano, Sandy Rihana, Dang K Nguyen, and Mohamad Sawan. Bispectrum features and multilayer perceptron classifier to enhance seizure prediction. *Scientific reports*, 8(1):1–8, 2018.

[33] Mary AB Brazier and JS Barlow. Some applications of correlation analysis to clinical problems in electroencephalography. *Electroencephalography and clinical Neurophysiology*, 8(2):325–331, 1956.

[34] C. T. Briels, C. J. Stam, P. Scheltens, S. Bruins, I. Lues, and A. A. Gouw. In pursuit of a sensitive EEG functional connectivity outcome measure for clinical trials in Alzheimer's disease. *Clinical Neurophysiology*, 131(1):88–95, January 2020. ISSN 1388-2457. doi: 10.1016/j.clinph.2019.09.014.

[35] Casper T Briels, Deborah N Schoonhoven, Cornelis J Stam, Hanneke de Waal, Philip Scheltens, and Alida A Gouw. Reproducibility of EEG functional connectivity in Alzheimer's disease. *Alzheimer's research & therapy*, 12(1):1–14, 2020.

[36] Matthew R Brier, Jewell B Thomas, and Beau M Ances. Network dysfunction in Alzheimer's disease: Refining the disconnection hypothesis. *Brain connectivity*, 4(5):299–311, 2014.

[37] Michael M. Bronstein, Joan Bruna, Yann LeCun, Arthur Szlam, and Pierre Vandergheynst. Geometric Deep Learning: Going beyond Euclidean data. *IEEE Signal Processing Magazine*, 34(4):18–42, July 2017. ISSN 1558-0792. doi: 10.1109/MSP.2017.2693418.

[38] Matthew J Brookes, Prejaas K Tewarie, Benjamin AE Hunt, Sian E Robson, Lauren E Gascoyne, Elizabeth B Liddle, Peter F Liddle, and Peter G Morris. A multi-layer network approach to MEG connectivity analysis. *Neuroimage*, 132: 425–438, 2016.

[39] Andreas Bruns and Reinhard Eckhorn. Task-related coupling from high-to low-frequency signals among visual cortical areas in human subdural recordings. *International journal of psychophysiology*, 51(2):97–116, 2004.

[40] Ed Bullmore and Olaf Sporns. Complex brain networks: Graph theoretical analysis of structural and functional systems. *Nature Reviews Neuroscience*, 10(3): 186–198, March 2009. ISSN 1471-0048. doi: 10.1038/nrn2575.

[41] György Buzsáki, Nikos Logothetis, and Wolf Singer. Scaling brain size, keeping timing: Evolutionary preservation of brain rhythms. *Neuron*, 80(3):751–764, 2013.

[42] Lihui Cai, Xile Wei, Jiang Wang, Haitao Yu, Bin Deng, and Ruofan Wang. Reconstruction of functional brain network in Alzheimer's disease via cross-frequency phase synchronization. *Neurocomputing*, 314:490–500, November 2018. ISSN 0925-2312. doi: 10.1016/j.neucom.2018.07.019.

[43] Lihui Cai, Xile Wei, Jing Liu, Lin Zhu, Jiang Wang, Bin Deng, Haitao Yu, and Ruofan Wang. Functional Integration and Segregation in Multiplex Brain Networks for Alzheimer's Disease. *Frontiers in Neuroscience*, 14, 2020. ISSN 1662-453X.

[44] R. T. Canolty, E. Edwards, S. S. Dalal, M. Soltani, S. S. Nagarajan, H. E. Kirsch, M. S. Berger, N. M. Barbaro, and R. T. Knight. High gamma power is phase-locked to theta oscillations in human neocortex. *Science*, 313(5793): 1626–1628, 2006. ISSN 0036-8075. doi: 10.1126/science.1128115. URL https://science.sciencemag.org/content/313/5793/1626.

[45] Ryan T. Canolty and Robert T. Knight. The functional role of cross-frequency coupling. *Trends in Cognitive Sciences*, 14(11):506–515, 2010. ISSN 1364-6613. doi: https://doi.org/10.1016/j.tics.2010.09.001. URL https://www.sciencedirect.com/science/article/pii/S1364661310002068.

[46] Giuseppe Caravaglios, Giuseppe Castro, Erminio Costanzo, Giulia Di Maria, Danielle Mancuso, and Emma Gabriella Muscoso. Theta power responses in mild Alzheimer's disease during an auditory oddball paradigm: Lack of theta enhancement during stimulus processing. *Journal of Neural Transmission*, 117 (10):1195–1208, October 2010. ISSN 1435-1463. doi: 10.1007/s00702-010-0488-2.

[47] Francesca Caso, Marco Cursi, Giuseppe Magnani, Giovanna Fanelli, Monica Falautano, Giancarlo Comi, Letizia Leocani, and Fabio Minicucci. Quantitative EEG and LORETA: Valuable tools in discerning FTD from AD? *Neurobiology of Aging*, 33(10):2343–2356, October 2012. ISSN 0197-4580. doi: 10.1016/j.neurobiolaging.2011.12.011.

[48] Qi Chang, Cancheng Li, Qing Tian, Qijing Bo, Jicong Zhang, Yanbing Xiong, and Chuanyue Wang. Classification of first-episode schizophrenia, chronic schizophrenia and healthy control based on brain network of mismatch negativity by graph neural network. *IEEE Transactions on Neural Systems and Rehabilitation Engineering*, 29:1784–1794, 2021.

[49] Yu-San Chang, Hsiang-Lan Chen, Chung-Yao Hsu, Shu-Hui Tang, and Ching-Kuan Liu. Parallel Improvement of Cognitive Functions and P300 Latency Following Donepezil Treatment in Patients With Alzheimer's Disease: A-

Case–Control Study. *Journal of Clinical Neurophysiology*, 31(1):81, February 2014. ISSN 0736-0258. doi: 10.1097/01.wnp.0000436899.48243.5e.

[50] Nitin Kumar Chauhan and Krishna Singh. A Review on Conventional Machine Learning vs Deep Learning. In *2018 International Conference on Computing, Power and Communication Technologies (GUCON)*, pages 347–352, September 2018. doi: 10.1109/GUCON.2018.8675097.

[51] Federico Chella, Laura Marzetti, Vittorio Pizzella, Filippo Zappasodi, and Guido Nolte. Third order spectral analysis robust to mixing artifacts for mapping cross frequency interactions in EEG/MEG. *Neuroimage*, 91:146–161, 2014.

[52] Jiangkuan Chen, Cong Liu, Chung-Kang Peng, Jong-Ling Fuh, Fengzhen Hou, and Albert C. Yang. Topological reorganization of EEG functional network is associated with the severity and cognitive impairment in Alzheimer's disease. *Physica A: Statistical Mechanics and its Applications*, 513:588–597, January 2019. ISSN 0378-4371. doi: 10.1016/j.physa.2018.09.043.

[53] Jianhui Chen, Hui Qian, and Xiaoliang Gong. Bayesian graph neural networks for EEG-Based emotion recognition. In *Clinical Image-Based Procedures, Distributed and Collaborative Learning, Artificial Intelligence for Combating COVID-19 and Secure and Privacy-Preserving Machine Learning*, pages 24–33. Springer, 2021.

[54] Tao Chen, Yanrong Guo, Shijie Hao, and Richang Hong. Exploring self-attention graph pooling with EEG-Based topological structure and soft label for depression detection. *IEEE Transactions on Affective Computing*, pages 2106–2118, 2022.

[55] Zhiqian Chen, Fanglan Chen, Lei Zhang, Taoran Ji, Kaiqun Fu, Liang Zhao, Feng Chen, Lingfei Wu, Charu Aggarwal, and Chang-Tien Lu. Bridging the gap between spatial and spectral domains: A survey on graph neural networks, July 2021.

[56] Kyunghyun Cho, Bart Van Merriënboer, Dzmitry Bahdanau, and Yoshua Bengio. On the properties of neural machine translation: Encoder-decoder approaches. *arXiv preprint arXiv:1409.1259*, 2014.

[57] Jacob Cohen. *Statistical Power Analysis for the Behavioral Sciences*. Routledge, 2013.

[58] Michael X Cohen. Assessing transient cross-frequency coupling in eeg data. *Journal of neuroscience methods*, 168(2):494–499, 2008.

[59] Michael X. Cohen. Assessing transient cross-frequency coupling in EEG data. *Journal of Neuroscience Methods*, 168(2):494–499, March 2008. ISSN 0165-0270. doi: 10.1016/j.jneumeth.2007.10.012.

[60] Nicolas Coquelet, Xavier De Tiège, Florian Destoky, Liliia Roshchupkina, Mathieu Bourguignon, Serge Goldman, Philippe Peigneux, and Vincent Wens. Comparing meg and high-density eeg for intrinsic functional connectivity mapping. *NeuroImage*, 210:116556, 2020.

[61] Ian C Covert, Balu Krishnan, Imad Najm, Jiening Zhan, Matthew Shore, John Hixson, and Ming Jack Po. Temporal graph convolutional networks for automatic seizure detection. In *Machine Learning for Healthcare Conference*, pages 160–180. PMLR, 2019.

[62] Helder Frederico da Silva Lopes, Jair M. Abe, and Renato Anghinah. Application of Paraconsistent Artificial Neural Networks as a Method of Aid in the Diagnosis of Alzheimer Disease. *Journal of Medical Systems*, 34(6):1073–1081, December 2010. ISSN 1573-689X. doi: 10.1007/s10916-009-9325-2.

[63] Zhengjia Dai, Qixiang Lin, Tao Li, Xiao Wang, Huishu Yuan, Xin Yu, Yong He, and Huali Wang. Disrupted structural and functional brain networks in Alzheimer's disease. *Neurobiology of aging*, 75:71–82, 2019.

[64] Marcello D'Amelio and Paolo Maria Rossini. Brain excitability and connectivity of neuronal assemblies in Alzheimer's disease: From animal models to human findings. *Progress in Neurobiology*, 99(1):42–60, October 2012. ISSN 0301-0082. doi: 10.1016/j.pneurobio.2012.07.001.

[65] Surya Das and Subha D. Puthankattil. Complex network analysis of MCI-AD EEG signals under cognitive and resting state. *Brain Research*, 1735:146743, May 2020. ISSN 0006-8993. doi: 10.1016/j.brainres.2020.146743.

[66] Serena Dattola, Nadia Mammone, Francesco Carlo Morabito, Domenico Rosaci, Giuseppe Maria Luigi Sarné, and Fabio La Foresta. Testing Graph Robustness Indexes for EEG Analysis in Alzheimer's Disease Diagnosis. *Electronics*, 10(12): 1440, January 2021. ISSN 2079-9292. doi: 10.3390/electronics10121440.

[67] J. Dauwels, F. Vialatte, and A. Cichocki. Diagnosis of Alzheimer's Disease from EEG Signals: Where Are We Standing? *Current Alzheimer Research*, 7(6): 487–505, September 2010. doi: 10.2174/156720510792231720.

[68] Justin Dauwels, François Vialatte, Toshimitsu Musha, and Andrzej Cichocki. A comparative study of synchrony measures for the early diagnosis of Alzheimer's disease based on EEG. *NeuroImage*, 49(1):668–693, 2010.

[69] Olivier David, Diego Cosmelli, and Karl J Friston. Evaluation of different measures of functional connectivity using a neural mass model. *Neuroimage*, 21(2): 659–673, 2004.

[70] Manlio De Domenico, Shuntaro Sasai, and Alex Arenas. Mapping multiplex hubs in human functional brain networks. *Frontiers in neuroscience*, 10:1–14, 2016.

[71] W. de Haan, Y.A.L. Pijnenburg, R.L.M. Strijers, Y. van der Made, W.M. van der Flier, P. Scheltens, and C.J. Stam. Functional neural network analysis in frontotemporal dementia and Alzheimer's disease using EEG and graph theory. *BMC Neuroscience*, 10, 2009. ISSN 1471-2202. doi: 10.1186/1471-2202-10-101.

[72] Willem de Haan, Wiesje M van der Flier, T Koene, Lieke L Smits, Philip Scheltens, and Cornelis J Stam. Disrupted modular brain dynamics reflect cognitive dysfunction in Alzheimer's disease. *Neuroimage*, 59(4):3085–3093, 2012.

[73] Floris De Lange, Ole Jensen, Markus Bauer, and Ivan Toni. Interactions between posterior gamma and frontal alpha/beta oscillations during imagined actions. *Frontiers in Human Neuroscience*, 2, 2008. ISSN 1662-5161.

[74] Floris P De Lange, Ole Jensen, Markus Bauer, and Ivan Toni. Interactions between posterior gamma and frontal alpha/beta oscillations during imagined actions. *Frontiers in human neuroscience*, 2:7, 2008.

[75] Michaël Defferrard, Xavier Bresson, and Pierre Vandergheynst. Convolutional neural networks on graphs with fast localized spectral filtering. In *Advances in Neural Information Processing Systems*, volume 29, pages 1–19. Curran Associates, Inc., 2016.

[76] Xavier Delbeuck, Martial Van der Linden, and Fabienne Collette. Alzheimer'disease as a disconnection syndrome? *Neuropsychology review*, 13(2):79–92, June 2003. ISSN 1573-6660. doi: 10.1023/A:1023832305702.

[77] Andac Demir, Toshiaki Koike-Akino, Ye Wang, Masaki Haruna, and Deniz Erdogmus. EEG-GNN: Graph neural networks for classification of electroencephalogram (EEG) signals. In *2021 43rd Annual International Conference of the IEEE Engineering in Medicine & Biology Society (EMBC)*, pages 1061–1067. IEEE, 2021.

[78] Stavros I Dimitriadis, Christos Salis, Ioannis Tarnanas, and David E Linden. Topological filtering of dynamic functional brain networks unfolds informative chronnectomics: A novel data-driven thresholding scheme based on orthogonal minimal spanning trees (OMSTs). *Frontiers in neuroinformatics*, 11:28, 2017. ISSN 1662-5196.

[79] Stavros I. Dimitriadis, María Eugenia López, Fernando Maestu, and Ernesto Pereda. Modeling the Switching Behavior of Functional Connectivity Microstates (FCμstates) as a Novel Biomarker for Mild Cognitive Impairment. *Frontiers in Neuroscience*, 13, 2019. ISSN 1662-453X.

[80] Yi Ding, Neethu Robinson, Qiuhao Zeng, and Cuntai Guan. LGGNet: Learning from Local-global-graph representations for brain-computer interface. *arXiv preprint arXiv:2105.02786*, 2021.

[81] Theekshana Dissanayake, Tharindu Fernando, Simon Denman, Sridha Sridharan, and Clinton Fookes. Geometric deep learning for subject independent epileptic seizure prediction using scalp EEG signals. *IEEE Journal of Biomedical and Health Informatics*, 26(2):527–538, 2021.

[82] Leide C. dos Santos Picanco, Priscilla F. Ozela, Maiara de Fatima de Brito Brito, Abraao A. Pinheiro, Elias C. Padilha, Francinaldo S. Braga, Carlos H. T. de Paula da Silva, Cleydson Breno Rodrigues dos Santos, Joaquín M. C. Rosa, and Lorane Izabel da Silva Hage-Melim. Alzheimer's disease: A review from the pathophysiology to diagnosis, new perspectives for pharmacological treatment. *Current Medicinal Chemistry*, 25(26):3141–3159, -08-01-2018. doi: 10.2174/0929867323666161213101126.

[83] Guanglong Du, Jinshao Su, Linlin Zhang, Kang Su, Xueqian Wang, Shaohua Teng, and Peter Xiaoping Liu. A multi-dimensional graph convolution network for EEG emotion recognition. *IEEE Transactions on Instrumentation and Measurement*, 71:1–11, 2022.

[84] Feng Duan, Zihao Huang, Zhe Sun, Yu Zhang, Qibin Zhao, Andrzej Cichocki, Zhenglu Yang, and Jordi Solé-Casals. Topological Network Analysis of Early Alzheimer's Disease Based on Resting State EEG. *IEEE Transactions on Neural Systems and Rehabilitation Engineering*, 28(10):2164–2172, October 2020. ISSN 1558-0210. doi: 10.1109/TNSRE.2020.3014951.

[85] M. M. A. Engels, M. Yu, C. J. Stam, A. A. Gouw, W. M. van der Flier, Ph. Scheltens, E. C. W. van Straaten, and A. Hillebrand. Directional information flow in patients with Alzheimer's disease. A source space resting state MEG study. *NeuroImage: Clinical*, 15:673–681, January 2017. ISSN 2213-1582. doi: 10.1016/j.nicl.2017.06.025.

[86] Lin Feng, Cheng Cheng, Mingyan Zhao, Huiyuan Deng, and Yong Zhang. EEG Based emotion recognition using spatial temporal graph convolutional LSTM with attention mechanism. *IEEE Journal of Biomedical and Health Informatics*, 2022.

[87] Alberto Fernández, Juan Arrazola, Fernando Maestú, Carlos Amo, Pedro Gil Gregorio, Christian Wienbruch, and Tomás Ortiz. Correlations of Hippocampal Atrophy and Focal Low Frequency Magnetic Activity in Alzheimer Disease: Volumetric MR Imaging Magnetoencephalographic Study. *American Journal of Neuroradiology*, 24(3):481–487, March 2003. ISSN 0195-6108, 1936-959X.

[88] Manuel Fernández, Ana L. Gobartt, Montse Balañá, and the COOPERA Study Group. Behavioural symptoms in patients with Alzheimer's disease and their association with cognitive impairment. *BMC Neurology*, 10(1):87, September 2010. ISSN 1471-2377. doi: 10.1186/1471-2377-10-87.

[89] Matthias Fey and Jan E. Lenssen. Fast graph representation learning with PyTorch Geometric. In *ICLR Workshop on Representation Learning on Graphs and Manifolds*, 2019.

[90] L. C. Fonseca, G. M. a. S. Tedrus, L. R. Prandi, and A. C. A. Andrade. Quantitative electroencephalography power and coherence measurements in the diagnosis of mild and moderate Alzheimer's disease. *Arquivos de Neuro-Psiquiatria*, 69: 297–303, 2011. ISSN 0004-282X, 1678-4227. doi: 10.1590/S0004-282X2011000300006.

[91] Lineu C. Fonseca, Gloria M. A. S. Tedrus, Larissa R. Prandi, Adriana M. Almeida, and Danilo S. Furlanetto. Alzheimer's disease: Relationship between cognitive aspects and power and coherence EEG measures. *Arquivos de Neuro-Psiquiatria*, 69:875–881, December 2011. ISSN 0004-282X, 1678-4227. doi: 10.1590/S0004-282X2011000700005.

[92] Francisco J Fraga, Tiago H Falk, Paulo AM Kanda, and Renato Anghinah. Characterizing Alzheimer's disease severity via resting-awake EEG amplitude modulation analysis. *PloS one*, 8(8):e72240, 2013.

[93] Raffaella Franciotti, Nicola Walter Falasca, Dario Arnaldi, Francesco Famà, Claudio Babiloni, Marco Onofrj, Flavio Mariano Nobili, and Laura Bonanni. Cortical network topology in prodromal and mild dementia due to Alzheimer's disease: Graph theory applied to resting state EEG. *Brain Topography*, 32(1):127–141, January 2019. ISSN 1573-6792. doi: 10.1007/s10548-018-0674-3.

[94] Sivasharmini Ganeshamoorthy, Laura Roden, Dominik Klepl, and Fei He. Gene Regulatory Network Inference through Link Prediction using Graph Neural Network. In *2022 IEEE Signal Processing in Medicine and Biology Symposium (SPMB)*, pages 1–5, December 2022. doi: 10.1109/SPMB55497.2022.10014835.

[95] Chen Gao, Yu Zheng, Nian Li, Yinfeng Li, Yingrong Qin, Jinghua Piao, Yuhan Quan, Jianxin Chang, Depeng Jin, Xiangnan He, and Yong Li. A survey of graph neural networks for recommender systems: Challenges, methods, and directions. *ACM Transactions on Recommender Systems*, 1(1):3:1–3:51, March 2023. doi: 10.1145/3568022.

[96] Hongyang Gao, Yi Liu, and Shuiwang Ji. Topology-aware graph pooling networks. *IEEE Transactions on Pattern Analysis and Machine Intelligence*, 43(12): 4512–4518, December 2021. ISSN 1939-3539. doi: 10.1109/TPAMI.2021.3062794.

[97] Xing Gao, Wenrui Dai, Chenglin Li, Hongkai Xiong, and Pascal Frossard. iPool–Information-Based pooling in hierarchical graph neural networks. *IEEE Transactions on Neural Networks and Learning Systems*, 33(9):5032–5044, September 2022. ISSN 2162-2388. doi: 10.1109/TNNLS.2021.3067441.

[98] Parham Ghorbanian, David M Devilbiss, Terry Hess, Allan Bernstein, Adam J Simon, and Hashem Ashrafiuon. Exploration of EEG features of Alzheimer's

disease using continuous wavelet transform. *Medical & biological engineering & computing*, 53(9):843–855, 2015.

[99] Sayantani Ghosh, Amit Konar, and Atulya K Nagar. Decoding subjective creativity skill from visuo-spatial reasoning ability using capsule graph neural network. In *2021 International Joint Conference on Neural Networks (IJCNN)*, pages 1–8. IEEE, 2021.

[100] Michelle Girvan and Mark EJ Newman. Community structure in social and biological networks. *Proceedings of the national academy of sciences*, 99(12): 7821–7826, 2002.

[101] Andreina Giustiniani, Laura Danesin, Beatrice Bozzetto, AnnaRita Macina, Silvia Benavides-Varela, and Francesca Burgio. Functional changes in brain oscillations in dementia: A review. *Reviews in the Neurosciences*, 34(1):25–47, January 2023. ISSN 2191-0200. doi: 10.1515/revneuro-2022-0010.

[102] Alida A. Gouw, Astrid M. Alsema, Betty M. Tijms, Andreas Borta, Philip Scheltens, Cornelis J. Stam, and Wiesje M. van der Flier. EEG spectral analysis as a putative early prognostic biomarker in nondemented, amyloid positive subjects. *Neurobiology of Aging*, 57:133–142, September 2017. ISSN 0197-4580. doi: 10.1016/j.neurobiolaging.2017.05.017.

[103] Jérémy Guillon, Yohan Attal, Olivier Colliot, Valentina La Corte, Bruno Dubois, Denis Schwartz, Mario Chavez, and F De Vico Fallani. Loss of brain inter-frequency hubs in Alzheimer's disease. *Scientific reports*, 7(1):1–13, 2017.

[104] Jeremy Guillon, Mario Chavez, Federico Battiston, Yohan Attal, Valentina La Corte, Michel Thiebaut de Schotten, Bruno Dubois, Denis Schwartz, Olivier Colliot, and Fabrizio de Vico Fallani. Disrupted core-periphery structure of multimodal brain networks in Alzheimer's disease. *Network Neuroscience*, 3(2):635–652, 2019.

[105] Simon Hanslmayr, Joachim Gross, Wolfgang Klimesch, and Kimron L. Shapiro. The role of alpha oscillations in temporal attention. *Brain Research Reviews*, 67 (1):331–343, June 2011. ISSN 0165-0173. doi: 10.1016/j.brainresrev.2011.04.002.

[106] Masahiro Hata, Hiroaki Kazui, Toshihisa Tanaka, Ryouhei Ishii, Leonides Canuet, Roberto D. Pascual-Marqui, Yasunori Aoki, Shunichiro Ikeda, Hideki

Kanemoto, Kenji Yoshiyama, Masao Iwase, and Masatoshi Takeda. Functional connectivity assessed by resting state EEG correlates with cognitive decline of Alzheimer's disease — An eLORETA study. *Clinical Neurophysiology*, 127(2): 1269–1278, February 2016. ISSN 1388-2457. doi: 10.1016/j.clinph.2015.10.030.

[107] Fei He and Yuan Yang. Nonlinear system identification of neural systems from neurophysiological signals. *Neuroscience*, 458:213–228, 2021. ISSN 0306-4522.

[108] Jiatong He, Jia Cui, Gaobo Zhang, Mingrui Xue, Dengyu Chu, and Yanna Zhao. Spatial-temporal seizure detection with graph attention network and bi-directional LSTM architecture. *Biomedical Signal Processing and Control*, 78: 103908, 2022.

[109] Christoph S. Herrmann, Matthias H. J. Munk, and Andreas K. Engel. Cognitive functions of gamma-band activity: Memory match and utilization. *Trends in Cognitive Sciences*, 8(8):347–355, August 2004. ISSN 1364-6613. doi: 10.1016/j.tics.2004.06.006.

[110] Timothy J. Hohman, Doug Tommet, Shawn Marks, Joey Contreras, Rich Jones, and Dan Mungas. Evaluating Alzheimer's disease biomarkers as mediators of age-related cognitive decline. *Neurobiology of Aging*, 58:120–128, October 2017. ISSN 0197-4580. doi: 10.1016/j.neurobiolaging.2017.06.022.

[111] Paul Hollingworth, Denise Harold, Lesley Jones, Michael J. Owen, and Julie Williams. Alzheimer's disease genetics: Current knowledge and future challenges. *International Journal of Geriatric Psychiatry*, 26(8):793–802, 2011. ISSN 1099-1166. doi: 10.1002/gps.2628.

[112] Yimin Hou, Shuyue Jia, Xiangmin Lun, Yan Shi, and Yang Li. Deep feature mining via attention-based BiLSTM-GCN for human motor imagery recognition. *arXiv preprint arXiv:2005.00777*, 2020.

[113] Yimin Hou, Shuyue Jia, Xiangmin Lun, Ziqian Hao, Yan Shi, Yang Li, Rui Zeng, and Jinglei Lv. GCNs-net: A graph convolutional neural network approach for decoding time-resolved eeg motor imagery signals. *IEEE Transactions on Neural Networks and Learning Systems*, 2022.

[114] C Huang, L. O Wahlund, T Dierks, P Julin, B Winblad, and V Jelic. Discrimination of Alzheimer's disease and mild cognitive impairment by equivalent EEG

sources: A cross-sectional and longitudinal study. *Clinical Neurophysiology*, 111 (11):1961–1967, November 2000. ISSN 1388-2457. doi: 10.1016/S1388-2457(00)00454-5.

[115] Cameron J Huggins, Javier Escudero, Mario A Parra, Brian Scally, Renato Anghinah, Amanda Vitória Lacerda De Araújo, Luis F Basile, and Daniel Abasolo. Deep learning of resting-state electroencephalogram signals for three-class classification of Alzheimer's disease, mild cognitive impairment and healthy ageing. *Journal of Neural Engineering*, 18(4):046087, June 2021. ISSN 1741-2552. doi: 10.1088/1741-2552/ac05d8.

[116] Mareike J Hülsemann, Ewald Naumann, and Björn Rasch. Quantification of phase-amplitude coupling in neuronal oscillations: comparison of phase-locking value, mean vector length, modulation index, and generalized-linear-modeling-cross-frequency-coupling. *Frontiers in neuroscience*, 13:573, 2019.

[117] René J. Huster, Stefanie Enriquez-Geppert, Christina F. Lavallee, Michael Falkenstein, and Christoph S. Herrmann. Electroencephalography of response inhibition tasks: Functional networks and cognitive contributions. *International Journal of Psychophysiology*, 87(3):217–233, March 2013. ISSN 0167-8760. doi: 10.1016/j.ijpsycho.2012.08.001.

[118] Cosimo Ieracitano, Nadia Mammone, Alessia Bramanti, Amir Hussain, and Francesco C Morabito. A convolutional neural network approach for classification of dementia stages based on 2D-spectral representation of EEG recordings. *Neurocomputing*, 323:96–107, January 2019. ISSN 0925-2312. doi: 10.1016/j.neucom.2018.09.071.

[119] Laura Sophie Imperatori, Monica Betta, Luca Cecchetti, Andrés Canales-Johnson, Emiliano Ricciardi, Francesca Siclari, Pietro Pietrini, Srivas Chennu, and Giulio Bernardi. Eeg functional connectivity metrics wpli and wsmi account for distinct types of brain functional interactions. *Scientific reports*, 9(1):1–15, 2019.

[120] Sergey Ioffe and Christian Szegedy. Batch normalization: Accelerating deep network training by reducing internal covariate shift. In *International Conference on Machine Learning*, pages 448–456. PMLR, 2015.

[121] Ryouhei Ishii, Leonides Canuet, Yasunori Aoki, Masahiro Hata, Masao Iwase, Shunichiro Ikeda, Keiichiro Nishida, and Manabu Ikeda. Healthy and Pathological Brain Aging: From the Perspective of Oscillations, Functional Connectivity, and Signal Complexity. *Neuropsychobiology*, 75(4):151–161, February 2018. ISSN 0302-282X. doi: 10.1159/000486870.

[122] Mahdi Jalili. Functional Brain Networks: Does the Choice of Dependency Estimator and Binarization Method Matter? *Scientific Reports*, 6(1):29780, July 2016. ISSN 2045-2322. doi: 10.1038/srep29780.

[123] Mahdi Jalili. Graph theoretical analysis of Alzheimer's disease: Discrimination of AD patients from healthy subjects. *Information Sciences*, 384:145–156, April 2017. ISSN 0020-0255. doi: 10.1016/j.ins.2016.08.047.

[124] Soobeom Jang, Seong-Eun Moon, and Jong-Seok Lee. EEG-based video identification using graph signal modeling and graph convolutional neural network. In *2018 IEEE International Conference on Acoustics, Speech and Signal Processing (ICASSP)*, pages 3066–3070. IEEE, 2018.

[125] Ole Jensen and Laura L Colgin. Cross-frequency coupling between neuronal oscillations. *Trends in cognitive sciences*, 11(7):267–269, 2007.

[126] Ole Jensen and Laura L. Colgin. Cross-frequency coupling between neuronal oscillations. *Trends in Cognitive Sciences*, 11(7):267–269, July 2007. ISSN 1364-6613, 1879-307X. doi: 10.1016/j.tics.2007.05.003.

[127] Dong-Hwa Jeong, Young-Do Kim, In-Uk Song, Yong-An Chung, and Jaeseung Jeong. Wavelet energy and wavelet coherence as EEG biomarkers for the diagnosis of Parkinson's disease-related dementia and Alzheimer's disease. *Entropy. An International and Interdisciplinary Journal of Entropy and Information Studies*, 18(1):8, 2016.

[128] Jaeseung Jeong. EEG dynamics in patients with Alzheimer's disease. *Clinical neurophysiology*, 115(7):1490–1505, 2004.

[129] Jaeseung Jeong, John C Gore, and Bradley S Peterson. Mutual information analysis of the eeg in patients with alzheimer's disease. *Clinical neurophysiology*, 112(5):827–835, May 2001. ISSN 1388-2457. doi: 10.1016/S1388-2457(01)00513-2.

[130] Jingjing Jia, Bofeng Zhang, Hehe Lv, Zhikang Xu, Shengxiang Hu, and Haiyan Li. CR-GCN: Channel-relationships-based graph convolutional network for EEG emotion recognition. *Brain Sciences*, 12(8):987, 2022.

[131] Manhua Jia, Wenjian Liu, Junwei Duan, Long Chen, CL Philip Chen, Qun Wang, and Zhiguo Zhou. Efficient graph convolutional networks for seizure prediction using scalp EEG. *Frontiers in Neuroscience*, 16:967116–967116, 2022.

[132] Ziyu Jia, Youfang Lin, Jing Wang, Ronghao Zhou, Xiaojun Ning, Yuanlai He, and Yaoshuai Zhao. GraphSleepNet: Adaptive spatial-temporal graph convolutional networks for sleep stage classification. In *IJCAI*, pages 1324–1330, 2020.

[133] Ziyu Jia, Youfang Lin, Jing Wang, Xiaojun Ning, Yuanlai He, Ronghao Zhou, Yuhan Zhou, and H Lehman Li-wei. Multi-view spatial-temporal graph convolutional networks with domain generalization for sleep stage classification. *IEEE Transactions on Neural Systems and Rehabilitation Engineering*, 29:1977–1986, 2021.

[134] Weiwei Jiang and Jiayun Luo. Graph neural network for traffic forecasting: A survey. *Expert Systems with Applications*, 207:117921, November 2022. ISSN 0957-4174. doi: 10.1016/j.eswa.2022.117921.

[135] Viktor Jirsa and Viktor Müller. Cross-frequency coupling in real and virtual brain networks. *Frontiers in Computational Neuroscience*, 7:78, 2013. ISSN 1662-5188.

[136] A Kabbara, H Eid, W El Falou, M Khalil, F Wendling, and M Hassan. Reduced integration and improved segregation of functional brain networks in Alzheimer's disease. *Journal of neural engineering*, 15(2):026023, 2018.

[137] Kedar Karhadkar, Pradeep Kr Banerjee, and Guido Montúfar. FoSR: First-order spectral rewiring for addressing oversquashing in GNNs, February 2023.

[138] Nastaran Khaleghi, Tohid Yousefi Rezaii, Soosan Beheshti, and Saeed Meshgini. Developing an efficient functional connectivity-based geometric deep network for automatic EEG-based visual decoding. *Biomedical Signal Processing and Control*, 80:104221, 2023.

[139] Mitsuru Kikuchi, Yuji Wada, and Yoshifumi Koshino. Differences in EEG Harmonic Driving Responses to Photic Stimulation between Normal Aging and

Alzheimer's Disease. *Clinical Electroencephalography*, 33(2):86–92, April 2002. ISSN 0009-9155. doi: 10.1177/155005940203300208.

[140] Ji-Sun Kim, Seung-Hwan Lee, Gewnhi Park, Sangrae Kim, Sung-Man Bae, Do-Won Kim, and Chang-Hwan Im. Clinical Implications of Quantitative Electroencephalography and Current Source Density in Patients with Alzheimer's Disease. *Brain Topography*, 25(4):461–474, October 2012. ISSN 1573-6792. doi: 10.1007/s10548-012-0234-1.

[141] Dominik Klepl, Fei He, Wu Min, Daniel Blackburn, and Ptolemaios Sarrigiannis. Bispectrum-based Cross-frequency Functional Connectivity: Classification of Alzheimer's disease. In *2022 44th Annual International Conference of the IEEE Engineering in Medicine & Biology Society (EMBC)*, pages 305–308, July 2022. doi: 10.1109/EMBC48229.2022.9871366.

[142] Dominik Klepl, Fei He, Min Wu, Daniel J. Blackburn, and Ptolemaios Sarrigiannis. EEG-Based Graph Neural Network Classification of Alzheimer's Disease: An Empirical Evaluation of Functional Connectivity Methods. *IEEE Transactions on Neural Systems and Rehabilitation Engineering*, 30:2651–2660, 2022. ISSN 1558-0210. doi: 10.1109/TNSRE.2022.3204913.

[143] Dominik Klepl, Fei He, Min Wu, Matteo De Marco, Daniel J. Blackburn, and Ptolemaios G. Sarrigiannis. Characterising Alzheimer's Disease With EEG-Based Energy Landscape Analysis. *IEEE Journal of Biomedical and Health Informatics*, 26(3):992–1000, March 2022. ISSN 2168-2208. doi: 10.1109/JBHI.2021.3105397.

[144] Dominik Klepl, Fei He, Min Wu, Daniel J. Blackburn, and Ptolemaios Sarrigiannis. Adaptive Gated Graph Convolutional Network for Explainable Diagnosis of Alzheimer's Disease Using EEG Data. *IEEE Transactions on Neural Systems and Rehabilitation Engineering*, 31:3978–3987, 2023. ISSN 1558-0210. doi: 10.1109/TNSRE.2023.3321634.

[145] Dominik Klepl, Fei He, Min Wu, Daniel J. Blackburn, and Ptolemaios G. Sarrigiannis. Cross-Frequency Multilayer Network Analysis with Bispectrum-based Functional Connectivity: A Study of Alzheimer's Disease. *Neuroscience*, 521:77–88, June 2023. ISSN 0306-4522. doi: 10.1016/j.neuroscience.2023.04.008.

[146] Dominik Klepl, Min Wu, and Fei He. Graph Neural Network-Based EEG Classification: A Survey. *IEEE Transactions on Neural Systems and Rehabilitation Engineering*, 32:493–503, 2024. ISSN 1558-0210. doi: 10.1109/TNSRE.2024.3355750.

[147] V Knott, E Mohr, C Mahoney, and V Ilivitsky. Quantitative electroencephalography in Alzheimer's disease: Comparison with a control group, population norms and mental status. *Journal of Psychiatry and Neuroscience*, 26(2):106–116, March 2001. ISSN 1180-4882.

[148] T. Koenig, L. Prichep, T. Dierks, D. Hubl, L. O. Wahlund, E. R. John, and V. Jelic. Decreased EEG synchronization in Alzheimer's disease and mild cognitive impairment. *Neurobiology of Aging*, 26(2):165–171, February 2005. ISSN 0197-4580. doi: 10.1016/j.neurobiolaging.2004.03.008.

[149] Wanzeng Kong, Min Qiu, Menghang Li, Xuanyu Jin, and Li Zhu. Causal graph convolutional neural network for emotion recognition. *IEEE Transactions on Cognitive and Developmental Systems*, 2022.

[150] Thomas König, L Prichep, Thomas Dierks, Daniela Hubl, LO Wahlund, ER John, and V Jelic. Decreased EEG synchronization in Alzheimer's disease and mild cognitive impairment. *Neurobiology of aging*, 26(2):165–171, 2005.

[151] Christopher K Kovach, Hiroyuki Oya, and Hiroto Kawasaki. The bispectrum and its relationship to phase-amplitude coupling. *Neuroimage*, 173:518–539, 2018.

[152] Devin Kreuzer, Dominique Beaini, Will Hamilton, Vincent Létourneau, and Prudencio Tossou. Rethinking Graph Transformers with Spectral Attention. In *Advances in Neural Information Processing Systems*, volume 34, pages 21618–21629. Curran Associates, Inc., 2021.

[153] Max Kuhn. *Caret: Classification and Regression Training*, 2021.

[154] N. N. Kulkarni and V. K. Bairagi. Extracting Salient Features for EEG-based Diagnosis of Alzheimer's Disease Using Support Vector Machine Classifier. *IETE Journal of Research*, 63(1):11–22, January 2017. ISSN 0377-2063. doi: 10.1080/03772063.2016.1241164.

[155] Youngchul Kwak, Woo-Jin Song, and Seong-Eun Kim. Graph neural network with multilevel feature fusion for EEG based brain-computer interface.

In *2020 IEEE International Conference on Consumer Electronics-Asia (ICCE-Asia)*, pages 1–3. IEEE, 2020.

[156] Fabio La Foresta, Francesco Carlo Morabito, Silvia Marino, and Serena Dattola. High-Density EEG Signal Processing Based on Active Source Reconstruction for Brain Network Analysis in Alzheimer's Disease. *Electronics*, 8(9):1031, September 2019. ISSN 2079-9292. doi: 10.3390/electronics8091031.

[157] Chiou-Lian Lai, Ruey-Tay Lin, Li-Min Liou, and Ching-Kuan Liu. The role of event-related potentials in cognitive decline in Alzheimer's disease. *Clinical Neurophysiology*, 121(2):194–199, February 2010. ISSN 1388-2457. doi: 10.1016/j.clinph.2009.11.001.

[158] Vito Latora and Massimo Marchiori. Vulnerability and protection of infrastructure networks. *Physical Review E*, 71(1):015103, 2005.

[159] Junhyun Lee, Inyeop Lee, and Jaewoo Kang. Self-attention graph pooling. In *Proceedings of the 36th International Conference on Machine Learning*, pages 3734–3743. PMLR, May 2019.

[160] Chao Li, Yong Sheng, Haishuai Wang, Mingyue Niu, Peiguang Jing, Ziping Zhao, and Björn W Schuller. EEG emotion recognition based on self-attention dynamic graph neural networks. In *2022 44th Annual International Conference of the IEEE Engineering in Medicine & Biology Society (EMBC)*, pages 292–296. IEEE, 2022.

[161] Hanyu Li, Xu Zhang, and Ying Xia. EEG emotion recognition based on dynamically organized graph neural network. In *International Conference on Multimedia Modeling*, pages 344–355. Springer, 2022.

[162] Jingcong Li, Shuqi Li, Jiahui Pan, and Fei Wang. Cross-subject EEG emotion recognition with self-organized graph neural network. *Frontiers in Neuroscience*, page 689, 2021.

[163] Lu-Bao Li, Tian Chen, Fu-Ji Ren, and Bei-Bei Luo. Bimodal emotion recognition method based on graph neural networks and attention. *Journal of Computer Applications*, 43(3):700–705, 2022.

[164] Menglei Li, Hongbo Chen, and Zixue Cheng. An attention-guided spatiotemporal graph convolutional network for sleep stage classification. *Life*, 12(5):622, 2022.

[165] Rihui Li, Thinh Nguyen, Thomas Potter, and Yingchun Zhang. Dynamic cortical connectivity alterations associated with Alzheimer's disease: An EEG and fNIRS integration study. *NeuroImage: Clinical*, 21:101622, January 2019. ISSN 2213-1582. doi: 10.1016/j.nicl.2018.101622.

[166] Rui Li, Yiting Wang, and Bao-Liang Lu. A multi-domain adaptive graph convolutional network for EEG-based emotion recognition. In *Proceedings of the 29th ACM International Conference on Multimedia*, pages 5565–5573, 2021.

[167] Rui Li, Xin Yuan, Mohsen Radfar, Peter Marendy, Wei Ni, Terrence J. O'Brien, and Pablo M. Casillas-Espinosa. Graph signal processing, graph neural network and graph learning on biological data: A systematic review. *IEEE Reviews in Biomedical Engineering*, 16:109–135, 2023. ISSN 1941-1189. doi: 10.1109/RBME.2021.3122522.

[168] Xiang Li, Jing Li, Yazhou Zhang, and Prayag Tiwari. Emotion recognition from multi-channel EEG data through a dual-pipeline graph attention network. In *2021 IEEE International Conference on Bioinformatics and Biomedicine (BIBM)*, pages 3642–3647. IEEE, 2021.

[169] Xiaowei Li, Rong La, Ying Wang, Bin Hu, and Xuemin Zhang. A deep learning approach for mild depression recognition based on functional connectivity using electroencephalography. *Frontiers in neuroscience*, 14:192, 2020.

[170] Xiaoxu Li, Wenming Zheng, Yuan Zong, Hongli Chang, and Cheng Lu. Attention-based spatio-temporal graphic LSTM for EEG emotion recognition. In *2021 International Joint Conference on Neural Networks (IJCNN)*, pages 1–8. IEEE, 2021.

[171] Xiaoyu Li, Buyue Qian, Jishang Wei, An Li, Xuan Liu, and Qinghua Zheng. Classify EEG and reveal latent graph structure with spatio-temporal graph convolutional neural network. In *2019 IEEE International Conference on Data Mining (ICDM)*, pages 389–398. IEEE, 2019.

[172] Xin Li, Changjie Yang, Ping Xie, Ying Han, Rui Su, Zhenyang Li, and Yi Liu. The diagnosis of amnestic mild cognitive impairment by combining the characteristics of brain functional network and support vector machine classifier. *Journal of Neuroscience Methods*, 363:109334, November 2021. ISSN 0165-0270. doi: 10.1016/j.jneumeth.2021.109334.

[173] Yan Li, Ning Zhong, David Taniar, and Haolan Zhang. Mutualgraphnet: A novel model for motor imagery classification. *arXiv preprint arXiv:2109.04361*, 2021.

[174] Yang Li, Yu Liu, Yu-Zhu Guo, Xiao-Feng Liao, Bin Hu, and Tao Yu. Spatio-temporal-spectral hierarchical graph convolutional network with semisupervised active learning for patient-specific seizure prediction. *IEEE Transactions on Cybernetics*, 2021.

[175] Yujia Li, Richard Zemel, Marc Brockschmidt, and Daniel Tarlow. Gated graph sequence neural networks. In *Proceedings of ICLR'16*, 2016.

[176] Qi Lian, Yu Qi, Gang Pan, and Yueming Wang. Learning graph in graph convolutional neural networks for robust seizure prediction. *Journal of Neural Engineering*, 17(3):035004, 2020.

[177] Zhiqiang Lin, Taorong Qiu, Ping Liu, Lingyun Zhang, Siwei Zhang, and Zhendong Mu. Fatigue driving recognition based on deep learning and graph neural network. *Biomedical Signal Processing and Control*, 68:102598, 2021.

[178] Hanjie Liu, Jinren Zhang, Qingshan Liu, and Jinde Cao. Minimum spanning tree based graph neural network for emotion classification using EEG. *Neural Networks*, 145:308–318, 2022.

[179] Roberta Lizio, Claudio Del Percio, Nicola Marzano, Andrea Soricelli, Görsev G. Yener, Erol Başar, Ciro Mundi, Salvatore De Rosa, Antonio Ivano Triggiani, Raffaele Ferri, Dario Arnaldi, Flavio Mariano Nobili, Susanna Cordone, Susanna Lopez, Filippo Carducci, Giulia Santi, Loreto Gesualdo, Paolo M. Rossini, Enrica Cavedo, Margherita Mauri, Giovanni B. Frisoni, and Claudio Babiloni. Neurophysiological Assessment of Alzheimer's Disease Individuals by a Single Electroencephalographic Marker. *Journal of Alzheimer's Disease*, 49(1):159–177, January 2016. ISSN 1387-2877. doi: 10.3233/JAD-143042.

[180] Maria E. López, Marjolein M. A. Engels, Elisabeth C. W. van Straaten, Ricardo Bajo, María L. Delgado, Philip Scheltens, Arjan Hillebrand, Cornelis J. Stam, and Fernando Maestú. MEG Beamformer-Based Reconstructions of Functional Networks in Mild Cognitive Impairment. *Frontiers in Aging Neuroscience*, 9, 2017. ISSN 1663-4365.

[181] Jianchao Lu, Yuzhe Tian, Shuang Wang, Michael Sheng, and Xi Zheng. PearNet: A pearson correlation-based graph attention network for sleep stage recognition. *arXiv preprint arXiv:2209.13645*, 2022.

[182] Mingqi Lv, Zhaoxiong Hong, Ling Chen, Tieming Chen, Tiantian Zhu, and Shouling Ji. Temporal multi-graph convolutional network for traffic flow prediction. *IEEE Transactions on Intelligent Transportation Systems*, 22(6):3337–3348, June 2021. ISSN 1558-0016. doi: 10.1109/TITS.2020.2983763.

[183] Naghmeh Mahmoodian, Axel Boese, Michael Friebe, and Javad Haddadnia. Epileptic seizure detection using cross-bispectrum of electroencephalogram signal. *Seizure : the journal of the British Epilepsy Association*, 66:4–11, 2019.

[184] Masoud Malekzadeh, Parisa Hajibabaee, Maryam Heidari, Samira Zad, Ozlem Uzuner, and James H Jones. Review of graph neural network in text classification. In *2021 IEEE 12th Annual Ubiquitous Computing, Electronics & Mobile Communication Conference (UEMCON)*, pages 0084–0091, December 2021. doi: 10.1109/UEMCON53757.2021.9666633.

[185] Nadia Mammone, Cosimo Ieracitano, Hojjat Adeli, Alessia Bramanti, and Francesco C. Morabito. Permutation Jaccard Distance-Based Hierarchical Clustering to Estimate EEG Network Density Modifications in MCI Subjects. *IEEE Transactions on Neural Networks and Learning Systems*, 29(10):5122–5135, October 2018. ISSN 2162-237X, 2162-2388. doi: 10.1109/TNNLS.2018.2791644.

[186] Nadia Mammone, Simona De Salvo, Lilla Bonanno, Cosimo Ieracitano, Silvia Marino, Angela Marra, Alessia Bramanti, and Francesco C. Morabito. Brain Network Analysis of Compressive Sensed High-Density EEG Signals in AD and MCI Subjects. *IEEE Transactions on Industrial Informatics*, 15(1):527–536, January 2019. ISSN 1551-3203, 1941-0050. doi: 10.1109/TII.2018.2868431.

[187] Aarón Maturana-Candelas, Carlos Gómez, Jesús Poza, Saúl J Ruiz-Gómez, and Roberto Hornero. Inter-band bispectral analysis of EEG background activity to characterize alzheimer's disease continuum. *Frontiers in Computational Neuroscience*, 14, 2020.

[188] Ali Mazaheri, Katrien Segaert, John Olichney, Jin-Chen Yang, Yu-Qiong Niu, Kim Shapiro, and Howard Bowman. EEG oscillations during word processing

predict MCI conversion to Alzheimer's disease. *NeuroImage: Clinical*, 17:188–197, January 2018. ISSN 2213-1582. doi: 10.1016/j.nicl.2017.10.009.

[189] Joseph McBride, Xiaopeng Zhao, Nancy Munro, Gregory Jicha, Charles Smith, and Yang Jiang. Discrimination of mild cognitive impairment and alzheimer's disease using transfer entropy measures of scalp eeg. *Journal of healthcare engineering*, 6(1):55–70, 2015.

[190] Ramtin Mehraram, Marcus Kaiser, Ruth Cromarty, Sara Graziadio, John T. O'Brien, Alison Killen, John-Paul Taylor, and Luis R. Peraza. Weighted network measures reveal differences between dementia types: An EEG study. *Human Brain Mapping*, 41(6):1573–1590, 2020. ISSN 1097-0193. doi: 10.1002/hbm.24896.

[191] Andreas Miltiadous, Katerina D. Tzimourta, Theodora Afrantou, Panagiotis Ioannidis, Nikolaos Grigoriadis, Dimitrios G. Tsalikakis, Pantelis Angelidis, Markos G. Tsipouras, Euripidis Glavas, Nikolaos Giannakeas, and Alexandros T. Tzallas. A Dataset of Scalp EEG Recordings of Alzheimer's Disease, Frontotemporal Dementia and Healthy Subjects from Routine EEG. *Data*, 8(6):95, June 2023. ISSN 2306-5729. doi: 10.3390/data8060095.

[192] D. V. Moretti, C. Fracassi, M. Pievani, C. Geroldi, G. Binetti, O. Zanetti, K. Sosta, P. M. Rossini, and G. B. Frisoni. Increase of theta/gamma ratio is associated with memory impairment. *Clinical Neurophysiology*, 120(2):295–303, February 2009. ISSN 1388-2457. doi: 10.1016/j.clinph.2008.11.012.

[193] D. V. Moretti, G. B. Frisoni, C. Fracassi, M. Pievani, C. Geroldi, G. Binetti, P. M. Rossini, and O. Zanetti. MCI patients' EEGs show group differences between those who progress and those who do not progress to AD. *Neurobiology of Aging*, 32(4):563–571, April 2011. ISSN 0197-4580. doi: 10.1016/j.neurobiolaging.2009.04.003.

[194] Florian Mormann, Juergen Fell, Nikolai Axmacher, Bernd Weber, Klaus Lehnertz, Christian E. Elger, and Guillén Fernández. Phase/amplitude reset and theta–gamma interaction in the human medial temporal lobe during a continuous word recognition memory task. *Hippocampus*, 15(7):890–900, 2005.

[195] Christopher Morris, Martin Ritzert, Matthias Fey, William L Hamilton, Jan Eric Lenssen, Gaurav Rattan, and Martin Grohe. Weisfeiler and Leman go neural:

Higher-order graph neural networks. In *Proceedings of the AAAI Conference on Artificial Intelligence*, volume 33, pages 4602–4609, 2019.

[196] Sarah Feldt Muldoon and Danielle S. Bassett. Network and Multilayer Network Approaches to Understanding Human Brain Dynamics. *Philosophy of Science*, 83 (5):710–720, December 2016. ISSN 0031-8248, 1539-767X. doi: 10.1086/687857.

[197] Christian Sandøe Musaeus, Knut Engedal, Peter Høgh, Vesna Jelic, Morten Mørup, Mala Naik, Anne-Rita Oeksengaard, Jon Snaedal, Lars-Olof Wahlund, Gunhild Waldemar, and Birgitte Bo Andersen. Oscillatory connectivity as a diagnostic marker of dementia due to Alzheimer's disease. *Clinical Neurophysiology*, 130(10):1889–1899, October 2019. ISSN 1388-2457. doi: 10.1016/j.clinph.2019.07.016.

[198] Christian Sandøe Musaeus, Malene Schjønning Nielsen, Jørgen Sandøe Musaeus, and Peter Høgh. Electroencephalographic cross-frequency coupling as a sign of disease progression in patients with mild cognitive impairment: A pilot study. *Frontiers in neuroscience*, page 790, 2020.

[199] C Neuper and G Pfurtscheller. Event-related dynamics of cortical rhythms: Frequency-specific features and functional correlates. *International Journal of Psychophysiology*, 43(1):41–58, December 2001. ISSN 0167-8760. doi: 10.1016/S0167-8760(01)00178-7.

[200] Volker Nimmrich, Andreas Draguhn, and Nikolai Axmacher. Neuronal Network Oscillations in Neurodegenerative Diseases. *NeuroMolecular Medicine*, 17(3):270–284, September 2015. ISSN 1559-1174. doi: 10.1007/s12017-015-8355-9.

[201] Stephanie Noble, Dustin Scheinost, and R Todd Constable. A decade of test-retest reliability of functional connectivity: A systematic review and meta-analysis. *Neuroimage*, 203:116157, 2019.

[202] Sou Nobukawa, Teruya Yamanishi, Shinya Kasakawa, Haruhiko Nishimura, Mitsuru Kikuchi, and Tetsuya Takahashi. Classification methods based on complexity and synchronization of electroencephalography signals in Alzheimer's disease. *Frontiers in psychiatry*, 11:255, 2020. ISSN 1664-0640.

[203] Guido Nolte, Ou Bai, Lewis Wheaton, Zoltan Mari, Sherry Vorbach, and Mark

Hallett. Identifying true brain interaction from EEG data using the imaginary part of coherency. *Clinical neurophysiology*, 115(10):2292–2307, 2004.

[204] Paul L. Nunez and Ramesh Srinivasan. *Electric Fields of the Brain: The Neurophysics of EEG*. Oxford University Press, 2006. ISBN 978-0-19-505038-7.

[205] Adam Paszke, Sam Gross, Francisco Massa, Adam Lerer, James Bradbury, Gregory Chanan, Trevor Killeen, Zeming Lin, Natalia Gimelshein, Luca Antiga, Alban Desmaison, Andreas Kopf, Edward Yang, Zachary DeVito, Martin Raison, Alykhan Tejani, Sasank Chilamkurthy, Benoit Steiner, Lu Fang, Junjie Bai, and Soumith Chintala. PyTorch: An imperative style, high-performance deep learning library. In *Advances in Neural Information Processing Systems 32*, pages 8024–8035. Curran Associates, Inc., 2019.

[206] The-Hanh Pham, Jahmunah Vicnesh, Joel Koh En Wei, Shu Lih Oh, N Arunkumar, Enas W Abdulhay, Edward J Ciaccio, and U Rajendra Acharya. Autism spectrum disorder diagnostic system using HOS bispectrum with EEG signals. *International journal of environmental research and public health*, 17(3):971, 2020.

[207] Michela Pievani, Willem de Haan, Tao Wu, William W Seeley, and Giovanni B Frisoni. Functional network disruption in the degenerative dementias. *The Lancet Neurology*, 10(9):829–843, 2011.

[208] Rok Požar, Bruno Giordani, and Voyko Kavcic. Effective differentiation of mild cognitive impairment by functional brain graph analysis and computerized testing. *PLOS ONE*, 15(3):e0230099, March 2020. ISSN 1932-6203. doi: 10.1371/journal.pone.0230099.

[209] Robert Clay Prim. Shortest connection networks and some generalizations. *The Bell System Technical Journal*, 36(6):1389–1401, 1957.

[210] Darshana Priyasad, Tharindu Fernando, Simon Denman, Sridha Sridharan, and Clinton Fookes. Affect recognition from scalp-EEG using channel-wise encoder networks coupled with geometric deep learning and multi-channel feature fusion. *Knowledge-Based Systems*, page 109038, 2022.

[211] Serge Przedborski, Miquel Vila, and Vernice Jackson-Lewis. Series Introduction: Neurodegeneration: What is it and where are we? *The Journal of Clinical*

Investigation, 111(1):3–10, January 2003. ISSN 0021-9738. doi: 10.1172/JCI17522.

[212] Sandra Pusil, Stavros I. Dimitriadis, María Eugenia López, Ernesto Pereda, and Fernando Maestú. Aberrant MEG multi-frequency phase temporal synchronization predicts conversion from mild cognitive impairment-to-Alzheimer's disease. *NeuroImage: Clinical*, 24:101972, January 2019. ISSN 2213-1582. doi: 10.1016/j.nicl.2019.101972.

[213] R Core Team. *R: A Language and Environment for Statistical Computing*. Vienna, Austria, 2021.

[214] Khadijeh Raeisi, Mohammad Khazaei, Pierpaolo Croce, Gabriella Tamburro, Silvia Comani, and Filippo Zappasodi. A GRAPH CONVOLUTIONAL NEURAL NETWORK FOR THE AUTOMATED DETECTION OF SEIZURES IN THE NEONATAL EEG. *Computer Methods and Programs in Biomedicine*, page 106950, 2022.

[215] Ekagra Ranjan, Soumya Sanyal, and Partha Talukdar. Asap: Adaptive structure aware pooling for learning hierarchical graph representations. In *Proceedings of the AAAI Conference on Artificial Intelligence*, volume 34, pages 5470–5477, 2020.

[216] Patrick Reiser, Marlen Neubert, André Eberhard, Luca Torresi, Chen Zhou, Chen Shao, Houssam Metni, Clint van Hoesel, Henrik Schopmans, Timo Sommer, and Pascal Friederich. Graph neural networks for materials science and chemistry. *Communications Materials*, 3(1):1–18, November 2022. ISSN 2662-4443. doi: 10.1038/s43246-022-00315-6.

[217] Francisco Aparecido Rodrigues, Caroline Alves, Aruane Pineda, Kirstin Roster, and Cristiane Thielemann. EEG functional connectivity and deep learning for automatic diagnosis of brain disorders: Alzheimer's disease and schizophrenia. *Journal of Physics: Complexity*, pages 1–13, 2022.

[218] Pedro Rodrigues and João Paulo Teixeira. Artificial Neural Networks in the Discrimination of Alzheimer's Disease. In Maria Manuela Cruz-Cunha, João Varajão, Philip Powell, and Ricardo Martinho, editors, *ENTERprise Information Systems*, Communications in Computer and Information Science, pages 272–281,

Berlin, Heidelberg, 2011. Springer. ISBN 978-3-642-24352-3. doi: 10.1007/978-3--642-24352-3_29.

[219] Jee Hoon Roh, Moon Ho Park, Deokwon Ko, Kun-Woo Park, Dae-Hie Lee, Changsu Han, Sangmee Anh Jo, Kyung-Sook Yang, and Ki-Young Jung. Region- and frequency-specific changes of spectral power in Alzheimer's disease and mild cognitive impairment. *Clinical Neurophysiology*, 122(11):2169–2176, November 2011. ISSN 1388-2457. doi: 10.1016/j.clinph.2011.03.023.

[220] Gonzalo M Rojas, Carolina Alvarez, Carlos E Montoya, María de la Iglesia-Vayá, Jaime E Cisternas, and Marcelo Gálvez. Study of resting-state functional connectivity networks using eeg electrodes position as seed. *Frontiers in neuroscience*, 12:235, 2018.

[221] P. M. Rossini, C. Del Percio, P. Pasqualetti, E. Cassetta, G. Binetti, G. Dal Forno, F. Ferreri, G. Frisoni, P. Chiovenda, C. Miniussi, L. Parisi, M. Tombini, F. Vecchio, and C. Babiloni. Conversion from mild cognitive impairment to Alzheimer's disease is predicted by sources and coherence of brain electroencephalography rhythms. *Neuroscience*, 143(3):793–803, December 2006. ISSN 0306-4522. doi: 10.1016/j.neuroscience.2006.08.049.

[222] Paolo M. Rossini, Simone Rossi, Claudio Babiloni, and John Polich. Clinical neurophysiology of aging brain: From normal aging to neurodegeneration. *Progress in Neurobiology*, 83(6):375–400, December 2007. ISSN 0301-0082. doi: 10.1016/j.pneurobio.2007.07.010.

[223] Mikail Rubinov and Olaf Sporns. Complex network measures of brain connectivity: Uses and interpretations. *NeuroImage*, 52(3):1059–1069, September 2010. ISSN 1053-8119. doi: 10.1016/j.neuroimage.2009.10.003.

[224] Vangelis Sakkalis. Review of advanced techniques for the estimation of brain connectivity measured with eeg/meg. *Computers in biology and medicine*, 41 (12):1110–1117, 2011.

[225] Jorge E. Santos Toural, Arquímedes Montoya Pedrón, and Enrique J. Marañón Reyes. A new method for classification of subjects with major cognitive disorder, Alzheimer type, based on electroencephalographic biomarkers. *Informatics in Medicine Unlocked*, 23:100537, January 2021. ISSN 2352-9148. doi: 10.1016/j.imu.2021.100537.

[226] B Schack, Wolfgang Klimesch, and Paul Sauseng. Phase synchronization between theta and upper alpha oscillations in a working memory task. *International Journal of Psychophysiology*, 57(2):105–114, 2005.

[227] Alfons Schnitzler and Joachim Gross. Normal and pathological oscillatory communication in the brain. *Nature Reviews Neuroscience*, 6(4):285–296, April 2005. ISSN 1471-0048. doi: 10.1038/nrn1650.

[228] Youngjoo Seo, Michaël Defferrard, Pierre Vandergheynst, and Xavier Bresson. Structured sequence modeling with graph convolutional recurrent networks. In Long Cheng, Andrew Chi Sing Leung, and Seiichi Ozawa, editors, *Neural Information Processing*, Lecture Notes in Computer Science, pages 362–373, Cham, 2018. Springer International Publishing. ISBN 978-3-030-04167-0. doi: 10.1007/978-3-030-04167-0_33.

[229] Xiaocai Shan, Jun Cao, Shoudong Huo, Liangyu Chen, Ptolemaios Georgios Sarrigiannis, and Yifan Zhao. Spatial–temporal graph convolutional network for Alzheimer classification based on brain functional connectivity imaging of electroencephalogram. *Human Brain Mapping*, 2022.

[230] Yunsheng Shi, Zhengjie Huang, Shikun Feng, Hui Zhong, Wenjin Wang, and Yu Sun. Masked label prediction: Unified message passing model for semi-supervised classification, May 2021.

[231] Markus Siegel, Tobias H. Donner, and Andreas K. Engel. Spectral fingerprints of large-scale neuronal interactions. *Nature Reviews Neuroscience*, 13(2):121–134, February 2012. ISSN 1471-0048. doi: 10.1038/nrn3137.

[232] Wolf Singer. Consciousness and the Binding Problem. *Annals of the New York Academy of Sciences*, 929(1):123–146, 2001. ISSN 1749-6632. doi: 10.1111/j.1749-6632.2001.tb05712.x.

[233] Una Smailovic, Thomas Koenig, Ingemar Kåreholt, Thomas Andersson, Milica Gregoric Kramberger, Bengt Winblad, and Vesna Jelic. Quantitative EEG power and synchronization correlate with Alzheimer's disease CSF biomarkers. *Neurobiology of Aging*, 63:88–95, March 2018. ISSN 0197-4580. doi: 10.1016/j.neurobiolaging.2017.11.005.

[234] Tengfei Song, Suyuan Liu, Wenming Zheng, Yuan Zong, and Zhen Cui. Instance-adaptive graph for EEG emotion recognition. In *Proceedings of the AAAI Conference on Artificial Intelligence*, volume 34(03), pages 2701–2708, 2020.

[235] Tengfei Song, Suyuan Liu, Wenming Zheng, Yuan Zong, Zhen Cui, Yang Li, and Xiaoyan Zhou. Variational instance-adaptive graph for EEG emotion recognition. *IEEE Transactions on Affective Computing*, 2021.

[236] Zhenxi Song, Bin Deng, Jiang Wang, and Ruofan Wang. Biomarkers for Alzheimer's disease defined by a novel brain functional network measure. *IEEE Transactions on Biomedical Engineering*, 66(1):41–49, January 2018. ISSN 1558-2531. doi: 10.1109/TBME.2018.2834546.

[237] C. J. Stam, B. F. Jones, I. Manshanden, A. M. van Cappellen van Walsum, T. Montez, J. P. A. Verbunt, J. C. de Munck, B. W. van Dijk, H. W. Berendse, and P. Scheltens. Magnetoencephalographic evaluation of resting-state functional connectivity in Alzheimer's disease. *NeuroImage*, 32(3):1335–1344, September 2006. ISSN 1053-8119. doi: 10.1016/j.neuroimage.2006.05.033.

[238] C. J. Stam, W. de Haan, A. Daffertshofer, B. F. Jones, I. Manshanden, A. M. van Cappellen van Walsum, T. Montez, J. P. A. Verbunt, J. C. de Munck, B. W. van Dijk, H. W. Berendse, and P. Scheltens. Graph theoretical analysis of magnetoencephalographic functional connectivity in Alzheimer's disease. *Brain*, 132 (1):213–224, January 2009. ISSN 0006-8950. doi: 10.1093/brain/awn262.

[239] C.J. Stam, A.M. Van Cappellen van Walsum, Y.A.L. Pijnenburg, H.W. Berendse, J.C. De Munck, P. Scheltens, and B.W. Van Dijk. Generalized synchronization of MEG recordings in Alzheimer's disease: Evidence for involvement of the gamma band. *Journal of Clinical Neurophysiology*, 19(6):562–574, 2002. ISSN 0736-0258. doi: 10.1097/00004691-200212000-00010.

[240] Cornelis J Stam, BF Jones, G Nolte, M Breakspear, and Ph Scheltens. Small-world networks and functional connectivity in Alzheimer's disease. *Cerebral cortex*, 17(1):92–99, 2007. ISSN 1460-2199. doi: 10.1093/cercor/bhj127.

[241] Cornelis J Stam, Guido Nolte, and Andreas Daffertshofer. Phase lag index: Assessment of functional connectivity from multi channel EEG and MEG with diminished bias from common sources. *Human brain mapping*, 28(11):1178–1193, 2007.

[242] Biao Sun, Han Zhang, Zexu Wu, Yunyan Zhang, and Ting Li. Adaptive spatiotemporal graph convolutional networks for motor imagery classification. *IEEE Signal Processing Letters*, 28:219–223, 2021.

[243] Mengying Sun, Sendong Zhao, Coryandar Gilvary, Olivier Elemento, Jiayu Zhou, and Fei Wang. Graph convolutional networks for computational drug development and discovery. *Briefings in Bioinformatics*, 21(3):919–935, May 2020. ISSN 1477-4054. doi: 10.1093/bib/bbz042.

[244] Mingyi Sun, Weigang Cui, Shuyue Yu, Hongbin Han, Bin Hu, and Yang Li. A dual-branch dynamic graph convolution based adaptive transformer feature fusion network for EEG emotion recognition. *IEEE Transactions on Affective Computing*, 2022.

[245] Shuting Sun, Xiaowei Li, Jing Zhu, Ying Wang, Rong La, Xuemin Zhang, Liuqing Wei, and Bin Hu. Graph theory analysis of functional connectivity in major depression disorder with high density resting state EEG data. *IEEE Transactions on Neural Systems and Rehabilitation Engineering*, 27(3):429–439, 2019.

[246] Xinlin Sun, Chao Ma, Peiyin Chen, Mengyu Li, He Wang, Weidong Dang, Chaoxu Mu, and Zhongke Gao. A novel complex network-based graph convolutional network in major depressive disorder detection. *IEEE Transactions on Instrumentation and Measurement*, 2022.

[247] Kaustubh Supekar, Vinod Menon, Daniel Rubin, Mark Musen, and Michael D Greicius. Network analysis of intrinsic functional brain connectivity in Alzheimer's disease. *PLoS computational biology*, 4(6):e1000100, 2008.

[248] Gabriella Tamburro, Selenia di Fronso, Claudio Robazza, Maurizio Bertollo, and Silvia Comani. Modulation of brain functional connectivity and efficiency during an endurance cycling task: a source level eeg and graph theory approach. *Frontiers in Human Neuroscience*, 14:243, 2020.

[249] Siyi Tang, Jared Dunnmon, Khaled Kamal Saab, Xuan Zhang, Qianying Huang, Florian Dubost, Daniel Rubin, and Christopher Lee Messer. Self supervised graph neural networks for improved electroencephalographic seizure analysis. In *International Conference on Learning Representations*, 2021.

[250] Tian–li Tao, Liang–hu Guo, Qiang He, Han Zhang, and Lin Xu. Seizure detection by brain-connectivity analysis using dynamic graph isomorphism network. In *2022 44th Annual International Conference of the IEEE Engineering in Medicine & Biology Society (EMBC)*, pages 2302–2305. IEEE, 2022.

[251] P. Tass, M. G. Rosenblum, J. Weule, J. Kurths, A. Pikovsky, J. Volkmann, A. Schnitzler, and H.-J. Freund. Detection of $\mathit{n}:\mathit{m}$ Phase Locking from Noisy Data: Application to Magnetoencephalography. *Physical Review Letters*, 81(15):3291–3294, October 1998. doi: 10.1103/PhysRevLett.81.3291.

[252] Robert D. Terry, Eliezer Masliah, David P. Salmon, Nelson Butters, Richard DeTeresa, Robert Hill, Lawrence A. Hansen, and Robert Katzman. Physical basis of cognitive alterations in alzheimer's disease: Synapse loss is the major correlate of cognitive impairment. *Annals of Neurology*, 30(4):572–580, 1991. ISSN 1531-8249. doi: 10.1002/ana.410300410.

[253] P. Tewarie, E. van Dellen, A. Hillebrand, and C. J. Stam. The minimum spanning tree: An unbiased method for brain network analysis. *NeuroImage*, 104:177–188, January 2015. ISSN 1053-8119. doi: 10.1016/j.neuroimage.2014.10.015.

[254] Prejaas Tewarie, Arjan Hillebrand, Bob W van Dijk, Cornelis J Stam, George C O'Neill, Piet Van Mieghem, Jil M Meier, Mark W Woolrich, Peter G Morris, and Matthew J Brookes. Integrating cross-frequency and within band functional networks in resting-state MEG: A multi-layer network approach. *Neuroimage*, 142:324–336, 2016.

[255] James Theiler, Stephen Eubank, André Longtin, Bryan Galdrikian, and J Doyne Farmer. Testing for nonlinearity in time series: The method of surrogate data. *Physica D: Nonlinear Phenomena*, 58(1-4):77–94, 1992.

[256] Jake Topping, Francesco Di Giovanni, Benjamin Paul Chamberlain, Xiaowen Dong, and Michael M. Bronstein. Understanding over-squashing and bottlenecks on graphs via curvature, November 2022.

[257] Adriano B. L. Tort, Robert Komorowski, Howard Eichenbaum, and Nancy Kopell. Measuring Phase-Amplitude Coupling Between Neuronal Oscillations of Different Frequencies. *Journal of Neurophysiology*, 104(2):1195–1210, August 2010. ISSN 0022-3077. doi: 10.1152/jn.00106.2010.

[258] Adriano BL Tort, Mark A Kramer, Catherine Thorn, Daniel J Gibson, Yasuo Kubota, Ann M Graybiel, and Nancy J Kopell. Dynamic cross-frequency couplings of local field potential oscillations in rat striatum and hippocampus during performance of a t-maze task. *Proceedings of the National Academy of Sciences*, 105(51):20517–20522, 2008.

[259] Jacques Touchon and Karen Ritchie. Prodromal cognitive disorder in Alzheimer's disease. *International Journal of Geriatric Psychiatry*, 14(7):556–563, 1999. ISSN 1099-1166. doi: 10.1002/(SICI)1099-1166(199907)14:7⟨556::AID-GPS982⟩3.0.CO;2-4.

[260] Guillaume T. Vallet, Carol Hudon, Martine Simard, and Rémy Versace. The disconnection syndrome in the Alzheimer's disease: The cross-modal priming example. *Cortex*, 49(9):2402–2415, October 2013. ISSN 0010-9452. doi: 10.1016/j.cortex.2012.10.010.

[261] F. Vecchio, F. Miraglia, D. Quaranta, G. Granata, R. Romanello, C. Marra, P. Bramanti, and P. M. Rossini. Cortical connectivity and memory performance in cognitive decline: A study via graph theory from EEG data. *Neuroscience*, 316:143–150, March 2016. ISSN 0306-4522. doi: 10.1016/j.neuroscience.2015.12.036.

[262] Fabrizio Vecchio, Francesca Miraglia, Francesca Piludu, Giuseppe Granata, Roberto Romanello, Massimo Caulo, Valeria Onofrj, Placido Bramanti, Cesare Colosimo, and Paolo Maria Rossini. "Small World" architecture in brain connectivity and hippocampal volume in Alzheimer's disease: A study via graph theory from EEG data. *Brain Imaging and Behavior*, 11(2):473–485, April 2017. ISSN 1931-7565. doi: 10.1007/s11682-016-9528-3.

[263] Fabrizio Vecchio, Francesca Miraglia, Francesca Alú, Alessandro Orticoni, Elda Judica, Maria Cotelli, and Paolo Maria Rossini. Contribution of graph theory applied to EEG data analysis for Alzheimer's disease versus vascular dementia diagnosis. *Journal of Alzheimer's Disease*, 82(2):871–879, 2021.

[264] Petar Veličković, Guillem Cucurull, Arantxa Casanova, Adriana Romero, Pietro Liò, and Yoshua Bengio. Graph attention networks, February 2018.

[265] Martin Vinck, Robert Oostenveld, Marijn Van Wingerden, Franscesco Battaglia, and Cyriel MA Pennartz. An improved index of phase-synchronization for elec-

trophysiological data in the presence of volume-conduction, noise and sample-size bias. *Neuroimage*, 55(4):1548–1565, 2011.

[266] Astrid von Stein and Johannes Sarnthein. Different frequencies for different scales of cortical integration: From local gamma to long range alpha/theta synchronization. *International Journal of Psychophysiology*, 38(3):301–313, December 2000. ISSN 0167-8760. doi: 10.1016/S0167-8760(00)00172-0.

[267] O. Vyšata, M. Vališ, A. Procházka, R. Rusina, and L. Pazdera. Linear and nonlinear EEG synchronization in Alzheimer's disease. *Neurophysiology*, 47(1): 46–52, 2015.

[268] Matthias Wacker and Herbert Witte. On the stability of the n: m phase synchronization index. *IEEE Transactions on Biomedical Engineering*, 58(2):332–338, 2010.

[269] Neeraj Wagh and Yogatheesan Varatharajah. EEG-GCNN: Augmenting electroencephalogram-based neurological disease diagnosis using a domain-guided graph convolutional neural network. In *Machine Learning for Health*, pages 367–378. PMLR, 2020.

[270] Bo Wang, Hui Shen, Gai Lu, Yingxin Liu, et al. Graph learning with co-teaching for EEG-Based motor imagery recognition. *IEEE Transactions on Cognitive and Developmental Systems*, 2022.

[271] Chao Wang, Jin Xu, Songzhen Zhao, and Wutao Lou. Graph theoretical analysis of EEG effective connectivity in vascular dementia patients during a visual oddball task. *Clinical Neurophysiology*, 127(1):324–334, January 2016. ISSN 1388-2457. doi: 10.1016/j.clinph.2015.04.063.

[272] Dixin Wang, Chang Lei, Xuan Zhang, Hongtong Wu, Shuzhen Zheng, Jinlong Chao, and Hong Peng. Identification of depression with a semi-supervised GCN based on EEG data. In *2021 IEEE International Conference on Bioinformatics and Biomedicine (BIBM)*, pages 2338–2345. IEEE, 2021.

[273] Jiang Wang, Chen Yang, Ruofan Wang, Haitao Yu, Yibin Cao, and Jing Liu. Functional brain networks in Alzheimer's disease: EEG analysis based on limited penetrable visibility graph and phase space method. *Physica A: Statistical*

Mechanics and its Applications, 460:174–187, October 2016. ISSN 0378-4371. doi: 10.1016/j.physa.2016.05.012.

[274] Jianian Wang, Sheng Zhang, Yanghua Xiao, and Rui Song. A review on graph neural network methods in financial applications, April 2022.

[275] Jing Wang, Yuxing Fang, Xiao Wang, Huichao Yang, Xin Yu, and Huali Wang. Enhanced gamma activity and cross-frequency interaction of resting-state electroencephalographic oscillations in patients with Alzheimer's disease. *Frontiers in aging neuroscience*, 9:243, July 2017. ISSN 1663-4365. doi: 10.3389/fnagi.2017.00243.

[276] Kun Wang, Meng Liang, Liang Wang, Lixia Tian, Xinqing Zhang, Kuncheng Li, and Tianzi Jiang. Altered functional connectivity in early alzheimer's disease: A resting-state fmri study. *Human brain mapping*, 28(10):967–978, 2007.

[277] Ruofan Wang, Jiang Wang, Haitao Yu, Xile Wei, Chen Yang, and Bin Deng. Decreased coherence and functional connectivity of electroencephalograph in Alzheimer's disease. *Chaos: An Interdisciplinary Journal of Nonlinear Science*, 24(3):033136, 2014.

[278] Ruofan Wang, Jiang Wang, Shunan Li, Haitao Yu, Bin Deng, and Xile Wei. Multiple feature extraction and classification of electroencephalograph signal for Alzheimers' with spectrum and bispectrum. *Chaos: An Interdisciplinary Journal of Nonlinear Science*, 25(1):013110, 2015.

[279] Yucheng Wang, Min Wu, Xiaoli Li, Lihua Xie, and Zhenghua Chen. Multivariate time series representation learning via hierarchical correlation pooling boosted graph neural network. *IEEE Transactions on Artificial Intelligence*, pages 1–13, 2023. ISSN 2691-4581. doi: 10.1109/TAI.2023.3241896.

[280] Oliver Wieder, Stefan Kohlbacher, Mélaine Kuenemann, Arthur Garon, Pierre Ducrot, Thomas Seidel, and Thierry Langer. A compact review of molecular property prediction with graph neural networks. *Drug Discovery Today: Technologies*, 37:1–12, December 2020. ISSN 1740-6749. doi: 10.1016/j.ddtec.2020.11.009.

[281] Tomasz Wierciński, Mateusz Rock, Robert Zwierzycki, Teresa Zawadzka, and Michał Zawadzki. Emotion recognition from physiological channels using graph neural network. *Sensors*, 22(8):2980, 2022.

[282] Herbert Witte, Peter Putsche, Claudia Hemmelmann, Christoph Schelenz, and Lutz Leistritz. Analysis and modeling of time-variant amplitude–frequency couplings of and between oscillations of eeg bursts. *Biological Cybernetics*, 99(2): 139–157, 2008.

[283] Lingfei Wu, Yu Chen, Kai Shen, Xiaojie Guo, Hanning Gao, Shucheng Li, Jian Pei, and Bo Long. Graph neural networks for natural language processing: A survey. *Foundations and Trends® in Machine Learning*, 16(2):119–328, January 2023. ISSN 1935-8237, 1935-8245. doi: 10.1561/2200000096.

[284] Shiwen Wu, Fei Sun, Wentao Zhang, Xu Xie, and Bin Cui. Graph neural networks in recommender systems: A survey. *ACM Computing Surveys*, 55(5):97:1–97:37, December 2022. ISSN 0360-0300. doi: 10.1145/3535101.

[285] Zonghan Wu, Shirui Pan, Fengwen Chen, Guodong Long, Chengqi Zhang, and Philip S. Yu. A comprehensive survey on graph neural networks. *IEEE Transactions on Neural Networks and Learning Systems*, 32(1):4–24, January 2021. ISSN 2162-2388. doi: 10.1109/TNNLS.2020.2978386.

[286] Teng Xie and Yong He. Mapping the Alzheimer's Brain with Connectomics. *Frontiers in Psychiatry*, 2, 2012. ISSN 1664-0640.

[287] Jiacheng Xiong, Zhaoping Xiong, Kaixian Chen, Hualiang Jiang, and Mingyue Zheng. Graph neural networks for automated de novo drug design. *Drug Discovery Today*, 26(6):1382–1393, June 2021. ISSN 1359-6446. doi: 10.1016/j.drudis.2021.02.011.

[288] Mengjia Xu, David Lopez Sanz, Pilar Garces, Fernando Maestu, Quanzheng Li, and Dimitrios Pantazis. A Graph Gaussian Embedding Method for Predicting Alzheimer's Disease Progression With MEG Brain Networks. *IEEE Transactions on Biomedical Engineering*, 68(5):1579–1588, May 2021. ISSN 1558-2531. doi: 10.1109/TBME.2021.3049199.

[289] Tao Xu, Wang Dang, Jiabao Wang, and Yun Zhou. DAGAM: A domain adversarial graph attention model for subject independent EEG-Based emotion recognition. *arXiv preprint arXiv:2202.12948*, 2022.

[290] Yunlong Xue, Wenming Zheng, Yuan Zong, Hongli Chang, and Xingxun Jiang. Adaptive hierarchical graph convolutional network for EEG emotion recognition.

In *2022 International Joint Conference on Neural Networks (IJCNN)*, pages 1–8. IEEE, 2022.

[291] Yongqiang Yin, Xiangwei Zheng, Bin Hu, Yuang Zhang, and Xinchun Cui. EEG emotion recognition using fusion model of graph convolutional neural networks and LSTM. *Applied Soft Computing*, 100:106954, 2021.

[292] Chengxuan Ying, Tianle Cai, Shengjie Luo, Shuxin Zheng, Guolin Ke, Di He, Yanming Shen, and Tie-Yan Liu. Do Transformers Really Perform Badly for Graph Representation? In *Advances in Neural Information Processing Systems*, volume 34, pages 28877–28888. Curran Associates, Inc., 2021.

[293] Zhitao Ying, Jiaxuan You, Christopher Morris, Xiang Ren, Will Hamilton, and Jure Leskovec. Hierarchical graph representation learning with differentiable pooling. In *Advances in Neural Information Processing Systems*, volume 31. Curran Associates, Inc., 2018.

[294] Nadia Youssef, Shasha Xiao, Meng Liu, Haipeng Lian, Renren Li, Xi Chen, Wei Zhang, Xiaoran Zheng, Yunxia Li, and Yingjie Li. Functional Brain Networks in Mild Cognitive Impairment Based on Resting Electroencephalography Signals. *Frontiers in Computational Neuroscience*, 15, 2021. ISSN 1662-5188.

[295] Haitao Yu, Xinyu Lei, Zhenxi Song, Jiang Wang, Xile Wei, and Baoqi Yu. Functional brain connectivity in Alzheimer's disease: An EEG study based on permutation disalignment index. *Physica A: Statistical Mechanics and its Applications*, 506:1093–1103, September 2018. ISSN 0378-4371. doi: 10.1016/j.physa.2018.05.009.

[296] Haitao Yu, Xinyu Lei, Zhenxi Song, Chen Liu, and Jiang Wang. Supervised network-based fuzzy learning of EEG signals for Alzheimer's disease identification. *IEEE Transactions on Fuzzy Systems*, 28(1):60–71, January 2019. ISSN 1063-6706, 1941-0034. doi: 10.1109/TFUZZ.2019.2903753.

[297] Meichen Yu, Alida A. Gouw, Arjan Hillebrand, Betty M. Tijms, Cornelis Jan Stam, Elisabeth C.W. Van Straaten, and Yolande A.L. Pijnenburg. Different functional connectivity and network topology in behavioral variant of frontotemporal dementia and Alzheimer's disease: An EEG study. *Neurobiology of Aging*, 42:150–162, June 2016. ISSN 01974580. doi: 10.1016/j.neurobiolaging.2016.03.018.

[298] Meichen Yu, Marjolein MA Engels, Arjan Hillebrand, Elisabeth CW Van Straaten, Alida A Gouw, Charlotte Teunissen, Wiesje M Van Der Flier, Philip Scheltens, and Cornelis J Stam. Selective impairment of hippocampus and posterior hub areas in Alzheimer's disease: An MEG-based multiplex network study. *Brain : a journal of neurology*, 140(5):1466–1485, 2017.

[299] Rajamanickam Yuvaraj, U Rajendra Acharya, and Yuki Hagiwara. A novel Parkinson's Disease Diagnosis Index using higher-order spectra features in EEG signals. *Neural Computing and Applications*, 30(4):1225–1235, 2018.

[300] Difei Zeng, Kejie Huang, Cenglin Xu, Haibin Shen, and Zhong Chen. Hierarchy graph convolution network and tree classification for epileptic detection on electroencephalography signals. *IEEE Transactions on Cognitive and Developmental Systems*, 13(4):955–968, 2020.

[301] Hong Zeng, Qi Wu, Yanping Jin, Haohao Zheng, Mingming Li, Yue Zhao, Hua Hu, and Wanzeng Kong. Siam-GCAN: A siamese graph convolutional attention network for EEG emotion recognition. *IEEE Transactions on Instrumentation and Measurement*, 2022.

[302] Honghui Zhang, Andrew J. Watrous, Ansh Patel, and Joshua Jacobs. Theta and Alpha Oscillations Are Traveling Waves in the Human Neocortex. *Neuron*, 98 (6):1269–1281.e4, June 2018. ISSN 08966273. doi: 10.1016/j.neuron.2018.05.019.

[303] Tong Zhang, Xuehan Wang, Xiangmin Xu, and CL Philip Chen. GCB-Net: Graph convolutional broad network and its application in emotion recognition. *IEEE Transactions on Affective Computing*, 13(1):379–388, 2019.

[304] Xiao-Meng Zhang, Li Liang, Lin Liu, and Ming-Jing Tang. Graph neural networks and their current applications in bioinformatics. *Frontiers in Genetics*, 12, 2021. ISSN 1664-8021. doi: 10.3389/fgene.2021.690049.

[305] Yanna Zhao, Changxu Dong, Gaobo Zhang, Yaru Wang, Xin Chen, Weikuan Jia, Qi Yuan, Fangzhou Xu, and Yuanjie Zheng. EEG-Based Seizure detection using linear graph convolution network with focal loss. *Computer Methods and Programs in Biomedicine*, 208:106277, 2021.

[306] Yifan Zhao, Yitian Zhao, Pholpat Durongbhan, Liangyu Chen, Jiang Liu, S. A. Billings, Panagiotis Zis, Zoe C. Unwin, Matteo De Marco, Annalena Venneri,

Daniel J. Blackburn, and Ptolemaios G. Sarrigiannis. Imaging of Nonlinear and Dynamic Functional Brain Connectivity Based on EEG Recordings With the Application on the Diagnosis of Alzheimer's Disease. *IEEE Transactions on Medical Imaging*, 39(5):1571–1581, May 2020. ISSN 0278-0062, 1558-254X. doi: 10.1109/TMI.2019.2953584.

[307] Maksim Zhdanov, Saskia Steinmann, and Nico Hoffmann. Investigating brain connectivity with graph neural networks and GNNExplainer. *arXiv preprint arXiv:2206.01930*, pages 5155–5161, 2022.

[308] Fa Zheng, Bin Hu, Shilin Zhang, Yalin Li, and Xiangwei Zheng. EEG emotion recognition based on hierarchy graph convolution network. In *2021 IEEE International Conference on Bioinformatics and Biomedicine (BIBM)*, pages 1628–1632. IEEE, 2021.

[309] Wei-Long Zheng and Bao-Liang Lu. Investigating Critical Frequency Bands and Channels for EEG-Based Emotion Recognition with Deep Neural Networks. *IEEE Transactions on Autonomous Mental Development*, 7(3):162–175, September 2015. ISSN 1943-0612. doi: 10.1109/TAMD.2015.2431497.

[310] Jiang Zheng-yan. Abnormal cortical functional connections in Alzheimer's disease: Analysis of inter- and intra-hemispheric EEG coherence. *Journal of Zhejiang University Science B*, 6(4):259–264, April 2005. ISSN 1862-1783. doi: 10.1007/BF02842462.

[311] Peixiang Zhong, Di Wang, and Chunyan Miao. EEG-based emotion recognition using regularized graph neural networks. *IEEE Transactions on Affective Computing*, 2020. doi: 10.1109/TAFFC.2020.2994159.

[312] Jie Zhou, Ganqu Cui, Shengding Hu, Zhengyan Zhang, Cheng Yang, Zhiyuan Liu, Lifeng Wang, Changcheng Li, and Maosong Sun. Graph neural networks: A review of methods and applications. *AI Open*, 1:57–81, January 2020. ISSN 2666-6510. doi: 10.1016/j.aiopen.2021.01.001.

[313] Yiwen Zhu, Kaiyu Gan, and Zhong Yin. Locally temporal-spatial pattern learning with graph attention mechanism for EEG-based emotion recognition. *arXiv preprint arXiv:2208.11087*, 2022.

Appendices

Appendix A

Additional results from Cross-Frequency Multilayer Network Analysis with Bispectrum-based Functional Connectivity (Chapter 4)

A.1 Statistical power

We calculate the statistical power given our sample size ($N = 40$) as a function of the effect size (Cohen's d) of a two-sample t-test with a two-sided alternative hypothesis and a significant p-value of 0.05 (Figure A.1). Sufficient power (80%) is reached with an effect size ≥ 0.45.

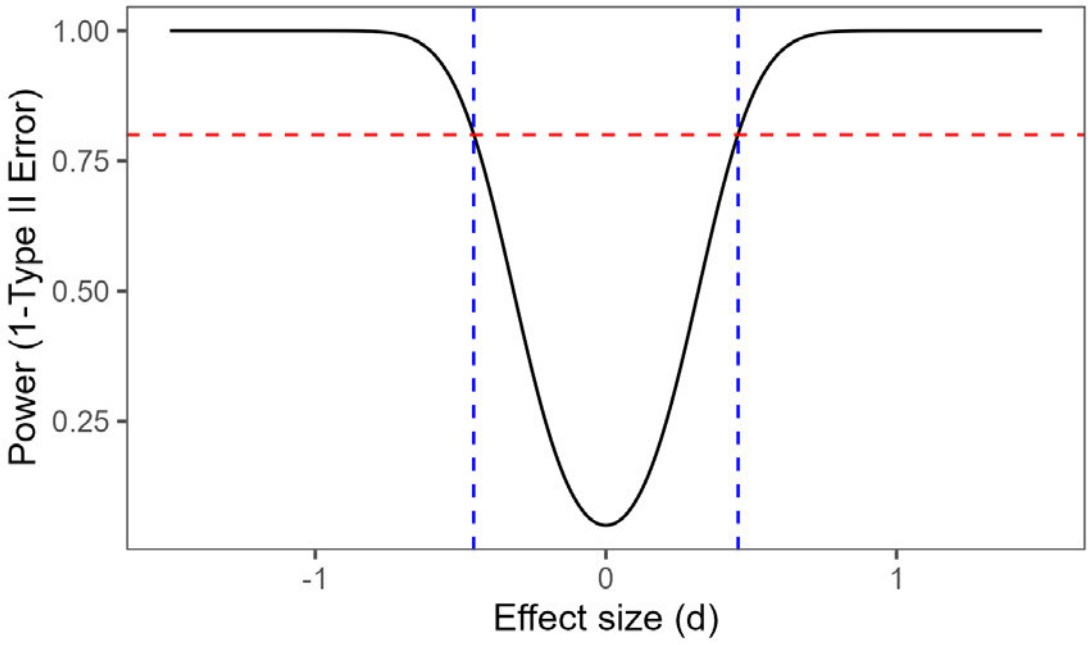

Figure A.1: Statistical power for different Cohen's d effect size values with sample size 40.

A.2 Results for epoch 1

In this section, we report the results of the statistical comparisons and corresponding figures using only data from the first epoch.

The comparisons of average coupling computed with CS and CBS are shown in Tables A.1 and A.2, respectively. Additionally, the corresponding figures of connectivity matrices computed with CS and CBS are shown in Figures A.2 and A.3.

The comparisons of node strength computed with CS and CBS are shown in Table A.3 and Figure A.4, and Table A.4 and Figure A.5, respectively.

Results of comparisons of the unweighted multilayer network metrics are reported in Tables A.5, A.6 and A.7 for edge betweenness, global vulnerability and local vulnerability, respectively. The corresponding figures are; edge betweenness (Figure A.6), global vulnerability (Figure A.7) and local vulnerability (Figure A.8).

Results of comparisons of the weighted multilayer network metrics are reported in Tables A.8, A.9 and A.10 for edge betweenness, global vulnerability and local vulnerability, respectively. The corresponding figures are; edge betweenness (Figure A.9), global vulnerability (Figure A.10) and local vulnerability (Figure A.11).

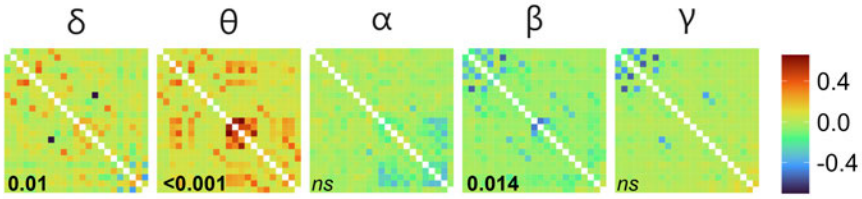

Figure A.2: Difference of average connectivity matrices (AD − HC) measured with CS in epoch 1 of (A) AD and (B) HC. For visualisation purposes, the values were min-max normalised. Digits in black denote a p-value testing for the difference in global coupling ($p < 0.05$ in bold, in italics otherwise).

Table A.1: Comparisons of the mean of adjacency matrix constructed with CS in epoch 1. The results are reported as follows: statistics value (degrees of freedom), p-value of the test, Cohen's d effect size (or nonparametric alternative), number of epochs where significant differences were observed (E), difference estimate μ with 95% confidence interval. Reliable differences (significant in all three epochs) are highlighted with bold text.

Frequency band	Test	Difference estimate (95% CI)
α	U=337, p=0.227, d=0.17, E=1	μ = −0.27 (-0.79 0.25)
β	**t(36.97)=-2.72, p=0.014, d=-0.72, E=3**	μ = −0.68 (-1.18 -0.18)
δ	**t(35.89)=2.99, p=0.01, d=0.78, E=3**	μ = 0.73 (0.24 1.22)
γ	t(36.45)=-1.22, p=0.227, d=-0.32, E=0	μ = −0.32 (-0.84 0.2)
θ	**t(36.85)=5.47, p¡0.001, d=1.44, E=3**	μ = 1.17 (0.74 1.6)

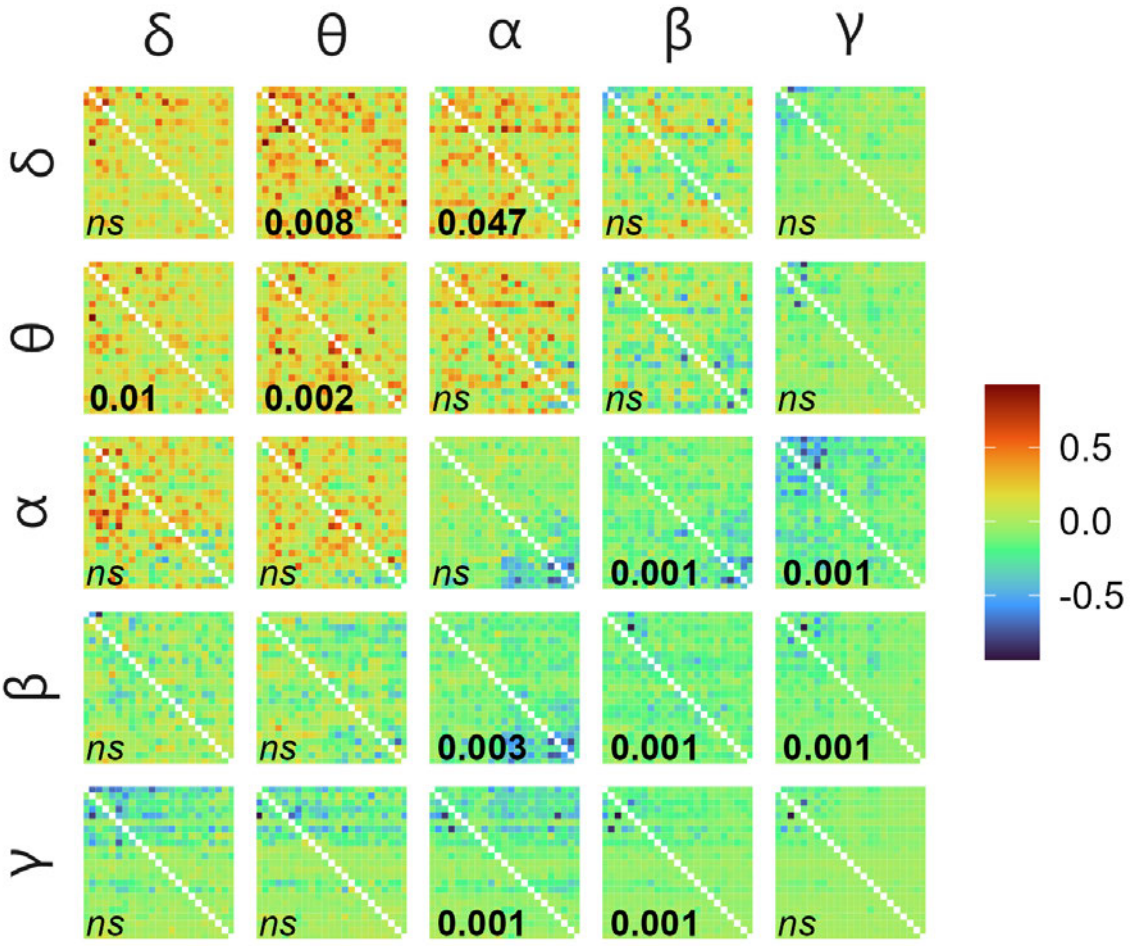

Figure A.3: Difference of average connectivity matrices (AD – HC) measured with CBS with input frequency on the vertical facets and output frequency on the horizontal. For visualisation purposes, the values were min-max normalised. Digits in black denote a p-value testing for the difference in global coupling ($p < 0.05$ in bold, in italics otherwise).

Table A.2: Comparisons of the mean of adjacency matrix constructed with CBS in epoch 1. The results are reported as follows: statistics value (degrees of freedom), p-value of the test, Cohen's d effect size (or nonparametric alternative), number of epochs where significant differences were observed (E), difference estimate μ with 95% confidence interval. Reliable differences (significant in all three epochs) are highlighted with bold text.

	δ	θ	α	β	γ
δ	t(27.35)=2.19, p=0.055, d=0.57, E=2, μ =0.55(0.04 1.05)	**t(24.81)=3.13, p=0.008, d=0.81, E=3, μ =0.75(0.27 1.24)**	**t(24.35)=2.33, p=0.047, d=0.61, E=3, μ =0.58(0.08 1.08)**	t(34.64)=-0.91, p=0.368, d=-0.24, E=0, μ =−0.24(-0.76 0.29)	U=332, p=0.182, d=0.18, E=0, μ =−0.33(-0.8 0.11)
θ	**t(27.46)=3, p=0.01, d=0.78, E=3, μ =0.73(0.24 1.21)**	**t(33.06)=3.7, p=0.002, d=0.97, E=3, μ =0.87(0.4 1.34)**	t(24.48)=1.99, p=0.069, d=0.52, E=1, μ =0.5(-0.01 1.01)	t(25.38)=-1.75, p=0.104, d=-0.45, E=1, μ =−0.44(-0.95 0.07)	U=275, p=0.047, d=0.3, E=1, μ =−0.5(-1.03 -0.08)
α	t(29.63)=1.49, p=0.161, d=0.39, E=2, μ =0.38(-0.13 0.9)	t(28.61)=2.22, p=0.055, d=0.58, E=1, μ =0.56(0.05 1.06)	t(36.22)=-2.16, p=0.055, d=-0.57, E=1, μ =−0.55(-1.05 -0.04)	**t(36.89)=-3.8, p=0.001, d=-1, E=3, μ =−0.9(-1.37 -0.42)**	**t(35.38)=-3.92, p=0.001, d=-1.03, E=3, μ =−0.91(-1.38 -0.45)**
β	t(32.77)=-1.79, p=0.099, d=-0.47, E=0, μ =−0.46(-0.97 0.05)	t(22.34)=-1.48, p=0.161, d=-0.38, E=1, μ =−0.38(-0.89 0.14)	**t(36.77)=-3.5, p=0.003, d=-0.92, E=3, μ =−0.84(-1.32 -0.36)**	**t(36.41)=-3.89, p=0.001, d=-1.02, E=3, μ =−0.91(-1.38 -0.44)**	**t(33.54)=-3.99, p=0.001, d=-1.04, E=3, μ =−0.93(-1.39 -0.46)**
γ	U=289, p=0.058, d=0.27, E=0, μ =−0.43(-0.97 -0.02)	U=288, p=0.058, d=0.27, E=0, μ =−0.46(-1.08 -0.02)	**t(36.04)=-3.87, p=0.001, d=-1.01, E=3, μ =−0.91(-1.38 -0.44)**	**t(34.55)=-3.83, p=0.001, d=-1, E=3, μ =−0.9(-1.37 -0.43)**	U=229, p=0.007, d=0.39, E=1, μ =−0.73(-1.21 -0.27)

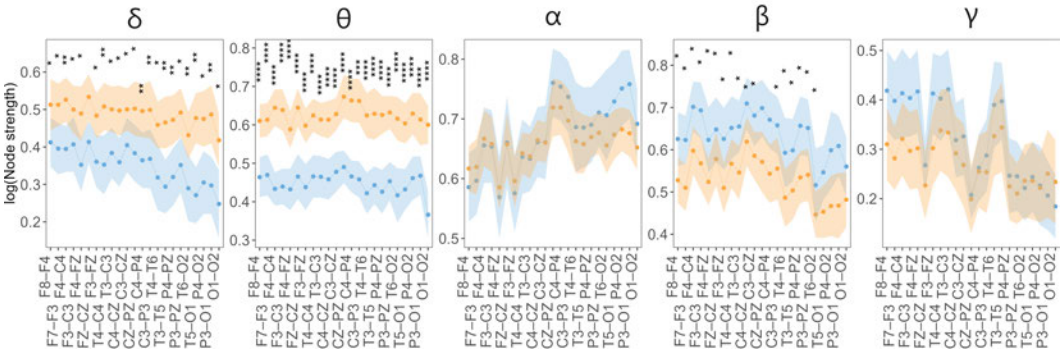

Figure A.4: Node strength (min-max normalised) measured with CS in epoch 1 of HC (blue) and AD (orange): mean with 95% confidence intervals. Significant differences ($p \leq 0.05$) observed in at least ten thresholded networks are encoded by asterisks. The number of asterisks corresponds to the p-value (FDR corrected), i.e. $p \leq 0.0001$ "****", $p \leq 0.001$ "***", $p \leq 0.01$ "**", and $p \leq 0.05$ "*".

Table A.3: Comparisons of node strength measured with CS in epoch 1. The results are reported as follows: statistics value (degrees of freedom), p-value of the test, Cohen's d effect size (or nonparametric alternative), number of epochs where significant differences were observed (E), and difference estimate μ with 95% confidence interval (CI). Reliable differences (significant in all three epochs) are highlighted with bold text.

channel	δ	θ	α	β	γ
F8–F4	t(36.66)=-2.16, p=0.038, d=-0.57, E=3, $\mu = -0.55$ (-1.06 -0.04)	t(35.85)=-4.45, p<0.001, d=-1.16, E=3, $\mu = -1.01$ (-1.46 -0.55)	**t(30.27)=-0.93, p=0.749, d=-0.24, E=0, $\mu = -0.24$ (-0.76 0.28)**	t(36.15)=2.4, p=0.041, d=0.63, E=3, $\mu = 0.6$ (0.1 1.11)	**U=543, p=0.32, d=0.25, E=0, $\mu = 0.5$ (-0.04 1.08)**
F7–F3	t(35.61)=-2.7, p=0.014, d=-0.71, E=3, $\mu = -0.67$ (-1.17 -0.17)	t(35.35)=-4.27, p<0.001, d=-1.12, E=3, $\mu = -0.98$ (-1.44 -0.52)	**t(35.59)=-0.65, p=0.861, d=-0.17, E=0, $\mu = -0.17$ (-0.7 0.35)**	t(36.99)=2.9, p=0.034, d=0.76, E=3, $\mu = 0.72$ (0.22 1.21)	**t(35.4)=2.33, p=0.32, d=0.61, E=0, $\mu = 0.59$ (0.08 1.09)**
F4–C4	t(37)=-3.16, p=0.01, d=-0.83, E=3, $\mu = -0.77$ (-1.26 -0.28)	t(36.07)=-6.72, p<0.001, d=-1.77, E=3, $\mu = -1.33$ (-1.72 -0.93)	**t(33.41)=-0.29, p=0.969, d=-0.08, E=0, $\mu = -0.08$ (-0.6 0.45)**	t(36.99)=2.59, p=0.035, d=0.68, E=3, $\mu = 0.65$ (0.15 1.15)	**t(35.73)=1.62, p=0.388, d=0.42, E=0, $\mu = 0.42$ (-0.1 0.93)**
F3–C3	**t(36.34)=-1.97, p=0.054, d=-0.51, E=0, $\mu = -0.5$ (-1.01 0.01)**	t(35.29)=-5.79, p<0.001, d=-1.52, E=3, $\mu = -1.22$ (-1.64 -0.8)	**t(34.49)=-0.11, p=0.969, d=-0.03, E=0, $\mu = -0.03$ (-0.56 0.5)**	t(36.96)=2.82, p=0.034, d=0.74, E=3, $\mu = 0.7$ (0.2 1.19)	**U=537, p=0.32, d=0.24, E=0, $\mu = 0.54$ (-0.04 1.08)**
F4–FZ	U=245, p=0.011, d=0.36, E=3, $\mu = -0.72$ (-1.33 -0.22)	t(36.67)=-4.42, p<0.001, d=-1.16, E=3, $\mu = -1$ (-1.46 -0.55)	**U=423, p=0.969, d=0.01, E=0, $\mu = 0.01$ (-0.42 0.5)**	t(32.52)=2.13, p=0.049, d=0.56, E=3, $\mu = 0.54$ (0.03 1.04)	**U=549, p=0.32, d=0.26, E=0, $\mu = 0.55$ (0.01 1.12)**
FZ–CZ	t(36.37)=-2.97, p=0.01, d=-0.78, E=3, $\mu = -0.73$ (-1.23 -0.24)	t(36.2)=-4.78, p<0.001, d=-1.25, E=3, $\mu = -1.06$ (-1.51 -0.62)	**U=458, p=0.861, d=0.08, E=0, $\mu = 0.14$ (-0.33 0.61)**	**t(35.7)=1.45, p=0.159, d=0.38, E=0, $\mu = 0.38$ (-0.14 0.89)**	**U=521, p=0.388, d=0.21, E=0, $\mu = 0.39$ (-0.12 0.84)**
F3–FZ	t(36.5)=-2.74, p=0.014, d=-0.72, E=3, $\mu = -0.68$ (-1.17 -0.18)	t(33.84)=-4.38, p<0.001, d=-1.15, E=3, $\mu = -0.99$ (-1.45 -0.54)	**U=416, p=0.969, d=0.01, E=0, $\mu = -0.03$ (-0.48 0.42)**	t(35.05)=2.53, p=0.037, d=0.66, E=3, $\mu = 0.63$ (0.13 1.13)	**t(36.82)=2.05, p=0.32, d=0.54, E=0, $\mu = 0.52$ (0.01 1.03)**
T4–C4	t(35.2)=-3.15, p=0.01, d=-0.82, E=3, $\mu = -0.76$ (-1.25 -0.28)	t(34.66)=-4.63, p<0.001, d=-1.21, E=3, $\mu = -1.04$ (-1.49 -0.59)	**U=428, p=0.969, d=0.02, E=0, $\mu = 0.03$ (-0.43 0.48)**	**t(34.47)=1.84, p=0.082, d=0.48, E=0, $\mu = 0.47$ (-0.04 0.98)**	**t(36.99)=1.11, p=0.592, d=0.29, E=0, $\mu = 0.29$ (-0.23 0.81)**
T3–C3	t(36.64)=-2.64, p=0.014, d=-0.69, E=3, $\mu = -0.66$ (-1.16 -0.16)	t(35.14)=-4.42, p<0.001, d=-1.16, E=3, $\mu = -1$ (-1.46 -0.55)	**t(31.65)=-0.13, p=0.969, d=-0.03, E=0, $\mu = -0.03$ (-0.56 0.49)**	U=585, p=0.034, d=0.34, E=3, $\mu = 0.66$ (0.14 1.18)	**t(35.93)=1.47, p=0.42, d=0.39, E=0, $\mu = 0.38$ (-0.14 0.91)**
C4–CZ	t(36.72)=-3.03, p=0.01, d=-0.8, E=3, $\mu = -0.74$ (-1.24 -0.25)	t(36.89)=-4.42, p<0.001, d=-1.16, E=3, $\mu = -1.01$ (-1.46 -0.55)	**U=459, p=0.861, d=0.08, E=0, $\mu = 0.14$ (-0.37 0.65)**	t(36.95)=2.19, p=0.049, d=0.57, E=3, $\mu = 0.55$ (0.05 1.06)	**U=453, p=0.818, d=0.07, E=0, $\mu = 0.12$ (-0.37 0.61)**
C3–CZ	t(34.34)=-2.13, p=0.039, d=-0.56, E=3, $\mu = -0.54$ (-1.04 -0.03)	t(35.35)=-4.63, p<0.001, d=-1.21, E=3, $\mu = -1.04$ (-1.49 -0.59)	**U=441, p=0.969, d=0.04, E=0, $\mu = 0.07$ (-0.42 0.53)**	t(34.44)=2.12, p=0.049, d=0.55, E=3, $\mu = 0.54$ (0.03 1.04)	**U=507, p=0.46, d=0.18, E=0, $\mu = 0.3$ (-0.15 0.76)**
CZ–PZ	t(37)=-2.33, p=0.027, d=-0.61, E=3, $\mu = -0.59$ (-1.09 -0.08)	t(32.04)=-5.32, p<0.001, d=-1.4, E=3, $\mu = -1.16$ (-1.59 -0.72)	**t(36.07)=1.13, p=0.749, d=0.3, E=0, $\mu = 0.29$ (-0.23 0.82)**	t(36.49)=2.66, p=0.034, d=0.7, E=3, $\mu = 0.67$ (0.16 1.17)	**U=471, p=0.681, d=0.1, E=0, $\mu = 0.17$ (-0.29 0.66)**
C4–P4	t(36.99)=-2.63, p=0.014, d=-0.69, E=3, $\mu = -0.66$ (-1.16 -0.16)	U=123, p<0.001, d=0.61, E=3, $\mu = -1.39$ (-1.74 -0.89)	**t(35.04)=0.98, p=0.749, d=0.26, E=0, $\mu = 0.26$ (-0.27 0.78)**	t(36.88)=2.69, p=0.034, d=0.71, E=3, $\mu = 0.67$ (0.17 1.17)	**U=441, p=0.818, d=0.04, E=0, $\mu = 0.08$ (-0.48 0.56)**
C3–P3	t(37)=-2.44, p=0.022, d=-0.64, E=3, $\mu = -0.61$ (-1.12 -0.11)	t(34.15)=-5.64, p<0.001, d=-1.49, E=3, $\mu = -1.2$ (-1.62 -0.77)	**t(36.66)=1.01, p=0.749, d=0.27, E=0, $\mu = 0.26$ (-0.26 0.79)**	t(36.36)=2.12, p=0.049, d=0.56, E=3, $\mu = 0.54$ (0.03 1.05)	**U=470, p=0.681, d=0.1, E=0, $\mu = 0.2$ (-0.27 0.68)**
T4–T6	t(32.57)=-2.68, p=0.014, d=-0.7, E=3, $\mu = -0.66$ (-1.16 -0.17)	t(36.14)=-5.24, p<0.001, d=-1.38, E=3, $\mu = -1.14$ (-1.57 -0.7)	**t(32.51)=0.53, p=0.861, d=0.14, E=0, $\mu = 0.14$ (-0.39 0.66)**	**t(35.8)=2.02, p=0.058, d=0.53, E=0, $\mu = 0.51$ (0.01 1.02)**	**t(36.85)=1.08, p=0.592, d=0.28, E=0, $\mu = 0.28$ (-0.24 0.81)**
T3–T5	U=194, p=0.004, d=0.46, E=3, $\mu = -0.92$ (-1.44 -0.43)	t(30.79)=-4.57, p<0.001, d=-1.21, E=3, $\mu = -1.04$ (-1.5 -0.59)	**t(33.11)=0.68, p=0.861, d=0.18, E=0, $\mu = 0.18$ (-0.35 0.7)**	U=565, p=0.042, d=0.3, E=3, $\mu = 0.55$ (0.08 1.07)	**t(35.22)=0.91, p=0.679, d=0.24, E=0, $\mu = 0.24$ (-0.29 0.77)**
P4–PZ	t(36.07)=-3.11, p=0.01, d=-0.81, E=3, $\mu = -0.76$ (-1.24 -0.27)	t(36.38)=-5.44, p<0.001, d=-1.43, E=3, $\mu = -1.16$ (-1.59 -0.73)	**U=492, p=0.749, d=0.15, E=0, $\mu = 0.3$ (-0.2 0.72)**	t(36.53)=2.71, p=0.034, d=0.71, E=3, $\mu = 0.67$ (0.18 1.17)	**U=441, p=0.818, d=0.04, E=0, $\mu = 0.07$ (-0.33 0.49)**
P3–PZ	t(36.54)=-2.93, p=0.01, d=-0.77, E=3, $\mu = -0.72$ (-1.21 -0.23)	t(36.17)=-5.58, p<0.001, d=-1.46, E=3, $\mu = -1.18$ (-1.61 -0.76)	**U=490, p=0.749, d=0.14, E=0, $\mu = 0.24$ (-0.2 0.85)**	t(36.81)=2.48, p=0.037, d=0.65, E=3, $\mu = 0.62$ (0.12 1.12)	**U=464, p=0.72, d=0.09, E=0, $\mu = 0.12$ (-0.28 0.7)**
T6–O2	t(32.69)=-2.68, p=0.014, d=-0.7, E=3, $\mu = -0.66$ (-1.16 -0.17)	t(35.19)=-4.53, p<0.001, d=-1.19, E=3, $\mu = -1.02$ (-1.47 -0.57)	**U=569, p=0.153, d=0.3, E=0, $\mu = 0.47$ (0.08 0.95)**	**t(29.14)=1.39, p=0.172, d=0.36, E=0, $\mu = 0.36$ (-0.16 0.87)**	**U=388, p=0.818, d=0.04, E=0, $\mu = -0.08$ (-0.54 0.45)**
T5–O1	t(35.44)=-4.21, p=0.002, d=-1.11, E=3, $\mu = -0.98$ (-1.44 -0.51)	t(36)=-4.71, p<0.001, d=-1.25, E=3, $\mu = -1.06$ (-1.51 -0.61)	**t(28.04)=1.47, p=0.749, d=0.39, E=0, $\mu = 0.38$ (-0.14 0.91)**	**t(35.97)=2.14, p=0.049, d=0.57, E=2, $\mu = 0.55$ (0.03 1.06)**	**U=430, p=0.818, d=0.05, E=0, $\mu = 0.07$ (-0.4 0.56)**
P4–O2	t(34.63)=-3.1, p=0.01, d=-0.83, E=3, $\mu = -0.77$ (-1.26 -0.27)	t(35.97)=-4.4, p<0.001, d=-1.16, E=3, $\mu = -1.01$ (-1.47 -0.55)	**U=570, p=0.153, d=0.35, E=0, $\mu = 0.66$ (0.16 1.1)**	t(33.26)=2.32, p=0.042, d=0.61, E=3, $\mu = 0.59$ (0.08 1.1)	**U=399, p=0.918, d=0.01, E=0, $\mu = -0.02$ (-0.48 0.43)**
P3–O1	t(35.93)=-3.59, p=0.005, d=-0.95, E=3, $\mu = -0.86$ (-1.35 -0.38)	t(31.25)=-3.55, p=0.001, d=-0.94, E=3, $\mu = -0.86$ (-1.35 -0.37)	**t(29.98)=2.43, p=0.153, d=0.64, E=0, $\mu = 0.61$ (0.11 1.12)**	t(35.58)=2.74, p=0.034, d=0.73, E=3, $\mu = 0.69$ (0.18 1.19)	**U=379, p=0.818, d=0.06, E=0, $\mu = -0.09$ (-0.65 0.28)**
O1–O2	t(30.32)=-3.03, p=0.01, d=-0.82, E=3, $\mu = -0.76$ (-1.27 -0.26)	U=97, p<0.001, d=0.65, E=3, $\mu = -1.32$ (-1.76 -0.86)	**t(27.04)=1.19, p=0.749, d=0.32, E=0, $\mu = 0.32$ (-0.22 0.85)**	**t(34.76)=1.69, p=0.106, d=0.45, E=0, $\mu = 0.44$ (-0.08 0.97)**	**U=338, p=0.679, d=0.12, E=0, $\mu = -0.14$ (-0.71 0.27)**

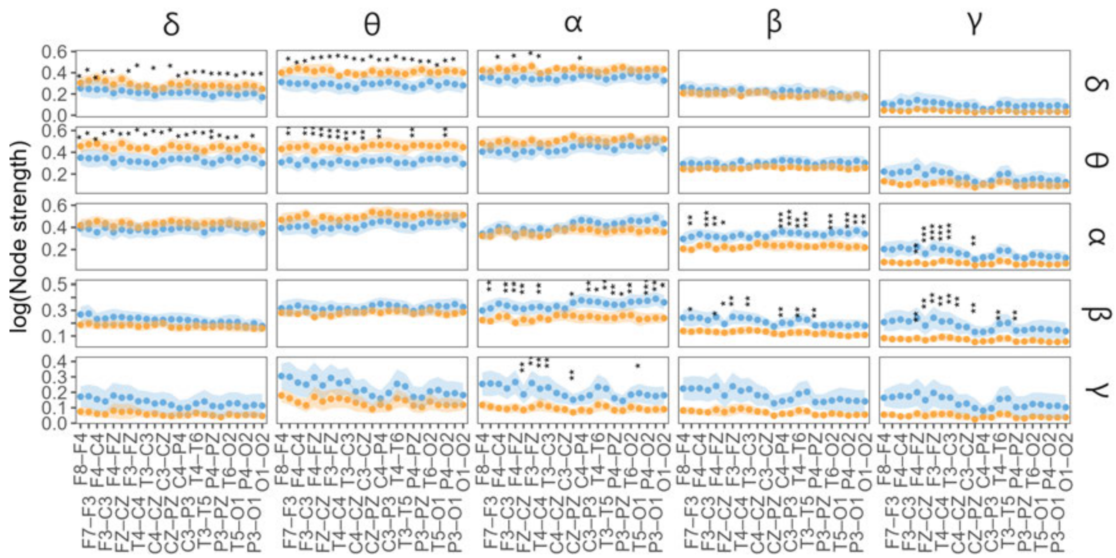

Figure A.5: Node strength (min-max normalised) measured with CBS in epoch 1 of HC (blue) and AD (orange): mean with 95% confidence intervals. The input frequency is on the vertical facets, and the output frequency is on the horizontal. Significant differences ($p \leq 0.05$) observed in at least ten thresholded networks are encoded by asterisks. The number of asterisks corresponds to the p-value (FDR corrected), i.e. $p \leq 0.0001$ "****", $p \leq 0.001$ "***", $p \leq 0.01$ "**", and $p \leq 0.05$ "*".

Table A.4: Comparisons of node strength measured with CBS in epoch 1. The results are reported as follows: statistics value (degrees of freedom), p-value of the test, Cohen's d effect size (or nonparametric alternative), number of epochs where significant differences were observed (E), and difference estimate μ with 95% confidence interval (CI). Reliable differences (significant in all three epochs) are highlighted with bold text.

from	channel	δ	θ	α	β	γ
δ	F8–F4	**U=328, p=0.156, d=0.19, E=0, μ =-0.35 (-0.94 0.18)**	t(36.08)=-2.06, p=0.048, d=-0.54, E=3, μ =-0.52 (-1.03 -0.02)	**U=293, p=0.093, d=0.26, E=0, μ =-0.52 (-0.99 0)**	**U=524, p=0.928, d=0.21, E=0, μ =0.3 (-0.09 0.79)**	**U=612, p=0.056, d=0.39, E=0, μ =0.45 (0.14 0.84)**
δ	F7–F3	U=286, p=0.043, d=0.27, E=3, μ =-0.66 (-1.08 -0.03)	t(27.65)=-2.62, p=0.015, d=-0.68, E=3, μ =-0.64 (-1.14 -0.15)	**U=285, p=0.078, d=0.28, E=0, μ =-0.48 (-0.9 -0.04)**	**U=453, p=0.928, d=0.07, E=0, μ =0.08 (-0.25 0.58)**	**U=533, p=0.342, d=0.23, E=0, μ =0.17 (-0.02 0.42)**
δ	F4–C4	U=246, p=0.029, d=0.36, E=3, μ =-0.75 (-1.14 -0.22)	t(31.71)=-3.04, p=0.011, d=-0.79, E=3, μ =-0.74 (-1.22 -0.25)	t(34.36)=-2.98, p=0.036, d=-0.78, E=3, μ =-0.73 (-1.22 -0.24)	**U=463, p=0.928, d=0.09, E=0, μ =0.19 (-0.34 0.72)**	**U=518, p=0.342, d=0.2, E=0, μ =0.07 (-0.03 0.24)**
δ	F3–C3	**t(34.07)=-1.76, p=0.088, d=-0.46, E=0, μ =-0.45 (-0.96 0.06)**	t(33.09)=-3.02, p=0.011, d=-0.79, E=3, μ =-0.74 (-1.22 -0.25)	**t(27.54)=-1.67, p=0.138, d=-0.43, E=0, μ =-0.42 (-0.94 0.09)**	**U=439, p=0.928, d=0.04, E=0, μ =0.06 (-0.31 0.44)**	**U=568, p=0.175, d=0.3, E=0, μ =0.14 (0.02 0.34)**
δ	F4–FZ	**U=293, p=0.053, d=0.26, E=0, μ =-0.42 (-0.89 0)**	t(36.93)=-2.74, p=0.014, d=-0.72, E=3, μ =-0.68 (-1.18 -0.18)	**t(35.8)=-2.47, p=0.064, d=-0.65, E=0, μ =-0.62 (-1.12 -0.12)**	**U=460, p=0.928, d=0.08, E=0, μ =0.1 (-0.28 0.52)**	**U=519, p=0.342, d=0.2, E=0, μ =0.1 (-0.03 0.3)**
δ	FZ–CZ	t(36.27)=-2.4, p=0.039, d=-0.63, E=3, μ =-0.6 (-1.11 -0.1)	t(35.68)=-3.05, p=0.011, d=-0.8, E=3, μ =-0.74 (-1.23 -0.25)	**t(29.45)=-2.24, p=0.078, d=-0.58, E=0, μ =-0.56 (-1.06 -0.06)**	**t(34.99)=0.98, p=0.928, d=0.26, E=0, μ =0.25 (-0.27 0.78)**	**U=520, p=0.342, d=0.2, E=0, μ =0.08 (-0.02 0.24)**
δ	F3–FZ	U=286, p=0.043, d=0.27, E=3, μ =-0.54 (-1 -0.05)	t(36.29)=-2.62, p=0.015, d=-0.69, E=3, μ =-0.65 (-1.15 -0.15)	t(34.63)=-2.77, p=0.036, d=-0.72, E=3, μ =-0.68 (-1.18 -0.19)	**U=402, p=0.928, d=0.04, E=0, μ =-0.06 (-0.54 0.45)**	**U=517, p=0.342, d=0.2, E=0, μ =0.11 (-0.03 0.24)**
δ	T4–C4	U=258, p=0.037, d=0.33, E=3, μ =-0.65 (-1.02 -0.19)	U=225, p=0.01, d=0.4, E=3, μ =-0.83 (-1.25 -0.34)	**U=286, p=0.078, d=0.27, E=0, μ =-0.49 (-0.92 -0.03)**	**U=512, p=0.928, d=0.19, E=0, μ =0.32 (-0.12 0.79)**	**U=509, p=0.366, d=0.18, E=0, μ =0.08 (-0.04 0.23)**
δ	T3–C3	U=274, p=0.039, d=0.3, E=3, μ =-0.61 (-1.12 -0.08)	t(25.36)=-2.9, p=0.012, d=-0.75, E=3, μ =-0.7 (-1.19 -0.22)	**t(28.32)=-1.8, p=0.121, d=-0.47, E=0, μ =-0.46 (-0.97 0.05)**	**U=405, p=0.928, d=0.03, E=0, μ =-0.04 (-0.53 0.51)**	**U=540, p=0.342, d=0.25, E=0, μ =0.13 (0 0.3)**
δ	C4–CZ	U=280, p=0.043, d=0.29, E=3, μ =-0.6 (-1.16 -0.05)	U=226, p=0.01, d=0.4, E=3, μ =-0.97 (-1.44 -0.38)	t(31.13)=-3.03, p=0.036, d=-0.79, E=3, μ =-0.74 (-1.22 -0.25)	**U=443, p=0.928, d=0.05, E=0, μ =0.06 (-0.51 0.67)**	**U=496, p=0.464, d=0.16, E=0, μ =0.1 (-0.04 0.3)**
δ	C3–CZ	U=285, p=0.043, d=0.28, E=3, μ =-0.46 (-0.85 -0.03)	**t(22.59)=-1.96, p=0.056, d=-0.51, E=0, μ =-0.49 (-1 0.01)**	**t(21.97)=-1.71, p=0.135, d=-0.45, E=0, μ =-0.43 (-0.94 0.08)**	**t(36.7)=0.44, p=0.928, d=0.11, E=0, μ =0.11 (-0.41 0.64)**	**U=566, p=0.175, d=0.3, E=0, μ =0.15 (0.01 0.31)**
δ	CZ–PZ	U=250, p=0.029, d=0.35, E=3, μ =-0.59 (-1.07 -0.18)	t(35.46)=-2.93, p=0.011, d=-0.77, E=3, μ =-0.72 (-1.21 -0.23)	t(36.62)=-2.79, p=0.036, d=-0.73, E=3, μ =-0.69 (-1.19 -0.19)	**U=459, p=0.928, d=0.08, E=0, μ =0.15 (-0.32 0.86)**	**U=465, p=0.666, d=0.09, E=0, μ =0.02 (-0.04 0.13)**
δ	C4–P4	U=273, p=0.039, d=0.3, E=3, μ =-0.51 (-0.91 -0.1)	t(33.98)=-2.24, p=0.034, d=-0.58, E=3, μ =-0.56 (-1.07 -0.06)	**t(36.23)=-1.48, p=0.173, d=-0.39, E=0, μ =-0.38 (-0.9 0.13)**	**U=493, p=0.928, d=0.15, E=0, μ =0.32 (-0.23 0.97)**	**U=465, p=0.666, d=0.09, E=0, μ =0.04 (-0.1 0.27)**
δ	C3–P3	U=244, p=0.029, d=0.36, E=3, μ =-0.61 (-1.03 -0.2)	t(34.36)=-2.27, p=0.033, d=-0.59, E=3, μ =-0.57 (-1.07 -0.07)	**t(30.48)=-1.44, p=0.179, d=-0.38, E=0, μ =-0.37 (-0.89 0.15)**	**U=468, p=0.928, d=0.1, E=0, μ =0.17 (-0.31 0.82)**	**U=451, p=0.734, d=0.06, E=0, μ =0.03 (-0.09 0.24)**
δ	T4–T6	U=270, p=0.039, d=0.31, E=3, μ =-0.47 (-0.86 -0.08)	U=249, p=0.013, d=0.35, E=3, μ =-0.62 (-1.08 -0.17)	**t(31.24)=-1, p=0.324, d=-0.26, E=0, μ =-0.26 (-0.78 0.26)**	**U=450, p=0.928, d=0.06, E=0, μ =0.11 (-0.24 0.6)**	**U=476, p=0.642, d=0.11, E=0, μ =0.06 (-0.07 0.2)**
δ	T3–T5	U=245, p=0.029, d=0.36, E=3, μ =-0.71 (-1.12 -0.25)	t(34.26)=-2.84, p=0.012, d=-0.74, E=3, μ =-0.7 (-1.19 -0.2)	**t(32.62)=-1.82, p=0.121, d=-0.48, E=0, μ =-0.46 (-0.98 0.05)**	**U=464, p=0.928, d=0.09, E=0, μ =0.13 (-0.25 0.59)**	**U=487, p=0.536, d=0.14, E=0, μ =0.06 (-0.05 0.2)**

δ	P4–PZ	U=238, p=0.029, d=0.37, E=3, μ =-0.79 (-1.14 -0.26)	U=206, p=0.01, d=0.44, E=3, μ =-1.02 (-1.53 -0.43)	**t(36.08)=-2.35, p=0.074, d=-0.61, E=0, μ =-0.59 (-1.09 -0.09)**	**U=482, p=0.928, d=0.13, E=0, μ =0.28 (-0.26 0.86)**	**U=469, p=0.666, d=0.1, E=0, μ =0.03 (-0.04 0.13)**
δ	P3–PZ	U=275, p=0.039, d=0.3, E=3, μ =-0.46 (-0.92 -0.06)	t(36.39)=-3.37, p=0.01, d=-0.88, E=3, μ =-0.81 (-1.29 -0.33)	**t(33.6)=-2.14, p=0.078, d=-0.56, E=0, μ =-0.54 (-1.05 -0.03)**	**U=422, p=0.982, d=0, E=0, μ =0.01 (-0.46 0.56)**	**U=508, p=0.366, d=0.18, E=0, μ =0.06 (-0.02 0.14)**
δ	T6–O2	U=281, p=0.043, d=0.28, E=3, μ =-0.41 (-0.87 -0.03)	**t(30.46)=-1.98, p=0.055, d=-0.52, E=0, μ =-0.5 (-1.01 0.01)**	**U=339, p=0.222, d=0.17, E=0, μ =-0.34 (-0.79 0.21)**	**U=435, p=0.928, d=0.03, E=0, μ =0.03 (-0.33 0.34)**	**U=458, p=0.718, d=0.08, E=0, μ =0.02 (-0.07 0.13)**
δ	T5–O1	U=263, p=0.039, d=0.32, E=3, μ =-0.62 (-0.98 -0.17)	t(34.26)=-2.71, p=0.014, d=-0.71, E=3, μ =-0.67 (-1.16 -0.17)	**t(27.33)=-1.53, p=0.169, d=-0.4, E=0, μ =-0.39 (-0.9 0.12)**	**U=424, p=0.982, d=0.01, E=0, μ =0.02 (-0.39 0.54)**	**U=451, p=0.734, d=0.06, E=0, μ =0.02 (-0.07 0.19)**
δ	P4–O2	U=268, p=0.039, d=0.31, E=3, μ =-0.55 (-1.02 -0.12)	t(30.49)=-2.66, p=0.015, d=-0.69, E=3, μ =-0.65 (-1.15 -0.16)	**t(26.21)=-1.97, p=0.097, d=-0.51, E=0, μ =-0.5 (-1 0.01)**	**U=382, p=0.928, d=0.08, E=0, μ =-0.13 (-0.55 0.27)**	**U=445, p=0.737, d=0.05, E=0, μ =0.01 (-0.06 0.1)**
δ	P3–O1	U=283, p=0.043, d=0.28, E=3, μ =-0.48 (-1.07 -0.04)	t(30.66)=-3, p=0.011, d=-0.78, E=3, μ =-0.73 (-1.22 -0.24)	**t(29.79)=-1.41, p=0.18, d=-0.37, E=0, μ =-0.36 (-0.88 0.15)**	**U=433, p=0.928, d=0.03, E=0, μ =0.03 (-0.47 0.48)**	**U=445, p=0.737, d=0.05, E=0, μ =0.01 (-0.06 0.13)**
δ	O1–O2	U=226, p=0.029, d=0.4, E=3, μ =-0.53 (-0.86 -0.21)	U=216, p=0.01, d=0.42, E=3, μ =-0.84 (-1.27 -0.42)	t(30.41)=-2.82, p=0.036, d=-0.74, E=3, μ =-0.69 (-1.18 -0.2)	**U=373, p=0.928, d=0.1, E=0, μ =-0.14 (-0.52 0.36)**	**U=400, p=0.763, d=0.04, E=0, μ =-0.01 (-0.09 0.07)**
θ	F8–F4	t(35.97)=-2.35, p=0.027, d=-0.62, E=3, μ =-0.59 (-1.09 -0.09)	t(36.95)=-2.9, p=0.007, d=-0.76, E=3, μ =-0.72 (-1.21 -0.22)	**t(36.02)=-1.94, p=0.148, d=-0.51, E=0, μ =-0.49 (-1 0.02)**	**U=517, p=0.342, d=0.2, E=0, μ =0.37 (-0.11 0.89)**	**U=593, p=0.065, d=0.35, E=0, μ =0.59 (0.2 1.03)**
θ	F7–F3	t(30.41)=-2.59, p=0.022, d=-0.67, E=3, μ =-0.64 (-1.14 -0.14)	t(36.91)=-2.47, p=0.017, d=-0.65, E=3, μ =-0.62 (-1.12 -0.12)	**t(34.39)=-0.91, p=0.403, d=-0.24, E=0, μ =-0.24 (-0.76 0.29)**	**U=488, p=0.4, d=0.14, E=0, μ =0.19 (-0.17 0.65)**	**U=514, p=0.26, d=0.19, E=0, μ =0.19 (-0.08 0.55)**
θ	F4–C4	t(34.05)=-2.77, p=0.019, d=-0.72, E=3, μ =-0.68 (-1.18 -0.19)	t(36.27)=-3.85, p=0.003, d=-1.01, E=3, μ =-0.9 (-1.37 -0.43)	**t(33.75)=-2.46, p=0.09, d=-0.64, E=0, μ =-0.61 (-1.11 -0.11)**	**U=489, p=0.4, d=0.14, E=0, μ =0.27 (-0.24 0.78)**	**U=556, p=0.103, d=0.28, E=0, μ =0.31 (0.02 0.71)**
θ	F3–C3	t(34.51)=-2.24, p=0.032, d=-0.59, E=3, μ =-0.56 (-1.07 -0.06)	t(36.15)=-2.9, p=0.007, d=-0.76, E=3, μ =-0.71 (-1.21 -0.22)	**t(30.01)=-1.82, p=0.154, d=-0.47, E=0, μ =-0.46 (-0.97 0.05)**	**U=479, p=0.442, d=0.12, E=0, μ =0.18 (-0.18 0.47)**	**U=594, p=0.065, d=0.36, E=0, μ =0.33 (0.09 0.65)**
θ	F4–FZ	U=264, p=0.024, d=0.32, E=3, μ =-0.67 (-1.18 -0.09)	t(36.77)=-2.83, p=0.008, d=-0.74, E=3, μ =-0.7 (-1.2 -0.21)	**t(33.06)=-2.07, p=0.13, d=-0.54, E=0, μ =-0.52 (-1.03 -0.02)**	**U=540, p=0.276, d=0.25, E=0, μ =0.4 (-0.02 0.82)**	**U=588, p=0.065, d=0.34, E=0, μ =0.37 (0.08 0.73)**
θ	FZ–CZ	t(35.78)=-3.12, p=0.018, d=-0.82, E=3, μ =-0.76 (-1.25 -0.27)	**t(36.93)=-3.8, p=0.003, d=-1, E=2, μ =-0.9 (-1.37 -0.42)**	**t(28.02)=-1.79, p=0.154, d=-0.47, E=0, μ =-0.45 (-0.96 0.06)**	**t(28.13)=0.68, p=0.524, d=0.18, E=0, μ =0.18 (-0.35 0.7)**	**U=535, p=0.156, d=0.23, E=0, μ =0.17 (-0.01 0.39)**
θ	F3–FZ	t(34.28)=-2.67, p=0.019, d=-0.7, E=3, μ =-0.66 (-1.16 -0.17)	t(35.71)=-3.11, p=0.006, d=-0.81, E=3, μ =-0.76 (-1.24 -0.27)	**t(31.92)=-2.34, p=0.09, d=-0.61, E=0, μ =-0.58 (-1.09 -0.08)**	**U=485, p=0.406, d=0.13, E=0, μ =0.24 (-0.27 0.68)**	**U=573, p=0.092, d=0.31, E=0, μ =0.32 (0.07 0.63)**
θ	T4–C4	t(25.95)=-2.76, p=0.019, d=-0.72, E=3, μ =-0.67 (-1.17 -0.18)	**t(36.93)=-2.33, p=0.024, d=-0.61, E=2, μ =-0.59 (-1.09 -0.08)**	**t(29.78)=-1.04, p=0.368, d=-0.27, E=0, μ =-0.27 (-0.79 0.25)**	**U=585, p=0.224, d=0.34, E=0, μ =0.58 (0.13 1.16)**	**U=555, p=0.103, d=0.28, E=0, μ =0.29 (0.02 0.62)**
θ	T3–C3	t(27.51)=-3.12, p=0.018, d=-0.81, E=3, μ =-0.75 (-1.24 -0.27)	**t(34.46)=-3.3, p=0.005, d=-0.86, E=2, μ =-0.79 (-1.28 -0.31)**	**t(34.11)=-1.67, p=0.177, d=-0.44, E=0, μ =-0.43 (-0.94 0.08)**	**U=428, p=0.908, d=0.02, E=0, μ =0.03 (-0.43 0.55)**	**U=564, p=0.095, d=0.29, E=0, μ =0.35 (0.05 0.64)**

θ	C4–CZ	t(35.54)=-2.94, p=0.019, d=-0.77, E=3, μ =-0.72 (-1.21 -0.23)	**t(34.62)=-3.41, p=0.005, d=-0.89, E=2, μ =-0.82 (-1.3 -0.34)**	**t(28.26)=-2.5, p=0.09, d=-0.65, E=0, μ =-0.62 (-1.12 -0.12)**	**U=506, p=0.364, d=0.18, E=0, μ =0.33 (-0.19 0.83)**	**U=539, p=0.149, d=0.24, E=0, μ =0.18 (-0.02 0.41)**
θ	C3–CZ	t(23.6)=-2.49, p=0.024, d=-0.65, E=3, μ =-0.62 (-1.11 -0.12)	**t(33.44)=-2.97, p=0.007, d=-0.78, E=2, μ =-0.73 (-1.21 -0.24)**	**t(22.5)=-2.39, p=0.09, d=-0.62, E=0, μ =-0.59 (-1.09 -0.09)**	**t(33.59)=0.86, p=0.454, d=0.22, E=0, μ =0.22 (-0.3 0.75)**	**U=569, p=0.092, d=0.3, E=0, μ =0.3 (0.04 0.59)**
θ	CZ–PZ	t(37)=-2.82, p=0.019, d=-0.74, E=3, μ =-0.7 (-1.19 -0.2)	t(36.79)=-3.37, p=0.005, d=-0.89, E=3, μ =-0.81 (-1.3 -0.33)	**t(35.33)=-2.36, p=0.09, d=-0.62, E=0, μ =-0.59 (-1.09 -0.09)**	**t(34.44)=1.7, p=0.31, d=0.44, E=0, μ =0.44 (-0.08 0.95)**	**U=496, p=0.327, d=0.16, E=0, μ =0.14 (-0.11 0.42)**
θ	C4–P4	t(36.99)=-2.31, p=0.028, d=-0.61, E=3, μ =-0.58 (-1.09 -0.08)	t(36.11)=-3.02, p=0.007, d=-0.79, E=3, μ =-0.74 (-1.24 -0.25)	**t(34.42)=-1.21, p=0.294, d=-0.32, E=0, μ =-0.31 (-0.83 0.21)**	**U=536, p=0.276, d=0.24, E=0, μ =0.41 (-0.06 0.94)**	**U=464, p=0.511, d=0.09, E=0, μ =0.11 (-0.21 0.45)**
θ	C3–P3	t(36.15)=-2.71, p=0.019, d=-0.71, E=3, μ =-0.67 (-1.17 -0.17)	t(36.81)=-2.96, p=0.007, d=-0.78, E=3, μ =-0.73 (-1.22 -0.24)	**t(36.38)=-1.24, p=0.294, d=-0.33, E=0, μ =-0.32 (-0.84 0.2)**	**t(27.93)=1.9, p=0.276, d=0.49, E=0, μ =0.48 (-0.03 0.99)**	**U=500, p=0.313, d=0.16, E=0, μ =0.2 (-0.1 0.6)**
θ	T4–T6	**t(29.21)=-1.6, p=0.115, d=-0.42, E=0, μ =-0.41 (-0.92 0.1)**	t(36.75)=-3.25, p=0.005, d=-0.85, E=3, μ =-0.79 (-1.27 -0.3)	**t(29.92)=-1.48, p=0.224, d=-0.39, E=0, μ =-0.38 (-0.89 0.14)**	**U=524, p=0.31, d=0.21, E=0, μ =0.38 (-0.11 1.05)**	**U=509, p=0.279, d=0.18, E=0, μ =0.2 (-0.06 0.53)**
θ	T3–T5	t(34.61)=-2.39, p=0.027, d=-0.63, E=3, μ =-0.6 (-1.1 -0.1)	**t(36.98)=-2.66, p=0.012, d=-0.7, E=2, μ =-0.66 (-1.16 -0.16)**	**t(35.41)=-0.94, p=0.403, d=-0.25, E=0, μ =-0.25 (-0.77 0.28)**	**U=493, p=0.4, d=0.15, E=0, μ =0.34 (-0.18 0.87)**	**U=518, p=0.249, d=0.2, E=0, μ =0.18 (-0.07 0.5)**
θ	P4–PZ	t(36.29)=-3.83, p=0.008, d=-1, E=3, μ =-0.9 (-1.37 -0.43)	t(36.56)=-4.44, p=0.001, d=-1.16, E=3, μ =-1.01 (-1.46 -0.55)	**t(28.93)=-2.56, p=0.09, d=-0.67, E=0, μ =-0.63 (-1.13 -0.14)**	**t(32.45)=1.08, p=0.4, d=0.28, E=0, μ =0.28 (-0.24 0.8)**	**U=484, p=0.417, d=0.13, E=0, μ =0.08 (-0.08 0.32)**
θ	P3–PZ	t(36.71)=-2.89, p=0.019, d=-0.76, E=3, μ =-0.71 (-1.2 -0.22)	**t(33.34)=-3.28, p=0.005, d=-0.86, E=2, μ =-0.79 (-1.27 -0.31)**	**t(30.05)=-1.52, p=0.222, d=-0.4, E=0, μ =-0.39 (-0.9 0.12)**	**U=505, p=0.364, d=0.17, E=0, μ =0.34 (-0.21 0.79)**	**U=539, p=0.149, d=0.24, E=0, μ =0.21 (-0.02 0.46)**
θ	T6–O2	**t(32.28)=-1.67, p=0.107, d=-0.43, E=0, μ =-0.43 (-0.94 0.09)**	**t(35.67)=-2.63, p=0.012, d=-0.69, E=2, μ =-0.65 (-1.15 -0.15)**	**t(24.55)=-1.81, p=0.154, d=-0.47, E=0, μ =-0.46 (-0.97 0.05)**	**U=464, p=0.524, d=0.09, E=0, μ =0.17 (-0.29 0.56)**	**U=478, p=0.453, d=0.12, E=0, μ =0.09 (-0.12 0.41)**
θ	T5–O1	t(33.94)=-2.48, p=0.024, d=-0.65, E=3, μ =-0.62 (-1.12 -0.12)	**t(37)=-2.69, p=0.012, d=-0.7, E=2, μ =-0.67 (-1.17 -0.17)**	**t(31.79)=-0.87, p=0.409, d=-0.23, E=0, μ =-0.22 (-0.75 0.3)**	**t(31.1)=1.99, p=0.276, d=0.52, E=0, μ =0.5 (0 1.01)**	**U=501, p=0.313, d=0.17, E=0, μ =0.13 (-0.07 0.51)**
θ	P4–O2	t(31.92)=-2.67, p=0.019, d=-0.7, E=3, μ =-0.66 (-1.15 -0.16)	**t(32.72)=-3.16, p=0.006, d=-0.82, E=2, μ =-0.76 (-1.25 -0.28)**	**t(29.64)=-1.38, p=0.252, d=-0.36, E=0, μ =-0.35 (-0.87 0.16)**	**U=489, p=0.4, d=0.14, E=0, μ =0.24 (-0.19 0.74)**	**U=468, p=0.511, d=0.1, E=0, μ =0.06 (-0.11 0.33)**
θ	P3–O1	t(34.2)=-2.35, p=0.027, d=-0.62, E=3, μ =-0.59 (-1.09 -0.09)	**t(36.13)=-2.96, p=0.007, d=-0.77, E=2, μ =-0.72 (-1.22 -0.23)**	**t(33.7)=-0.67, p=0.503, d=-0.18, E=0, μ =-0.18 (-0.7 0.35)**	**U=555, p=0.276, d=0.28, E=0, μ =0.58 (0.04 1.12)**	**U=463, p=0.511, d=0.09, E=0, μ =0.07 (-0.11 0.41)**
θ	O1–O2	U=222, p=0.018, d=0.4, E=3, μ =-0.67 (-1.01 -0.34)	t(36.47)=-3.58, p=0.004, d=-0.94, E=3, μ =-0.85 (-1.33 -0.38)	**t(24.68)=-2.06, p=0.13, d=-0.54, E=0, μ =-0.52 (-1.02 -0.01)**	**U=508, p=0.364, d=0.18, E=0, μ =0.26 (-0.09 0.74)**	**U=377, p=0.511, d=0.09, E=0, μ =-0.05 (-0.28 0.18)**
α	F8–F4	**t(36.24)=-0.71, p=0.581, d=-0.19, E=0, μ =-0.19 (-0.71 0.34)**	**t(37)=-1.84, p=0.113, d=-0.48, E=0, μ =-0.47 (-0.99 0.04)**	U=440, p=0.763, d=0.04, E=0, μ =0.06 (-0.34 0.49)	**U=611, p=0.003, d=0.39, E=2, μ =0.65 (0.25 1.06)**	**U=657, p=0.001, d=0.48, E=2, μ =0.61 (0.27 0.92)**
α	F7–F3	**U=292, p=0.244, d=0.26, E=0, μ =-0.53 (-0.94 -0.01)**	U=281, p=0.087, d=0.28, E=0, μ =-0.57 (-1.02 -0.07)	U=470, p=0.567, d=0.1, E=0, μ =-0.13 (-0.27 0.54)	**U=642, p=0.001, d=0.45, E=2, μ =0.76 (0.37 1.07)**	**U=608, p=0.004, d=0.38, E=2, μ =0.42 (0.11 0.77)**

α	F4–C4	**t(35.66)=-2.52, p=0.244, d=-0.66, E=0, μ =-0.63 (-1.13 -0.13)**	**t(32)=-2.23, p=0.087, d=-0.58, E=0, μ =-0.56 (-1.06 -0.06)**	**t(35.35)=1.01, p=0.483, d=0.27, E=0, μ =0.26 (-0.26 0.79)**	**U=632, p=0.001, d=0.43, E=2, μ =0.8 (0.39 1.27)**	U=663, p=0.001, d=0.5, E=3, μ =0.65 (0.29 1.11)
α	F3–C3	**t(29.47)=-0.98, p=0.452, d=-0.25, E=0, μ =-0.25 (-0.77 0.27)**	**t(31.94)=-2.27, p=0.087, d=-0.59, E=0, μ =-0.57 (-1.07 -0.07)**	**U=451, p=0.667, d=0.06, E=0, μ =0.11 (-0.4 0.57)**	U=579, p=0.014, d=0.32, E=3, μ =0.52 (0.11 0.91)	U=669, p=0.001, d=0.51, E=3, μ =0.61 (0.29 0.93)
α	F4–FZ	**t(35.99)=-1.18, p=0.371, d=-0.31, E=0, μ =-0.31 (-0.83 0.21)**	**t(35.99)=-1.7, p=0.12, d=-0.45, E=0, μ =-0.44 (-0.95 0.08)**	**t(31.17)=0.64, p=0.637, d=0.17, E=0, μ =0.17 (-0.36 0.69)**	**t(33.22)=3.7, p=0.001, d=0.97, E=1, μ =0.87 (0.4 1.34)**	U=659, p=0.001, d=0.49, E=3, μ =0.52 (0.23 0.89)
α	FZ–CZ	**t(35.03)=-1.82, p=0.244, d=-0.48, E=0, μ =-0.46 (-0.98 0.05)**	**t(32.72)=-2.56, p=0.087, d=-0.67, E=0, μ =-0.64 (-1.13 -0.14)**	**t(36.87)=0.96, p=0.494, d=0.25, E=0, μ =0.25 (-0.27 0.77)**	**t(36.94)=2.47, p=0.017, d=0.65, E=2, μ =0.62 (0.12 1.12)**	U=642, p=0.002, d=0.45, E=3, μ =0.52 (0.22 0.85)
α	F3–FZ	**t(34.01)=-1.47, p=0.343, d=-0.38, E=0, μ =-0.38 (-0.89 0.14)**	**t(33.83)=-1.83, p=0.113, d=-0.48, E=0, μ =-0.47 (-0.98 0.04)**	**t(32.46)=0.77, p=0.567, d=0.2, E=0, μ =0.2 (-0.32 0.72)**	**U=647, p=0.001, d=0.46, E=2, μ =0.81 (0.4 1.19)**	U=666, p=0.001, d=0.5, E=3, μ =0.55 (0.25 0.89)
α	T4–C4	**t(25.09)=-0.54, p=0.651, d=-0.14, E=0, μ =-0.14 (-0.66 0.38)**	**t(34.35)=-1.34, p=0.195, d=-0.35, E=0, μ =-0.35 (-0.86 0.17)**	**t(32.7)=2.13, p=0.144, d=0.56, E=0, μ =0.54 (0.03 1.04)**	**U=652, p=0.001, d=0.47, E=2, μ =0.94 (0.45 1.31)**	**U=618, p=0.004, d=0.4, E=2, μ =0.45 (0.16 0.77)**
α	T3–C3	**t(32.4)=-1.53, p=0.343, d=-0.4, E=0, μ =-0.39 (-0.91 0.12)**	**t(34.34)=-2.13, p=0.087, d=-0.56, E=0, μ =-0.54 (-1.04 -0.03)**	**U=458, p=0.646, d=0.08, E=0, μ =0.19 (-0.3 0.67)**	**t(34.7)=3.04, p=0.005, d=0.79, E=2, μ =0.74 (0.25 1.23)**	**U=633, p=0.002, d=0.44, E=2, μ =0.56 (0.22 0.94)**
α	C4–CZ	**t(36.79)=-2.01, p=0.244, d=-0.53, E=0, μ =-0.51 (-1.02 0)**	**t(30.78)=-2.7, p=0.087, d=-0.71, E=0, μ =-0.67 (-1.16 -0.17)**	**U=488, p=0.483, d=0.14, E=0, μ =0.26 (-0.22 0.71)**	**U=617, p=0.003, d=0.4, E=2, μ =0.68 (0.27 1.11)**	**U=616, p=0.004, d=0.4, E=2, μ =0.39 (0.16 0.66)**
α	C3–CZ	**t(24.59)=-1.39, p=0.351, d=-0.36, E=0, μ =-0.36 (-0.87 0.16)**	**t(29.58)=-1.95, p=0.113, d=-0.51, E=0, μ =-0.49 (-1 0.02)**	**t(35.05)=0.53, p=0.657, d=0.14, E=0, μ =0.14 (-0.39 0.66)**	**t(37)=2.31, p=0.025, d=0.61, E=2, μ =0.58 (0.08 1.09)**	**U=626, p=0.003, d=0.42, E=2, μ =0.68 (0.27 1.06)**
α	CZ–PZ	**t(35.49)=-1.97, p=0.244, d=-0.52, E=0, μ =-0.5 (-1.01 0.01)**	**t(35.95)=-2.45, p=0.087, d=-0.64, E=0, μ =-0.61 (-1.11 -0.11)**	**t(37)=1.37, p=0.31, d=0.36, E=0, μ =0.36 (-0.16 0.88)**	t(34.37)=3.33, p=0.003, d=0.88, E=3, μ =0.81 (0.32 1.3)	U=612, p=0.004, d=0.39, E=3, μ =0.55 (0.15 1.02)
α	C4–P4	**t(36.51)=-1.25, p=0.353, d=-0.33, E=0, μ =-0.33 (-0.85 0.19)**	**t(36.36)=-1.81, p=0.113, d=-0.47, E=0, μ =-0.46 (-0.98 0.05)**	**t(36.98)=2.29, p=0.119, d=0.6, E=0, μ =0.58 (0.07 1.09)**	U=673, p|0.001, d=0.52, E=3, μ =0.87 (0.47 1.31)	**U=590, p=0.009, d=0.35, E=1, μ =0.54 (0.13 0.99)**
α	C3–P3	**t(36.1)=-1.28, p=0.353, d=-0.34, E=0, μ =-0.33 (-0.85 0.19)**	**t(36.53)=-1.79, p=0.113, d=-0.47, E=0, μ =-0.46 (-0.97 0.05)**	**U=580, p=0.118, d=0.33, E=0, μ =0.62 (0.1 1.04)**	t(36.73)=3.25, p=0.003, d=0.85, E=3, μ =0.79 (0.3 1.28)	**U=608, p=0.004, d=0.38, E=1, μ =0.57 (0.17 0.98)**
α	T4–T6	**t(31.91)=-0.54, p=0.651, d=-0.14, E=0, μ =-0.14 (-0.66 0.38)**	**t(34.88)=-1.89, p=0.113, d=-0.49, E=0, μ =-0.48 (-0.99 0.03)**	**t(36.8)=1.9, p=0.151, d=0.5, E=0, μ =0.49 (-0.03 1)**	U=671, p|0.001, d=0.51, E=3, μ =0.99 (0.56 1.38)	**U=598, p=0.007, d=0.36, E=1, μ =0.43 (0.13 0.82)**
α	T3–T5	**t(35.65)=-2, p=0.244, d=-0.52, E=0, μ =-0.51 (-1.02 0)**	**t(36.39)=-1.75, p=0.117, d=-0.46, E=0, μ =-0.45 (-0.96 0.07)**	**U=510, p=0.31, d=0.18, E=0, μ =0.37 (-0.17 0.82)**	U=641, p=0.001, d=0.45, E=3, μ =0.81 (0.39 1.26)	**U=619, p=0.004, d=0.41, E=2, μ =0.6 (0.22 1.04)**
α	P4–PZ	**t(34.44)=-1.35, p=0.351, d=-0.35, E=0, μ =-0.35 (-0.87 0.17)**	**t(33.72)=-2.59, p=0.087, d=-0.68, E=0, μ =-0.64 (-1.14 -0.15)**	**t(36.7)=1.88, p=0.151, d=0.49, E=0, μ =0.48 (-0.03 0.99)**	**t(33.06)=4.29, p|0.001, d=1.12, E=2, μ =0.98 (0.52 1.44)**	**U=608, p=0.004, d=0.38, E=1, μ =0.5 (0.14 0.92)**
α	P3–PZ	**t(28.47)=-1.51, p=0.343, d=-0.39, E=0, μ =-0.39 (-0.9 0.13)**	**t(30.04)=-2.31, p=0.087, d=-0.6, E=0, μ =-0.58 (-1.08 -0.07)**	**t(37)=1.67, p=0.211, d=0.44, E=0, μ =0.43 (-0.09 0.95)**	t(35.97)=2.76, p=0.009, d=0.73, E=3, μ =0.69 (0.19 1.19)	**U=620, p=0.004, d=0.41, E=2, μ =0.7 (0.25 1.08)**

α	T6–O2	**t(30.27)=-0.36, p=0.752, d=-0.09, E=0, μ =-0.09 (-0.62 0.43)**	**t(32.47)=-1.68, p=0.12, d=-0.44, E=0, μ =-0.43 (-0.94 0.08)**	**t(35.57)=1.98, p=0.151, d=0.52, E=0, μ =0.5 (-0.01 1.01)**	t(36.88)=2.84, p=0.008, d=0.75, E=3, μ =0.7 (0.21 1.2)	**U=597, p=0.007, d=0.36, E=1, μ =0.47 (0.13 0.87)**
α	T5–O1	**U=366, p=0.521, d=0.11, E=0, μ =-0.18 (-0.64 0.24)**	**t(34.59)=-1.56, p=0.143, d=-0.41, E=0, μ =-0.4 (-0.92 0.11)**	**t(36.62)=2.5, p=0.118, d=0.65, E=0, μ =0.63 (0.12 1.13)**	t(36.79)=3.42, p=0.002, d=0.9, E=3, μ =0.82 (0.34 1.31)	**U=575, p=0.017, d=0.32, E=1, μ =0.37 (0.06 0.95)**
α	P4–O2	**t(31.54)=-1.03, p=0.443, d=-0.27, E=0, μ =-0.27 (-0.79 0.25)**	**t(30.38)=-1.34, p=0.195, d=-0.35, E=0, μ =-0.34 (-0.86 0.17)**	**t(28.88)=2.39, p=0.118, d=0.62, E=0, μ =0.6 (0.1 1.1)**	U=655, p=0.001, d=0.48, E=3, μ =0.77 (0.43 1.23)	**U=571, p=0.019, d=0.31, E=1, μ =0.37 (0.07 0.68)**
α	P3–O1	**U=399, p=0.752, d=0.04, E=0, μ =-0.06 (-0.54 0.43)**	**t(33.55)=-0.9, p=0.373, d=-0.23, E=0, μ =-0.23 (-0.76 0.29)**	**t(34.03)=3.15, p=0.062, d=0.82, E=0, μ =0.76 (0.28 1.25)**	t(36.78)=4.26, p|0.001, d=1.12, E=3, μ =0.98 (0.52 1.44)	**U=592, p=0.008, d=0.35, E=1, μ =0.46 (0.11 0.86)**
α	O1–O2	**t(36.08)=-1.86, p=0.244, d=-0.49, E=0, μ =-0.47 (-0.99 0.04)**	**t(29.2)=-2.17, p=0.087, d=-0.57, E=0, μ =-0.55 (-1.05 -0.04)**	**t(25.85)=1.93, p=0.151, d=0.5, E=0, μ =0.49 (-0.02 0.99)**	U=655, p=0.001, d=0.48, E=3, μ =0.88 (0.47 1.37)	**U=526, p=0.101, d=0.22, E=0, μ =0.22 (-0.05 0.53)**
β	F8–F4	**U=551, p=0.418, d=0.27, E=0, μ =0.41 (0.02 0.82)**	**U=470, p=0.537, d=0.1, E=0, μ =0.19 (-0.23 0.64)**	**U=595, p=0.008, d=0.36, E=2, μ =0.55 (0.17 0.93)**	**U=612, p=0.005, d=0.39, E=2, μ =0.51 (0.2 0.85)**	**U=659, p=0.001, d=0.49, E=2, μ =0.57 (0.23 0.99)**
β	F7–F3	**U=525, p=0.418, d=0.21, E=0, μ =0.29 (-0.06 0.71)**	**U=461, p=0.588, d=0.08, E=0, μ =0.1 (-0.23 0.47)**	**U=613, p=0.004, d=0.39, E=1, μ =0.64 (0.26 0.98)**	**U=607, p=0.006, d=0.38, E=2, μ =0.41 (0.14 0.72)**	U=627, p=0.002, d=0.42, E=3, μ =0.45 (0.15 0.81)
β	F4–C4	**U=497, p=0.418, d=0.16, E=0, μ =0.32 (-0.14 0.88)**	**t(21.09)=2.13, p=0.227, d=0.55, E=0, μ =0.53 (0.03 1.03)**	t(36.83)=3.1, p=0.005, d=0.81, E=3, μ =0.76 (0.27 1.24)	**U=603, p=0.006, d=0.37, E=1, μ =0.63 (0.22 1.13)**	U=654, p=0.001, d=0.48, E=3, μ =0.65 (0.22 0.99)
β	F3–C3	**U=484, p=0.5, d=0.13, E=0, μ =0.24 (-0.19 0.62)**	**U=459, p=0.588, d=0.08, E=0, μ =0.16 (-0.3 0.56)**	U=598, p=0.007, d=0.36, E=3, μ =0.6 (0.2 0.95)	U=583, p=0.012, d=0.33, E=3, μ =0.49 (0.12 0.86)	U=660, p=0.001, d=0.49, E=3, μ =0.59 (0.24 0.91)
β	F4–FZ	**U=499, p=0.418, d=0.16, E=0, μ =0.23 (-0.11 0.59)**	**U=566, p=0.175, d=0.3, E=0, μ =0.45 (0.05 0.81)**	**t(30.06)=3.79, p=0.001, d=0.99, E=2, μ =0.89 (0.42 1.36)**	U=641, p=0.003, d=0.45, E=3, μ =0.69 (0.32 1.14)	U=643, p=0.001, d=0.46, E=3, μ =0.48 (0.2 0.83)
β	FZ–CZ	**U=523, p=0.418, d=0.21, E=0, μ =0.37 (-0.06 0.84)**	**t(25.79)=1.13, p=0.429, d=0.29, E=0, μ =0.29 (-0.23 0.81)**	t(36.66)=2.43, p=0.02, d=0.64, E=3, μ =0.61 (0.11 1.12)	**t(35.15)=3.42, p=0.003, d=0.9, E=1, μ =0.82 (0.34 1.3)**	U=647, p=0.001, d=0.46, E=3, μ =0.44 (0.16 0.76)
β	F3–FZ	**U=499, p=0.418, d=0.16, E=0, μ =0.27 (-0.17 0.72)**	**U=566, p=0.175, d=0.3, E=0, μ =0.46 (0.07 0.92)**	**U=626, p=0.003, d=0.42, E=2, μ =0.74 (0.33 1.13)**	U=658, p=0.003, d=0.49, E=3, μ =0.68 (0.33 1.05)	U=654, p=0.001, d=0.48, E=3, μ =0.52 (0.19 0.89)
β	T4–C4	**U=566, p=0.418, d=0.3, E=0, μ =0.51 (0.09 1.04)**	**U=500, p=0.429, d=0.16, E=0, μ =0.31 (-0.19 0.85)**	**U=599, p=0.007, d=0.37, E=2, μ =0.7 (0.2 1.22)**	**U=626, p=0.003, d=0.42, E=2, μ =0.72 (0.28 1.12)**	**U=632, p=0.002, d=0.43, E=2, μ =0.48 (0.21 0.77)**
β	T3–C3	**U=527, p=0.418, d=0.22, E=0, μ =0.38 (-0.05 0.97)**	**t(32.3)=0.91, p=0.487, d=0.24, E=0, μ =0.24 (-0.29 0.76)**	U=577, p=0.016, d=0.32, E=3, μ =0.55 (0.17 1.05)	**U=616, p=0.004, d=0.4, E=2, μ =0.73 (0.25 1.21)**	**U=649, p=0.001, d=0.47, E=2, μ =0.54 (0.26 0.95)**
β	C4–CZ	**U=506, p=0.418, d=0.18, E=0, μ =0.32 (-0.17 0.91)**	**U=422, p=0.982, d=0, E=0, μ =0.02 (-0.43 0.55)**	**U=610, p=0.005, d=0.39, E=2, μ =0.65 (0.23 1.06)**	**U=599, p=0.007, d=0.37, E=2, μ =0.62 (0.17 1.13)**	**U=616, p=0.003, d=0.4, E=2, μ =0.43 (0.15 0.69)**
β	C3–CZ	**U=467, p=0.571, d=0.1, E=0, μ =0.18 (-0.35 0.66)**	**t(32.68)=1.09, p=0.429, d=0.28, E=0, μ =0.28 (-0.24 0.8)**	**t(36.22)=1.66, p=0.103, d=0.43, E=0, μ =0.43 (-0.09 0.94)**	**t(35.09)=3.36, p=0.003, d=0.88, E=2, μ =0.81 (0.33 1.29)**	**U=640, p=0.001, d=0.45, E=2, μ =0.63 (0.26 1.03)**
β	CZ–PZ	**U=515, p=0.418, d=0.19, E=0, μ =0.46 (-0.17 1.1)**	**t(30.19)=1.55, p=0.368, d=0.4, E=0, μ =0.4 (-0.12 0.91)**	U=622, p=0.003, d=0.41, E=3, μ =0.69 (0.26 1.12)	U=568, p=0.021, d=0.3, E=3, μ =0.65 (0.11 1.22)	U=603, p=0.005, d=0.37, E=3, μ =0.41 (0.12 0.81)

β	C4–P4	**U=517, p=0.418, d=0.2, E=0, μ =0.46 (-0.12 1.07)**	**U=525, p=0.368, d=0.21, E=0, μ =0.41 (-0.1 1.03)**	U=667, p=0.001, d=0.5, E=3, μ =0.87 (0.46 1.32)	**U=637, p=0.003, d=0.44, E=2, μ =0.79 (0.34 1.3)**	**U=601, p=0.005, d=0.37, E=2, μ =0.56 (0.13 1.15)**
β	C3–P3	**U=506, p=0.418, d=0.18, E=0, μ =0.36 (-0.14 0.95)**	**U=499, p=0.429, d=0.16, E=0, μ =0.33 (-0.16 0.86)**	U=644, p=0.001, d=0.46, E=3, μ =0.82 (0.37 1.24)	U=584, p=0.012, d=0.34, E=3, μ =0.63 (0.15 1.23)	**U=607, p=0.004, d=0.38, E=2, μ =0.55 (0.15 1.08)**
β	T4–T6	**U=476, p=0.5, d=0.11, E=0, μ =0.19 (-0.29 0.78)**	**U=495, p=0.429, d=0.15, E=0, μ =0.26 (-0.24 0.83)**	U=680, p¡0.001, d=0.53, E=3, μ =0.86 (0.5 1.28)	**U=632, p=0.003, d=0.43, E=1, μ =0.74 (0.28 1.21)**	**U=623, p=0.003, d=0.41, E=1, μ =0.48 (0.16 0.85)**
β	T3–T5	**U=482, p=0.5, d=0.13, E=0, μ =0.25 (-0.2 0.77)**	**t(29.71)=0.92, p=0.487, d=0.24, E=0, μ =0.24 (-0.28 0.76)**	U=637, p=0.002, d=0.44, E=3, μ =0.75 (0.38 1.23)	**U=631, p=0.003, d=0.43, E=2, μ =0.89 (0.41 1.36)**	**U=620, p=0.003, d=0.41, E=2, μ =0.5 (0.17 0.92)**
β	P4–PZ	**U=476, p=0.5, d=0.11, E=0, μ =0.22 (-0.24 0.92)**	**t(31.53)=0.88, p=0.487, d=0.23, E=0, μ =0.23 (-0.29 0.75)**	t(36.94)=3.07, p=0.005, d=0.81, E=3, μ =0.75 (0.26 1.24)	U=626, p=0.003, d=0.42, E=3, μ =0.78 (0.3 1.35)	U=621, p=0.003, d=0.41, E=3, μ =0.48 (0.16 0.87)
β	P3–PZ	**U=478, p=0.5, d=0.12, E=0, μ =0.33 (-0.27 0.91)**	**U=498, p=0.429, d=0.16, E=0, μ =0.3 (-0.15 0.74)**	t(36.96)=2.33, p=0.024, d=0.61, E=3, μ =0.59 (0.08 1.1)	U=595, p=0.008, d=0.36, E=3, μ =0.74 (0.21 1.2)	U=633, p=0.002, d=0.44, E=3, μ =0.52 (0.23 0.91)
β	T6–O2	**U=451, p=0.699, d=0.06, E=0, μ =0.1 (-0.31 0.66)**	**U=458, p=0.588, d=0.08, E=0, μ =0.11 (-0.39 0.58)**	t(36.19)=2.59, p=0.015, d=0.68, E=3, μ =0.65 (0.15 1.14)	**U=577, p=0.015, d=0.32, E=1, μ =0.49 (0.08 1.02)**	**U=580, p=0.013, d=0.33, E=1, μ =0.33 (0.08 0.67)**
β	T5–O1	**U=460, p=0.623, d=0.08, E=0, μ =0.13 (-0.23 0.67)**	**t(29.21)=1.93, p=0.273, d=0.5, E=0, μ =0.49 (-0.02 1)**	t(36.63)=3.92, p=0.001, d=1.03, E=3, μ =0.92 (0.45 1.39)	**U=605, p=0.006, d=0.38, E=2, μ =0.65 (0.17 1.15)**	**U=584, p=0.011, d=0.34, E=1, μ =0.27 (0.04 0.71)**
β	P4–O2	**U=436, p=0.848, d=0.03, E=0, μ =0.05 (-0.39 0.52)**	**U=519, p=0.368, d=0.2, E=0, μ =0.38 (-0.11 0.83)**	t(32.51)=3.97, p=0.001, d=1.04, E=3, μ =0.92 (0.46 1.39)	**U=590, p=0.009, d=0.35, E=2, μ =0.55 (0.16 0.95)**	**U=584, p=0.011, d=0.34, E=1, μ =0.29 (0.07 0.53)**
β	P3–O1	**U=504, p=0.418, d=0.17, E=0, μ =0.4 (-0.18 0.9)**	**t(29.35)=2.48, p=0.175, d=0.65, E=0, μ =0.61 (0.12 1.11)**	t(35.09)=4.55, p¡0.001, d=1.19, E=3, μ =1.02 (0.57 1.47)	**U=621, p=0.003, d=0.41, E=2, μ =0.71 (0.31 1.14)**	**U=613, p=0.003, d=0.39, E=2, μ =0.36 (0.1 0.77)**
β	O1–O2	**U=431, p=0.871, d=0.02, E=0, μ =0.03 (-0.42 0.46)**	**U=503, p=0.429, d=0.17, E=0, μ =0.27 (-0.15 0.77)**	**t(31.39)=3.51, p=0.002, d=0.92, E=2, μ =0.83 (0.36 1.31)**	U=591, p=0.009, d=0.35, E=3, μ =0.67 (0.18 1.12)	**U=568, p=0.021, d=0.3, E=1, μ =0.24 (0.03 0.53)**
γ	F8–F4	**U=609, p=0.033, d=0.39, E=1, μ =0.35 (0.11 0.65)**	**U=570, p=0.109, d=0.31, E=0, μ =0.48 (0.05 0.89)**	**U=644, p=0.002, d=0.46, E=2, μ =0.6 (0.26 0.95)**	**U=658, p=0.001, d=0.49, E=2, μ =0.62 (0.29 0.98)**	**U=686, p¡0.001, d=0.54, E=2, μ =0.65 (0.37 0.96)**
γ	F7–F3	**U=568, p=0.06, d=0.3, E=0, μ =0.22 (0.04 0.48)**	**U=546, p=0.109, d=0.26, E=0, μ =0.36 (0 0.77)**	**U=624, p=0.003, d=0.42, E=2, μ =0.57 (0.2 0.89)**	**U=624, p=0.002, d=0.42, E=2, μ =0.47 (0.15 0.87)**	**U=624, p=0.004, d=0.42, E=2, μ =0.35 (0.1 0.56)**
γ	F4–C4	**U=539, p=0.129, d=0.24, E=0, μ =0.14 (-0.01 0.35)**	**U=547, p=0.109, d=0.26, E=0, μ =0.3 (0 0.88)**	U=655, p=0.001, d=0.48, E=3, μ =0.69 (0.26 1.28)	**U=660, p=0.001, d=0.49, E=2, μ =0.64 (0.22 1.01)**	**U=634, p=0.004, d=0.44, E=2, μ =0.32 (0.11 0.63)**
γ	F3–C3	**U=584, p=0.038, d=0.34, E=1, μ =0.21 (0.06 0.47)**	**U=593, p=0.109, d=0.35, E=0, μ =0.41 (0.1 0.88)**	U=655, p=0.001, d=0.48, E=3, μ =0.57 (0.27 0.9)	**U=660, p=0.001, d=0.49, E=2, μ =0.54 (0.25 0.83)**	**U=650, p=0.003, d=0.47, E=2, μ =0.3 (0.13 0.56)**
γ	F4–FZ	**U=583, p=0.038, d=0.33, E=1, μ =0.2 (0.04 0.42)**	**U=574, p=0.109, d=0.31, E=0, μ =0.33 (0.05 0.73)**	U=680, p=0.001, d=0.53, E=3, μ =0.65 (0.31 1.02)	**U=652, p=0.001, d=0.47, E=2, μ =0.47 (0.19 0.86)**	**U=628, p=0.004, d=0.42, E=2, μ =0.29 (0.11 0.64)**
γ	FZ–CZ	**U=581, p=0.038, d=0.33, E=1, μ =0.17 (0.03 0.39)**	**U=552, p=0.109, d=0.27, E=0, μ =0.19 (0.01 0.47)**	U=634, p=0.002, d=0.44, E=3, μ =0.5 (0.21 0.75)	**U=646, p=0.001, d=0.46, E=2, μ =0.37 (0.16 0.65)**	**U=619, p=0.004, d=0.41, E=1, μ =0.18 (0.06 0.31)**
γ	F3–FZ	**U=594, p=0.038, d=0.36, E=1, μ =0.2 (0.06 0.43)**	**U=575, p=0.109, d=0.32, E=0, μ =0.39 (0.08 0.83)**	U=642, p=0.002, d=0.45, E=3, μ =0.56 (0.23 1)	**U=647, p=0.001, d=0.46, E=2, μ =0.44 (0.16 0.79)**	**U=627, p=0.004, d=0.42, E=1, μ =0.3 (0.11 0.62)**
γ	T4–C4	**U=538, p=0.129, d=0.24, E=0, μ =0.16 (-0.01 0.38)**	**U=556, p=0.109, d=0.28, E=0, μ =0.29 (0.02 0.58)**	U=573, p=0.017, d=0.31, E=3, μ =0.32 (0.05 0.63)	**U=615, p=0.003, d=0.4, E=2, μ =0.38 (0.14 0.68)**	**U=614, p=0.005, d=0.4, E=1, μ =0.23 (0.09 0.55)**

γ	T3–C3	U=617, p=0.033, d=0.4, E=1, μ =0.26 (0.1 0.48)	U=563, p=0.109, d=0.29, E=0, μ =0.34 (0.04 0.72)	U=607, p=0.004, d=0.38, E=2, μ =0.42 (0.14 0.82)	U=647, p=0.001, d=0.46, E=2, μ =0.54 (0.25 0.9)	U=636, p=0.004, d=0.44, E=2, μ =0.31 (0.11 0.6)
γ	C4–CZ	U=515, p=0.218, d=0.19, E=0, μ =0.1 (-0.03 0.29)	U=536, p=0.128, d=0.24, E=0, μ =0.26 (-0.02 0.6)	U=615, p=0.004, d=0.4, E=1, μ =0.45 (0.13 0.79)	U=615, p=0.003, d=0.4, E=2, μ =0.41 (0.14 0.78)	U=619, p=0.004, d=0.41, E=1, μ =0.22 (0.06 0.54)
γ	C3–CZ	U=588, p=0.038, d=0.34, E=1, μ =0.22 (0.05 0.4)	U=539, p=0.124, d=0.24, E=0, μ =0.27 (-0.01 0.67)	U=607, p=0.004, d=0.38, E=2, μ =0.5 (0.17 0.92)	U=627, p=0.002, d=0.42, E=2, μ =0.5 (0.18 0.89)	U=623, p=0.004, d=0.41, E=2, μ =0.24 (0.08 0.47)
γ	CZ–PZ	U=524, p=0.191, d=0.21, E=0, μ =0.08 (-0.01 0.25)	U=554, p=0.109, d=0.27, E=0, μ =0.26 (0.01 0.57)	U=653, p=0.001, d=0.48, E=1, μ =0.74 (0.33 1.19)	U=631, p=0.002, d=0.43, E=2, μ =0.44 (0.16 0.83)	U=578, p=0.018, d=0.32, E=1, μ =0.13 (0.02 0.27)
γ	C4–P4	U=496, p=0.293, d=0.16, E=0, μ =0.1 (-0.07 0.34)	U=482, p=0.357, d=0.13, E=0, μ =0.13 (-0.14 0.52)	U=634, p=0.002, d=0.44, E=1, μ =0.58 (0.21 0.98)	U=593, p=0.008, d=0.35, E=2, μ =0.45 (0.1 0.98)	U=566, p=0.029, d=0.3, E=1, μ =0.28 (0.03 0.7)
γ	C3–P3	U=494, p=0.293, d=0.15, E=0, μ =0.09 (-0.05 0.32)	U=545, p=0.109, d=0.26, E=0, μ =0.25 (0 0.65)	U=622, p=0.003, d=0.41, E=1, μ =0.48 (0.21 0.87)	U=610, p=0.004, d=0.39, E=2, μ =0.46 (0.14 0.98)	U=578, p=0.018, d=0.32, E=1, μ =0.23 (0.05 0.55)
γ	T4–T6	U=504, p=0.264, d=0.17, E=0, μ =0.13 (-0.07 0.37)	U=524, p=0.17, d=0.21, E=0, μ =0.22 (-0.05 0.58)	U=594, p=0.007, d=0.36, E=1, μ =0.43 (0.11 0.75)	U=621, p=0.003, d=0.41, E=1, μ =0.42 (0.13 0.73)	U=593, p=0.012, d=0.35, E=1, μ =0.24 (0.06 0.56)
γ	T3–T5	U=538, p=0.129, d=0.24, E=0, μ =0.14 (-0.01 0.34)	U=523, p=0.17, d=0.21, E=0, μ =0.29 (-0.07 0.61)	U=599, p=0.006, d=0.37, E=2, μ =0.54 (0.17 0.98)	U=625, p=0.002, d=0.42, E=2, μ =0.47 (0.17 0.85)	U=587, p=0.015, d=0.34, E=1, μ =0.25 (0.06 0.51)
γ	P4–PZ	U=521, p=0.194, d=0.21, E=0, μ =0.08 (-0.03 0.25)	U=507, p=0.218, d=0.18, E=0, μ =0.14 (-0.06 0.38)	U=611, p=0.004, d=0.39, E=1, μ =0.58 (0.19 1.02)	U=620, p=0.003, d=0.41, E=2, μ =0.44 (0.16 0.85)	U=578, p=0.018, d=0.32, E=1, μ =0.12 (0.02 0.32)
γ	P3–PZ	U=549, p=0.115, d=0.26, E=0, μ =0.12 (0 0.31)	U=507, p=0.218, d=0.18, E=0, μ =0.18 (-0.08 0.48)	U=617, p=0.004, d=0.4, E=2, μ =0.6 (0.24 1)	U=647, p=0.001, d=0.46, E=2, μ =0.49 (0.21 0.81)	U=606, p=0.006, d=0.38, E=1, μ =0.18 (0.05 0.32)
γ	T6–O2	U=506, p=0.264, d=0.18, E=0, μ =0.09 (-0.04 0.25)	U=515, p=0.204, d=0.19, E=0, μ =0.19 (-0.07 0.52)	U=585, p=0.01, d=0.34, E=1, μ =0.52 (0.13 1)	U=570, p=0.019, d=0.31, E=1, μ =0.27 (0.04 0.53)	U=543, p=0.065, d=0.25, E=0, μ =0.12 (-0.01 0.31)
γ	T5–O1	U=494, p=0.293, d=0.15, E=0, μ =0.08 (-0.05 0.31)	U=500, p=0.251, d=0.16, E=0, μ =0.19 (-0.1 0.57)	U=610, p=0.004, d=0.39, E=1, μ =0.5 (0.15 0.87)	U=580, p=0.013, d=0.33, E=1, μ =0.26 (0.04 0.61)	U=539, p=0.071, d=0.24, E=0, μ =0.11 (-0.01 0.37)
γ	P4–O2	U=467, p=0.493, d=0.1, E=0, μ =0.03 (-0.08 0.18)	U=513, p=0.204, d=0.19, E=0, μ =0.12 (-0.05 0.39)	U=615, p=0.004, d=0.4, E=1, μ =0.51 (0.21 0.9)	U=603, p=0.005, d=0.37, E=1, μ =0.27 (0.08 0.47)	U=545, p=0.063, d=0.26, E=0, μ =0.1 (0 0.31)
γ	P3–O1	U=464, p=0.501, d=0.09, E=0, μ =0.04 (-0.06 0.21)	U=495, p=0.272, d=0.15, E=0, μ =0.15 (-0.1 0.66)	U=606, p=0.004, d=0.38, E=2, μ =0.49 (0.18 0.79)	U=596, p=0.007, d=0.36, E=1, μ =0.29 (0.07 0.61)	U=528, p=0.099, d=0.22, E=0, μ =0.09 (-0.01 0.34)
γ	O1–O2	U=480, p=0.391, d=0.12, E=0, μ =0.05 (-0.07 0.19)	U=469, p=0.453, d=0.1, E=0, μ =0.11 (-0.15 0.45)	U=594, p=0.007, d=0.36, E=2, μ =0.47 (0.14 0.85)	U=573, p=0.018, d=0.31, E=1, μ =0.23 (0.03 0.51)	U=488, p=0.296, d=0.14, E=0, μ =0.05 (-0.04 0.19)

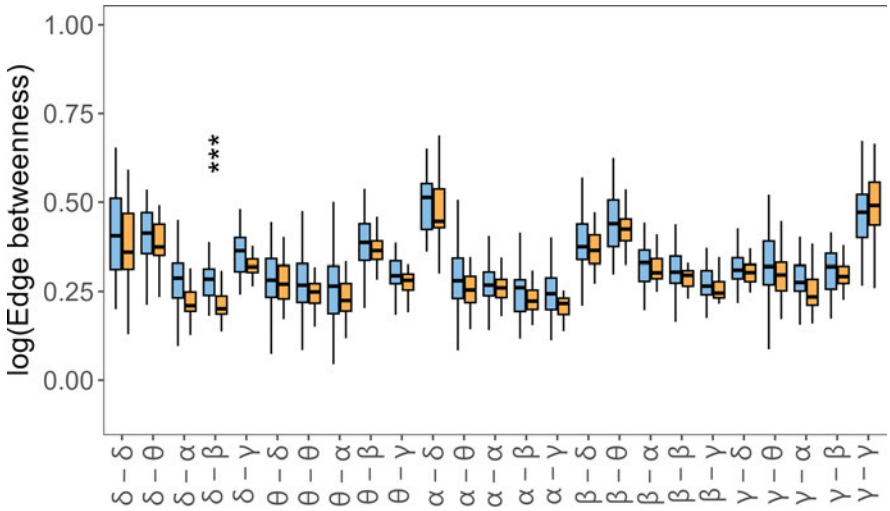

Figure A.6: Importance of each type of frequency coupling of HC (blue) and AD (orange) measured by edge betweenness in epoch 1. Significant differences ($p \leq 0.05$) observed in at least ten thresholded networks are encoded by asterisks. The number of asterisks corresponds to the p-value (FDR corrected), i.e. $p \leq 0.0001$ "****", $p \leq 0.001$ "***", $p \leq 0.01$ "**", and $p \leq 0.05$ "*".

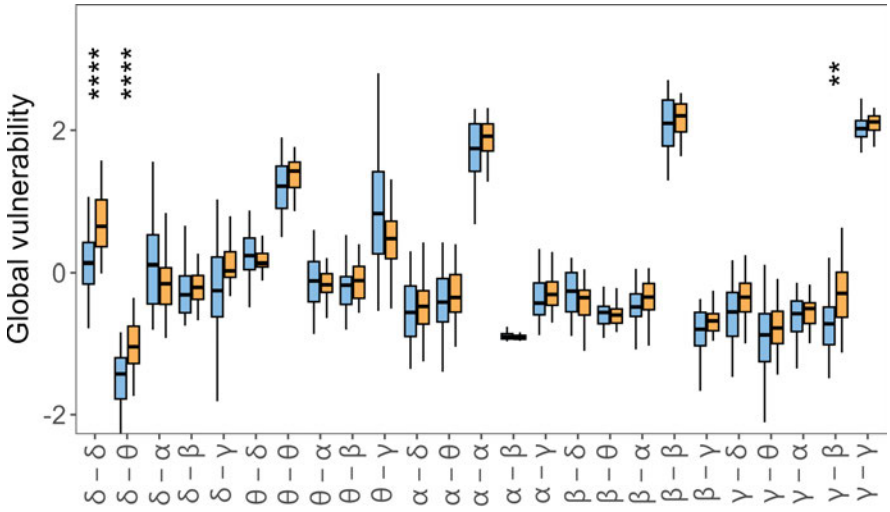

Figure A.7: Global vulnerability of HC (blue) and AD (orange) in epoch 1. Significant differences ($p \leq 0.05$) observed in at least ten thresholded networks are encoded by asterisks. The number of asterisks corresponds to the p-value (FDR corrected), i.e. $p \leq 0.0001$ "****", $p \leq 0.001$ "***", $p \leq 0.01$ "**", and $p \leq 0.05$ "*".

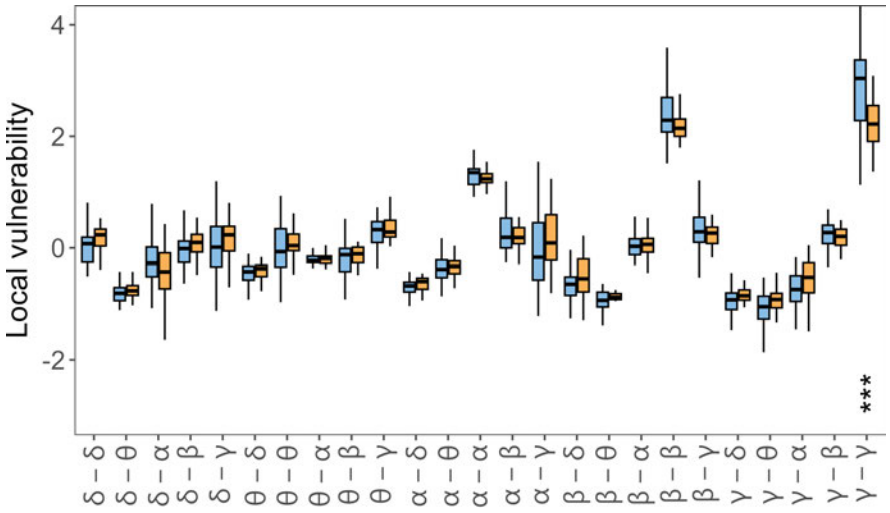

Figure A.8: Local vulnerability of HC (blue) and AD (orange) in epoch 1. Significant differences ($p \leq 0.05$) observed in at least ten thresholded networks are encoded by asterisks. The number of asterisks corresponds to the p-value (FDR corrected), i.e. $p \leq 0.0001$ "****", $p \leq 0.001$ "***", $p \leq 0.01$ "**", and $p \leq 0.05$ "*".

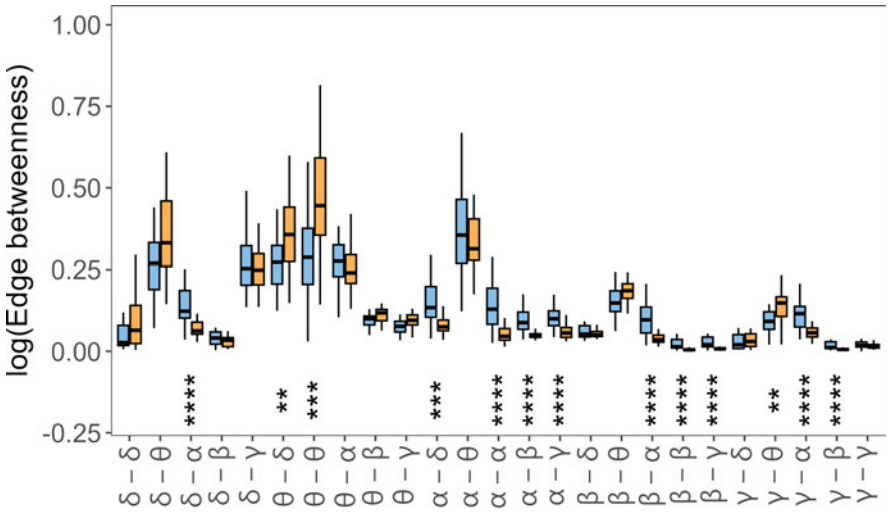

Figure A.9: Importance of each type of frequency coupling of HC (blue) and AD (orange) measured by weighted edge betweenness in epoch 1. Significant differences ($p \leq 0.05$) observed in at least ten thresholded networks are encoded by asterisks. The number of asterisks corresponds to the p-value (FDR corrected), i.e. $p \leq 0.0001$ "****", $p \leq 0.001$ "***", $p \leq 0.01$ "**", and $p \leq 0.05$ "*".

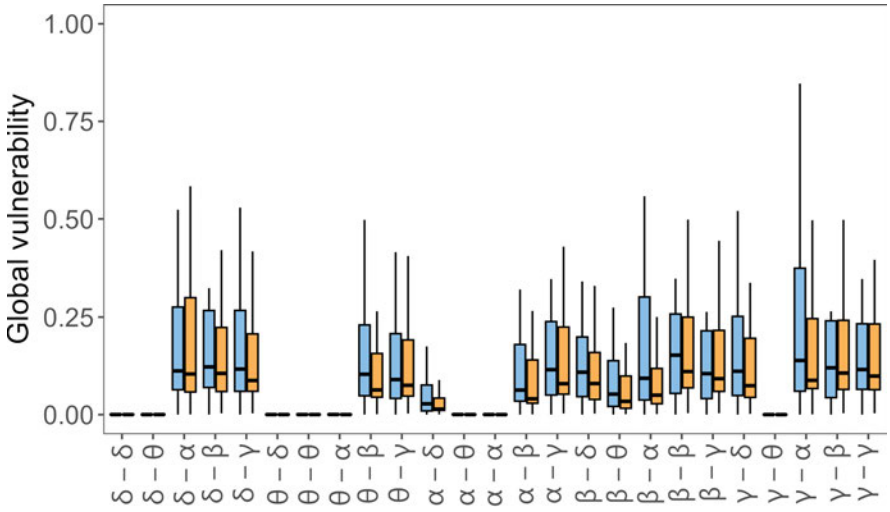

Figure A.10: Weighted global vulnerability of HC (blue) and AD (orange) in epoch 1. Significant differences ($p \leq 0.05$) observed in at least ten thresholded networks are encoded by asterisks.
The number of asterisks corresponds to the p-value (FDR corrected), i.e. $p \leq 0.0001$ "****", $p \leq 0.001$ "***", $p \leq 0.01$ "**", and $p \leq 0.05$ "*".

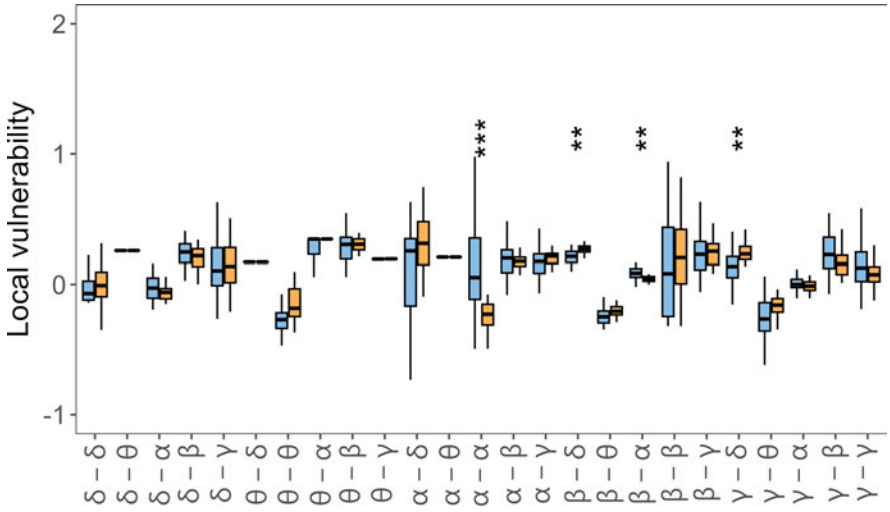

Figure A.11: Weighted local vulnerability of HC (blue) and AD (orange) in epoch 1. Significant differences ($p \leq 0.05$) observed in at least ten thresholded networks are encoded by asterisks. The number of asterisks corresponds to the p-value (FDR corrected), i.e. $p \leq 0.0001$ "****", $p \leq 0.001$ "***", $p \leq 0.01$ "**", and $p \leq 0.05$ "*".

Table A.5: Results from epoch 1 comparing unweighted edge betweenness. The results are reported as follows: statistics value (degrees of freedom), p-value of the test, Cohen's d effect size or nonparameteric alternative, number of thresholds where significant differences were observed (T), number of epochs where significant differences were observed (E), group difference estimate (95% CI). Reliable differences (significant in all three epochs) are highlighted with bold text.

	δ	θ	α	β	γ
δ	t(36.68)=0.95, p=0.348, d=0.25, T=1, E=0, μ = 0.25 (-0.28 0.77)	U=508, p=0.175, d=0.18, T=0, E=0, μ = 0.31 (-0.15 0.74)	U=591, p=0.007, d=0.35, T=16, E=2, μ = 0.62 (0.19 1.09)	**U=636, p=0.001, d=0.44, T=17, E=3,** μ = 0.7 **(0.33 1.1)**	U=542, p=0.058, d=0.25, T=9, E=0, μ = 0.32 (0 0.54)
θ	U=455, p=0.594, d=0.07, T=0, E=0, μ = 0.11 (-0.28 0.55)	U=513, p=0.151, d=0.19, T=3, E=0, μ = 0.28 (-0.15 0.71)	U=500, p=0.218, d=0.16, T=0, E=0, μ = 0.28 (-0.15 0.76)	U=517, p=0.134, d=0.2, T=0, E=0, μ = 0.33 (-0.11 0.73)	U=498, p=0.23, d=0.16, T=0, E=0, μ = 0.2 (-0.13 0.57)
α	t(36.86)=1.34, p=0.185, d=0.35, T=0, E=0, μ = 0.35 (-0.17 0.87)	t(30.26)=1.16, p=0.25, d=0.3, T=0, E=0, μ = 0.3 (-0.22 0.82)	U=483, p=0.333, d=0.13, T=0, E=0, μ = 0.18 (-0.3 0.64)	U=521, p=0.118, d=0.21, T=0, E=0, μ = 0.31 (-0.1 0.73)	U=528, p=0.095, d=0.22, T=3, E=0, μ = 0.19 (-0.04 0.42)
β	U=489, p=0.289, d=0.14, T=0, E=0, μ = 0.19 (-0.15 0.54)	U=475, p=0.399, d=0.11, T=0, E=0, μ = 0.15 (-0.23 0.59)	U=472, p=0.426, d=0.11, T=0, E=0, μ = 0.18 (-0.25 0.66)	U=494, p=0.255, d=0.15, T=1, E=0, μ = 0.23 (-0.18 0.66)	U=508, p=0.175, d=0.18, T=1, E=0, μ = 0.27 (-0.14 0.6)
γ	U=475, p=0.399, d=0.11, T=0, E=0, μ = 0.15 (-0.22 0.52)	U=504, p=0.195, d=0.17, T=0, E=0, μ = 0.2 (-0.13 0.53)	U=548, p=0.047, d=0.26, T=11, E=2, μ = 0.25 (0.01 0.48)	U=479, p=0.365, d=0.12, T=0, E=0, μ = 0.16 (-0.18 0.44)	U=360, p=0.357, d=0.12, T=0, E=0, μ = −0.22 (-0.68 0.23)

Table A.6: Results from epoch 1 comparing unweighted global vulnerability. The results are reported as follows: statistics value (degrees of freedom), p-value of the test, Cohen's d effect size or nonparameteric alternative, number of thresholds where significant differences were observed (T), number of epochs where significant differences were observed (E), group difference estimate (95% CI). Reliable differences (significant in all three epochs) are highlighted with bold text.

	δ	θ	α	β	γ
δ	**t(33.22)=-4.38, p¡0.001, d=-1.14, T=17, E=3,** μ = −0.99**(-1.45 -0.54)**	**U=168, p¡0.001, d=0.51, T=18, E=3,** μ = −0.91**(-1.35 -0.48)**	U=532, p=0.083, d=0.23, T=8, E=0, μ = 0.44(-0.06 0.96)	U=352, p=0.294, d=0.14, T=3, E=0, μ = −0.22(-0.62 0.22)	t(32.49)=-1.94, p=0.058, d=-0.51, T=9, E=0, μ = −0.49(-1 0.02)
θ	t(30.36)=0.98, p=0.33, d=0.26, T=0, E=0, μ = 0.25(-0.27 0.78)	U=326, p=0.147, d=0.19, T=0, E=0, μ = −0.41(-0.95 0.14)	t(31.47)=0.67, p=0.503, d=0.18, T=0, E=0, μ = 0.18(-0.35 0.7)	U=341, p=0.224, d=0.16, T=0, E=0, μ = −0.26(-0.8 0.17)	U=546, p=0.05, d=0.26, T=9, E=0, μ = 0.49(-0.01 0.95)
α	t(32.58)=-0.95, p=0.344, d=-0.25, T=4, E=0, μ = −0.25(-0.77 0.27)	t(36.41)=-0.83, p=0.412, d=-0.22, T=0, E=0, μ = −0.22(-0.74 0.31)	U=352, p=0.296, d=0.14, T=0, E=0, μ = −0.28(-0.81 0.2)	U=473, p=0.414, d=0.11, T=3, E=0, μ = 0.03(-0.04 0.1)	U=356, p=0.326, d=0.13, T=1, E=0, μ = −0.21(-0.6 0.24)
β	t(36.92)=1.48, p=0.145, d=0.39, T=8, E=0, μ = 0.38(-0.14 0.9)	U=455, p=0.594, d=0.07, T=0, E=0, μ = 0.08(-0.31 0.49)	t(36.76)=-0.95, p=0.349, d=-0.25, T=4, E=0, μ = −0.25(-0.78 0.28)	t(30.7)=-0.86, p=0.392, d=-0.23, T=3, E=0, μ = −0.22(-0.75 0.3)	U=321, p=0.126, d=0.2, T=7, E=0, μ = −0.39(-0.84 0.11)
γ	U=327, p=0.151, d=0.19, T=2, E=0, μ = −0.23(-0.54 0.08)	t(32.84)=-1.36, p=0.179, d=-0.36, T=0, E=0, μ = −0.35(-0.87 0.17)	U=370, p=0.444, d=0.1, T=1, E=0, μ = −0.2(-0.68 0.26)	**U=235, p=0.004, d=0.38, T=13, E=3,** μ = −0.61**(-1.02 -0.2)**	t(36.21)=-1.79, p=0.079, d=-0.47, T=7, E=0, μ = −0.46(-0.97 0.06)

Table A.7: Results from epoch 1 comparing unweighted local vulnerability. The results are reported as follows: statistics value (degrees of freedom), p-value of the test, Cohen's d effect size or nonparameteric alternative, number of thresholds where significant differences were observed (T), number of epochs where significant differences were observed (E), group difference estimate (95% CI). Reliable differences (significant in all three epochs) are highlighted with bold text.

	δ	θ	α	β	γ
δ	U=308, p=0.083, d=0.23, T=9, E=0, $\mu = -0.4$ (-0.82 0.06)	t(36.15)=-0.87, p=0.389, d=-0.23, T=2, E=0, $\mu = -0.23$ (-0.75 0.3)	t(37)=1.86, p=0.068, d=0.49, T=9, E=0, $\mu = 0.48$ (-0.04 0.99)	t(35.43)=-1.95, p=0.056, d=-0.51, T=7, E=0, $\mu = -0.5$ (-1.01 0.01)	t(34.87)=-1.11, p=0.27, d=-0.29, T=0, E=0, $\mu = -0.29$ (-0.81 0.23)
θ	U=361, p=0.365, d=0.12, T=0, E=0, $\mu = -0.21$ (-0.65 0.26)	t(32.16)=-0.52, p=0.606, d=-0.14, T=2, E=0, $\mu = -0.14$ (-0.66 0.39)	U=389, p=0.638, d=0.06, T=0, E=0, $\mu = -0.08$ (-0.45 0.29)	t(29.01)=-0.85, p=0.399, d=-0.22, T=0, E=0, $\mu = -0.22$ (-0.74 0.3)	t(36.97)=-0.56, p=0.581, d=-0.15, T=0, E=0, $\mu = -0.15$ (-0.67 0.38)
α	t(35.69)=-1.77, p=0.082, d=-0.46, T=9, E=0, $\mu = -0.45$ (-0.97 0.06)	t(36.82)=-0.42, p=0.677, d=-0.11, T=0, E=0, $\mu = -0.11$ (-0.64 0.42)	U=504, p=0.195, d=0.17, T=5, E=0, $\mu = 0.3$ (-0.19 0.61)	t(29.31)=1.25, p=0.216, d=0.33, T=3, E=0, $\mu = 0.32$ (-0.2 0.84)	t(34.1)=-1.23, p=0.223, d=-0.32, T=0, E=0, $\mu = -0.32$ (-0.84 0.2)
β	t(36.26)=-1.61, p=0.114, d=-0.42, T=5, E=0, $\mu = -0.42$ (-0.94 0.1)	U=360, p=0.357, d=0.12, T=0, E=0, $\mu = -0.27$ (-0.74 0.25)	t(36.89)=-0.95, p=0.344, d=-0.25, T=2, E=0, $\mu = -0.25$ (-0.77 0.27)	U=519, p=0.126, d=0.2, T=1, E=0, $\mu = 0.39$ (-0.08 0.96)	t(23.65)=0.83, p=0.409, d=0.22, T=4, E=0, $\mu = 0.22$ (-0.31 0.74)
γ	U=283, p=0.033, d=0.28, T=11, E=1, $\mu = -0.4$ (-0.81 -0.03)	t(32.95)=-2.29, p=0.026, d=-0.6, T=11, E=1, $\mu = -0.58$ (-1.08 -0.07)	t(36.03)=-1.93, p=0.059, d=-0.51, T=9, E=0, $\mu = -0.5$ (-1.01 0.02)	U=474, p=0.408, d=0.11, T=2, E=0, $\mu = 0.16$ (-0.26 0.61)	**U=635, p=0.001, d=0.44, T=13, E=3,** $\mu = 0.3$ **(0.12 0.49)**

Table A.8: Results from epoch 1 comparing weighted edge betweenness. The results are reported as follows: statistics value (degrees of freedom), p-value of the test, Cohen's d effect size or nonparameteric alternative, number of thresholds where significant differences were observed (T), number of epochs where significant differences were observed (E), group difference estimate (95% CI). Reliable differences (significant in all three epochs) are highlighted with bold text.

	δ	θ	α	β	γ
δ	**U=666, p¡0.001, d=0.53, T=19, E=3,** $\mu = 0.23$ **(0.15 0.41)**	**U=603, p¡0.001, d=0.49, T=14, E=3,** $\mu = 0$ **(0 0.18)**	**U=693.5, p¡0.001, d=0.59, T=19, E=3,** $\mu = 0.38$ **(0.02 0.75)**	**U=704, p¡0.001, d=0.58, T=19, E=3,** $\mu = 0.97$ **(0.58 1.33)**	**U=635, p=0.001, d=0.44, T=18, E=3,** $\mu = 0.68$ **(0.32 1.01)**
θ	**U=660.5, p¡0.001, d=0.54, T=17, E=3,** $\mu = 0.29$ **(0.01 0.66)**	**U=675.5, p¡0.001, d=0.54, T=12, E=3,** $\mu = 0.43$ **(0.03 0.84)**	U=461, p=0.195, d=0.17, T=2, E=0, $\mu = 0$ (0 0)	U=518, p=0.027, d=0.29, T=18, E=1, $\mu = 0$ (0 0)	U=389, p=0.638, d=0.06, T=1, E=0, $\mu = -0.06$ (-0.3 0.23)
α	U=563, p=0.011, d=0.33, T=18, E=2, $\mu = 0$ (0 0.36)	U=488, p=0.096, d=0.22, T=5, E=0, $\mu = 0$ (0 0)	U=297.5, p=0.058, d=0.25, T=10, E=1, $\mu = -0.31$ (-0.64 0)	U=346, p=0.255, d=0.15, T=2, E=0, $\mu = -0.14$ (-0.43 0.13)	U=481, p=0.349, d=0.12, T=1, E=0, $\mu = 0.04$ (-0.04 0.12)
β	**U=694, p¡0.001, d=0.56, T=18, E=3,** $\mu = 0.34$ **(0.16 0.62)**	U=458, p=0.559, d=0.08, T=4, E=0, $\mu = 0.01$ (-0.12 0.17)	U=377.5, p=0.481, d=0.09, T=6, E=0, $\mu = 0$ (-0.06 0)	U=356, p=0.323, d=0.13, T=4, E=0, $\mu = -0.05$ (-0.17 0.06)	**U=178, p¡0.001, d=0.49, T=18, E=3,** $\mu = -0.74$ **(-1.18 -0.36)**
γ	**U=625, p=0.001, d=0.42, T=18, E=3,** $\mu = 1.06$ **(0.45 1.49)**	U=337, p=0.201, d=0.17, T=2, E=0, $\mu = -0.23$ (-0.71 0.13)	U=390, p=0.649, d=0.06, T=1, E=0, $\mu = -0.03$ (-0.15 0.13)	**U=194, p¡0.001, d=0.46, T=14, E=3,** $\mu = -0.72$ **(-1.1 -0.37)**	**t(36.57)=-4.16, p¡0.001, d=-1.09, T=19, E=3,** $\mu = -0.96$ **(-1.42 -0.5)**

Table A.9: Results from epoch 1 comparing weighted global vulnerability. The results are reported as follows: statistics value (degrees of freedom), p-value of the test, Cohen's d effect size or nonparameteric alternative, number of thresholds where significant differences were observed (T), number of epochs where significant differences were observed (E), group difference estimate (95% CI). Reliable differences (significant in all three epochs) are highlighted with bold text.

	δ	θ	α	β	γ
δ	U=354, p=0.311, d=0.13, T=2, E=0, μ = 0 (0 0)	U=284, p=0.034, d=0.28, T=12, E=1, μ = 0 (0 0)	U=384, p=0.583, d=0.07, T=6, E=0, μ = 0 (0 0)	**U=670, p¡0.001, d=0.51, T=19, E=3,** μ = 0.01 **(0 0.13)**	t(27.29)=2.9, p=0.006, d=0.75, T=15, E=2, μ = 0.71 (0.22 1.2)
θ	U=480, p=0.357, d=0.12, T=1, E=0, μ = 0 (0 0)	U=286, p=0.037, d=0.27, T=13, E=1, μ = 0 (0 0)	U=302, p=0.067, d=0.24, T=7, E=0, μ = 0 (0 0)	U=373, p=0.472, d=0.1, T=0, E=0, μ = 0 (0 0)	U=494, p=0.255, d=0.15, T=1, E=0, μ = 0.22 (-0.19 0.71)
α	U=366, p=0.408, d=0.11, T=3, E=0, μ = 0 (0 0)	U=306, p=0.077, d=0.23, T=9, E=0, μ = 0 (0 0)	U=301, p=0.065, d=0.24, T=8, E=0, μ = −0.07 (-0.17 0)	U=359, p=0.349, d=0.12, T=1, E=0, μ = 0 (0 0)	t(35.04)=-0.66, p=0.515, d=-0.17, T=5, E=0, μ = −0.17 (-0.7 0.35)
β	**U=617, p=0.002, d=0.4, T=12, E=3,** μ = 0.02 **(0 0.13)**	U=341, p=0.224, d=0.16, T=3, E=0, μ = 0 (0 0)	U=303, p=0.07, d=0.24, T=9, E=0, μ = 0 (0 0)	U=459, p=0.552, d=0.08, T=6, E=0, μ = 0.01 (-0.05 0.06)	**U=214, p=0.001, d=0.42, T=13, E=3,** μ = −0.7 **(-1.07 -0.34)**
γ	t(35.38)=-1.22, p=0.228, d=-0.32, T=0, E=0, μ = −0.32 (-0.85 0.21)	U=444, p=0.717, d=0.05, T=0, E=0, μ = 0.03 (-0.19 0.31)	U=339, p=0.212, d=0.17, T=0, E=0, μ = −0.15 (-0.46 0.07)	**t(36.15)=-5.79, p¡0.001, d=-1.52, T=20, E=3,** μ = −1.22 **(-1.64 -0.79)**	**U=186, p¡0.001, d=0.48, T=18, E=3,** μ = −0.98 **(-1.44 -0.49)**

Table A.10: Results from epoch 1 comparing weighted local vulnerability. The results are reported as follows: statistics value (degrees of freedom), p-value of the test, Cohen's d effect size or nonparameteric alternative, number of thresholds where significant differences were observed (T), number of epochs where significant differences were observed (E), group difference estimate (95% CI). Reliable differences (significant in all three epochs) are highlighted with bold text.

	δ	θ	α	β	γ
δ	**U=634, p=0.001, d=0.44, T=19, E=3,** μ = 0.9 **(0.43 1.28)**	**U=691, p¡0.001, d=0.55, T=18, E=3,** μ = 0.96 **(0.61 1.38)**	**U=242, p=0.005, d=0.36, T=11, E=3,** μ = −0.56 **(-0.95 -0.18)**	**t(34.01)=-3.9, p¡0.001, d=-1.02, T=11, E=3,** μ = −0.91 **(-1.38 -0.44)**	U=478, p=0.374, d=0.12, T=0, E=0, μ = 0.15 (-0.22 0.6)
θ	**t(29.56)=3.73, p¡0.001, d=0.97, T=19, E=3,** μ = 0.87 **(0.4 1.34)**	**U=705, p¡0.001, d=0.58, T=17, E=3,** μ = 1.01 **(0.63 1.35)**	U=296, p=0.054, d=0.25, T=9, E=0, μ = −0.43 (-0.8 0.01)	**t(36.97)=-4.26, p¡0.001, d=-1.12, T=12, E=3,** μ = −0.98 **(-1.44 -0.52)**	t(35.47)=-1.44, p=0.156, d=-0.38, T=3, E=0, μ = −0.37 (-0.89 0.15)
α	**t(29.91)=3.86, p¡0.001, d=1.01, T=18, E=3,** μ = 0.9 **(0.43 1.37)**	**U=674, p¡0.001, d=0.52, T=17, E=3,** μ = 1 **(0.59 1.35)**	**U=233, p=0.003, d=0.38, T=11, E=3,** μ = −0.66 **(-1 -0.26)**	**U=192, p¡0.001, d=0.47, T=14, E=3,** μ = −0.87 **(-1.31 -0.46)**	U=325, p=0.142, d=0.19, T=5, E=0, μ = −0.25 (-0.64 0.08)
β	**t(31.81)=2.97, p=0.004, d=0.78, T=18, E=3,** μ = 0.72 **(0.24 1.21)**	**U=690, p¡0.001, d=0.55, T=15, E=3,** μ = 0.83 **(0.53 1.14)**	U=296, p=0.054, d=0.25, T=9, E=0, μ = −0.45 (-0.88 0.01)	**U=215, p=0.001, d=0.42, T=11, E=3,** μ = −0.8 **(-1.22 -0.36)**	t(36.94)=-1.63, p=0.11, d=-0.43, T=7, E=0, μ = −0.42 (-0.94 0.1)
γ	t(33.07)=0.65, p=0.519, d=0.17, T=3, E=0, μ = 0.17 (-0.35 0.69)	U=527, p=0.098, d=0.22, T=4, E=0, μ = 0.41 (-0.13 0.95)	U=360, p=0.357, d=0.12, T=0, E=0, μ = −0.13 (-0.47 0.21)	**U=207, p=0.001, d=0.44, T=15, E=3,** μ = −0.72 **(-1.07 -0.36)**	**U=162, p¡0.001, d=0.53, T=16, E=3,** μ = −0.81 **(-1.28 -0.47)**

Table A.11: Comparisons of the mean of adjacency matrix constructed with CS in epoch 2. The results are reported as follows: statistics value (degrees of freedom), p-value of the test, Cohen's d effect size (or nonparametric alternative), number of epochs where significant differences were observed (E), difference estimate μ with 95% confidence interval. Reliable differences (significant in all three epochs) are highlighted with bold text.

Frequency band	Test	Difference estimate (95% CI)
α	U=313, p=0.122, d=0.22, E=1	μ = −0.4 (-0.87 0.09)
β	**U=225, p=0.003, d=0.4, E=3**	μ = −0.73 (-1.23 -0.25)
δ	**U=657, p¡0.001, d=0.48, E=3**	μ = 0.93 (0.46 1.4)
γ	t(32.53)=-1.53, p=0.132, d=-0.4, E=0	μ = −0.4 (-0.93 0.12)
θ	**t(36.34)=4.5, p¡0.001, d=1.18, E=3**	μ = 1.02 (0.56 1.47)

A.3 Results of statistical tests for epoch 2

In this section, we report the detailed results of the statistical comparisons accompanying the figures reported in the main text computed using only data from the second epoch. The comparisons of average coupling computed with CS and CBS are shown in Tables A.11 and A.12, respectively. The comparisons of node strength computed with CS and CBS are shown in Tables A.13 and A.14, respectively. Results of comparisons of the unweighted multilayer network metrics are reported in Tables A.15, A.16 and A.17 for edge betweenness, global vulnerability and local vulnerability, respectively. Results of comparisons of the weighted multilayer network metrics are reported in Tables A.18, A.19 and A.20 for edge betweenness, global vulnerability and local vulnerability, respectively.

Table A.12: Comparisons of the mean of adjacency matrix constructed with CBS in epoch 2. The results are reported as follows: statistics value (degrees of freedom), p-value of the test, Cohen's d effect size (or nonparametric alternative), number of epochs where significant differences were observed (E), difference estimate μ with 95% confidence interval. Reliable differences (significant in all three epochs) are highlighted with bold text.

	δ	θ	α	β	γ
δ	t(35.95)=3.8, p=0.002, d=0.99, E=2, μ =0.89(0.42 1.36)	**t(35.54)=4.66, p|0.001, d=1.22, E=3, μ =1.04(0.59 1.49)**	**t(35.53)=4.07, p=0.001, d=1.06, E=3, μ =0.94(0.48 1.41)**	t(36.46)=0.1, p=0.919, d=0.03, E=0, μ =0.03(-0.5 0.55)	U=386, p=0.688, d=0.07, E=0, μ =−0.12(-0.58 0.35)
θ	**t(35.54)=4.66, p|0.001, d=1.22, E=3, μ =1.04(0.59 1.49)**	**t(35.55)=3.77, p=0.002, d=0.99, E=3, μ =0.89(0.42 1.36)**	t(32.41)=2.24, p=0.049, d=0.58, E=1, μ =0.56(0.06 1.07)	t(35.24)=-1.53, p=0.193, d=-0.4, E=1, μ =−0.4(-0.91 0.12)	U=347, p=0.343, d=0.15, E=1, μ =−0.31(-0.79 0.17)
α	t(33.87)=3.92, p=0.002, d=1.02, E=2, μ =0.91(0.45 1.38)	t(33)=2.65, p=0.02, d=0.69, E=1, μ =0.66(0.16 1.15)	t(35.33)=-0.39, p=0.755, d=-0.1, E=1, μ =−0.1(-0.64 0.43)	**t(29.7)=-2.76, p=0.017, d=-0.73, E=3, μ =−0.69(-1.2 -0.19)**	**t(34.87)=-2.91, p=0.013, d=-0.77, E=3, μ =−0.72(-1.22 -0.22)**
β	t(36.51)=-0.26, p=0.831, d=-0.07, E=0, μ =−0.07(-0.6 0.46)	t(34.36)=-0.84, p=0.506, d=-0.22, E=1, μ =−0.22(-0.74 0.3)	**t(28.17)=-2.39, p=0.038, d=-0.63, E=3, μ =−0.61(-1.12 -0.1)**	**t(33.65)=-2.89, p=0.013, d=-0.76, E=3, μ =−0.72(-1.22 -0.22)**	**t(36.98)=-3.22, p=0.008, d=-0.85, E=3, μ =−0.78(-1.27 -0.3)**
γ	U=384, p=0.688, d=0.07, E=0, μ =−0.13(-0.65 0.31)	t(36.82)=-1.32, p=0.268, d=-0.35, E=0, μ =−0.34(-0.86 0.18)	**t(34.36)=-2.88, p=0.013, d=-0.76, E=3, μ =−0.72(-1.21 -0.22)**	**t(36.88)=-3.15, p=0.008, d=-0.83, E=3, μ =−0.77(-1.25 -0.28)**	U=301, p=0.101, d=0.24, E=1, μ =−0.52(-0.98 0.03)

Table A.13: Comparisons of node strength measured with CS in epoch 2. The results are reported as follows: statistics value (degrees of freedom), p-value of the test, Cohen's d effect size (or nonparametric alternative), number of epochs where significant differences were observed (E), and difference estimate μ with 95% confidence interval (CI). Reliable differences (significant in all three epochs) are highlighted with bold text.

channel	δ	θ	α	β	γ
F8–F4	**t(36.8)=-3.65, p=0.001, d=-0.96, E=3, μ = −0.87 (-1.35 -0.39)**	**t(36.25)=-4.24, p¡0.001, d=-1.11, E=3, μ = −0.97 (-1.43 -0.51)**	t(34.7)=0.06, p=0.994, d=0.02, E=0, μ = 0.02 (-0.51 0.54)	**t(36.3)=3.83, p=0.002, d=1.01, E=3, μ = 0.91 (0.43 1.38)**	U=557, p=0.108, d=0.28, E=0, μ = 0.6 (0.03 1.16)
F7–F3	**t(36.82)=-4.23, p¡0.001, d=-1.11, E=3, μ = −0.97 (-1.43 -0.51)**	**t(32.41)=-3.79, p=0.001, d=-0.99, E=3, μ = −0.89 (-1.36 -0.42)**	U=369, p=0.625, d=0.1, E=0, μ = −0.25 (-0.77 0.28)	**t(36.88)=3.46, p=0.003, d=0.91, E=3, μ = 0.83 (0.35 1.31)**	U=586, p=0.104, d=0.34, E=0, μ = 0.71 (0.17 1.19)
F4–C4	**t(36.76)=-4.36, p¡0.001, d=-1.15, E=3, μ = −1 (-1.46 -0.54)**	**t(36.35)=-4.39, p¡0.001, d=-1.15, E=3, μ = −1 (-1.46 -0.55)**	t(36.42)=0.44, p=0.848, d=0.11, E=0, μ = 0.11 (-0.41 0.64)	**t(34.27)=3.9, p=0.002, d=1.03, E=3, μ = 0.92 (0.45 1.39)**	U=568, p=0.108, d=0.3, E=0, μ = 0.59 (0.08 1.12)
F3–C3	t(36.86)=-3.4, p=0.001, d=-0.89, E=2, μ = −0.82 (-1.3 -0.34)	**t(36.2)=-4.77, p¡0.001, d=-1.26, E=3, μ = −1.07 (-1.52 -0.62)**	t(36.86)=0.01, p=0.994, d=0, E=0, μ = 0 (-0.53 0.53)	**t(28.26)=4.39, p=0.001, d=1.16, E=3, μ = 1.01 (0.55 1.48)**	U=589, p=0.104, d=0.35, E=0, μ = 0.67 (0.13 1.22)
F4–FZ	**t(36.77)=-3.79, p=0.001, d=-0.99, E=3, μ = −0.89 (-1.37 -0.42)**	**U=176, p¡0.001, d=0.5, E=3, μ = −0.86 (-1.33 -0.42)**	U=416, p=0.994, d=0.01, E=0, μ = −0.01 (-0.44 0.44)	**t(35.62)=2.66, p=0.02, d=0.7, E=3, μ = 0.66 (0.16 1.16)**	t(35.96)=2.24, p=0.108, d=0.59, E=0, μ = 0.57 (0.06 1.07)
FZ–CZ	**t(36.61)=-4.23, p¡0.001, d=-1.11, E=3, μ = −0.98 (-1.44 -0.51)**	**t(36.78)=-3.52, p=0.001, d=-0.92, E=3, μ = −0.84 (-1.32 -0.36)**	U=533, p=0.294, d=0.23, E=0, μ = 0.44 (-0.04 0.9)	U=610, p=0.007, d=0.39, E=2, μ = 0.69 (0.24 1.17)	U=507, p=0.395, d=0.18, E=0, μ = 0.35 (-0.15 0.86)
F3–FZ	**t(36.97)=-3.05, p=0.004, d=-0.8, E=3, μ = −0.75 (-1.24 -0.26)**	**U=217, p=0.002, d=0.41, E=3, μ = −0.75 (-1.16 -0.32)**	U=421, p=0.994, d=0, E=0, μ = 0 (-0.54 0.52)	**t(36.99)=2.6, p=0.021, d=0.68, E=3, μ = 0.65 (0.15 1.15)**	U=578, p=0.104, d=0.32, E=0, μ = 0.63 (0.18 1.18)
T4–C4	**t(36.79)=-4.14, p¡0.001, d=-1.08, E=3, μ = −0.96 (-1.42 -0.49)**	**t(31.35)=-4.21, p¡0.001, d=-1.1, E=3, μ = −0.96 (-1.42 -0.5)**	U=545, p=0.24, d=0.26, E=0, μ = 0.47 (-0.01 0.9)	t(36.72)=2.31, p=0.032, d=0.61, E=2, μ = 0.58 (0.08 1.09)	U=516, p=0.395, d=0.2, E=0, μ = 0.37 (-0.14 0.87)
T3–C3	**t(34.89)=-4.41, p¡0.001, d=-1.15, E=3, μ = −1 (-1.46 -0.55)**	**t(31.3)=-3.33, p=0.002, d=-0.87, E=3, μ = −0.8 (-1.28 -0.32)**	t(36.43)=-0.02, p=0.994, d=0, E=0, μ = 0 (-0.53 0.52)	**t(36.18)=3.63, p=0.002, d=0.95, E=3, μ = 0.87 (0.39 1.35)**	t(36.61)=2.24, p=0.108, d=0.59, E=0, μ = 0.57 (0.06 1.07)
C4–CZ	**t(36.77)=-2.84, p=0.006, d=-0.75, E=3, μ = −0.7 (-1.2 -0.21)**	**t(36.9)=-4.08, p¡0.001, d=-1.07, E=3, μ = −0.95 (-1.41 -0.48)**	U=498, p=0.353, d=0.16, E=0, μ = 0.31 (-0.19 0.72)	**t(35.84)=2.34, p=0.032, d=0.62, E=3, μ = 0.59 (0.09 1.1)**	U=480, p=0.547, d=0.12, E=0, μ = 0.26 (-0.26 0.78)
C3–CZ	**t(36.69)=-2.98, p=0.004, d=-0.78, E=3, μ = −0.73 (-1.22 -0.24)**	**t(36.77)=-3.27, p=0.002, d=-0.86, E=3, μ = −0.79 (-1.28 -0.31)**	U=465, p=0.666, d=0.09, E=0, μ = 0.15 (-0.35 0.63)	**t(35.91)=2.77, p=0.016, d=0.73, E=3, μ = 0.69 (0.19 1.19)**	U=512, p=0.395, d=0.19, E=0, μ = 0.36 (-0.11 0.91)
CZ–PZ	**t(37)=-4, p¡0.001, d=-1.05, E=3, μ = −0.93 (-1.4 -0.47)**	**t(35.55)=-4.88, p¡0.001, d=-1.28, E=3, μ = −1.09 (-1.53 -0.64)**	t(36.91)=1.44, p=0.299, d=0.38, E=0, μ = 0.37 (-0.15 0.89)	**U=638, p=0.002, d=0.45, E=3, μ = 0.84 (0.4 1.33)**	U=452, p=0.687, d=0.07, E=0, μ = 0.12 (-0.36 0.47)
C4–P4	**t(36.53)=-4.28, p¡0.001, d=-1.13, E=3, μ = −0.99 (-1.45 -0.52)**	**t(36.78)=-5.04, p¡0.001, d=-1.32, E=3, μ = −1.11 (-1.55 -0.67)**	U=522, p=0.294, d=0.21, E=0, μ = 0.42 (-0.1 0.9)	**t(30.59)=3.39, p=0.004, d=0.9, E=3, μ = 0.83 (0.34 1.31)**	U=457, p=0.659, d=0.08, E=0, μ = 0.13 (-0.4 0.52)
C3–P3	**t(36.05)=-4.06, p¡0.001, d=-1.06, E=3, μ = −0.94 (-1.41 -0.48)**	**t(36.78)=-5.16, p¡0.001, d=-1.36, E=3, μ = −1.13 (-1.56 -0.69)**	t(36.98)=1.27, p=0.353, d=0.33, E=0, μ = 0.33 (-0.19 0.85)	**t(30.61)=4.03, p=0.002, d=1.07, E=3, μ = 0.95 (0.48 1.42)**	U=480, p=0.547, d=0.12, E=0, μ = 0.18 (-0.27 0.62)
T4–T6	**U=203, p=0.001, d=0.44, E=3, μ = −1.05 (-1.57 -0.45)**	**t(35.99)=-4.05, p¡0.001, d=-1.06, E=3, μ = −0.94 (-1.4 -0.47)**	U=522, p=0.294, d=0.21, E=0, μ = 0.42 (-0.09 0.86)	t(30.07)=1.5, p=0.153, d=0.4, E=0, μ = 0.39 (-0.13 0.92)	t(34.14)=0.62, p=0.659, d=0.16, E=0, μ = 0.16 (-0.37 0.7)
T3–T5	**t(36.03)=-3.71, p=0.001, d=-0.97, E=3, μ = −0.88 (-1.35 -0.4)**	**t(36.81)=-4.3, p¡0.001, d=-1.13, E=3, μ = −0.98 (-1.44 -0.53)**	U=499, p=0.353, d=0.16, E=0, μ = 0.33 (-0.19 0.81)	**t(34.53)=2.8, p=0.016, d=0.74, E=3, μ = 0.7 (0.2 1.2)**	t(33.29)=0.93, p=0.547, d=0.25, E=0, μ = 0.25 (-0.28 0.78)
P4–PZ	**t(37)=-3.4, p=0.001, d=-0.89, E=3, μ = −0.82 (-1.3 -0.34)**	**t(36.88)=-4.39, p¡0.001, d=-1.15, E=3, μ = −1 (-1.46 -0.54)**	t(35.75)=1.51, p=0.299, d=0.39, E=0, μ = 0.39 (-0.13 0.91)	**t(35.16)=2.48, p=0.025, d=0.65, E=3, μ = 0.63 (0.12 1.13)**	U=410, p=0.923, d=0.02, E=0, μ = −0.03 (-0.58 0.48)
P3–PZ	**U=180, p¡0.001, d=0.49, E=3, μ = −1.1 (-1.67 -0.61)**	**t(36.4)=-3.49, p=0.001, d=-0.92, E=3, μ = −0.84 (-1.31 -0.36)**	t(32.48)=1.7, p=0.294, d=0.44, E=0, μ = 0.44 (-0.08 0.95)	**U=577, p=0.023, d=0.32, E=3, μ = 0.65 (0.13 1.24)**	U=469, p=0.613, d=0.1, E=0, μ = 0.14 (-0.35 0.56)
T6–O2	**U=194, p=0.001, d=0.46, E=3, μ = −1.09 (-1.59 -0.52)**	**t(35.12)=-4.06, p¡0.001, d=-1.06, E=3, μ = −0.94 (-1.4 -0.48)**	U=610, p=0.063, d=0.39, E=0, μ = 0.68 (0.29 1.1)	t(36.92)=1.41, p=0.163, d=0.37, E=0, μ = 0.37 (-0.15 0.89)	U=324, p=0.395, d=0.17, E=0, μ = −0.25 (-0.63 0.13)
T5–O1	**t(30.73)=-4.33, p¡0.001, d=-1.14, E=3, μ = −0.99 (-1.46 -0.53)**	**t(34.14)=-3.45, p=0.001, d=-0.91, E=3, μ = −0.83 (-1.32 -0.35)**	t(32.43)=2.69, p=0.111, d=0.71, E=0, μ = 0.67 (0.17 1.17)	t(32.71)=1.62, p=0.128, d=0.43, E=0, μ = 0.42 (-0.1 0.95)	U=369, p=0.659, d=0.08, E=0, μ = −0.11 (-0.5 0.25)
P4–O2	**U=191, p=0.001, d=0.45, E=3, μ = −1.2 (-1.59 -0.56)**	**t(32.17)=-3.35, p=0.002, d=-0.88, E=3, μ = −0.81 (-1.3 -0.33)**	U=545, p=0.151, d=0.29, E=0, μ = 0.5 (0.04 0.95)	**U=540, p=0.039, d=0.28, E=3, μ = 0.57 (0.07 0.96)**	U=358, p=0.613, d=0.1, E=0, μ = −0.15 (-0.6 0.22)
P3–O1	**U=189, p=0.001, d=0.44, E=3, μ = −0.99 (-1.51 -0.41)**	**t(35.98)=-4.04, p¡0.001, d=-1.07, E=3, μ = −0.95 (-1.42 -0.48)**	t(35.57)=1.48, p=0.299, d=0.39, E=0, μ = 0.39 (-0.14 0.91)	**t(25.07)=2.35, p=0.032, d=0.62, E=3, μ = 0.6 (0.09 1.12)**	U=409, p=0.968, d=0.01, E=0, μ = 0.01 (-0.42 0.38)
O1–O2	**t(33.25)=-3.72, p=0.001, d=-1, E=3, μ = −0.9 (-1.39 -0.42)**	**t(33.89)=-4.4, p¡0.001, d=-1.19, E=3, μ = −1.03 (-1.49 -0.56)**	t(34.89)=2.31, p=0.151, d=0.62, E=0, μ = 0.59 (0.08 1.11)	t(29.68)=1.46, p=0.158, d=0.39, E=0, μ = 0.39 (-0.15 0.92)	U=314, p=0.395, d=0.17, E=0, μ = −0.2 (-0.6 0.12)

Table A.14: Comparisons of node strength measured with CBS in epoch 2. The results are reported as follows: statistics value (degrees of freedom), p-value of the test, Cohen's d effect size (or nonparametric alternative), number of epochs where significant differences were observed (E), and difference estimate μ with 95% confidence interval (CI). Reliable differences (significant in all three epochs) are highlighted with bold text.

from	channel	δ	θ	α	β	γ
δ	F8–F4	U=238, p=0.005, d=0.37, E=2, μ =-0.73 (-1.25 -0.23)	**t(36.72)=-3.87, p¡0.001, d=-1.01, E=3, μ =-0.91 (-1.38 -0.44)**	t(35.73)=-2.77, p=0.008, d=-0.73, E=2, μ =-0.69 (-1.18 -0.19)	U=413, p=0.982, d=0.01, E=0, μ =-0.01 (-0.45 0.39)	U=519, p=0.715, d=0.2, E=0, μ =0.34 (-0.13 0.71)
δ	F7–F3	**U=224, p=0.003, d=0.4, E=3, μ =-0.77 (-1.27 -0.32)**	**t(36.93)=-3.82, p¡0.001, d=-1, E=3, μ =-0.9 (-1.37 -0.43)**	t(36.92)=-3.8, p=0.001, d=-1, E=2, μ =-0.9 (-1.37 -0.42)	U=393, p=0.982, d=0.06, E=0, μ =-0.11 (-0.48 0.49)	U=511, p=0.715, d=0.19, E=0, μ =0.2 (-0.08 0.44)
δ	F4–C4	**U=227, p=0.003, d=0.39, E=3, μ =-0.8 (-1.19 -0.37)**	**U=152, p¡0.001, d=0.55, E=3, μ =-1.16 (-1.58 -0.66)**	**t(32.42)=-4.89, p¡0.001, d=-1.29, E=3, μ =-1.09 (-1.54 -0.64)**	U=390, p=0.982, d=0.06, E=0, μ =-0.11 (-0.58 0.36)	U=506, p=0.715, d=0.18, E=0, μ =0.1 (-0.05 0.26)
δ	F3–C3	U=198, p=0.001, d=0.45, E=2, μ =-0.82 (-1.16 -0.41)	**t(36.6)=-5, p¡0.001, d=-1.31, E=3, μ =-1.1 (-1.54 -0.66)**	t(36.22)=-4.03, p=0.001, d=-1.06, E=2, μ =-0.94 (-1.41 -0.47)	U=418, p=0.982, d=0, E=0, μ =0 (-0.5 0.43)	U=480, p=0.746, d=0.12, E=0, μ =0.08 (-0.07 0.26)
δ	F4–FZ	U=198, p=0.001, d=0.45, E=2, μ =-0.89 (-1.36 -0.45)	**t(33.13)=-3.8, p¡0.001, d=-0.99, E=3, μ =-0.89 (-1.36 -0.42)**	t(34.81)=-3.66, p=0.001, d=-0.96, E=2, μ =-0.87 (-1.34 -0.39)	U=376, p=0.982, d=0.09, E=0, μ =-0.14 (-0.53 0.33)	U=524, p=0.715, d=0.21, E=0, μ =0.14 (-0.04 0.23)
δ	FZ–CZ	**U=199, p=0.001, d=0.45, E=3, μ =-0.81 (-1.23 -0.41)**	**t(35.9)=-4.23, p¡0.001, d=-1.11, E=3, μ =-0.98 (-1.44 -0.51)**	t(35.39)=-3.98, p=0.001, d=-1.05, E=2, μ =-0.93 (-1.4 -0.46)	U=417, p=0.982, d=0.01, E=0, μ =-0.02 (-0.5 0.39)	U=514, p=0.715, d=0.19, E=0, μ =0.06 (-0.03 0.18)
δ	F3–FZ	**t(37)=-3.51, p=0.002, d=-0.92, E=3, μ =-0.84 (-1.32 -0.36)**	**t(35.14)=-3.36, p=0.001, d=-0.88, E=3, μ =-0.81 (-1.29 -0.33)**	**t(36.97)=-3.65, p=0.001, d=-0.96, E=3, μ =-0.87 (-1.34 -0.39)**	U=417, p=0.982, d=0.01, E=0, μ =-0.01 (-0.44 0.4)	U=468, p=0.862, d=0.1, E=0, μ =0.07 (-0.12 0.2)
δ	T4–C4	**U=176, p=0.001, d=0.5, E=3, μ =-0.94 (-1.36 -0.49)**	**t(36.75)=-4.36, p¡0.001, d=-1.15, E=3, μ =-1 (-1.46 -0.54)**	t(36.44)=-3.22, p=0.004, d=-0.84, E=1, μ =-0.78 (-1.27 -0.29)	U=418, p=0.982, d=0, E=0, μ =-0.01 (-0.38 0.36)	U=462, p=0.862, d=0.09, E=0, μ =0.04 (-0.09 0.15)
δ	T3–C3	**U=204, p=0.002, d=0.44, E=3, μ =-0.94 (-1.49 -0.39)**	**t(37)=-4.67, p¡0.001, d=-1.22, E=3, μ =-1.05 (-1.5 -0.6)**	t(35.81)=-3.42, p=0.002, d=-0.9, E=1, μ =-0.83 (-1.31 -0.34)	U=347, p=0.858, d=0.15, E=0, μ =-0.22 (-0.57 0.18)	U=490, p=0.715, d=0.14, E=0, μ =0.08 (-0.06 0.21)
δ	C4–CZ	**t(35.74)=-2.24, p=0.029, d=-0.59, E=3, μ =-0.57 (-1.08 -0.06)**	**t(37)=-3.54, p=0.001, d=-0.93, E=3, μ =-0.85 (-1.33 -0.37)**	**U=254, p=0.009, d=0.34, E=3, μ =-0.66 (-1.14 -0.18)**	U=481, p=0.982, d=0.12, E=0, μ =0.23 (-0.22 0.67)	U=504, p=0.715, d=0.17, E=0, μ =0.07 (-0.04 0.2)
δ	C3–CZ	**t(35.77)=-3.17, p=0.003, d=-0.83, E=3, μ =-0.78 (-1.27 -0.28)**	t(36.74)=-3.42, p=0.001, d=-0.9, E=2, μ =-0.82 (-1.31 -0.34)	t(35.57)=-2.79, p=0.008, d=-0.73, E=1, μ =-0.69 (-1.18 -0.19)	U=446, p=0.982, d=0.05, E=0, μ =0.09 (-0.32 0.61)	U=490, p=0.715, d=0.14, E=0, μ =0.07 (-0.05 0.2)
δ	CZ–PZ	**U=198, p=0.001, d=0.45, E=3, μ =-0.85 (-1.29 -0.35)**	**t(35.98)=-6.3, p¡0.001, d=-1.66, E=3, μ =-1.28 (-1.69 -0.87)**	**t(35.45)=-4.18, p=0.001, d=-1.1, E=3, μ =-0.97 (-1.44 -0.5)**	U=439, p=0.982, d=0.04, E=0, μ =0.08 (-0.49 0.63)	U=438, p=0.905, d=0.04, E=0, μ =0.02 (-0.09 0.15)
δ	C4–P4	**U=231, p=0.003, d=0.39, E=3, μ =-0.71 (-1.08 -0.28)**	**t(36.65)=-5.29, p¡0.001, d=-1.39, E=3, μ =-1.15 (-1.58 -0.71)**	t(36.68)=-4.07, p=0.001, d=-1.07, E=2, μ =-0.95 (-1.41 -0.48)	U=450, p=0.982, d=0.06, E=0, μ =0.09 (-0.36 0.59)	U=393, p=0.905, d=0.06, E=0, μ =-0.04 (-0.29 0.23)

δ	C3–P3	**U=207, p=0.002, d=0.44, E=3, μ =-0.81 (-1.34 -0.38)**	**U=151, p¡0.001, d=0.55, E=3, μ =-1.13 (-1.67 -0.67)**	t(36.61)=-3.86, p=0.001, d=-1.01, E=2, μ =-0.91 (-1.38 -0.44)	U=426, p=0.982, d=0.01, E=0, μ =0.02 (-0.43 0.56)	U=417, p=0.969, d=0.01, E=0, μ =0 (-0.32 0.33)
δ	T4–T6	**U=180, p=0.001, d=0.49, E=3, μ =-0.98 (-1.36 -0.56)**	**t(36.88)=-4.44, p¡0.001, d=-1.16, E=3, μ =-1.01 (-1.46 -0.55)**	t(36.03)=-3.01, p=0.005, d=-0.79, E=2, μ =-0.74 (-1.23 -0.25)	U=382, p=0.982, d=0.08, E=0, μ =-0.11 (-0.49 0.28)	U=395, p=0.905, d=0.05, E=0, μ =-0.02 (-0.16 0.1)
δ	T3–T5	**U=238, p=0.005, d=0.37, E=3, μ =-0.76 (-1.11 -0.31)**	**t(36.48)=-3.79, p¡0.001, d=-0.99, E=3, μ =-0.89 (-1.36 -0.42)**	t(36.55)=-2.81, p=0.008, d=-0.74, E=1, μ =-0.69 (-1.19 -0.2)	U=317, p=0.695, d=0.21, E=0, μ =-0.27 (-0.61 0.11)	U=444, p=0.905, d=0.05, E=0, μ =0.02 (-0.12 0.16)
δ	P4–PZ	**U=211, p=0.002, d=0.43, E=3, μ =-0.83 (-1.27 -0.38)**	**t(36.79)=-4.4, p¡0.001, d=-1.16, E=3, μ =-1 (-1.46 -0.55)**	t(36.59)=-3.64, p=0.001, d=-0.95, E=1, μ =-0.86 (-1.34 -0.39)	U=428, p=0.982, d=0.02, E=0, μ =0.03 (-0.38 0.49)	U=432, p=0.937, d=0.02, E=0, μ =0.01 (-0.11 0.15)
δ	P3–PZ	**U=242, p=0.005, d=0.36, E=3, μ =-0.87 (-1.27 -0.29)**	**t(32.55)=-4.26, p¡0.001, d=-1.11, E=3, μ =-0.97 (-1.43 -0.51)**	t(31.72)=-3.03, p=0.005, d=-0.79, E=1, μ =-0.74 (-1.22 -0.25)	U=414, p=0.982, d=0.01, E=0, μ =-0.02 (-0.35 0.36)	U=411, p=0.937, d=0.02, E=0, μ =-0.01 (-0.1 0.09)
δ	T6–O2	**U=222, p=0.003, d=0.4, E=3, μ =-0.72 (-1.12 -0.33)**	t(36.48)=-2.98, p=0.004, d=-0.78, E=2, μ =-0.73 (-1.22 -0.24)	U=251, p=0.008, d=0.35, E=2, μ =-0.6 (-1.01 -0.19)	U=323, p=0.695, d=0.2, E=0, μ =-0.2 (-0.46 0.09)	U=382, p=0.862, d=0.08, E=0, μ =-0.03 (-0.12 0.08)
δ	T5–O1	**U=226, p=0.003, d=0.4, E=3, μ =-0.76 (-1.17 -0.3)**	**t(36.83)=-3.6, p=0.001, d=-0.95, E=3, μ =-0.86 (-1.34 -0.38)**	t(34.35)=-3.11, p=0.005, d=-0.81, E=2, μ =-0.76 (-1.24 -0.27)	U=312, p=0.695, d=0.22, E=0, μ =-0.27 (-0.56 0.07)	U=354, p=0.715, d=0.13, E=0, μ =-0.04 (-0.12 0.05)
δ	P4–O2	**U=185, p=0.001, d=0.48, E=3, μ =-0.9 (-1.37 -0.44)**	**t(36.93)=-4.77, p¡0.001, d=-1.25, E=3, μ =-1.06 (-1.51 -0.62)**	t(37)=-2.85, p=0.008, d=-0.75, E=2, μ =-0.71 (-1.2 -0.21)	U=345, p=0.858, d=0.15, E=0, μ =-0.22 (-0.54 0.18)	U=400, p=0.905, d=0.04, E=0, μ =-0.01 (-0.09 0.06)
δ	P3–O1	**U=214, p=0.002, d=0.42, E=3, μ =-0.7 (-1.12 -0.31)**	**t(36.41)=-4.13, p¡0.001, d=-1.08, E=3, μ =-0.95 (-1.42 -0.49)**	t(35.57)=-3.36, p=0.003, d=-0.88, E=2, μ =-0.81 (-1.29 -0.33)	U=315, p=0.695, d=0.21, E=0, μ =-0.29 (-0.6 0.09)	U=379, p=0.862, d=0.08, E=0, μ =-0.02 (-0.09 0.05)
δ	O1–O2	**U=203, p=0.002, d=0.44, E=3, μ =-0.9 (-1.37 -0.44)**	**U=124, p¡0.001, d=0.6, E=3, μ =-1.32 (-1.76 -0.86)**	**t(36.46)=-4.94, p¡0.001, d=-1.3, E=3, μ =-1.09 (-1.54 -0.65)**	U=327, p=0.695, d=0.19, E=0, μ =-0.25 (-0.77 0.1)	U=351, p=0.715, d=0.14, E=0, μ =-0.04 (-0.12 0.05)
θ	F8–F4	**t(36.09)=-3.76, p=0.001, d=-0.98, E=3, μ =-0.88 (-1.36 -0.41)**	**t(36.3)=-2.93, p=0.008, d=-0.77, E=3, μ =-0.72 (-1.21 -0.23)**	t(33.68)=-2.11, p=0.083, d=-0.55, E=0, μ =-0.53 (-1.04 -0.03)	U=470, p=0.716, d=0.1, E=0, μ =0.24 (-0.24 0.68)	U=524, p=0.322, d=0.21, E=0, μ =0.39 (-0.11 0.81)
θ	F7–F3	**t(35.36)=-4.13, p¡0.001, d=-1.08, E=3, μ =-0.95 (-1.41 -0.49)**	**t(36.89)=-2.94, p=0.008, d=-0.77, E=3, μ =-0.72 (-1.22 -0.23)**	t(35.49)=-2.15, p=0.083, d=-0.56, E=0, μ =-0.54 (-1.05 -0.04)	t(36.1)=0.4, p=0.926, d=0.11, E=0, μ =0.11 (-0.42 0.63)	U=519, p=0.322, d=0.2, E=0, μ =0.43 (-0.1 0.94)
θ	F4–C4	**U=144, p¡0.001, d=0.56, E=3, μ =-1.22 (-1.58 -0.72)**	**t(35.62)=-4.24, p=0.001, d=-1.12, E=3, μ =-0.98 (-1.44 -0.52)**	t(36.53)=-3.47, p=0.024, d=-0.91, E=1, μ =-0.83 (-1.31 -0.35)	t(36.97)=0.3, p=0.926, d=0.08, E=0, μ =0.08 (-0.45 0.61)	U=555, p=0.274, d=0.28, E=0, μ =0.36 (0.03 0.66)
θ	F3–C3	**t(36.96)=-4.95, p¡0.001, d=-1.3, E=3, μ =-1.09 (-1.54 -0.65)**	**t(35.37)=-4.58, p=0.001, d=-1.21, E=3, μ =-1.04 (-1.49 -0.58)**	t(36.95)=-2.77, p=0.058, d=-0.73, E=0, μ =-0.69 (-1.18 -0.19)	t(34.79)=0.73, p=0.716, d=0.19, E=0, μ =0.19 (-0.34 0.73)	U=533, p=0.322, d=0.23, E=0, μ =0.25 (-0.02 0.56)
θ	F4–FZ	**t(29.34)=-3.71, p=0.001, d=-0.97, E=3, μ =-0.87 (-1.34 -0.4)**	**t(36.35)=-3.53, p=0.003, d=-0.93, E=3, μ =-0.84 (-1.32 -0.36)**	t(34.01)=-2.95, p=0.054, d=-0.77, E=0, μ =-0.72 (-1.21 -0.23)	t(32.83)=0.76, p=0.716, d=0.2, E=0, μ =0.2 (-0.32 0.72)	U=607, p=0.074, d=0.38, E=0, μ =0.44 (0.16 0.67)

θ	FZ–CZ	**t(36.97)=-4.93, p¡0.001, d=-1.29, E=3, μ =-1.09 (-1.53 -0.65)**	t(35.18)=-3.6, p=0.003, d=-0.95, E=2, μ =-0.86 (-1.34 -0.38)	t(36)=-2.43, p=0.061, d=-0.64, E=0, μ =-0.61 (-1.12 -0.11)	t(35.99)=0.33, p=0.926, d=0.09, E=0, μ =0.09 (-0.44 0.62)	U=513, p=0.347, d=0.19, E=0, μ =0.18 (-0.09 0.43)
θ	F3–FZ	**t(33.07)=-3.78, p=0.001, d=-0.99, E=3, μ =-0.89 (-1.36 -0.41)**	**t(31.27)=-2.15, p=0.036, d=-0.56, E=3, μ =-0.54 (-1.05 -0.04)**	t(33.5)=-2.07, p=0.083, d=-0.54, E=0, μ =-0.52 (-1.03 -0.02)	t(35.99)=0.1, p=0.982, d=0.03, E=0, μ =0.03 (-0.5 0.55)	U=531, p=0.322, d=0.23, E=0, μ =0.28 (-0.03 0.58)
θ	T4–C4	**t(36.94)=-4.5, p¡0.001, d=-1.18, E=3, μ =-1.02 (-1.48 -0.57)**	t(31.3)=-2.91, p=0.008, d=-0.76, E=2, μ =-0.71 (-1.2 -0.22)	t(27.44)=-2.56, p=0.061, d=-0.67, E=0, μ =-0.63 (-1.13 -0.13)	U=422, p=0.982, d=0, E=0, μ =0.01 (-0.5 0.53)	U=480, p=0.746, d=0.12, E=0, μ =0.1 (-0.15 0.35)
θ	T3–C3	**t(37)=-4.34, p¡0.001, d=-1.14, E=3, μ =-0.99 (-1.45 -0.54)**	t(36.92)=-2.91, p=0.008, d=-0.76, E=2, μ =-0.72 (-1.21 -0.22)	t(36.99)=-2.1, p=0.083, d=-0.55, E=0, μ =-0.53 (-1.05 -0.02)	t(36.69)=0.21, p=0.96, d=0.05, E=0, μ =0.06 (-0.47 0.58)	U=575, p=0.177, d=0.32, E=0, μ =0.4 (0.08 0.72)
θ	C4–CZ	**t(35.15)=-3.35, p=0.002, d=-0.88, E=3, μ =-0.8 (-1.29 -0.32)**	t(35.78)=-2.63, p=0.012, d=-0.69, E=2, μ =-0.65 (-1.15 -0.16)	t(36.7)=-2.2, p=0.083, d=-0.58, E=0, μ =-0.56 (-1.06 -0.05)	t(36.91)=-0.07, p=0.982, d=-0.02, E=0, μ =-0.02 (-0.55 0.51)	U=522, p=0.322, d=0.21, E=0, μ =0.18 (-0.05 0.39)
θ	C3–CZ	**t(35.99)=-3.73, p=0.001, d=-0.98, E=3, μ =-0.88 (-1.35 -0.41)**	t(32.08)=-2.73, p=0.01, d=-0.71, E=2, μ =-0.67 (-1.17 -0.18)	t(31.15)=-2.43, p=0.061, d=-0.64, E=0, μ =-0.61 (-1.11 -0.11)	t(36.56)=0.88, p=0.716, d=0.23, E=0, μ =0.23 (-0.29 0.75)	U=463, p=0.799, d=0.09, E=0, μ =0.07 (-0.19 0.34)
θ	CZ–PZ	**t(33.82)=-5.67, p¡0.001, d=-1.5, E=3, μ =-1.2 (-1.63 -0.78)**	**U=199, p=0.002, d=0.45, E=3, μ =-0.86 (-1.29 -0.38)**	t(36.91)=-1.86, p=0.121, d=-0.49, E=0, μ =-0.48 (-0.99 0.04)	t(35.23)=2.3, p=0.146, d=0.61, E=0, μ =0.58 (0.07 1.09)	U=471, p=0.77, d=0.1, E=0, μ =0.11 (-0.13 0.39)
θ	C4–P4	**t(36.05)=-4.95, p¡0.001, d=-1.3, E=3, μ =-1.1 (-1.54 -0.65)**	**t(36.75)=-3.19, p=0.006, d=-0.84, E=3, μ =-0.78 (-1.27 -0.29)**	t(37)=-1.27, p=0.266, d=-0.33, E=0, μ =-0.33 (-0.85 0.19)	t(35.84)=3.56, p=0.018, d=0.93, E=2, μ =0.85 (0.37 1.32)	U=422, p=0.982, d=0, E=0, μ =0 (-0.47 0.41)
θ	C3–P3	**t(35.11)=-4.82, p¡0.001, d=-1.27, E=3, μ =-1.08 (-1.53 -0.63)**	**t(30.94)=-3.26, p=0.006, d=-0.86, E=3, μ =-0.8 (-1.29 -0.31)**	t(34.92)=-1.31, p=0.266, d=-0.34, E=0, μ =-0.34 (-0.87 0.18)	t(36.83)=1.71, p=0.359, d=0.45, E=0, μ =0.44 (-0.08 0.96)	U=437, p=0.967, d=0.03, E=0, μ =0.04 (-0.47 0.48)
θ	T4–T6	t(36.96)=-4.21, p¡0.001, d=-1.11, E=2, μ =-0.97 (-1.43 -0.51)	**t(36.28)=-2.76, p=0.01, d=-0.72, E=3, μ =-0.68 (-1.18 -0.19)**	t(33.29)=-0.92, p=0.377, d=-0.24, E=0, μ =-0.24 (-0.76 0.28)	t(29.62)=2.34, p=0.146, d=0.61, E=0, μ =0.58 (0.08 1.09)	U=439, p=0.967, d=0.04, E=0, μ =0.06 (-0.22 0.29)
θ	T3–T5	**U=232, p=0.003, d=0.38, E=3, μ =-0.83 (-1.34 -0.34)**	t(35.2)=-2.84, p=0.009, d=-0.75, E=2, μ =-0.71 (-1.2 -0.21)	t(36.82)=-1.53, p=0.19, d=-0.4, E=0, μ =-0.4 (-0.91 0.12)	U=460, p=0.779, d=0.08, E=0, μ =0.16 (-0.34 0.61)	U=523, p=0.322, d=0.21, E=0, μ =0.32 (-0.1 0.67)
θ	P4–PZ	**t(36.96)=-4.47, p¡0.001, d=-1.17, E=3, μ =-1.02 (-1.47 -0.56)**	**t(36.84)=-3.97, p=0.002, d=-1.04, E=3, μ =-0.93 (-1.39 -0.46)**	U=268, p=0.061, d=0.31, E=0, μ =-0.64 (-1.21 -0.12)	t(36.5)=1.24, p=0.56, d=0.32, E=0, μ =0.32 (-0.2 0.84)	U=425, p=0.982, d=0.01, E=0, μ =0.02 (-0.31 0.33)
θ	P3–PZ	**t(30.35)=-2.96, p=0.005, d=-0.77, E=3, μ =-0.72 (-1.21 -0.23)**	t(32.17)=-2.74, p=0.01, d=-0.72, E=2, μ =-0.68 (-1.17 -0.18)	t(29.61)=-1.17, p=0.301, d=-0.3, E=0, μ =-0.3 (-0.82 0.22)	U=567, p=0.146, d=0.3, E=0, μ =0.51 (0.08 1.01)	U=442, p=0.967, d=0.04, E=0, μ =0.05 (-0.19 0.31)
θ	T6–O2	t(32.09)=-3.24, p=0.002, d=-0.85, E=2, μ =-0.78 (-1.26 -0.3)	t(36.57)=-2.97, p=0.008, d=-0.78, E=2, μ =-0.73 (-1.22 -0.24)	t(27.85)=-1.05, p=0.33, d=-0.27, E=0, μ =-0.27 (-0.79 0.25)	U=492, p=0.56, d=0.15, E=0, μ =0.26 (-0.17 0.68)	U=378, p=0.799, d=0.09, E=0, μ =-0.06 (-0.29 0.14)
θ	T5–O1	**U=200, p=0.001, d=0.45, E=3, μ =-1.02 (-1.47 -0.41)**	t(36.49)=-2.92, p=0.008, d=-0.76, E=2, μ =-0.72 (-1.21 -0.22)	t(31.06)=-1.57, p=0.189, d=-0.41, E=0, μ =-0.4 (-0.92 0.11)	U=495, p=0.56, d=0.15, E=0, μ =0.29 (-0.18 0.74)	U=367, p=0.77, d=0.11, E=0, μ =-0.06 (-0.23 0.1)
θ	P4–O2	**t(36.42)=-4.15, p¡0.001, d=-1.09, E=3, μ =-0.96 (-1.42 -0.5)**	t(36.89)=-2.61, p=0.012, d=-0.69, E=2, μ =-0.65 (-1.15 -0.15)	t(34.96)=-0.87, p=0.386, d=-0.23, E=0, μ =-0.23 (-0.75 0.3)	U=514, p=0.483, d=0.19, E=0, μ =0.31 (-0.11 0.74)	U=411, p=0.982, d=0.02, E=0, μ =-0.01 (-0.17 0.15)

θ	P3–O1	**t(36.88)=-3.74, p=0.001, d=-0.98, E=3, μ =-0.88 (-1.36 -0.41)**	t(36.73)=-3.19, p=0.006, d=-0.84, E=2, μ =-0.78 (-1.27 -0.29)	t(36.9)=-1.13, p=0.302, d=-0.3, E=0, μ =-0.3 (-0.82 0.23)	t(29.51)=2, p=0.235, d=0.52, E=0, μ =0.5 (0 1.01)	U=425, p=0.982, d=0.01, E=0, μ =0.01 (-0.17 0.21)
θ	O1–O2	**t(36.29)=-3.87, p=0.001, d=-1.01, E=3, μ =-0.91 (-1.38 -0.44)**	**t(36.95)=-3.05, p=0.008, d=-0.8, E=3, μ =-0.75 (-1.24 -0.26)**	t(33.7)=-1.61, p=0.187, d=-0.42, E=0, μ =-0.41 (-0.93 0.1)	U=509, p=0.489, d=0.18, E=0, μ =0.28 (-0.15 0.86)	U=392, p=0.965, d=0.06, E=0, μ =-0.03 (-0.25 0.17)
α	F8–F4	t(33.5)=-3.37, p=0.003, d=-0.88, E=2, μ =-0.81 (-1.29 -0.33)	t(35.07)=-2.68, p=0.03, d=-0.7, E=1, μ =-0.66 (-1.16 -0.17)	U=371, p=0.798, d=0.1, E=0, μ =-0.19 (-0.67 0.35)	t(36.85)=1.96, p=0.074, d=0.51, E=0, μ =0.5 (-0.01 1.01)	U=582, p=0.025, d=0.33, E=2, μ =0.53 (0.11 0.9)
α	F7–F3	t(36.66)=-3.96, p=0.001, d=-1.04, E=2, μ =-0.92 (-1.39 -0.46)	t(35.07)=-3.26, p=0.015, d=-0.85, E=1, μ =-0.79 (-1.27 -0.3)	t(32.72)=-1.69, p=0.791, d=-0.44, E=0, μ =-0.44 (-0.96 0.08)	t(36.34)=1.23, p=0.244, d=0.32, E=0, μ =0.32 (-0.2 0.85)	U=585, p=0.025, d=0.34, E=2, μ =0.43 (0.11 0.76)
α	F4–C4	t(32.9)=-4.25, p|0.001, d=-1.12, E=2, μ =-0.98 (-1.45 -0.52)	t(36.6)=-3.38, p=0.015, d=-0.89, E=1, μ =-0.82 (-1.3 -0.33)	U=416, p=0.957, d=0.01, E=0, μ =-0.02 (-0.48 0.48)	t(29.02)=1.31, p=0.227, d=0.35, E=0, μ =0.35 (-0.19 0.88)	**U=669, p=0.001, d=0.51, E=3, μ =0.66 (0.38 1.01)**
α	F3–C3	t(36.94)=-4.23, p|0.001, d=-1.11, E=2, μ =-0.98 (-1.44 -0.51)	t(36.72)=-3.46, p=0.015, d=-0.91, E=1, μ =-0.83 (-1.31 -0.35)	U=394, p=0.798, d=0.05, E=0, μ =-0.12 (-0.58 0.37)	**U=563, p=0.049, d=0.29, E=3, μ =0.55 (0.05 0.99)**	**U=670, p=0.001, d=0.51, E=3, μ =0.71 (0.33 0.99)**
α	F4–FZ	t(34.65)=-3.21, p=0.005, d=-0.84, E=2, μ =-0.78 (-1.26 -0.29)	t(35.75)=-2.96, p=0.021, d=-0.77, E=1, μ =-0.72 (-1.22 -0.23)	t(35.7)=-0.93, p=0.798, d=-0.24, E=0, μ =-0.24 (-0.77 0.28)	t(37)=1.76, p=0.102, d=0.46, E=0, μ =0.45 (-0.06 0.97)	**U=634, p=0.005, d=0.44, E=3, μ =0.57 (0.25 0.91)**
α	FZ–CZ	t(36.99)=-4.56, p|0.001, d=-1.2, E=1, μ =-1.03 (-1.48 -0.58)	t(36.73)=-2.88, p=0.022, d=-0.76, E=1, μ =-0.71 (-1.21 -0.22)	U=448, p=0.798, d=0.06, E=0, μ =0.08 (-0.38 0.55)	t(29.42)=1.16, p=0.263, d=0.31, E=0, μ =0.31 (-0.23 0.84)	**U=582, p=0.025, d=0.33, E=3, μ =0.38 (0.1 0.69)**
α	F3–FZ	t(37)=-3.81, p=0.001, d=-1, E=1, μ =-0.9 (-1.37 -0.43)	t(32.09)=-1.86, p=0.087, d=-0.49, E=0, μ =-0.47 (-0.98 0.04)	t(36.83)=-1.23, p=0.791, d=-0.32, E=0, μ =-0.32 (-0.84 0.2)	t(36.84)=0.87, p=0.386, d=0.23, E=0, μ =0.23 (-0.3 0.76)	**U=600, p=0.021, d=0.37, E=3, μ =0.52 (0.16 0.89)**
α	T4–C4	t(32.64)=-2.88, p=0.008, d=-0.75, E=1, μ =-0.7 (-1.2 -0.21)	t(26.92)=-2.19, p=0.059, d=-0.57, E=0, μ =-0.55 (-1.05 -0.05)	t(36.83)=-0.16, p=0.913, d=-0.04, E=0, μ =-0.04 (-0.57 0.49)	U=547, p=0.072, d=0.26, E=0, μ =0.45 (0.01 0.94)	U=576, p=0.025, d=0.32, E=2, μ =0.35 (0.08 0.64)
α	T3–C3	t(35.81)=-3.05, p=0.007, d=-0.8, E=1, μ =-0.75 (-1.24 -0.26)	t(36)=-2.65, p=0.03, d=-0.69, E=1, μ =-0.66 (-1.16 -0.16)	t(31.98)=-0.65, p=0.798, d=-0.17, E=0, μ =-0.17 (-0.71 0.36)	U=560, p=0.052, d=0.29, E=0, μ =0.6 (0.08 1.04)	U=626, p=0.006, d=0.42, E=2, μ =0.6 (0.22 0.95)
α	C4–CZ	t(34.74)=-2.36, p=0.024, d=-0.62, E=1, μ =-0.59 (-1.09 -0.09)	t(35)=-2.57, p=0.03, d=-0.67, E=1, μ =-0.64 (-1.14 -0.14)	U=404, p=0.888, d=0.03, E=0, μ =-0.05 (-0.48 0.37)	U=546, p=0.072, d=0.26, E=0, μ =0.45 (-0.02 0.85)	U=575, p=0.025, d=0.32, E=2, μ =0.36 (0.06 0.68)
α	C3–CZ	t(35.69)=-2.89, p=0.008, d=-0.76, E=1, μ =-0.71 (-1.2 -0.22)	t(29.85)=-2.29, p=0.055, d=-0.6, E=0, μ =-0.57 (-1.08 -0.07)	U=477, p=0.798, d=0.12, E=0, μ =0.19 (-0.3 0.54)	t(32.74)=2.09, p=0.068, d=0.55, E=0, μ =0.54 (0.02 1.05)	U=594, p=0.024, d=0.36, E=2, μ =0.5 (0.18 0.9)
α	CZ–PZ	t(36.56)=-4.71, p|0.001, d=-1.24, E=2, μ =-1.06 (-1.51 -0.61)	t(36.45)=-2.6, p=0.03, d=-0.68, E=1, μ =-0.65 (-1.15 -0.15)	U=491, p=0.791, d=0.15, E=0, μ =0.24 (-0.22 0.72)	**t(23.71)=2.68, p=0.024, d=0.71, E=3, μ =0.68 (0.17 1.19)**	**U=577, p=0.025, d=0.32, E=3, μ =0.45 (0.12 0.76)**
α	C4–P4	t(36.53)=-4.43, p|0.001, d=-1.16, E=2, μ =-1.01 (-1.46 -0.55)	t(35.3)=-2.02, p=0.076, d=-0.53, E=0, μ =-0.51 (-1.02 0)	U=514, p=0.791, d=0.19, E=0, μ =0.39 (-0.14 0.88)	**t(27.55)=3.46, p=0.011, d=0.92, E=3, μ =0.84 (0.35 1.33)**	U=535, p=0.101, d=0.23, E=0, μ =0.33 (-0.04 0.75)
α	C3–P3	t(36.17)=-3.54, p=0.002, d=-0.93, E=1, μ =-0.85 (-1.33 -0.37)	t(34.82)=-2.24, p=0.057, d=-0.59, E=0, μ =-0.57 (-1.08 -0.06)	U=463, p=0.798, d=0.09, E=0, μ =0.15 (-0.28 0.69)	**t(27.11)=2.69, p=0.024, d=0.71, E=3, μ =0.68 (0.17 1.19)**	U=527, p=0.114, d=0.22, E=0, μ =0.35 (-0.04 0.72)
α	T4–T6	t(34.51)=-2.91, p=0.008, d=-0.76, E=1, μ =-0.71 (-1.2 -0.22)	t(31.99)=-1.66, p=0.117, d=-0.43, E=0, μ =-0.42 (-0.94 0.09)	t(35.19)=0.84, p=0.798, d=0.22, E=0, μ =0.22 (-0.31 0.75)	**U=604, p=0.014, d=0.38, E=3, μ =0.75 (0.24 1.18)**	U=540, p=0.09, d=0.25, E=0, μ =0.29 (-0.02 0.59)
α	T3–T5	t(35.91)=-2.39, p=0.023, d=-0.63, E=1, μ =-0.6 (-1.1 -0.1)	t(36.99)=-2.01, p=0.076, d=-0.53, E=0, μ =-0.51 (-1.02 0)	U=451, p=0.798, d=0.06, E=0, μ =0.12 (-0.39 0.63)	**U=573, p=0.035, d=0.31, E=3, μ =0.61 (0.15 0.96)**	U=576, p=0.025, d=0.32, E=2, μ =0.44 (0.11 0.84)

α	P4–PZ	t(36.84)=-2.57, p=0.015, d=-0.68, E=1, μ =-0.64 (-1.15 -0.14)	t(36.32)=-3.05, p=0.02, d=-0.8, E=1, μ =-0.74 (-1.23 -0.25)	U=457, p=0.798, d=0.08, E=0, μ =0.12 (-0.29 0.63)	t(29.69)=1.86, p=0.089, d=0.49, E=0, μ =0.48 (-0.04 1.01)	U=546, p=0.077, d=0.26, E=0, μ =0.38 (0 0.81)
α	P3–PZ	t(25.4)=-2.18, p=0.034, d=-0.57, E=1, μ =-0.55 (-1.05 -0.04)	t(33.5)=-1.73, p=0.108, d=-0.45, E=0, μ =-0.44 (-0.96 0.07)	U=507, p=0.791, d=0.18, E=0, μ =0.36 (-0.11 0.81)	**t(34.15)=3.66, p=0.011, d=0.96, E=3, μ =0.88 (0.4 1.36)**	U=582, p=0.025, d=0.33, E=2, μ =0.52 (0.13 0.94)
α	T6–O2	U=195, p=0.001, d=0.46, E=1, μ =-0.78 (-1.16 -0.33)	t(32.47)=-1.94, p=0.079, d=-0.51, E=0, μ =-0.49 (-1 0.02)	t(34.76)=1.14, p=0.791, d=0.3, E=0, μ =0.3 (-0.22 0.82)	**U=600, p=0.015, d=0.37, E=3, μ =0.7 (0.21 1.14)**	U=522, p=0.12, d=0.21, E=0, μ =0.18 (-0.04 0.43)
α	T5–O1	t(33.16)=-2.75, p=0.01, d=-0.72, E=1, μ =-0.68 (-1.17 -0.18)	t(32.65)=-1.94, p=0.079, d=-0.51, E=0, μ =-0.49 (-1 0.02)	t(36.93)=1.65, p=0.791, d=0.43, E=0, μ =0.43 (-0.09 0.94)	**U=622, p=0.011, d=0.41, E=3, μ =0.84 (0.35 1.3)**	U=525, p=0.114, d=0.21, E=0, μ =0.19 (-0.04 0.48)
α	P4–O2	t(35.83)=-2.32, p=0.025, d=-0.61, E=1, μ =-0.58 (-1.09 -0.08)	t(34.25)=-1.46, p=0.15, d=-0.38, E=0, μ =-0.38 (-0.89 0.14)	t(36.55)=1.33, p=0.791, d=0.35, E=0, μ =0.35 (-0.17 0.87)	**U=591, p=0.021, d=0.35, E=3, μ =0.71 (0.19 1.15)**	U=525, p=0.114, d=0.21, E=0, μ =0.19 (-0.04 0.45)
α	P3–O1	t(36.28)=-2.9, p=0.008, d=-0.76, E=1, μ =-0.71 (-1.2 -0.22)	t(36.33)=-1.63, p=0.117, d=-0.43, E=0, μ =-0.42 (-0.94 0.1)	t(36.84)=0.71, p=0.798, d=0.19, E=0, μ =0.19 (-0.34 0.72)	**t(33.53)=3.05, p=0.014, d=0.8, E=3, μ =0.75 (0.26 1.25)**	U=530, p=0.113, d=0.22, E=0, μ =0.23 (-0.03 0.5)
α	O1–O2	t(37)=-2.99, p=0.007, d=-0.79, E=2, μ =-0.74 (-1.23 -0.24)	t(35.61)=-1.62, p=0.117, d=-0.42, E=0, μ =-0.42 (-0.93 0.1)	t(36.75)=0.51, p=0.798, d=0.13, E=0, μ =0.13 (-0.39 0.66)	**U=614, p=0.013, d=0.4, E=3, μ =0.7 (0.3 1.23)**	U=498, p=0.23, d=0.16, E=0, μ =0.15 (-0.1 0.48)
β	F8–F4	U=445, p=0.875, d=0.05, E=0, μ =0.07 (-0.3 0.46)	U=511, p=0.915, d=0.19, E=0, μ =0.35 (-0.15 0.76)	t(35.73)=1.81, p=0.087, d=0.48, E=0, μ =0.47 (-0.05 0.99)	U=612, p=0.03, d=0.39, E=2, μ =0.63 (0.23 1.06)	U=642, p=0.002, d=0.45, E=2, μ =0.62 (0.32 0.93)
β	F7–F3	U=446, p=0.875, d=0.05, E=0, μ =0.08 (-0.41 0.63)	t(34.81)=0.29, p=0.938, d=0.08, E=0, μ =0.08 (-0.46 0.61)	U=540, p=0.076, d=0.25, E=0, μ =0.43 (-0.03 0.91)	U=569, p=0.031, d=0.3, E=2, μ =0.41 (0.05 0.81)	**U=616, p=0.006, d=0.4, E=3, μ =0.45 (0.18 0.76)**
β	F4–C4	U=399, p=0.875, d=0.04, E=0, μ =-0.07 (-0.45 0.36)	t(36.62)=0.29, p=0.938, d=0.08, E=0, μ =0.08 (-0.45 0.61)	**U=556, p=0.049, d=0.28, E=3, μ =0.47 (0.04 0.95)**	U=549, p=0.054, d=0.26, E=0, μ =0.46 (0.01 0.89)	**U=647, p=0.002, d=0.46, E=3, μ =0.49 (0.27 0.84)**
β	F3–C3	U=450, p=0.875, d=0.06, E=0, μ =0.12 (-0.4 0.63)	t(34.2)=0.96, p=0.915, d=0.25, E=0, μ =0.26 (-0.28 0.79)	**U=583, p=0.027, d=0.33, E=3, μ =0.63 (0.16 0.99)**	**U=596, p=0.031, d=0.36, E=3, μ =0.63 (0.2 1.08)**	**U=685, p10.001, d=0.54, E=3, μ =0.52 (0.28 0.78)**
β	F4–FZ	U=453, p=0.875, d=0.07, E=0, μ =0.1 (-0.29 0.68)	t(31.05)=0.58, p=0.915, d=0.15, E=0, μ =0.15 (-0.37 0.68)	t(35.97)=1.76, p=0.092, d=0.46, E=0, μ =0.45 (-0.06 0.96)	**U=598, p=0.031, d=0.36, E=3, μ =0.62 (0.19 1.07)**	**U=662, p=0.001, d=0.49, E=3, μ =0.49 (0.24 0.73)**
β	FZ–CZ	U=392, p=0.875, d=0.06, E=0, μ =-0.1 (-0.6 0.29)	t(36.67)=0.53, p=0.915, d=0.14, E=0, μ =0.14 (-0.39 0.67)	**U=563, p=0.042, d=0.29, E=3, μ =0.51 (0.06 0.98)**	t(37)=1.79, p=0.082, d=0.47, E=0, μ =0.46 (-0.05 0.98)	**U=597, p=0.009, d=0.36, E=3, μ =0.33 (0.09 0.64)**
β	F3–FZ	U=429, p=0.896, d=0.02, E=0, μ =0.02 (-0.47 0.4)	U=382, p=0.915, d=0.08, E=0, μ =-0.14 (-0.61 0.32)	t(36.26)=1.06, p=0.293, d=0.28, E=0, μ =0.28 (-0.25 0.81)	**U=574, p=0.031, d=0.31, E=3, μ =0.55 (0.12 1.03)**	**U=633, p=0.003, d=0.44, E=3, μ =0.47 (0.19 0.78)**
β	T4–C4	U=395, p=0.875, d=0.05, E=0, μ =-0.08 (-0.4 0.32)	U=428, p=0.949, d=0.02, E=0, μ =0.02 (-0.48 0.56)	U=544, p=0.069, d=0.25, E=0, μ =0.45 (-0.02 0.88)	U=561, p=0.038, d=0.29, E=2, μ =0.49 (0.05 0.92)	U=606, p=0.008, d=0.38, E=2, μ =0.33 (0.12 0.57)
β	T3–C3	U=397, p=0.875, d=0.05, E=0, μ =-0.1 (-0.5 0.42)	t(36.85)=-0.32, p=0.938, d=-0.08, E=0, μ =-0.08 (-0.61 0.44)	**U=568, p=0.039, d=0.3, E=3, μ =0.57 (0.1 1.08)**	U=578, p=0.031, d=0.32, E=2, μ =0.56 (0.11 1.02)	U=622, p=0.005, d=0.41, E=2, μ =0.51 (0.21 0.82)
β	C4–CZ	U=498, p=0.875, d=0.16, E=0, μ =0.29 (-0.18 0.7)	t(36.67)=0.12, p=0.949, d=0.03, E=0, μ =0.03 (-0.5 0.56)	U=506, p=0.193, d=0.18, E=0, μ =0.27 (-0.15 0.67)	t(35.68)=2.48, p=0.031, d=0.65, E=2, μ =0.63 (0.12 1.13)	U=615, p=0.006, d=0.4, E=2, μ =0.34 (0.12 0.6)
β	C3–CZ	U=394, p=0.875, d=0.05, E=0, μ =-0.12 (-0.55 0.43)	t(33.42)=0.04, p=0.969, d=0.01, E=0, μ =0.01 (-0.52 0.54)	U=588, p=0.027, d=0.34, E=2, μ =0.52 (0.16 0.9)	t(36.04)=2.71, p=0.031, d=0.71, E=2, μ =0.68 (0.18 1.18)	U=605, p=0.008, d=0.38, E=2, μ =0.41 (0.14 0.72)
β	CZ–PZ	U=492, p=0.875, d=0.15, E=0, μ =0.29 (-0.26 0.84)	t(36.82)=1.17, p=0.915, d=0.31, E=0, μ =0.31 (-0.22 0.83)	**U=624, p=0.012, d=0.42, E=3, μ =0.74 (0.31 1.14)**	**t(36.87)=2.57, p=0.031, d=0.68, E=3, μ =0.64 (0.14 1.15)**	**U=596, p=0.009, d=0.36, E=3, μ =0.39 (0.12 0.73)**
β	C4–P4	U=500, p=0.875, d=0.16, E=0, μ =0.28 (-0.17 0.72)	t(35.13)=2.54, p=0.324, d=0.66, E=0, μ =0.63 (0.13 1.13)	**U=663, p=0.002, d=0.5, E=3, μ =0.83 (0.48 1.33)**	U=611, p=0.03, d=0.39, E=2, μ =0.75 (0.25 1.24)	U=571, p=0.026, d=0.31, E=2, μ =0.42 (0.07 0.9)

β	C3–P3	U=464, p=0.875, d=0.09, E=0, μ =0.17 (-0.26 0.69)	t(36.94)=1.04, p=0.915, d=0.27, E=0, μ =0.27 (-0.25 0.8)	**U=612, p=0.012, d=0.39, E=3, μ =0.66 (0.23 1.09)**	**U=583, p=0.031, d=0.33, E=3, μ =0.68 (0.17 1.08)**	U=561, p=0.038, d=0.29, E=2, μ =0.4 (0.04 0.73)
β	T4–T6	U=352, p=0.875, d=0.14, E=0, μ =-0.19 (-0.65 0.19)	t(35.21)=0.85, p=0.915, d=0.22, E=0, μ =0.22 (-0.3 0.74)	**U=578, p=0.028, d=0.32, E=3, μ =0.64 (0.15 1.09)**	U=530, p=0.088, d=0.22, E=0, μ =0.4 (-0.1 0.89)	U=538, p=0.081, d=0.24, E=0, μ =0.22 (-0.01 0.49)
β	T3–T5	U=390, p=0.875, d=0.06, E=0, μ =-0.09 (-0.5 0.32)	t(33.73)=0.38, p=0.938, d=0.1, E=0, μ =0.1 (-0.43 0.63)	**U=567, p=0.039, d=0.3, E=3, μ =0.58 (0.09 1)**	U=569, p=0.031, d=0.3, E=2, μ =0.5 (0.07 1.01)	U=572, p=0.026, d=0.31, E=2, μ =0.34 (0.06 0.66)
β	P4–PZ	U=439, p=0.875, d=0.04, E=0, μ =0.09 (-0.37 0.63)	t(36.47)=0.63, p=0.915, d=0.17, E=0, μ =0.17 (-0.36 0.69)	**U=584, p=0.027, d=0.34, E=3, μ =0.59 (0.16 1.11)**	**U=576, p=0.031, d=0.32, E=3, μ =0.6 (0.11 1.09)**	**U=596, p=0.009, d=0.36, E=3, μ =0.48 (0.14 0.8)**
β	P3–PZ	U=471, p=0.875, d=0.1, E=0, μ =0.13 (-0.23 0.55)	U=464, p=0.915, d=0.09, E=0, μ =0.15 (-0.32 0.63)	**U=583, p=0.027, d=0.33, E=3, μ =0.7 (0.18 1.13)**	**U=570, p=0.031, d=0.31, E=3, μ =0.61 (0.13 1.09)**	**U=596, p=0.009, d=0.36, E=3, μ =0.37 (0.09 0.7)**
β	T6–O2	U=366, p=0.875, d=0.11, E=0, μ =-0.12 (-0.43 0.19)	U=428, p=0.949, d=0.02, E=0, μ =0.03 (-0.44 0.51)	**U=580, p=0.028, d=0.33, E=3, μ =0.63 (0.14 1.11)**	U=538, p=0.074, d=0.24, E=0, μ =0.31 (-0.06 0.69)	U=525, p=0.109, d=0.21, E=0, μ =0.16 (-0.04 0.4)
β	T5–O1	U=342, p=0.875, d=0.16, E=0, μ =-0.22 (-0.54 0.14)	t(26.1)=0.53, p=0.915, d=0.14, E=0, μ =0.14 (-0.38 0.66)	**U=618, p=0.012, d=0.4, E=3, μ =0.8 (0.29 1.25)**	U=539, p=0.074, d=0.24, E=0, μ =0.37 (-0.05 0.78)	U=535, p=0.086, d=0.23, E=0, μ =0.16 (-0.01 0.39)
β	P4–O2	U=403, p=0.875, d=0.03, E=0, μ =-0.04 (-0.43 0.32)	t(31.27)=1.27, p=0.915, d=0.33, E=0, μ =0.33 (-0.19 0.85)	**U=611, p=0.012, d=0.39, E=3, μ =0.77 (0.27 1.2)**	U=569, p=0.031, d=0.3, E=2, μ =0.45 (0.07 0.92)	U=526, p=0.109, d=0.22, E=0, μ =0.15 (-0.02 0.36)
β	P3–O1	U=368, p=0.875, d=0.11, E=0, μ =-0.17 (-0.53 0.26)	t(34.59)=1.2, p=0.915, d=0.31, E=0, μ =0.31 (-0.21 0.83)	**t(33.3)=2.18, p=0.049, d=0.58, E=3, μ =0.56 (0.05 1.07)**	U=550, p=0.054, d=0.27, E=0, μ =0.46 (0.02 0.94)	U=556, p=0.044, d=0.28, E=2, μ =0.23 (0.01 0.49)
β	O1–O2	U=409, p=0.896, d=0.02, E=0, μ =-0.06 (-0.51 0.42)	t(32.53)=1.47, p=0.915, d=0.38, E=0, μ =0.38 (-0.14 0.89)	t(36.64)=2.03, p=0.064, d=0.53, E=0, μ =0.52 (0.01 1.03)	**U=564, p=0.036, d=0.29, E=3, μ =0.55 (0.07 1.04)**	U=523, p=0.111, d=0.21, E=0, μ =0.16 (-0.04 0.49)
γ	F8–F4	U=508, p=0.815, d=0.18, E=0, μ =0.19 (-0.1 0.43)	U=505, p=0.546, d=0.17, E=0, μ =0.41 (-0.19 0.88)	U=613, p=0.009, d=0.39, E=2, μ =0.69 (0.27 1.14)	U=671, p=0.001, d=0.51, E=2, μ =0.7 (0.42 1)	U=579, p=0.042, d=0.32, E=2, μ =0.47 (0.12 0.81)
γ	F7–F3	U=500, p=0.815, d=0.16, E=0, μ =0.14 (-0.07 0.42)	U=529, p=0.351, d=0.22, E=0, μ =0.44 (-0.09 0.89)	U=603, p=0.011, d=0.37, E=2, μ =0.53 (0.16 0.89)	U=606, p=0.007, d=0.38, E=2, μ =0.41 (0.17 0.69)	U=609, p=0.029, d=0.39, E=2, μ =0.39 (0.12 0.62)
γ	F4–C4	U=496, p=0.815, d=0.16, E=0, μ =0.1 (-0.07 0.26)	U=518, p=0.427, d=0.2, E=0, μ =0.26 (-0.1 0.58)	**U=617, p=0.009, d=0.4, E=3, μ =0.59 (0.24 0.95)**	U=659, p=0.001, d=0.49, E=2, μ =0.38 (0.19 0.64)	U=604, p=0.029, d=0.38, E=2, μ =0.24 (0.08 0.42)
γ	F3–C3	U=495, p=0.815, d=0.15, E=0, μ =0.09 (-0.06 0.24)	U=546, p=0.231, d=0.26, E=0, μ =0.33 (0 0.71)	**U=656, p=0.004, d=0.48, E=3, μ =0.68 (0.33 1.01)**	U=683, pi0.001, d=0.54, E=2, μ =0.47 (0.27 0.71)	U=617, p=0.029, d=0.4, E=2, μ =0.26 (0.08 0.45)
γ	F4–FZ	U=552, p=0.815, d=0.27, E=0, μ =0.13 (0.01 0.27)	U=555, p=0.231, d=0.28, E=0, μ =0.3 (0.02 0.58)	**U=617, p=0.009, d=0.4, E=3, μ =0.56 (0.25 0.96)**	U=636, p=0.003, d=0.44, E=2, μ =0.37 (0.19 0.6)	U=591, p=0.035, d=0.35, E=2, μ =0.21 (0.06 0.37)
γ	FZ–CZ	U=517, p=0.815, d=0.2, E=0, μ =0.08 (-0.03 0.19)	U=549, p=0.231, d=0.26, E=0, μ =0.21 (0 0.45)	**U=571, p=0.035, d=0.31, E=3, μ =0.41 (0.07 0.64)**	U=629, p=0.003, d=0.43, E=2, μ =0.31 (0.14 0.53)	U=564, p=0.062, d=0.29, E=0, μ =0.12 (0.02 0.23)
γ	F3–FZ	U=520, p=0.815, d=0.2, E=0, μ =0.12 (-0.03 0.29)	U=556, p=0.231, d=0.28, E=0, μ =0.33 (0.03 0.61)	**U=617, p=0.009, d=0.4, E=3, μ =0.57 (0.23 0.88)**	U=649, p=0.001, d=0.47, E=2, μ =0.47 (0.21 0.71)	U=568, p=0.06, d=0.3, E=0, μ =0.21 (0.03 0.41)
γ	T4–C4	U=399, p=0.96, d=0.04, E=0, μ =-0.03 (-0.19 0.13)	U=418, p=0.982, d=0, E=0, μ =0 (-0.33 0.3)	**U=575, p=0.032, d=0.32, E=3, μ =0.29 (0.07 0.59)**	U=622, p=0.004, d=0.41, E=2, μ =0.28 (0.11 0.51)	U=540, p=0.12, d=0.25, E=0, μ =0.12 (-0.01 0.25)
γ	T3–C3	U=445, p=0.96, d=0.05, E=0, μ =0.03 (-0.16 0.23)	U=560, p=0.231, d=0.29, E=0, μ =0.35 (0.03 0.73)	U=605, p=0.011, d=0.38, E=2, μ =0.5 (0.18 0.96)	U=634, p=0.003, d=0.44, E=2, μ =0.51 (0.24 0.81)	U=590, p=0.035, d=0.35, E=2, μ =0.29 (0.08 0.49)
γ	C4–CZ	U=470, p=0.96, d=0.1, E=0, μ =0.05 (-0.07 0.18)	U=463, p=0.784, d=0.09, E=0, μ =0.08 (-0.21 0.31)	U=543, p=0.066, d=0.25, E=0, μ =0.32 (-0.01 0.63)	U=612, p=0.006, d=0.39, E=2, μ =0.33 (0.14 0.57)	U=562, p=0.062, d=0.29, E=0, μ =0.14 (0.02 0.27)
γ	C3–CZ	U=461, p=0.96, d=0.08, E=0, μ =0.04 (-0.08 0.14)	U=451, p=0.878, d=0.06, E=0, μ =0.09 (-0.22 0.4)	U=614, p=0.009, d=0.4, E=2, μ =0.52 (0.24 0.92)	U=613, p=0.006, d=0.39, E=2, μ =0.39 (0.15 0.68)	U=582, p=0.042, d=0.33, E=2, μ =0.15 (0.04 0.36)

γ	CZ–PZ	U=479, p=0.96, d=0.12, E=0, μ =0.05 (-0.07 0.19)	U=466, p=0.784, d=0.09, E=0, μ =0.12 (-0.26 0.48)	U=550, p=0.059, d=0.27, E=0, μ =0.4 (0.01 0.71)	U=594, p=0.012, d=0.36, E=2, μ =0.34 (0.11 0.65)	U=508, p=0.268, d=0.18, E=0, μ =0.07 (-0.03 0.19)
γ	C4–P4	U=439, p=0.96, d=0.04, E=0, μ =0.02 (-0.11 0.15)	U=492, p=0.616, d=0.15, E=0, μ =0.2 (-0.13 0.56)	U=542, p=0.066, d=0.25, E=0, μ =0.37 (-0.02 0.79)	U=584, p=0.018, d=0.34, E=2, μ =0.4 (0.1 0.78)	U=482, p=0.436, d=0.13, E=0, μ =0.12 (-0.14 0.41)
γ	C3–P3	U=440, p=0.96, d=0.04, E=0, μ =0.03 (-0.14 0.17)	U=477, p=0.676, d=0.12, E=0, μ =0.13 (-0.2 0.43)	U=557, p=0.05, d=0.28, E=0, μ =0.45 (0.04 0.77)	U=583, p=0.018, d=0.33, E=2, μ =0.44 (0.1 0.76)	U=505, p=0.273, d=0.17, E=0, μ =0.17 (-0.07 0.4)
γ	T4–T6	U=420, p=1, d=0, E=0, μ =0 (-0.22 0.15)	U=450, p=0.878, d=0.06, E=0, μ =0.06 (-0.19 0.32)	U=550, p=0.059, d=0.27, E=0, μ =0.3 (0.01 0.58)	U=547, p=0.062, d=0.26, E=0, μ =0.21 (0 0.43)	U=528, p=0.167, d=0.22, E=0, μ =0.1 (-0.03 0.23)
γ	T3–T5	U=428, p=0.994, d=0.02, E=0, μ =0.01 (-0.18 0.18)	U=484, p=0.638, d=0.13, E=0, μ =0.19 (-0.2 0.62)	U=568, p=0.037, d=0.3, E=2, μ =0.48 (0.07 0.9)	U=566, p=0.033, d=0.3, E=2, μ =0.31 (0.05 0.61)	U=541, p=0.12, d=0.25, E=0, μ =0.18 (-0.01 0.35)
γ	P4–PZ	U=434, p=0.96, d=0.03, E=0, μ =0.02 (-0.09 0.16)	U=424, p=0.982, d=0.01, E=0, μ =0.01 (-0.26 0.28)	U=541, p=0.066, d=0.25, E=0, μ =0.39 (-0.02 0.73)	U=561, p=0.038, d=0.29, E=2, μ =0.35 (0.05 0.65)	U=482, p=0.436, d=0.13, E=0, μ =0.08 (-0.07 0.22)
γ	P3–PZ	U=423, p=1, d=0.01, E=0, μ =0 (-0.1 0.11)	U=499, p=0.572, d=0.16, E=0, μ =0.17 (-0.12 0.48)	U=565, p=0.039, d=0.3, E=2, μ =0.56 (0.07 0.97)	U=581, p=0.018, d=0.33, E=2, μ =0.31 (0.06 0.62)	U=518, p=0.214, d=0.2, E=0, μ =0.08 (-0.02 0.2)
γ	T6–O2	U=403, p=0.96, d=0.03, E=0, μ =-0.02 (-0.15 0.09)	U=406, p=0.96, d=0.03, E=0, μ =-0.03 (-0.36 0.21)	U=543, p=0.066, d=0.25, E=0, μ =0.28 (-0.02 0.52)	U=524, p=0.116, d=0.21, E=0, μ =0.13 (-0.03 0.32)	U=450, p=0.678, d=0.06, E=0, μ =0.02 (-0.06 0.11)
γ	T5–O1	U=399, p=0.96, d=0.04, E=0, μ =-0.01 (-0.12 0.1)	U=401, p=0.938, d=0.04, E=0, μ =-0.04 (-0.25 0.18)	U=529, p=0.092, d=0.22, E=0, μ =0.22 (-0.03 0.47)	U=523, p=0.116, d=0.21, E=0, μ =0.13 (-0.04 0.35)	U=457, p=0.628, d=0.08, E=0, μ =0.02 (-0.06 0.11)
γ	P4–O2	U=368, p=0.96, d=0.11, E=0, μ =-0.04 (-0.14 0.05)	U=422, p=0.982, d=0, E=0, μ =0 (-0.18 0.19)	U=538, p=0.07, d=0.24, E=0, μ =0.27 (-0.01 0.53)	U=545, p=0.063, d=0.26, E=0, μ =0.15 (0 0.32)	U=464, p=0.576, d=0.09, E=0, μ =0.02 (-0.04 0.09)
γ	P3–O1	U=378, p=0.96, d=0.09, E=0, μ =-0.03 (-0.14 0.08)	U=483, p=0.638, d=0.13, E=0, μ =0.09 (-0.13 0.32)	U=582, p=0.028, d=0.33, E=2, μ =0.37 (0.09 0.65)	U=541, p=0.069, d=0.25, E=0, μ =0.17 (-0.01 0.41)	U=472, p=0.516, d=0.11, E=0, μ =0.03 (-0.06 0.12)
γ	O1–O2	U=399, p=0.96, d=0.04, E=0, μ =-0.01 (-0.11 0.08)	U=398, p=0.938, d=0.04, E=0, μ =-0.04 (-0.3 0.21)	U=580, p=0.028, d=0.33, E=2, μ =0.42 (0.1 0.72)	U=503, p=0.201, d=0.17, E=0, μ =0.11 (-0.06 0.35)	U=405, p=0.823, d=0.03, E=0, μ =-0.01 (-0.08 0.08)

Table A.15: Results from epoch 2 comparing unweighted edge betweenness. The results are reported as follows: statistics value (degrees of freedom), p-value of the test, Cohen's d effect size or nonparameteric alternative, number of thresholds where significant differences were observed (T), number of epochs where significant differences were observed (E), and group difference estimate (95% CI). Reliable differences (significant in all three epochs) are highlighted with bold text.

	δ	θ	α	β	γ
δ	U=507, p=0.18, d=0.18, T=5, E=0, μ = 0.3 (-0.14 0.63)	U=574, p=0.016, d=0.31, T=13, E=1, μ = 0.56 (0.09 0.96)	t(33.13)=3.63, p=0.001, d=0.95, T=19, E=2, μ = 0.86 (0.38 1.33)	**U=650, p¡0.001, d=0.47, T=18, E=3,** μ = 0.85 **(0.4 1.24)**	U=506, p=0.185, d=0.18, T=9, E=0, μ = 0.2 (-0.08 0.47)
θ	U=489, p=0.289, d=0.14, T=0, E=0, μ = 0.18 (-0.18 0.54)	U=498, p=0.23, d=0.16, T=0, E=0, μ = 0.28 (-0.17 0.72)	U=536, p=0.072, d=0.24, T=5, E=0, μ = 0.43 (-0.04 0.9)	U=570, p=0.019, d=0.31, T=19, E=1, μ = 0.51 (0.08 0.93)	U=549, p=0.045, d=0.26, T=11, E=1, μ = 0.33 (0.01 0.64)
α	U=569, p=0.02, d=0.3, T=20, E=1, μ = 0.34 (0.04 0.65)	U=539, p=0.065, d=0.24, T=8, E=0, μ = 0.44 (-0.01 0.82)	U=555, p=0.036, d=0.28, T=13, E=1, μ = 0.49 (0.03 0.93)	U=599, p=0.005, d=0.37, T=19, E=1, μ = 0.59 (0.16 1.01)	U=627, p=0.001, d=0.42, T=18, E=1, μ = 0.38 (0.16 0.58)
β	U=561, p=0.028, d=0.29, T=14, E=1, μ = 0.39 (0.04 0.72)	U=527, p=0.098, d=0.22, T=4, E=0, μ = 0.34 (-0.07 0.71)	U=541, p=0.06, d=0.25, T=6, E=0, μ = 0.41 (-0.01 0.79)	t(31.53)=2.25, p=0.029, d=0.59, T=15, E=1, μ = 0.56 (0.06 1.07)	U=572, p=0.018, d=0.31, T=16, E=1, μ = 0.31 (0.06 0.48)
γ	t(35.3)=-1, p=0.321, d=-0.26, T=6, E=0, μ = −0.26 (-0.79 0.26)	U=509, p=0.17, d=0.18, T=3, E=0, μ = 0.23 (-0.12 0.65)	U=569, p=0.02, d=0.3, T=15, E=2, μ = 0.35 (0.06 0.65)	U=559, p=0.03, d=0.28, T=15, E=1, μ = 0.28 (0.04 0.53)	U=488, p=0.296, d=0.14, T=1, E=0, μ = 0.23 (-0.24 0.71)

Table A.16: Results from epoch 2 comparing unweighted global vulnerability. The results are reported as follows: statistics value (degrees of freedom), p-value of the test, Cohen's d effect size or nonparameteric alternative, number of thresholds where significant differences were observed (T), number of epochs where significant differences were observed (E), and group difference estimate (95% CI). Reliable differences (significant in all three epochs) are highlighted with bold text.

	δ	θ	α	β	γ
δ	**t(27.5)=-4.11, p¡0.001, d=-1.07, T=19, E=3,** μ = −0.94**(-1.4 -0.48)**	**t(37)=-4.64, p¡0.001, d=-1.22, T=16, E=3,** μ = −1.04**(-1.49 -0.59)**	t(36.96)=-1.31, p=0.194, d=-0.35, T=3, E=0, μ = −0.34(-0.87 0.18)	t(33.86)=-1.24, p=0.219, d=-0.33, T=2, E=0, μ = −0.32(-0.84 0.2)	t(36.99)=-1.78, p=0.08, d=-0.47, T=8, E=0, μ = −0.46(-0.97 0.06)
θ	t(35.35)=1.21, p=0.232, d=0.32, T=4, E=0, μ = 0.32(-0.21 0.84)	U=315, p=0.104, d=0.21, T=1, E=0, μ = −0.35(-0.87 0.08)	U=492, p=0.268, d=0.15, T=0, E=0, μ = 0.18(-0.14 0.51)	U=348, p=0.268, d=0.15, T=0, E=0, μ = −0.23(-0.77 0.27)	U=344, p=0.242, d=0.16, T=2, E=0, μ = −0.22(-0.66 0.17)
α	U=505, p=0.19, d=0.17, T=7, E=0, μ = 0.35(-0.14 0.88)	t(35.45)=-1.09, p=0.281, d=-0.29, T=5, E=0, μ = −0.29(-0.81 0.24)	U=511, p=0.16, d=0.19, T=5, E=0, μ = 0.28(-0.13 0.62)	t(34.49)=-0.74, p=0.461, d=-0.2, T=0, E=0, μ = −0.2(-0.73 0.33)	U=386, p=0.605, d=0.07, T=0, E=0, μ = −0.13(-0.63 0.35)
β	t(30.07)=-1.04, p=0.301, d=-0.27, T=6, E=0, μ = −0.27(-0.79 0.25)	t(36.97)=-0.74, p=0.462, d=-0.19, T=0, E=0, μ = −0.19(-0.72 0.33)	U=453, p=0.616, d=0.07, T=1, E=0, μ = 0.03(-0.07 0.12)	t(34.58)=2.73, p=0.008, d=0.72, T=10, E=1, μ = 0.68(0.18 1.19)	t(37)=-2.34, p=0.023, d=-0.61, T=12, E=2, μ = −0.59(-1.1 -0.08)
γ	U=370, p=0.444, d=0.1, T=6, E=0, μ = −0.12(-0.51 0.21)	t(36.76)=0.65, p=0.516, d=0.17, T=0, E=0, μ = 0.17(-0.36 0.7)	U=456, p=0.583, d=0.07, T=1, E=0, μ = 0.13(-0.34 0.6)	**t(34.2)=-3.94, p¡0.001, d=-1.04, T=14, E=3,** μ = −0.93**(-1.4 -0.45)**	t(36.54)=-1.63, p=0.109, d=-0.43, T=7, E=0, μ = −0.42(-0.94 0.1)

Table A.17: Results from epoch 2 comparing unweighted local vulnerability. The results are reported as follows: statistics value (degrees of freedom), p-value of the test, Cohen's d effect size or nonparameteric alternative, number of thresholds where significant differences were observed (T), number of epochs where significant differences were observed (E), and group difference estimate (95% CI). Reliable differences (significant in all three epochs) are highlighted with bold text.

	δ	θ	α	β	γ
δ	U=247, p=0.007, d=0.35, T=14, E=1, $\mu = -0.67$ (-1.12 -0.16)	t(34.75)=-1.66, p=0.104, d=-0.44, T=6, E=0, $\mu = -0.43$ (-0.95 0.09)	t(36.84)=-0.99, p=0.325, d=-0.26, T=2, E=0, $\mu = -0.26$ (-0.78 0.26)	t(34.9)=-0.48, p=0.633, d=-0.13, T=0, E=0, $\mu = -0.13$ (-0.66 0.41)	U=375, p=0.492, d=0.09, T=0, E=0, $\mu = -0.17$ (-0.67 0.29)
θ	t(34.18)=-1.47, p=0.148, d=-0.38, T=4, E=0, $\mu = -0.38$ (-0.89 0.14)	U=365, p=0.399, d=0.11, T=0, E=0, $\mu = -0.18$ (-0.79 0.24)	t(34.46)=0.86, p=0.392, d=0.23, T=1, E=0, $\mu = 0.23$ (-0.3 0.76)	t(36.55)=-0.72, p=0.476, d=-0.19, T=0, E=0, $\mu = -0.19$ (-0.71 0.34)	t(32.79)=-1.08, p=0.286, d=-0.28, T=2, E=0, $\mu = -0.28$ (-0.8 0.24)
α	t(34.6)=-1.41, p=0.164, d=-0.37, T=5, E=0, $\mu = -0.36$ (-0.88 0.15)	t(28.77)=-1.36, p=0.18, d=-0.36, T=3, E=0, $\mu = -0.36$ (-0.89 0.17)	U=520, p=0.122, d=0.2, T=7, E=0, $\mu = 0.43$ (-0.13 0.95)	t(33.16)=1.35, p=0.182, d=0.35, T=6, E=0, $\mu = 0.35$ (-0.17 0.87)	t(36.83)=-1.74, p=0.088, d=-0.46, T=4, E=0, $\mu = -0.45$ (-0.96 0.07)
β	t(35.19)=-2.09, p=0.042, d=-0.55, T=10, E=1, $\mu = -0.53$ (-1.05 -0.02)	U=529, p=0.092, d=0.22, T=6, E=0, $\mu = 0.35$ (-0.07 0.83)	t(36.22)=2.16, p=0.035, d=0.57, T=11, E=1, $\mu = 0.55$ (0.04 1.06)	U=617, p=0.002, d=0.4, T=12, E=1, $\mu = 0.66$ (0.23 1.1)	t(36.56)=-1.08, p=0.283, d=-0.28, T=4, E=0, $\mu = -0.28$ (-0.81 0.24)
γ	U=307, p=0.08, d=0.23, T=9, E=0, $\mu = -0.36$ (-0.76 0.03)	U=320, p=0.122, d=0.2, T=0, E=0, $\mu = -0.36$ (-0.8 0.08)	U=304, p=0.072, d=0.24, T=6, E=0, $\mu = -0.39$ (-0.81 0.04)	t(36.12)=-1.94, p=0.058, d=-0.51, T=8, E=0, $\mu = -0.49$ (-1.01 0.02)	**U=662, p¡0.001, d=0.49, T=19, E=3,** $\mu = 0.25$ **(0.12 0.43)**

Table A.18: Results from epoch 2 comparing weighted edge betweenness. The results are reported as follows: statistics value (degrees of freedom), p-value of the test, Cohen's d effect size or nonparameteric alternative, number of thresholds where significant differences were observed (T), number of epochs where significant differences were observed (E), and group difference estimate (95% CI). Reliable differences (significant in all three epochs) are highlighted with bold text.

	δ	θ	α	β	γ
δ	**U=608, p¡0.001, d=0.47, T=20, E=3,** $\mu = 0$ **(0 0.01)**	**U=618, p¡0.001, d=0.49, T=14, E=3,** $\mu = 0.03$ **(0 0.14)**	**U=681.5, p¡0.001, d=0.55, T=19, E=3,** $\mu = 0.45$ **(0.21 0.91)**	**U=671, p¡0.001, d=0.51, T=18, E=3,** $\mu = 0.25$ **(0.14 0.55)**	**U=639, p¡0.001, d=0.45, T=19, E=3,** $\mu = 0.95$ **(0.38 1.38)**
θ	**U=683.5, p¡0.001, d=0.54, T=10, E=3,** $\mu = 0.56$ **(0.3 1)**	**U=556.5, p=0.003, d=0.39, T=10, E=3,** $\mu = 0$ **(0 0)**	U=448, p=0.176, d=0.18, T=4, E=0, $\mu = 0$ (0 0)	U=478.5, p=0.367, d=0.12, T=1, E=0, $\mu = 0.07$ (-0.02 0.24)	U=480, p=0.357, d=0.12, T=1, E=0, $\mu = 0.13$ (-0.2 0.38)
α	U=504.5, p=0.065, d=0.24, T=10, E=2, $\mu = 0$ (0 0)	U=461, p=0.265, d=0.15, T=1, E=0, $\mu = 0$ (0 0)	U=458, p=0.354, d=0.12, T=0, E=0, $\mu = 0$ (0 0)	U=442, p=0.738, d=0.04, T=2, E=0, $\mu = 0.03$ (-0.15 0.27)	U=350, p=0.282, d=0.14, T=1, E=0, $\mu = -0.14$ (-0.44 0.15)
β	**U=686, p¡0.001, d=0.54, T=19, E=3,** $\mu = 0.71$ **(0.36 1.13)**	t(36.24)=0.53, p=0.6, d=0.14, T=0, E=0, $\mu = 0.14$ (-0.39 0.67)	U=389.5, p=0.51, d=0.09, T=0, E=0, $\mu = 0$ (0 0)	U=455, p=0.589, d=0.07, T=0, E=0, $\mu = 0$ (-0.02 0.04)	**U=176, p¡0.001, d=0.5, T=18, E=3,** $\mu = -0.77$ **(-1.13 -0.28)**
γ	**U=628, p=0.001, d=0.42, T=18, E=3,** $\mu = 1.05$ **(0.45 1.45)**	U=354, p=0.311, d=0.13, T=6, E=0, $\mu = -0.23$ (-0.7 0.18)	U=381, p=0.552, d=0.08, T=1, E=0, $\mu = -0.05$ (-0.22 0.12)	**U=207, p=0.001, d=0.44, T=14, E=3,** $\mu = -0.65$ **(-1.04 -0.27)**	**t(32)=-3.69, p=0.001, d=-0.96, T=17, E=3,** $\mu = -0.87$ **(-1.34 -0.4)**

Table A.19: Results from epoch 2 comparing weighted global vulnerability. The results are reported as follows: statistics value (degrees of freedom), p-value of the test, Cohen's d effect size or nonparameteric alternative, number of thresholds where significant differences were observed (T), number of epochs where significant diffferences were observed (E), group difference estimate (95% CI). Reliable differences (significant in all three epochs) are highlighted with bold text.

	δ	θ	α	β	γ
δ	U=389, p=0.638, d=0.06, T=3, E=0, μ = 0 (0 0)	U=387, p=0.616, d=0.07, T=2, E=0, μ = 0 (0 0)	U=467, p=0.472, d=0.1, T=3, E=0, μ = 0 (0 0)	**U=645, p¡0.001, d=0.46, T=19, E=3,** μ = 0.19 **(0.06 0.48)**	t(36.04)=1.44, p=0.154, d=0.38, T=2, E=0, μ = 0.37 (-0.14 0.89)
θ	U=377, p=0.511, d=0.09, T=3, E=0, μ = 0 (0 0)	U=483, p=0.333, d=0.13, T=0, E=0, μ = 0 (0 0.17)	U=388, p=0.627, d=0.07, T=0, E=0, μ = 0 (0 0)	U=386, p=0.605, d=0.07, T=0, E=0, μ = −0.01 (-0.06 0.03)	U=475, p=0.399, d=0.11, T=0, E=0, μ = 0.22 (-0.31 0.74)
α	U=483, p=0.333, d=0.13, T=5, E=0, μ = 0 (0 0)	U=388, p=0.627, d=0.07, T=0, E=0, μ = 0 (0 0)	U=400, p=0.763, d=0.04, T=0, E=0, μ = 0 (0 0)	U=388, p=0.627, d=0.07, T=0, E=0, μ = 0 (0 0)	U=355, p=0.318, d=0.13, T=2, E=0, μ = −0.22 (-0.74 0.3)
β	**U=644, p¡0.001, d=0.46, T=10, E=3,** μ = 0.4 **(0.03 0.62)**	U=379, p=0.531, d=0.08, T=0, E=0, μ = 0 (0 0)	U=459, p=0.552, d=0.08, T=0, E=0, μ = 0 (0 0)	U=458, p=0.562, d=0.08, T=2, E=0, μ = 0 (0 0)	**U=176, p¡0.001, d=0.5, T=18, E=3,** μ = −0.64 **(-0.96 -0.3)**
γ	U=532, p=0.083, d=0.23, T=4, E=0, μ = 0.35 (-0.03 0.83)	U=446, p=0.694, d=0.05, T=0, E=0, μ = 0.13 (-0.28 0.6)	U=396, p=0.717, d=0.05, T=0, E=0, μ = −0.08 (-0.51 0.28)	**t(35.65)=-3.68, p=0.001, d=-0.96, T=20, E=3,** μ = −0.87 **(-1.34 -0.4)**	**U=185, p¡0.001, d=0.48, T=18, E=3,** μ = −0.96 **(-1.5 -0.38)**

Table A.20: Results from epoch 2 comparing weighted local vulnerability. The results are reported as follows: statistics value (degrees of freedom), p-value of the test, Cohen's d effect size or nonparameteric alternative, number of thresholds where significant differences were observed (T), number of epochs where significant differences were observed (E), and group difference estimate (95% CI). Reliable differences (significant in all three epochs) are highlighted with bold text.

	δ	θ	α	β	γ
δ	**U=644, p¡0.001, d=0.46, T=17, E=3,** μ = 0.79 **(0.36 1.22)**	**U=657, p¡0.001, d=0.48, T=18, E=3,** μ = 0.86 **(0.46 1.29)**	**U=213, p=0.001, d=0.42, T=14, E=3,** μ = −0.76 **(-1.13 -0.39)**	**U=176, p¡0.001, d=0.5, T=14, E=3,** μ = −0.7 **(-0.97 -0.4)**	U=456, p=0.583, d=0.07, T=0, E=0, μ = 0.1 (-0.28 0.47)
θ	**t(28.75)=3.75, p¡0.001, d=0.98, T=19, E=3,** μ = 0.88 **(0.41 1.35)**	**t(36.76)=3.51, p=0.001, d=0.92, T=15, E=3,** μ = 0.84 **(0.36 1.32)**	U=263, p=0.014, d=0.32, T=12, E=2, μ = −0.57 (-0.91 -0.13)	**t(33.55)=-5.08, p¡0.001, d=-1.34, T=16, E=3,** μ = −1.12 **(-1.56 -0.68)**	U=349, p=0.275, d=0.15, T=0, E=0, μ = −0.15 (-0.46 0.13)
α	**t(36.95)=3.9, p¡0.001, d=1.02, T=19, E=3,** μ = 0.92 **(0.45 1.38)**	**t(34.18)=3.25, p=0.002, d=0.86, T=14, E=3,** μ = 0.79 **(0.3 1.28)**	**U=212, p=0.001, d=0.42, T=14, E=3,** μ = −0.82 **(-1.29 -0.34)**	**t(28.29)=-5.33, p¡0.001, d=-1.41, T=15, E=3,** μ = −1.16 **(-1.6 -0.72)**	U=349, p=0.275, d=0.15, T=5, E=0, μ = −0.21 (-0.62 0.14)
β	**t(33.58)=3.73, p¡0.001, d=0.97, T=18, E=3,** μ = 0.88 **(0.41 1.35)**	**U=610, p=0.003, d=0.39, T=11, E=3,** μ = 0.7 **(0.24 1.19)**	U=271, p=0.02, d=0.3, T=12, E=1, μ = −0.5 (-0.84 -0.07)	**U=177, p¡0.001, d=0.5, T=14, E=3,** μ = −0.87 **(-1.24 -0.51)**	U=320, p=0.122, d=0.2, T=6, E=0, μ = −0.26 (-0.59 0.05)
γ	U=547, p=0.048, d=0.26, T=10, E=1, μ = 0.48 (0 1.06)	t(32.94)=1.24, p=0.222, d=0.33, T=4, E=0, μ = 0.33 (-0.2 0.85)	t(33.97)=-0.65, p=0.521, d=-0.17, T=0, E=0, μ = −0.17 (-0.69 0.36)	**t(32.39)=-3.72, p¡0.001, d=-0.98, T=16, E=3,** μ = −0.89 **(-1.37 -0.41)**	**t(35.36)=-3.19, p=0.002, d=-0.83, T=11, E=3,** μ = −0.77 **(-1.26 -0.29)**

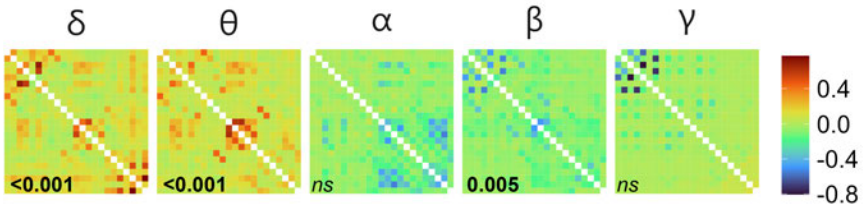

Figure A.12: Difference of average connectivity matrices (AD − HC) measured with CS in epoch 3. For visualisation purposes, the values were min-max normalised. Digits in black denote a p-value testing for the difference in global coupling ($p < 0.05$ in bold, in italics otherwise).

A.4 Results for epoch 3

In this section, we only report the results of the statistical comparisons and corresponding figures using data from the third epoch.

The comparisons of average coupling computed with CS and CBS are shown in Tables A.21 and A.22, respectively. Additionally, the corresponding figures of connectivity matrices computed with CS and CBS are shown in Figures A.12 and A.13.

The comparisons of node strength computed with CS and CBS are shown in Table A.23 and Figure A.14, and Table A.24 and Figure A.15, respectively.

Results of comparisons of the unweighted multilayer network metrics are reported in Tables A.25, A.26 and A.27 for edge betweenness, global vulnerability and local vulnerability, respectively. The corresponding figures are; edge betweenness (Figure A.16), global vulnerability (Figure A.17) and local vulnerability (Figure A.18).

Results of comparisons of the weighted multilayer network metrics are reported in Tables A.28, A.29 and A.30 for edge betweenness, global vulnerability and local vulnerability, respectively. The corresponding figures are; edge betweenness (Figure A.19), global vulnerability (Figure A.20) and local vulnerability (Figure A.21).

Table A.21: Comparisons of the mean of adjacency matrix constructed with CS in epoch 3. The results are reported as follows: statistics value (degrees of freedom), p-value of the test, Cohen's d effect size (or nonparametric alternative), number of epochs where significant differences were observed (E), difference estimate μ with 95% confidence interval. Reliable differences (significant in all three epochs) are highlighted with bold text.

Frequency band	Test	Difference estimate (95% CI)
α	t(34.87)=-2.12, p=0.049, d=-0.55, E=1	μ = −0.54 (-1.04 -0.03)
β	**U=231, p=0.005, d=0.39, E=3**	μ = −0.72 (-1.19 -0.2)
δ	**t(34.62)=4.82, p¡0.001, d=1.26, E=3**	μ = 1.07 (0.62 1.51)
γ	U=355, p=0.318, d=0.13, E=0	μ = −0.27 (-0.85 0.31)
θ	**t(32.41)=4.93, p¡0.001, d=1.3, E=3**	μ = 1.1 (0.65 1.54)

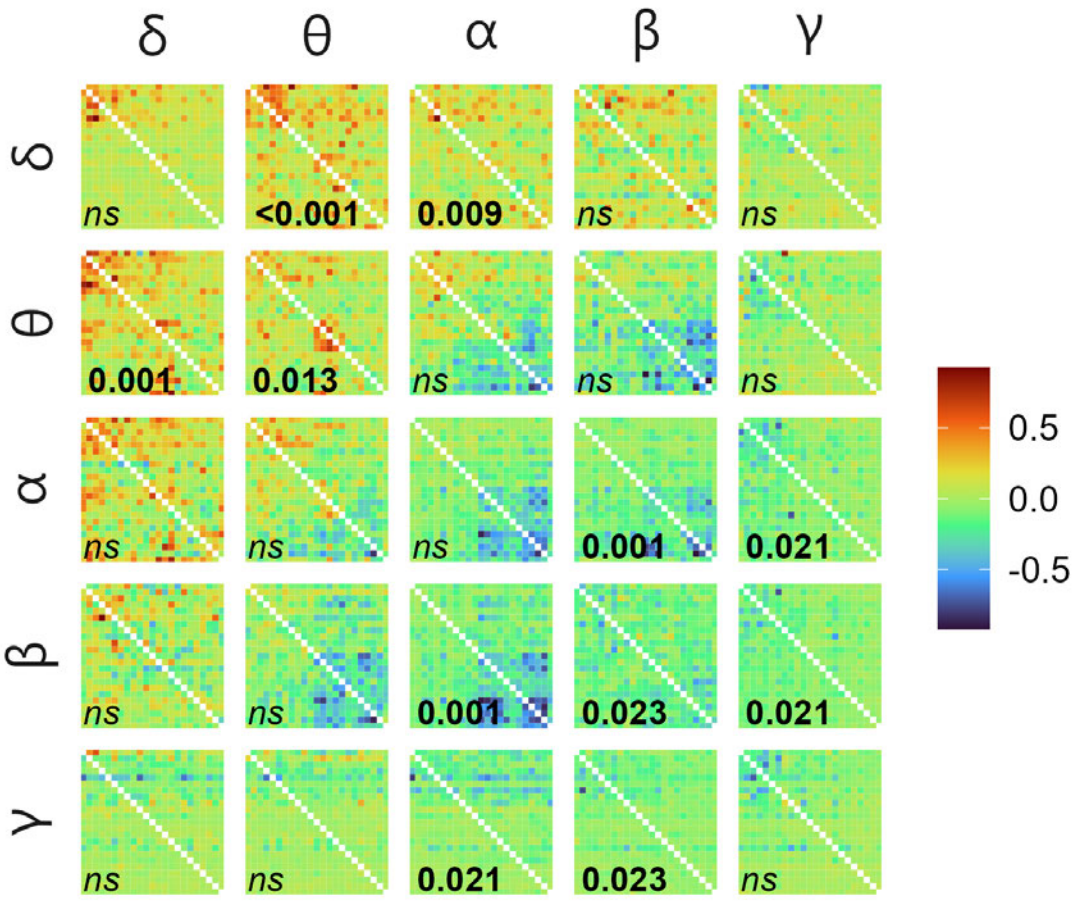

Figure A.13: Difference of average connectivity matrices (AD − HC) measured with CBS in epoch 3 with input frequency on the vertical facets and output frequency on the horizontal. For visualisation purposes, the values were min-max normalised. Digits in white denote a p-value testing for the difference in global coupling ($p < 0.05$ in bold, in italics otherwise).

	δ	θ	α	β	γ
δ	t(36.7)=3.5, p=0.005, d=0.92, E=2, μ =0.84(0.36 1.32)	**t(36.86)=4.74, p¡0.001, d=1.24, E=3, μ =1.06(0.61 1.51)**	**t(32.33)=3.21, p=0.009, d=0.84, E=3, μ =0.77(0.29 1.26)**	t(35.67)=0.47, p=0.763, d=0.12, E=0, μ =0.12(-0.4 0.65)	U=435, p=0.857, d=0.03, E=0, μ =0.04(-0.52 0.51)
θ	**t(36.75)=3.97, p=0.001, d=1.04, E=3, μ =0.93(0.46 1.4)**	**t(36.48)=3.03, p=0.013, d=0.8, E=3, μ =0.74(0.25 1.24)**	t(34.96)=0.4, p=0.783, d=0.11, E=1, μ =0.11(-0.42 0.63)	t(30.99)=-2.9, p=0.017, d=-0.76, E=1, μ =−0.71(-1.2 -0.22)	U=376, p=0.626, d=0.09, E=1, μ =−0.17(-0.66 0.29)
α	t(36.28)=2.49, p=0.026, d=0.65, E=2, μ =0.62(0.12 1.12)	t(36.75)=0.8, p=0.559, d=0.21, E=1, μ =0.21(-0.31 0.74)	t(36.79)=-2.57, p=0.023, d=-0.67, E=1, μ =−0.64(-1.14 -0.14)	**t(37)=-4.15, p=0.001, d=-1.09, E=3, μ =−0.96(-1.42 -0.5)**	**t(36.81)=-2.72, p=0.021, d=-0.71, E=3, μ =−0.68(-1.17 -0.18)**
β	t(33.54)=-0.09, p=0.928, d=-0.02, E=0, μ =−0.02(-0.55 0.5)	t(29.57)=-2.26, p=0.044, d=-0.59, E=1, μ =−0.57(-1.07 -0.06)	**t(37)=-4.04, p=0.001, d=-1.06, E=3, μ =−0.94(-1.41 -0.47)**	**t(36.54)=-2.63, p=0.023, d=-0.69, E=3, μ =−0.66(-1.16 -0.16)**	**t(36.29)=-2.77, p=0.021, d=-0.72, E=3, μ =−0.68(-1.18 -0.19)**
γ	U=399, p=0.817, d=0.04, E=0, μ =−0.07(-0.63 0.37)	t(36.58)=-1.13, p=0.368, d=-0.3, E=0, μ =−0.29(-0.82 0.23)	**t(36.98)=-2.69, p=0.021, d=-0.71, E=3, μ =−0.67(-1.17 -0.17)**	**t(35.97)=-2.58, p=0.023, d=-0.68, E=3, μ =−0.64(-1.14 -0.14)**	U=313, p=0.144, d=0.22, E=1, μ =−0.39(-0.91 0.08)

Table A.22: Comparisons of the mean of adjacency matrix constructed with CBS in epoch 3. The results are reported as follows: statistics value (degrees of freedom), p-value of the test, Cohen's d effect size (or nonparametric alternative), number of epochs where significant differences were observed (E), difference estimate μ with 95% confidence interval. Reliable differences (significant in all three epochs) are highlighted with bold text.

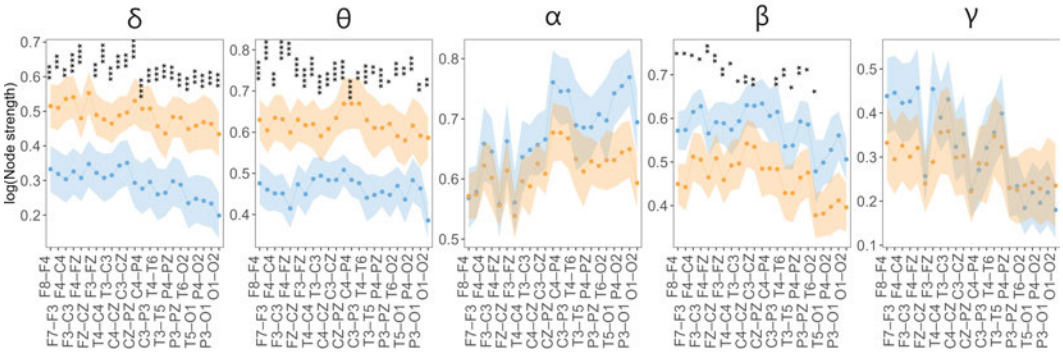

Figure A.14: Node strength (min-max normalised) measured with CS in epoch 3 of HC (blue) and AD (orange): mean with 95% confidence intervals. Significant differences ($p \leq 0.05$) observed in at least ten thresholded networks are encoded by asterisks. The number of asterisks corresponds to the p-value (FDR corrected), i.e. $p \leq 0.0001$ "****", $p \leq 0.001$ "***", $p \leq 0.01$ "**", and $p \leq 0.05$ "*".

Table A.23: Comparisons of node strength measured with CS in epoch 3. The results are reported as follows: statistics value (degrees of freedom), p-value of the test, Cohen's d effect size (or nonparametric alternative), number of epochs where significant differences were observed (E), and difference estimate μ with 95% confidence interval (CI). Reliable differences (significant in all three epochs) are highlighted with bold text.

channel	δ	θ	α	β	γ
F8–F4	t(36.96)=-4.06, p<0.001, d=-1.07, E=3, $\mu = -0.94$ (-1.41 -0.48)	t(36.99)=-4.51, p<0.001, d=-1.18, E=3, $\mu = -1.02$ (-1.48 -0.57)	**t(33.69)=-0.12, p=0.947, d=-0.03, E=0,** $\mu = -0.03$ **(-0.56 0.49)**	t(36.56)=4, p=0.004, d=1.05, E=3, $\mu = 0.94$ (0.47 1.4)	**t(37)=1.81, p=0.347, d=0.48, E=0,** $\mu = 0.47$ **(-0.05 0.98)**
F7–F3	t(36.99)=-4.21, p<0.001, d=-1.11, E=3, $\mu = -0.97$ (-1.43 -0.51)	t(36.67)=-3.91, p<0.001, d=-1.03, E=3, $\mu = -0.92$ (-1.39 -0.45)	**t(36.71)=0.15, p=0.947, d=0.04, E=0,** $\mu = 0.04$ **(-0.49 0.57)**	t(35.89)=3.78, p=0.004, d=0.99, E=3, $\mu = 0.9$ (0.42 1.37)	**t(36.95)=2.67, p=0.115, d=0.7, E=0,** $\mu = 0.66$ **(0.17 1.16)**
F4–C4	t(36.95)=-5.09, p<0.001, d=-1.34, E=3, $\mu = -1.11$ (-1.55 -0.68)	t(32.04)=-5.41, p<0.001, d=-1.43, E=3, $\mu = -1.17$ (-1.6 -0.73)	**t(30.83)=1, p=0.39, d=0.26, E=0,** $\mu = 0.26$ **(-0.26 0.78)**	U=563, p=0.027, d=0.29, E=3, $\mu = 0.6$ (0.06 1.17)	**t(36.63)=1.65, p=0.399, d=0.43, E=0,** $\mu = 0.43$ **(-0.09 0.94)**
F3–C3	**t(36.75)=-4.88, p¡0.001, d=-1.28, E=2,** $\mu = -1.08$ **(-1.52 -0.64)**	t(34.72)=-4.9, p<0.001, d=-1.29, E=3, $\mu = -1.09$ (-1.54 -0.64)	**t(36.93)=1.18, p=0.349, d=0.31, E=0,** $\mu = 0.31$ **(-0.21 0.83)**	U=608, p=0.008, d=0.38, E=3, $\mu = 0.74$ (0.21 1.17)	**U=536, p=0.347, d=0.24, E=0,** $\mu = 0.5$ **(-0.04 1.11)**
F4–FZ	t(36.65)=-3.93, p<0.001, d=-1.03, E=3, $\mu = -0.92$ (-1.39 -0.45)	t(36.94)=-5.59, p<0.001, d=-1.47, E=3, $\mu = -1.19$ (-1.61 -0.76)	**t(29.33)=0.07, p=0.947, d=0.02, E=0,** $\mu = 0.02$ **(-0.51 0.54)**	t(37)=2.88, p=0.01, d=0.76, E=3, $\mu = 0.71$ (0.22 1.21)	**t(36.59)=2.35, p=0.171, d=0.62, E=0,** $\mu = 0.59$ **(0.09 1.1)**
FZ–CZ	t(36.56)=-4.7, p<0.001, d=-1.23, E=3, $\mu = -1.05$ (-1.5 -0.6)	t(36.28)=-4.48, p<0.001, d=-1.18, E=3, $\mu = -1.02$ (-1.48 -0.56)	**t(34.16)=1.25, p=0.333, d=0.33, E=0,** $\mu = 0.32$ **(-0.2 0.84)**	**t(33.61)=2.31, p=0.027, d=0.61, E=2,** $\mu = 0.59$ **(0.08 1.1)**	**U=450, p=0.967, d=0.06, E=0,** $\mu = 0.11$ **(-0.5 0.62)**
F3–FZ	t(36.98)=-3.91, p<0.001, d=-1.03, E=3, $\mu = -0.92$ (-1.39 -0.45)	t(36.52)=-4.93, p<0.001, d=-1.29, E=3, $\mu = -1.09$ (-1.53 -0.65)	**t(32.14)=0.71, p=0.554, d=0.19, E=0,** $\mu = 0.18$ **(-0.34 0.71)**	t(35.75)=3.62, p=0.004, d=0.95, E=3, $\mu = 0.87$ (0.39 1.35)	**t(35.6)=2.92, p=0.115, d=0.76, E=0,** $\mu = 0.72$ **(0.22 1.21)**
T4–C4	t(34.8)=-3.92, p<0.001, d=-1.02, E=3, $\mu = -0.91$ (-1.38 -0.45)	t(35.28)=-3.45, p=0.001, d=-0.91, E=3, $\mu = -0.83$ (-1.32 -0.35)	**t(31.06)=1.12, p=0.363, d=0.29, E=0,** $\mu = 0.29$ **(-0.23 0.81)**	**t(36.97)=2.06, p=0.044, d=0.54, E=2,** $\mu = 0.53$ **(0.02 1.04)**	**t(34.44)=0.57, p=0.964, d=0.15, E=0,** $\mu = 0.15$ **(-0.38 0.68)**
T3–C3	t(36.63)=-3.51, p=0.001, d=-0.92, E=3, $\mu = -0.84$ (-1.32 -0.36)	t(31.13)=-2.55, p=0.014, d=-0.67, E=3, $\mu = -0.64$ (-1.15 -0.14)	**t(34.74)=1.9, p=0.131, d=0.5, E=0,** $\mu = 0.49$ **(-0.03 1.01)**	t(35.43)=2.63, p=0.016, d=0.69, E=3, $\mu = 0.66$ (0.16 1.16)	**U=485, p=0.914, d=0.13, E=0,** $\mu = 0.31$ **(-0.3 0.87)**
C4–CZ	t(35.21)=-3.41, p=0.001, d=-0.89, E=3, $\mu = -0.82$ (-1.3 -0.34)	t(34.33)=-3.79, p=0.001, d=-1, E=3, $\mu = -0.9$ (-1.38 -0.42)	**t(31.98)=1.02, p=0.39, d=0.27, E=0,** $\mu = 0.27$ **(-0.25 0.79)**	t(34.91)=2.53, p=0.018, d=0.67, E=3, $\mu = 0.64$ (0.13 1.14)	**U=458, p=0.964, d=0.08, E=0,** $\mu = 0.12$ **(-0.38 0.57)**
C3–CZ	t(32.98)=-3.64, p=0.001, d=-0.95, E=3, $\mu = -0.86$ (-1.33 -0.38)	t(36.99)=-4.57, p<0.001, d=-1.2, E=3, $\mu = -1.03$ (-1.49 -0.58)	**t(31.5)=1.94, p=0.131, d=0.51, E=0,** $\mu = 0.49$ **(-0.02 1)**	t(36.31)=2.55, p=0.017, d=0.67, E=3, $\mu = 0.64$ (0.14 1.14)	**U=477, p=0.964, d=0.12, E=0,** $\mu = 0.23$ **(-0.33 0.7)**
CZ–PZ	U=151, p<0.001, d=0.55, E=3, $\mu = -1.17$ (-1.66 -0.66)	t(24.48)=-4.39, p<0.001, d=-1.16, E=3, $\mu = -1.02$ (-1.48 -0.55)	**t(36.9)=2.35, p=0.073, d=0.62, E=0,** $\mu = 0.59$ **(0.09 1.1)**	t(35.42)=3.54, p=0.004, d=0.93, E=3, $\mu = 0.85$ (0.37 1.33)	**U=441, p=0.967, d=0.04, E=0,** $\mu = 0.07$ **(-0.46 0.53)**
C4–P4	U=156, p<0.001, d=0.54, E=3, $\mu = -1.18$ (-1.68 -0.67)	U=141, p<0.001, d=0.57, E=3, $\mu = -1.24$ (-1.65 -0.72)	**t(35.22)=1.94, p=0.131, d=0.51, E=0,** $\mu = 0.49$ **(-0.02 1)**	t(36.99)=2.89, p=0.01, d=0.76, E=3, $\mu = 0.71$ (0.22 1.21)	**U=403, p=0.967, d=0.03, E=0,** $\mu = -0.06$ **(-0.7 0.43)**
C3–P3	U=181, p<0.001, d=0.49, E=3, $\mu = -1.11$ (-1.64 -0.6)	t(28.76)=-5.3, p<0.001, d=-1.4, E=3, $\mu = -1.16$ (-1.6 -0.72)	**t(36.97)=2.2, p=0.093, d=0.58, E=0,** $\mu = 0.56$ **(0.05 1.06)**	t(36.91)=2.91, p=0.01, d=0.77, E=3, $\mu = 0.72$ (0.22 1.21)	**U=457, p=0.964, d=0.08, E=0,** $\mu = 0.13$ **(-0.43 0.66)**
T4–T6	t(35.96)=-4.11, p<0.001, d=-1.08, E=3, $\mu = -0.95$ (-1.41 -0.49)	t(34.59)=-4.35, p<0.001, d=-1.15, E=3, $\mu = -1$ (-1.46 -0.54)	**U=522, p=0.189, d=0.21, E=0,** $\mu = 0.4$ **(-0.09 0.98)**	**t(35.39)=2.7, p=0.014, d=0.71, E=1,** $\mu = 0.68$ **(0.18 1.18)**	**t(34.98)=0.15, p=0.967, d=0.04, E=0,** $\mu = 0.04$ **(-0.49 0.57)**
T3–T5	t(36.16)=-3.5, p=0.001, d=-0.92, E=3, $\mu = -0.84$ (-1.32 -0.36)	t(28.56)=-3.72, p=0.001, d=-0.98, E=3, $\mu = -0.89$ (-1.37 -0.41)	**t(36.99)=1.78, p=0.143, d=0.47, E=0,** $\mu = 0.46$ **(-0.06 0.97)**	t(34.46)=2.58, p=0.017, d=0.68, E=3, $\mu = 0.65$ (0.14 1.15)	**U=510, p=0.542, d=0.18, E=0,** $\mu = 0.34$ **(-0.18 0.9)**
P4–PZ	t(35.71)=-4.11, p<0.001, d=-1.07, E=3, $\mu = -0.95$ (-1.41 -0.49)	t(29.73)=-4.98, p<0.001, d=-1.31, E=3, $\mu = -1.11$ (-1.55 -0.66)	**t(34.46)=1.84, p=0.137, d=0.48, E=0,** $\mu = 0.47$ **(-0.04 0.98)**	t(34.29)=3.48, p=0.004, d=0.92, E=3, $\mu = 0.84$ (0.36 1.32)	**U=421, p=0.994, d=0, E=0,** $\mu = 0.01$ **(-0.54 0.51)**
P3–PZ	t(35.74)=-4.39, p<0.001, d=-1.15, E=3, $\mu = -1$ (-1.45 -0.54)	t(36.97)=-4.71, p<0.001, d=-1.23, E=3, $\mu = -1.05$ (-1.5 -0.61)	**t(36.15)=3.03, p=0.017, d=0.79, E=1,** $\mu = 0.74$ **(0.25 1.23)**	t(35.82)=2.98, p=0.01, d=0.78, E=3, $\mu = 0.73$ (0.24 1.23)	**U=440, p=0.967, d=0.04, E=0,** $\mu = 0.09$ **(-0.39 0.53)**
T6–O2	U=179, p<0.001, d=0.49, E=3, $\mu = -1.18$ (-1.58 -0.66)	t(30.88)=-3.19, p=0.003, d=-0.85, E=3, $\mu = -0.79$ (-1.29 -0.29)	**U=570, p=0.073, d=0.31, E=0,** $\mu = 0.55$ **(0.09 1.02)**	**t(32.84)=2.29, p=0.027, d=0.6, E=1,** $\mu = 0.57$ **(0.07 1.08)**	**U=369, p=0.964, d=0.08, E=0,** $\mu = -0.13$ **(-0.75 0.29)**
T5–O1	U=167, p<0.001, d=0.51, E=3, $\mu = -1.11$ (-1.63 -0.58)	t(35.61)=-3.52, p=0.001, d=-0.93, E=3, $\mu = -0.85$ (-1.34 -0.37)	**t(34.7)=3.24, p=0.016, d=0.86, E=1,** $\mu = 0.79$ **(0.3 1.28)**	**t(36)=3.27, p=0.006, d=0.87, E=2,** $\mu = 0.8$ **(0.31 1.29)**	**U=394, p=0.967, d=0.03, E=0,** $\mu = -0.04$ **(-0.61 0.39)**
P4–O2	U=164, p<0.001, d=0.5, E=3, $\mu = -1.18$ (-1.59 -0.59)	t(32.71)=-3.17, p=0.003, d=-0.84, E=3, $\mu = -0.78$ (-1.28 -0.29)	**t(36)=3.23, p=0.016, d=0.86, E=1,** $\mu = 0.79$ **(0.3 1.28)**	t(35.38)=2.7, p=0.014, d=0.72, E=3, $\mu = 0.68$ (0.17 1.18)	**U=387, p=0.967, d=0.04, E=0,** $\mu = -0.06$ **(-0.61 0.32)**
P3–O1	U=155, p<0.001, d=0.53, E=3, $\mu = -1.17$ (-1.67 -0.68)	t(26.51)=-2.89, p=0.006, d=-0.77, E=3, $\mu = -0.73$ (-1.23 -0.22)	**t(35.96)=3.66, p=0.013, d=0.97, E=1,** $\mu = 0.88$ **(0.4 1.36)**	t(34.03)=3.57, p=0.004, d=0.95, E=3, $\mu = 0.86$ (0.38 1.35)	**U=390, p=0.994, d=0, E=0,** $\mu = -0.01$ **(-0.59 0.37)**
O1–O2	U=118, p<0.001, d=0.6, E=3, $\mu = -1.25$ (-1.61 -0.85)	t(34.21)=-6.3, p<0.001, d=-1.68, E=3, $\mu = -1.29$ (-1.7 -0.88)	**t(32.21)=3.07, p=0.017, d=0.82, E=1,** $\mu = 0.76$ **(0.26 1.26)**	**t(33.58)=3.11, p=0.008, d=0.83, E=1,** $\mu = 0.77$ **(0.27 1.27)**	**U=345, p=0.964, d=0.07, E=0,** $\mu = -0.1$ **(-0.57 0.27)**

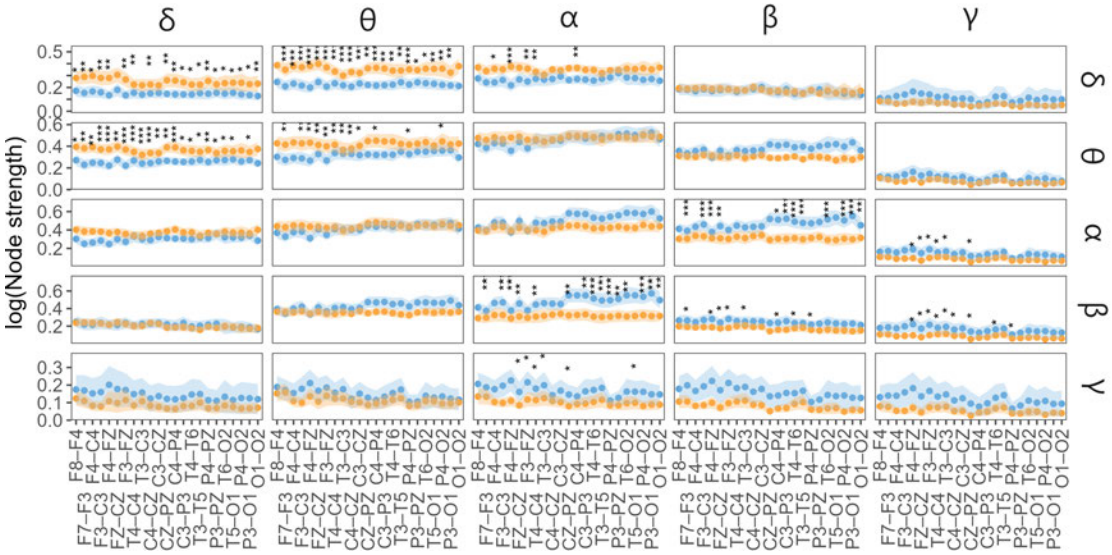

Figure A.15: Node strength (min-max normalised) measured with CBS in epoch 3 of HC (blue) and AD (orange): mean with 95% confidence intervals. The input frequency is on the vertical facets, and the output frequency is on the horizontal. Significant differences ($p \leq 0.05$) observed in at least ten thresholded networks are encoded by asterisks. The number of asterisks corresponds to the p-value (FDR corrected), i.e. $p \leq 0.0001$ "****", $p \leq 0.001$ "***", $p \leq 0.01$ "**", and $p \leq 0.05$ "*".

Table A.24: Comparisons of node strength measured with CBS in epoch 3. The results are reported as follows: statistics value (degrees of freedom), p-value of the test, Cohen's d effect size (or nonparametric alternative), number of epochs where significant differences were observed (E), and difference estimate μ with 95% confidence interval (CI). Reliable differences (significant in all three epochs) are highlighted with bold text.

from	channel	δ	θ	α	β	γ
δ	F8–F4	**U=237, p=0.007, d=0.37, E=2, μ =-0.77 (-1.43 -0.24)**	t(35.41)=-4.39, p¡0.001, d=-1.15, E=3, μ =-1 (-1.45 -0.54)	**t(36.81)=-2.75, p=0.017, d=-0.72, E=2, μ =-0.68 (-1.18 -0.18)**	**U=347, p=0.527, d=0.15, E=0, μ =-0.19 (-0.58 0.23)**	**U=419, p=1, d=0, E=0, μ =0 (-0.26 0.23)**
δ	F7–F3	U=210, p=0.003, d=0.43, E=3, μ =-0.89 (-1.4 -0.35)	t(34.06)=-3.99, p¡0.001, d=-1.05, E=3, μ =-0.94 (-1.41 -0.47)	**t(37)=-3.14, p=0.009, d=-0.82, E=2, μ =-0.77 (-1.25 -0.28)**	**U=343, p=0.527, d=0.16, E=0, μ =-0.24 (-0.6 0.2)**	**U=408, p=0.981, d=0.02, E=0, μ =-0.02 (-0.27 0.16)**
δ	F4–C4	U=208, p=0.003, d=0.43, E=3, μ =-0.74 (-1.32 -0.34)	t(36.96)=-4.3, p¡0.001, d=-1.13, E=3, μ =-0.99 (-1.45 -0.53)	t(36.72)=-3.73, p=0.003, d=-0.98, E=3, μ =-0.89 (-1.36 -0.41)	**U=306, p=0.497, d=0.23, E=0, μ =-0.35 (-0.7 0.04)**	**U=454, p=0.981, d=0.07, E=0, μ =0.04 (-0.1 0.16)**
δ	F3–C3	**U=224, p=0.005, d=0.4, E=2, μ =-0.73 (-1.24 -0.25)**	t(36.92)=-4.33, p¡0.001, d=-1.14, E=3, μ =-0.99 (-1.45 -0.53)	**t(32.71)=-2.55, p=0.023, d=-0.67, E=2, μ =-0.63 (-1.13 -0.13)**	**U=294, p=0.497, d=0.26, E=0, μ =-0.3 (-0.64 0)**	**U=439, p=0.981, d=0.04, E=0, μ =0.02 (-0.12 0.12)**
δ	F4–FZ	**U=180, p=0.002, d=0.49, E=2, μ =-0.8 (-1.38 -0.43)**	t(36.1)=-5.42, p¡0.001, d=-1.43, E=3, μ =-1.17 (-1.6 -0.73)	**t(35.97)=-4.74, p¡0.001, d=-1.24, E=2, μ =-1.06 (-1.5 -0.61)**	**U=346, p=0.527, d=0.15, E=0, μ =-0.22 (-0.65 0.18)**	**U=463, p=0.981, d=0.09, E=0, μ =0.03 (-0.1 0.14)**
δ	FZ–CZ	U=222, p=0.004, d=0.4, E=3, μ =-0.72 (-1.3 -0.26)	t(36.92)=-4.33, p¡0.001, d=-1.14, E=3, μ =-0.99 (-1.45 -0.53)	**t(36.78)=-2.8, p=0.016, d=-0.74, E=2, μ =-0.69 (-1.19 -0.2)**	**U=372, p=0.592, d=0.1, E=0, μ =-0.19 (-0.61 0.22)**	**U=440, p=0.981, d=0.04, E=0, μ =0.02 (-0.12 0.09)**
δ	F3–FZ	U=204, p=0.003, d=0.44, E=3, μ =-0.77 (-1.28 -0.37)	t(33.05)=-4.53, p¡0.001, d=-1.19, E=3, μ =-1.03 (-1.49 -0.58)	t(36.98)=-3.19, p=0.009, d=-0.84, E=3, μ =-0.78 (-1.26 -0.29)	**U=355, p=0.563, d=0.13, E=0, μ =-0.18 (-0.61 0.27)**	**U=435, p=0.981, d=0.03, E=0, μ =0.01 (-0.15 0.14)**
δ	T4–C4	U=250, p=0.013, d=0.35, E=3, μ =-0.57 (-1.05 -0.14)	t(36.93)=-3.08, p=0.004, d=-0.81, E=3, μ =-0.75 (-1.24 -0.26)	**t(32.23)=-1.65, p=0.122, d=-0.43, E=0, μ =-0.42 (-0.93 0.09)**	**U=362, p=0.573, d=0.12, E=0, μ =-0.23 (-0.68 0.25)**	**U=410, p=0.981, d=0.02, E=0, μ =-0.01 (-0.18 0.12)**
δ	T3–C3	U=276, p=0.029, d=0.29, E=3, μ =-0.54 (-1.06 -0.06)	t(37)=-2.55, p=0.014, d=-0.67, E=3, μ =-0.64 (-1.14 -0.14)	**U=306, p=0.094, d=0.23, E=0, μ =-0.36 (-0.92 0.04)**	**U=375, p=0.596, d=0.09, E=0, μ =-0.18 (-0.59 0.27)**	**U=445, p=0.981, d=0.05, E=0, μ =0.04 (-0.17 0.16)**
δ	C4–CZ	U=256, p=0.016, d=0.34, E=3, μ =-0.59 (-1.05 -0.14)	t(36.89)=-4.23, p¡0.001, d=-1.11, E=3, μ =-0.97 (-1.44 -0.51)	t(28.21)=-2.59, p=0.023, d=-0.67, E=3, μ =-0.64 (-1.13 -0.14)	**U=349, p=0.527, d=0.15, E=0, μ =-0.31 (-0.75 0.21)**	**U=411, p=0.981, d=0.02, E=0, μ =-0.01 (-0.14 0.13)**
δ	C3–CZ	U=285, p=0.039, d=0.28, E=3, μ =-0.42 (-0.88 -0.04)	**t(35.34)=-2.71, p=0.01, d=-0.71, E=2, μ =-0.67 (-1.17 -0.17)**	**t(30.17)=-1.5, p=0.146, d=-0.39, E=0, μ =-0.38 (-0.9 0.13)**	**U=404, p=0.848, d=0.03, E=0, μ =-0.05 (-0.43 0.4)**	**U=468, p=0.981, d=0.1, E=0, μ =0.05 (-0.11 0.19)**
δ	CZ–PZ	U=211, p=0.003, d=0.43, E=3, μ =-0.79 (-1.22 -0.33)	t(29.77)=-4.87, p¡0.001, d=-1.29, E=3, μ =-1.09 (-1.54 -0.64)	t(36.97)=-4.32, p=0.001, d=-1.13, E=3, μ =-0.99 (-1.45 -0.53)	**U=398, p=0.81, d=0.04, E=0, μ =-0.08 (-0.52 0.4)**	**U=405, p=0.981, d=0.03, E=0, μ =-0.01 (-0.12 0.08)**
δ	C4–P4	U=199, p=0.002, d=0.45, E=3, μ =-0.73 (-1.15 -0.33)	t(32.96)=-4.59, p¡0.001, d=-1.21, E=3, μ =-1.04 (-1.5 -0.59)	**t(36.64)=-3.52, p=0.004, d=-0.92, E=2, μ =-0.84 (-1.32 -0.36)**	**U=341, p=0.527, d=0.16, E=0, μ =-0.23 (-0.6 0.21)**	**U=385, p=0.981, d=0.07, E=0, μ =-0.03 (-0.2 0.1)**
δ	C3–P3	U=233, p=0.006, d=0.38, E=3, μ =-0.67 (-1.15 -0.21)	U=190, p¡0.001, d=0.47, E=3, μ =-0.93 (-1.41 -0.51)	**t(36.16)=-2.95, p=0.014, d=-0.77, E=2, μ =-0.72 (-1.21 -0.23)**	**U=423, p=0.969, d=0.01, E=0, μ =0.01 (-0.39 0.42)**	**U=420, p=1, d=0, E=0, μ =0 (-0.2 0.14)**
δ	T4–T6	U=265, p=0.02, d=0.32, E=3, μ =-0.54 (-0.99 -0.14)	t(34.98)=-3.25, p=0.003, d=-0.86, E=3, μ =-0.79 (-1.28 -0.3)	**t(34.95)=-2.82, p=0.016, d=-0.74, E=2, μ =-0.69 (-1.19 -0.2)**	**U=316, p=0.497, d=0.21, E=0, μ =-0.29 (-0.64 0.07)**	**U=394, p=0.981, d=0.05, E=0, μ =-0.02 (-0.15 0.09)**

δ	T3–T5	U=288, p=0.04, d=0.27, E=3, μ =-0.44 (-0.93 -0.02)	t(36.51)=-2.56, p=0.014, d=-0.67, E=3, μ =-0.64 (-1.15 -0.14)	**t(35.53)=-1.3, p=0.2, d=-0.34, E=0, μ =-0.34 (-0.86 0.18)**	**U=388, p=0.721, d=0.07, E=0, μ =-0.12 (-0.5 0.36)**	**U=429, p=0.981, d=0.02, E=0, μ =0.01 (-0.17 0.16)**
δ	P4–PZ	U=198, p=0.002, d=0.45, E=3, μ =-0.74 (-1.2 -0.31)	t(37)=-4.16, p|0.001, d=-1.09, E=3, μ =-0.96 (-1.43 -0.5)	**t(25.06)=-1.95, p=0.074, d=-0.51, E=0, μ =-0.49 (-1 0.02)**	**U=359, p=0.573, d=0.12, E=0, μ =-0.18 (-0.61 0.27)**	**U=408, p=0.981, d=0.02, E=0, μ =-0.01 (-0.2 0.12)**
δ	P3–PZ	U=287, p=0.04, d=0.27, E=3, μ =-0.52 (-1.01 -0.01)	t(35.97)=-3.39, p=0.002, d=-0.89, E=3, μ =-0.81 (-1.3 -0.33)	**U=324, p=0.146, d=0.2, E=0, μ =-0.38 (-0.87 0.13)**	**U=469, p=0.592, d=0.1, E=0, μ =0.16 (-0.27 0.64)**	**U=432, p=0.981, d=0.02, E=0, μ =0.01 (-0.11 0.13)**
δ	T6–O2	U=228, p=0.005, d=0.39, E=3, μ =-0.58 (-0.85 -0.23)	**U=175, p|0.001, d=0.5, E=2, μ =-0.79 (-1.12 -0.44)**	**U=259, p=0.022, d=0.33, E=2, μ =-0.54 (-0.93 -0.13)**	**U=307, p=0.497, d=0.23, E=0, μ =-0.2 (-0.46 0.02)**	**U=348, p=0.981, d=0.15, E=0, μ =-0.04 (-0.14 0.03)**
δ	T5–O1	U=267, p=0.02, d=0.31, E=3, μ =-0.58 (-1.01 -0.1)	t(33.99)=-3.42, p=0.002, d=-0.9, E=3, μ =-0.83 (-1.31 -0.34)	**t(34.13)=-2.17, p=0.047, d=-0.57, E=2, μ =-0.55 (-1.05 -0.04)**	**U=349, p=0.527, d=0.15, E=0, μ =-0.2 (-0.53 0.16)**	**U=374, p=0.981, d=0.09, E=0, μ =-0.02 (-0.16 0.06)**
δ	P4–O2	U=258, p=0.016, d=0.33, E=3, μ =-0.44 (-0.77 -0.09)	U=211, p=0.001, d=0.43, E=3, μ =-0.72 (-1.19 -0.3)	**U=268, p=0.027, d=0.31, E=2, μ =-0.55 (-0.98 -0.07)**	**U=345, p=0.527, d=0.15, E=0, μ =-0.15 (-0.42 0.12)**	**U=399, p=0.981, d=0.04, E=0, μ =-0.01 (-0.12 0.06)**
δ	P3–O1	U=264, p=0.02, d=0.32, E=3, μ =-0.57 (-1.11 -0.11)	t(28.68)=-3.16, p=0.003, d=-0.84, E=3, μ =-0.78 (-1.28 -0.28)	**t(37)=-2.42, p=0.027, d=-0.63, E=2, μ =-0.61 (-1.11 -0.1)**	**U=370, p=0.592, d=0.1, E=0, μ =-0.14 (-0.56 0.27)**	**U=398, p=0.981, d=0.04, E=0, μ =-0.01 (-0.15 0.06)**
δ	O1–O2	U=199, p=0.002, d=0.45, E=3, μ =-0.56 (-0.9 -0.27)	U=144, p|0.001, d=0.56, E=3, μ =-0.92 (-1.33 -0.52)	U=195, p=0.003, d=0.46, E=3, μ =-0.75 (-1.1 -0.33)	**U=315, p=0.497, d=0.21, E=0, μ =-0.24 (-0.51 0.06)**	**U=348, p=0.981, d=0.15, E=0, μ =-0.04 (-0.15 0.03)**
θ	F8–F4	t(36.96)=-3.54, p=0.002, d=-0.93, E=3, μ =-0.85 (-1.33 -0.37)	t(36.9)=-2.92, p=0.012, d=-0.77, E=3, μ =-0.72 (-1.21 -0.23)	**t(36.26)=-1.29, p=0.828, d=-0.34, E=0, μ =-0.33 (-0.85 0.19)**	**U=487, p=0.348, d=0.14, E=0, μ =0.25 (-0.21 0.83)**	**U=422, p=0.982, d=0, E=0, μ =0.01 (-0.36 0.34)**
θ	F7–F3	t(36.58)=-4.43, p|0.001, d=-1.17, E=3, μ =-1.01 (-1.47 -0.55)	t(35.49)=-3.33, p=0.009, d=-0.88, E=3, μ =-0.81 (-1.29 -0.32)	**t(36.86)=-1.78, p=0.621, d=-0.47, E=0, μ =-0.46 (-0.97 0.06)**	**t(36.99)=0.88, p=0.421, d=0.23, E=0, μ =0.23 (-0.3 0.76)**	**U=476, p=0.899, d=0.11, E=0, μ =0.12 (-0.18 0.43)**
θ	F4–C4	t(34.27)=-4.51, p|0.001, d=-1.19, E=3, μ =-1.03 (-1.49 -0.57)	t(35.56)=-3.78, p=0.005, d=-0.99, E=3, μ =-0.9 (-1.37 -0.42)	**t(36.89)=-1.34, p=0.828, d=-0.35, E=0, μ =-0.35 (-0.87 0.17)**	**U=514, p=0.216, d=0.19, E=0, μ =0.38 (-0.12 0.87)**	**U=527, p=0.899, d=0.22, E=0, μ =0.22 (-0.05 0.5)**
θ	F3–C3	t(36.97)=-3.73, p=0.001, d=-0.98, E=3, μ =-0.88 (-1.36 -0.41)	t(35.95)=-3.12, p=0.009, d=-0.82, E=3, μ =-0.76 (-1.26 -0.27)	**t(37)=-0.87, p=0.828, d=-0.23, E=0, μ =-0.23 (-0.75 0.3)**	**U=490, p=0.341, d=0.14, E=0, μ =0.28 (-0.19 0.77)**	**U=530, p=0.899, d=0.22, E=0, μ =0.21 (-0.03 0.41)**
θ	F4–FZ	t(34.48)=-4.57, p|0.001, d=-1.2, E=3, μ =-1.04 (-1.49 -0.58)	t(36.46)=-4.14, p=0.003, d=-1.09, E=3, μ =-0.96 (-1.43 -0.5)	**t(36.88)=-2.95, p=0.108, d=-0.77, E=0, μ =-0.72 (-1.22 -0.23)**	**t(36.87)=-0.48, p=0.66, d=-0.13, E=0, μ =-0.13 (-0.66 0.4)**	**U=496, p=0.899, d=0.16, E=0, μ =0.14 (-0.11 0.41)**
θ	FZ–CZ	t(36.82)=-3.46, p=0.002, d=-0.91, E=3, μ =-0.83 (-1.31 -0.35)	**U=297, p=0.081, d=0.25, E=0, μ =-0.44 (-0.93 0.03)**	**t(36.18)=-1.04, p=0.828, d=-0.27, E=0, μ =-0.27 (-0.79 0.25)**	**t(33.16)=1.62, p=0.195, d=0.42, E=0, μ =0.42 (-0.1 0.93)**	**U=508, p=0.899, d=0.18, E=0, μ =0.11 (-0.06 0.26)**
θ	F3–FZ	t(33.35)=-4.27, p|0.001, d=-1.13, E=3, μ =-0.99 (-1.45 -0.52)	U=213, p=0.008, d=0.42, E=3, μ =-0.72 (-1.21 -0.31)	**t(36.56)=-1.9, p=0.621, d=-0.5, E=0, μ =-0.49 (-1 0.03)**	**U=430, p=0.883, d=0.02, E=0, μ =0.01 (-0.36 0.47)**	**U=492, p=0.899, d=0.15, E=0, μ =0.14 (-0.11 0.36)**
θ	T4–C4	t(36.99)=-2.31, p=0.031, d=-0.61, E=3, μ =-0.58 (-1.09 -0.08)	**t(36.99)=-1.78, p=0.103, d=-0.47, E=0, μ =-0.46 (-0.97 0.06)**	**t(32.91)=-0.22, p=0.997, d=-0.06, E=0, μ =-0.06 (-0.58 0.47)**	**t(31.2)=1.46, p=0.216, d=0.38, E=0, μ =0.37 (-0.14 0.89)**	**U=451, p=0.946, d=0.06, E=0, μ =0.06 (-0.28 0.33)**
θ	T3–C3	t(35.94)=-2.18, p=0.036, d=-0.57, E=3, μ =-0.55 (-1.07 -0.04)	**U=360, p=0.357, d=0.12, E=0, μ =-0.25 (-0.73 0.29)**	**t(36.88)=0, p=0.997, d=0, E=0, μ =0 (-0.53 0.53)**	**U=551, p=0.096, d=0.27, E=0, μ =0.5 (0.01 0.97)**	**U=485, p=0.899, d=0.13, E=0, μ =0.15 (-0.16 0.4)**
θ	C4–CZ	t(36.98)=-3.03, p=0.006, d=-0.8, E=3, μ =-0.74 (-1.23 -0.25)	**U=345, p=0.259, d=0.15, E=0, μ =-0.33 (-0.79 0.2)**	**t(29.25)=-0.23, p=0.997, d=-0.06, E=0, μ =-0.06 (-0.58 0.46)**	**U=491, p=0.341, d=0.15, E=0, μ =0.26 (-0.19 0.8)**	**U=451, p=0.946, d=0.06, E=0, μ =0.04 (-0.2 0.25)**

θ	C3–CZ	t(36.99)=-2.3, p=0.031, d=-0.6, E=3, μ =-0.58 (-1.09 -0.07)	**t(37)=-2.18, p=0.06, d=-0.57, E=0, μ =-0.55 (-1.06 -0.04)**	**t(33.05)=-0.57, p=0.938, d=-0.15, E=0, μ =-0.15 (-0.67 0.38)**	**t(34.17)=1.41, p=0.225, d=0.37, E=0, μ =0.36 (-0.15 0.88)**	**U=478, p=0.899, d=0.12, E=0, μ =0.11 (-0.12 0.36)**
θ	CZ–PZ	U=175, p|0.001, d=0.5, E=3, μ =-0.88 (-1.38 -0.44)	U=223, p=0.009, d=0.4, E=3, μ =-0.8 (-1.23 -0.3)	**t(36.36)=-0.26, p=0.997, d=-0.07, E=0, μ =-0.07 (-0.6 0.46)**	**U=618, p=0.013, d=0.4, E=1, μ =0.66 (0.24 1.3)**	**U=480, p=0.899, d=0.12, E=0, μ =0.08 (-0.1 0.25)**
θ	C4–P4	U=181, p|0.001, d=0.49, E=3, μ =-0.84 (-1.32 -0.37)	U=231, p=0.009, d=0.39, E=3, μ =-0.7 (-1.2 -0.27)	**t(36.87)=-0.19, p=0.997, d=-0.05, E=0, μ =-0.05 (-0.58 0.48)**	**U=611, p=0.013, d=0.39, E=2, μ =0.67 (0.24 1.28)**	**U=403, p=0.946, d=0.03, E=0, μ =-0.03 (-0.28 0.19)**
θ	C3–P3	U=230, p=0.005, d=0.39, E=3, μ =-0.79 (-1.28 -0.28)	t(29.99)=-3.11, p=0.009, d=-0.82, E=3, μ =-0.77 (-1.27 -0.27)	**t(36.02)=-0.74, p=0.828, d=-0.19, E=0, μ =-0.19 (-0.72 0.33)**	**U=610, p=0.013, d=0.39, E=1, μ =0.64 (0.17 1.16)**	**U=416, p=0.982, d=0.01, E=0, μ =-0.01 (-0.24 0.19)**
θ	T4–T6	**t(34.38)=-2.76, p=0.012, d=-0.73, E=2, μ =-0.69 (-1.19 -0.19)**	t(35.43)=-2.63, p=0.023, d=-0.69, E=3, μ =-0.66 (-1.16 -0.16)	**t(34.88)=-0.1, p=0.997, d=-0.03, E=0, μ =-0.03 (-0.55 0.5)**	**U=536, p=0.148, d=0.24, E=0, μ =0.55 (-0.06 1.28)**	**U=442, p=0.946, d=0.04, E=0, μ =0.04 (-0.24 0.26)**
θ	T3–T5	t(35.99)=-2.17, p=0.036, d=-0.57, E=3, μ =-0.55 (-1.06 -0.04)	**t(28.64)=-1.69, p=0.118, d=-0.45, E=0, μ =-0.44 (-0.97 0.08)**	**t(36.81)=0.73, p=0.828, d=0.19, E=0, μ =0.19 (-0.34 0.72)**	**U=605, p=0.014, d=0.38, E=1, μ =0.7 (0.22 1.23)**	**U=449, p=0.946, d=0.06, E=0, μ =0.07 (-0.21 0.36)**
θ	P4–PZ	t(36.01)=-3.53, p=0.002, d=-0.93, E=3, μ =-0.85 (-1.33 -0.37)	U=264, p=0.028, d=0.32, E=3, μ =-0.6 (-1.05 -0.11)	**t(31.7)=-0.02, p=0.997, d=0, E=0, μ =0 (-0.53 0.52)**	**U=534, p=0.148, d=0.23, E=0, μ =0.51 (-0.06 0.99)**	**U=439, p=0.946, d=0.04, E=0, μ =0.04 (-0.28 0.34)**
θ	P3–PZ	t(36.17)=-2.07, p=0.044, d=-0.54, E=3, μ =-0.53 (-1.04 -0.02)	**t(36.1)=-1.95, p=0.081, d=-0.51, E=0, μ =-0.5 (-1.02 0.01)**	**t(31.87)=0.85, p=0.828, d=0.22, E=0, μ =0.22 (-0.3 0.74)**	**U=591, p=0.024, d=0.35, E=1, μ =0.7 (0.15 1.2)**	**U=443, p=0.946, d=0.05, E=0, μ =0.05 (-0.23 0.33)**
θ	T6–O2	**U=250, p=0.012, d=0.35, E=2, μ =-0.57 (-0.98 -0.17)**	**t(36.99)=-2.08, p=0.069, d=-0.55, E=0, μ =-0.53 (-1.04 -0.02)**	**t(32.29)=0.8, p=0.828, d=0.21, E=0, μ =0.21 (-0.31 0.73)**	**U=580, p=0.031, d=0.33, E=1, μ =0.43 (0.07 0.96)**	**U=377, p=0.946, d=0.09, E=0, μ =-0.04 (-0.2 0.07)**
θ	T5–O1	t(34.07)=-2.2, p=0.036, d=-0.58, E=3, μ =-0.56 (-1.08 -0.05)	**t(35.44)=-1.29, p=0.221, d=-0.34, E=0, μ =-0.34 (-0.86 0.19)**	**t(32.26)=0.86, p=0.828, d=0.22, E=0, μ =0.22 (-0.3 0.75)**	**t(32.37)=4.41, p=0.001, d=1.15, E=1, μ =1 (0.54 1.45)**	**U=423, p=0.982, d=0.01, E=0, μ =0.01 (-0.21 0.21)**
θ	P4–O2	U=269, p=0.026, d=0.31, E=3, μ =-0.51 (-1.02 -0.09)	**t(31.59)=-1.86, p=0.093, d=-0.49, E=0, μ =-0.48 (-1 0.04)**	**t(36.93)=0.16, p=0.997, d=0.04, E=0, μ =0.04 (-0.49 0.57)**	**U=581, p=0.031, d=0.33, E=1, μ =0.53 (0.13 1.06)**	**U=438, p=0.946, d=0.04, E=0, μ =0.02 (-0.14 0.16)**
θ	P3–O1	t(26.77)=-2.42, p=0.027, d=-0.64, E=3, μ =-0.62 (-1.13 -0.1)	**t(33.27)=-1.33, p=0.217, d=-0.35, E=0, μ =-0.35 (-0.88 0.18)**	**t(36.61)=0.89, p=0.828, d=0.23, E=0, μ =0.23 (-0.29 0.76)**	**U=685, p|0.001, d=0.54, E=1, μ =1 (0.56 1.46)**	**U=435, p=0.946, d=0.03, E=0, μ =0.03 (-0.22 0.18)**
θ	O1–O2	U=186, p=0.001, d=0.48, E=3, μ =-0.75 (-1.16 -0.4)	U=242, p=0.012, d=0.36, E=3, μ =-0.69 (-1.13 -0.21)	**t(35.23)=-0.48, p=0.966, d=-0.13, E=0, μ =-0.13 (-0.65 0.4)**	**U=517, p=0.216, d=0.2, E=0, μ =0.38 (-0.1 0.91)**	**U=362, p=0.899, d=0.12, E=0, μ =-0.08 (-0.36 0.09)**
α	F8–F4	**t(36.89)=-2.64, p=0.031, d=-0.69, E=2, μ =-0.66 (-1.16 -0.16)**	**t(36.91)=-1.7, p=0.433, d=-0.45, E=0, μ =-0.44 (-0.95 0.08)**	**t(35.69)=0.84, p=0.466, d=0.22, E=0, μ =0.22 (-0.3 0.74)**	**U=592, p=0.011, d=0.35, E=2, μ =0.71 (0.18 1.15)**	**U=541, p=0.093, d=0.25, E=0, μ =0.24 (-0.02 0.53)**
α	F7–F3	**t(35.86)=-3.76, p=0.006, d=-0.99, E=2, μ =-0.89 (-1.37 -0.42)**	**t(36.58)=-2.4, p=0.228, d=-0.63, E=0, μ =-0.61 (-1.11 -0.1)**	**t(35.12)=0.23, p=0.851, d=0.06, E=0, μ =0.06 (-0.47 0.6)**	**U=572, p=0.022, d=0.31, E=2, μ =0.53 (0.12 0.94)**	**U=551, p=0.093, d=0.27, E=0, μ =0.28 (0.02 0.6)**

α	F4–C4	**t(36.97)=-3.71, p=0.006, d=-0.97, E=2, μ =-0.88 (-1.35 -0.4)**	**t(36.96)=-1.8, p=0.433, d=-0.47, E=0, μ =-0.46 (-0.98 0.05)**	**U=512, p=0.207, d=0.19, E=0, μ =0.33 (-0.15 0.85)**	**t(36.15)=2.37, p=0.025, d=0.62, E=2, μ =0.6 (0.09 1.11)**	U=606, p=0.026, d=0.38, E=3, μ =0.42 (0.13 0.78)
α	F3–C3	**t(31.82)=-2.86, p=0.023, d=-0.75, E=2, μ =-0.7 (-1.19 -0.21)**	**t(36.98)=-1.39, p=0.656, d=-0.36, E=0, μ =-0.36 (-0.88 0.16)**	**t(36.82)=1.05, p=0.358, d=0.28, E=0, μ =0.28 (-0.25 0.8)**	U=603, p=0.007, d=0.37, E=3, μ =0.72 (0.24 1.25)	U=597, p=0.031, d=0.36, E=3, μ =0.37 (0.13 0.66)
α	F4–FZ	**t(36.84)=-3.53, p=0.006, d=-0.93, E=2, μ =-0.85 (-1.33 -0.37)**	**t(36.5)=-3.11, p=0.069, d=-0.82, E=0, μ =-0.76 (-1.25 -0.27)**	**t(36.92)=-0.51, p=0.668, d=-0.13, E=0, μ =-0.14 (-0.66 0.39)**	**t(36.79)=1.77, p=0.082, d=0.46, E=0, μ =0.45 (-0.06 0.97)**	U=633, p=0.016, d=0.44, E=3, μ =0.41 (0.15 0.68)
α	FZ–CZ	**t(36.32)=-2.26, p=0.072, d=-0.59, E=0, μ =-0.57 (-1.07 -0.06)**	**t(36.51)=-0.69, p=0.854, d=-0.18, E=0, μ =-0.18 (-0.71 0.34)**	**t(36.86)=1.42, p=0.207, d=0.37, E=0, μ =0.37 (-0.15 0.89)**	**U=610, p=0.005, d=0.39, E=2, μ =0.66 (0.24 1.14)**	U=613, p=0.026, d=0.39, E=3, μ =0.33 (0.1 0.58)
α	F3–FZ	**t(37)=-2.19, p=0.075, d=-0.58, E=0, μ =-0.56 (-1.07 -0.05)**	**t(36.91)=-1.94, p=0.433, d=-0.51, E=0, μ =-0.5 (-1.01 0.02)**	**t(36.97)=-0.19, p=0.851, d=-0.05, E=0, μ =-0.05 (-0.58 0.48)**	**t(36.06)=2.5, p=0.021, d=0.66, E=2, μ =0.63 (0.12 1.13)**	U=587, p=0.036, d=0.34, E=3, μ =0.38 (0.1 0.65)
α	T4–C4	**t(31.89)=-0.29, p=0.774, d=-0.08, E=0, μ =-0.08 (-0.6 0.45)**	**t(36.01)=-0.54, p=0.854, d=-0.14, E=0, μ =-0.14 (-0.67 0.39)**	**t(34.46)=1.66, p=0.171, d=0.43, E=0, μ =0.42 (-0.09 0.94)**	**U=588, p=0.012, d=0.34, E=2, μ =0.66 (0.15 1.23)**	**U=541, p=0.093, d=0.25, E=0, μ =0.33 (-0.02 0.67)**
α	T3–C3	**U=356, p=0.413, d=0.13, E=0, μ =-0.27 (-0.8 0.26)**	**t(34.8)=0.26, p=0.919, d=0.07, E=0, μ =0.07 (-0.47 0.6)**	**U=586, p=0.027, d=0.34, E=1, μ =0.64 (0.19 1.07)**	**U=611, p=0.005, d=0.39, E=2, μ =0.68 (0.25 1.19)**	**U=538, p=0.094, d=0.24, E=0, μ =0.3 (-0.04 0.59)**
α	C4–CZ	**t(29.63)=-2.04, p=0.089, d=-0.53, E=0, μ =-0.52 (-1.02 -0.01)**	**U=426, p=0.932, d=0.01, E=0, μ =0.05 (-0.54 0.55)**	**U=552, p=0.071, d=0.27, E=0, μ =0.43 (0.02 0.92)**	**U=548, p=0.049, d=0.26, E=2, μ =0.5 (0 1.03)**	**U=506, p=0.203, d=0.18, E=0, μ =0.16 (-0.09 0.45)**
α	C3–CZ	**t(31.44)=-1.23, p=0.303, d=-0.32, E=0, μ =-0.32 (-0.84 0.2)**	**t(35.2)=-0.89, p=0.854, d=-0.23, E=0, μ =-0.23 (-0.75 0.29)**	**t(36.2)=1.43, p=0.207, d=0.37, E=0, μ =0.37 (-0.15 0.89)**	**t(36.09)=2.14, p=0.04, d=0.56, E=2, μ =0.54 (0.03 1.05)**	**U=546, p=0.093, d=0.26, E=0, μ =0.24 (0 0.51)**
α	CZ–PZ	**t(35.34)=-2.7, p=0.03, d=-0.71, E=2, μ =-0.68 (-1.18 -0.17)**	**t(36.6)=-0.73, p=0.854, d=-0.19, E=0, μ =-0.19 (-0.72 0.34)**	**U=619, p=0.013, d=0.41, E=1, μ =0.74 (0.28 1.3)**	U=715, p|0.001, d=0.6, E=3, μ =1.02 (0.56 1.49)	U=586, p=0.036, d=0.34, E=3, μ =0.29 (0.06 0.56)
α	C4–P4	**t(32.52)=-3.17, p=0.013, d=-0.84, E=2, μ =-0.78 (-1.27 -0.29)**	**t(36.99)=-1.18, p=0.802, d=-0.31, E=0, μ =-0.31 (-0.83 0.22)**	**t(36.55)=2.8, p=0.023, d=0.73, E=1, μ =0.69 (0.2 1.19)**	U=695, pi0.001, d=0.56, E=3, μ =0.96 (0.55 1.44)	**U=500, p=0.218, d=0.16, E=0, μ =0.17 (-0.11 0.42)**
α	C3–P3	**t(36.96)=-2.1, p=0.084, d=-0.55, E=0, μ =-0.54 (-1.05 -0.03)**	**t(36.16)=-0.62, p=0.854, d=-0.16, E=0, μ =-0.16 (-0.69 0.37)**	**U=599, p=0.019, d=0.37, E=1, μ =0.67 (0.21 1.23)**	U=689, pi0.001, d=0.55, E=3, μ =0.94 (0.52 1.37)	**U=537, p=0.094, d=0.24, E=0, μ =0.2 (-0.02 0.44)**
α	T4–T6	**U=304, p=0.118, d=0.24, E=0, μ =-0.43 (-0.96 0.06)**	**t(36.95)=-0.65, p=0.854, d=-0.17, E=0, μ =-0.17 (-0.7 0.36)**	**t(34.54)=2.35, p=0.052, d=0.61, E=0, μ =0.59 (0.09 1.09)**	U=651, p=0.001, d=0.47, E=3, μ =0.9 (0.45 1.43)	**U=514, p=0.178, d=0.19, E=0, μ =0.22 (-0.08 0.48)**
α	T3–T5	**t(36.72)=-0.59, p=0.614, d=-0.15, E=0, μ =-0.15 (-0.68 0.37)**	**t(34.4)=0.27, p=0.919, d=0.07, E=0, μ =0.07 (-0.46 0.61)**	**t(37)=2.2, p=0.061, d=0.58, E=0, μ =0.56 (0.05 1.07)**	U=656, p=0.001, d=0.48, E=3, μ =0.85 (0.41 1.32)	**U=554, p=0.093, d=0.27, E=0, μ =0.31 (0.01 0.69)**
α	P4–PZ	**t(31.06)=-1.69, p=0.148, d=-0.44, E=0, μ =-0.43 (-0.94 0.08)**	**t(36.59)=-0.38, p=0.9, d=-0.1, E=0, μ =-0.1 (-0.63 0.43)**	**U=578, p=0.034, d=0.32, E=1, μ =0.64 (0.13 1.17)**	**U=625, p=0.002, d=0.42, E=2, μ =0.81 (0.34 1.27)**	**U=545, p=0.093, d=0.26, E=0, μ =0.35 (0 0.72)**
α	P3–PZ	**U=398, p=0.774, d=0.04, E=0, μ =-0.11 (-0.64 0.42)**	**t(37)=0.54, p=0.854, d=0.14, E=0, μ =0.14 (-0.39 0.67)**	**U=609, p=0.017, d=0.39, E=1, μ =0.69 (0.23 1.24)**	t(36.72)=3.79, p=0.001, d=1, E=3, μ =0.9 (0.42 1.37)	**U=566, p=0.075, d=0.3, E=0, μ =0.39 (0.06 0.81)**

α	T6–O2	**U=298, p=0.103, d=0.25, E=0, μ =-0.42 (-0.83 0.01)**	**t(35.21)=-0.13, p=0.932, d=-0.04, E=0, μ =-0.04 (-0.56 0.49)**	**U=604, p=0.017, d=0.38, E=1, μ =0.79 (0.27 1.35)**	U=671, p¡0.001, d=0.51, E=3, μ =0.88 (0.42 1.37)	**U=501, p=0.218, d=0.17, E=0, μ =0.11 (-0.09 0.32)**
α	T5–O1	**t(36.82)=-1.47, p=0.211, d=-0.39, E=0, μ =-0.38 (-0.9 0.14)**	**t(37)=0.43, p=0.9, d=0.11, E=0, μ =0.11 (-0.42 0.64)**	**t(33.5)=3.44, p=0.013, d=0.9, E=1, μ =0.82 (0.34 1.3)**	t(35.83)=4.96, p¡0.001, d=1.3, E=3, μ =1.09 (0.65 1.53)	**U=552, p=0.093, d=0.27, E=0, μ =0.26 (0.03 0.57)**
α	P4–O2	**U=358, p=0.413, d=0.13, E=0, μ =-0.24 (-0.71 0.27)**	**t(36.78)=-0.11, p=0.932, d=-0.03, E=0, μ =-0.03 (-0.56 0.5)**	**t(36.6)=2.3, p=0.052, d=0.6, E=0, μ =0.58 (0.08 1.09)**	U=643, p=0.001, d=0.46, E=3, μ =0.93 (0.4 1.4)	**U=542, p=0.093, d=0.25, E=0, μ =0.19 (-0.01 0.44)**
α	P3–O1	**t(35.2)=-0.77, p=0.511, d=-0.2, E=0, μ =-0.2 (-0.73 0.33)**	**t(37)=0.74, p=0.854, d=0.19, E=0, μ =0.19 (-0.33 0.72)**	**t(34.05)=3.3, p=0.013, d=0.86, E=1, μ =0.79 (0.31 1.28)**	U=714, p¡0.001, d=0.6, E=3, μ =1.15 (0.69 1.62)	**U=523, p=0.142, d=0.21, E=0, μ =0.17 (-0.04 0.41)**
α	O1–O2	**U=231, p=0.013, d=0.39, E=2, μ =-0.68 (-1.09 -0.23)**	**t(36.88)=-0.77, p=0.854, d=-0.2, E=0, μ =-0.2 (-0.73 0.32)**	**U=515, p=0.207, d=0.19, E=0, μ =0.35 (-0.13 0.95)**	U=571, p=0.022, d=0.31, E=3, μ =0.5 (0.07 1.03)	**U=512, p=0.179, d=0.19, E=0, μ =0.16 (-0.05 0.44)**
β	F8–F4	**U=403, p=0.962, d=0.03, E=0, μ =-0.05 (-0.56 0.37)**	**U=440, p=0.798, d=0.04, E=0, μ =0.1 (-0.41 0.68)**	**U=596, p=0.007, d=0.36, E=2, μ =0.76 (0.22 1.28)**	**U=531, p=0.123, d=0.23, E=0, μ =0.27 (-0.06 0.67)**	**U=558, p=0.05, d=0.28, E=0, μ =0.29 (0.03 0.58)**
β	F7–F3	**U=333, p=0.947, d=0.18, E=0, μ =-0.27 (-0.77 0.17)**	**U=391, p=0.723, d=0.06, E=0, μ =-0.13 (-0.64 0.44)**	**t(35.5)=1.88, p=0.066, d=0.49, E=0, μ =0.48 (-0.03 1)**	**U=538, p=0.103, d=0.24, E=0, μ =0.36 (-0.03 0.73)**	U=573, p=0.048, d=0.31, E=3, μ =0.33 (0.06 0.66)
β	F4–C4	**U=343, p=0.947, d=0.16, E=0, μ =-0.25 (-0.69 0.14)**	**t(32.08)=1.1, p=0.353, d=0.29, E=0, μ =0.29 (-0.23 0.8)**	U=617, p=0.003, d=0.4, E=3, μ =0.72 (0.27 1.18)	**U=516, p=0.151, d=0.2, E=0, μ =0.27 (-0.1 0.68)**	U=602, p=0.028, d=0.37, E=3, μ =0.36 (0.09 0.77)
β	F3–C3	**U=352, p=0.947, d=0.14, E=0, μ =-0.22 (-0.61 0.2)**	**t(31.61)=1.21, p=0.334, d=0.32, E=0, μ =0.31 (-0.21 0.83)**	U=618, p=0.003, d=0.4, E=3, μ =0.77 (0.33 1.24)	U=575, p=0.041, d=0.32, E=3, μ =0.42 (0.07 0.84)	U=594, p=0.029, d=0.36, E=3, μ =0.34 (0.12 0.64)
β	F4–FZ	**U=409, p=0.962, d=0.02, E=0, μ =-0.05 (-0.51 0.33)**	**t(36.08)=-0.19, p=0.847, d=-0.05, E=0, μ =-0.05 (-0.58 0.48)**	**t(36.99)=2.39, p=0.022, d=0.63, E=2, μ =0.6 (0.1 1.11)**	U=598, p=0.024, d=0.36, E=3, μ =0.51 (0.17 0.92)	U=618, p=0.028, d=0.4, E=3, μ =0.38 (0.15 0.65)
β	FZ–CZ	**U=337, p=0.947, d=0.17, E=0, μ =-0.3 (-0.77 0.12)**	**t(30.79)=1.16, p=0.34, d=0.3, E=0, μ =0.3 (-0.22 0.82)**	U=596, p=0.007, d=0.36, E=3, μ =0.67 (0.21 1.14)	**U=554, p=0.061, d=0.27, E=0, μ =0.45 (0.02 0.81)**	U=575, p=0.048, d=0.32, E=3, μ =0.24 (0.04 0.49)
β	F3–FZ	**U=402, p=0.962, d=0.04, E=0, μ =-0.06 (-0.53 0.4)**	**U=453, p=0.708, d=0.07, E=0, μ =0.13 (-0.33 0.57)**	**t(37)=2.13, p=0.039, d=0.56, E=2, μ =0.54 (0.03 1.05)**	U=602, p=0.024, d=0.37, E=3, μ =0.56 (0.16 0.99)	U=601, p=0.028, d=0.37, E=3, μ =0.35 (0.09 0.68)
β	T4–C4	**U=427, p=0.962, d=0.01, E=0, μ =0.03 (-0.45 0.48)**	**U=508, p=0.288, d=0.18, E=0, μ =0.43 (-0.18 0.96)**	**U=615, p=0.003, d=0.4, E=2, μ =0.81 (0.32 1.21)**	**U=523, p=0.143, d=0.21, E=0, μ =0.37 (-0.09 0.82)**	**U=551, p=0.05, d=0.27, E=0, μ =0.26 (0.01 0.58)**
β	T3–C3	**U=441, p=0.962, d=0.04, E=0, μ =0.06 (-0.39 0.53)**	**t(36.94)=1.55, p=0.242, d=0.41, E=0, μ =0.4 (-0.12 0.92)**	U=630, p=0.002, d=0.43, E=3, μ =0.77 (0.35 1.22)	**U=487, p=0.303, d=0.14, E=0, μ =0.23 (-0.17 0.67)**	**U=555, p=0.05, d=0.28, E=0, μ =0.32 (0.02 0.58)**
β	C4–CZ	**U=357, p=0.947, d=0.13, E=0, μ =-0.23 (-0.63 0.27)**	**U=499, p=0.334, d=0.16, E=0, μ =0.27 (-0.18 0.87)**	**U=603, p=0.006, d=0.37, E=2, μ =0.69 (0.23 1.12)**	**U=522, p=0.143, d=0.21, E=0, μ =0.37 (-0.12 0.85)**	**U=528, p=0.095, d=0.22, E=0, μ =0.2 (-0.03 0.46)**
β	C3–CZ	**U=401, p=0.962, d=0.04, E=0, μ =-0.09 (-0.59 0.48)**	**t(35.07)=0.89, p=0.456, d=0.23, E=0, μ =0.23 (-0.29 0.76)**	**U=593, p=0.008, d=0.35, E=2, μ =0.64 (0.17 1.05)**	**U=516, p=0.151, d=0.2, E=0, μ =0.32 (-0.12 0.77)**	**U=567, p=0.05, d=0.3, E=0, μ =0.3 (0.03 0.65)**
β	CZ–PZ	**U=472, p=0.947, d=0.11, E=0, μ =0.22 (-0.25 0.66)**	**U=582, p=0.052, d=0.33, E=0, μ =0.6 (0.12 1.11)**	U=688, p¡0.001, d=0.55, E=3, μ =0.96 (0.53 1.45)	U=619, p=0.024, d=0.41, E=3, μ =0.59 (0.2 1.01)	U=589, p=0.031, d=0.35, E=3, μ =0.24 (0.07 0.58)
β	C4–P4	**U=411, p=0.962, d=0.02, E=0, μ =-0.05 (-0.46 0.38)**	**U=570, p=0.063, d=0.31, E=0, μ =0.57 (0.1 1.1)**	U=695, p¡0.001, d=0.56, E=3, μ =0.95 (0.56 1.44)	**U=561, p=0.054, d=0.29, E=0, μ =0.44 (0.06 0.82)**	**U=530, p=0.095, d=0.22, E=0, μ =0.16 (-0.03 0.49)**
β	C3–P3	**U=469, p=0.947, d=0.1, E=0, μ =0.14 (-0.27 0.62)**	**U=566, p=0.066, d=0.3, E=0, μ =0.59 (0.11 1.12)**	U=666, p¡0.001, d=0.5, E=3, μ =0.88 (0.45 1.32)	U=572, p=0.041, d=0.31, E=3, μ =0.48 (0.08 0.91)	**U=557, p=0.05, d=0.28, E=0, μ =0.21 (0.02 0.52)**

β	T4–T6	**U=407, p=0.962, d=0.03, E=0, μ =-0.07 (-0.43 0.38)**	**U=544, p=0.139, d=0.25, E=0, μ =0.52 (0 1.17)**	U=664, p¡0.001, d=0.5, E=3, μ =0.93 (0.56 1.36)	**U=510, p=0.173, d=0.18, E=0, μ =0.34 (-0.1 0.75)**	**U=552, p=0.05, d=0.27, E=0, μ =0.24 (0.01 0.55)**
β	T3–T5	**U=478, p=0.947, d=0.12, E=0, μ =0.16 (-0.21 0.67)**	**U=585, p=0.052, d=0.34, E=0, μ =0.68 (0.2 1.24)**	U=627, p=0.002, d=0.42, E=3, μ =0.79 (0.35 1.29)	**U=521, p=0.143, d=0.21, E=0, μ =0.35 (-0.1 0.77)**	**U=553, p=0.05, d=0.27, E=0, μ =0.32 (0.02 0.66)**
β	P4–PZ	**U=421, p=0.994, d=0, E=0, μ =0 (-0.46 0.5)**	**U=571, p=0.063, d=0.31, E=0, μ =0.58 (0.1 1.08)**	U=642, p=0.001, d=0.45, E=3, μ =0.82 (0.39 1.29)	t(34.95)=2.45, p=0.041, d=0.64, E=3, μ =0.61 (0.11 1.11)	U=570, p=0.049, d=0.31, E=3, μ =0.37 (0.05 0.75)
β	P3–PZ	**U=487, p=0.947, d=0.14, E=0, μ =0.21 (-0.23 0.63)**	**U=582, p=0.052, d=0.33, E=0, μ =0.67 (0.14 1.24)**	U=665, p¡0.001, d=0.5, E=3, μ =0.93 (0.4 1.37)	U=599, p=0.024, d=0.37, E=3, μ =0.7 (0.2 1.2)	U=599, p=0.028, d=0.37, E=3, μ =0.39 (0.12 0.8)
β	T6–O2	**U=311, p=0.947, d=0.22, E=0, μ =-0.24 (-0.52 0.05)**	**U=539, p=0.149, d=0.24, E=0, μ =0.45 (-0.02 0.99)**	U=659, p¡0.001, d=0.49, E=3, μ =0.88 (0.4 1.52)	**U=563, p=0.054, d=0.29, E=0, μ =0.35 (0.05 0.67)**	**U=528, p=0.095, d=0.22, E=0, μ =0.11 (-0.02 0.31)**
β	T5–O1	**U=357, p=0.947, d=0.13, E=0, μ =-0.15 (-0.5 0.2)**	**t(33.87)=2.77, p=0.052, d=0.72, E=0, μ =0.68 (0.19 1.18)**	U=663, p¡0.001, d=0.5, E=3, μ =0.99 (0.5 1.53)	**U=591, p=0.028, d=0.35, E=2, μ =0.49 (0.14 0.88)**	**U=556, p=0.05, d=0.28, E=0, μ =0.19 (0.01 0.43)**
β	P4–O2	**U=382, p=0.962, d=0.08, E=0, μ =-0.12 (-0.43 0.24)**	**U=515, p=0.251, d=0.19, E=0, μ =0.44 (-0.13 0.97)**	U=647, p=0.001, d=0.46, E=3, μ =0.86 (0.38 1.41)	**U=559, p=0.054, d=0.28, E=0, μ =0.4 (0.04 0.78)**	**U=556, p=0.05, d=0.28, E=0, μ =0.17 (0.01 0.43)**
β	P3–O1	**U=412, p=0.962, d=0.02, E=0, μ =-0.02 (-0.43 0.39)**	**t(31.08)=3.11, p=0.052, d=0.81, E=0, μ =0.75 (0.27 1.24)**	U=691, p¡0.001, d=0.55, E=3, μ =1.06 (0.63 1.51)	**U=600, p=0.024, d=0.37, E=2, μ =0.64 (0.21 1.06)**	**U=557, p=0.05, d=0.28, E=0, μ =0.2 (0.01 0.51)**
β	O1–O2	**U=379, p=0.962, d=0.08, E=0, μ =-0.12 (-0.5 0.25)**	**t(23.97)=1.64, p=0.226, d=0.43, E=0, μ =0.42 (-0.09 0.93)**	**U=599, p=0.007, d=0.37, E=2, μ =0.66 (0.22 1.19)**	U=573, p=0.041, d=0.31, E=3, μ =0.43 (0.1 0.89)	**U=536, p=0.083, d=0.24, E=0, μ =0.15 (-0.02 0.39)**
γ	F8–F4	**U=439, p=0.982, d=0.04, E=0, μ =0.06 (-0.29 0.31)**	**U=464, p=0.894, d=0.09, E=0, μ =0.12 (-0.28 0.52)**	**U=556, p=0.072, d=0.28, E=0, μ =0.33 (0.04 0.64)**	**U=542, p=0.084, d=0.25, E=0, μ =0.23 (-0.01 0.5)**	**U=525, p=0.226, d=0.21, E=0, μ =0.17 (-0.04 0.4)**
γ	F7–F3	**U=432, p=0.982, d=0.02, E=0, μ =0.02 (-0.2 0.22)**	**U=420, p=1, d=0, E=0, μ =0 (-0.39 0.37)**	**U=518, p=0.142, d=0.2, E=0, μ =0.21 (-0.06 0.58)**	**U=576, p=0.056, d=0.32, E=0, μ =0.36 (0.08 0.69)**	**U=541, p=0.198, d=0.25, E=0, μ =0.19 (-0.01 0.38)**
γ	F4–C4	**U=469, p=0.982, d=0.1, E=0, μ =0.05 (-0.11 0.21)**	**U=504, p=0.894, d=0.17, E=0, μ =0.19 (-0.09 0.5)**	U=593, p=0.038, d=0.35, E=3, μ =0.44 (0.13 0.78)	**U=562, p=0.064, d=0.29, E=0, μ =0.3 (0.03 0.65)**	**U=565, p=0.136, d=0.3, E=0, μ =0.18 (0.02 0.49)**
γ	F3–C3	**U=481, p=0.982, d=0.12, E=0, μ =0.08 (-0.08 0.21)**	**U=543, p=0.894, d=0.25, E=0, μ =0.27 (-0.02 0.57)**	U=606, p=0.026, d=0.38, E=3, μ =0.37 (0.11 0.68)	**U=586, p=0.053, d=0.34, E=0, μ =0.3 (0.08 0.58)**	**U=583, p=0.136, d=0.33, E=0, μ =0.18 (0.05 0.34)**
γ	F4–FZ	**U=505, p=0.982, d=0.17, E=0, μ =0.1 (-0.05 0.28)**	**U=486, p=0.894, d=0.13, E=0, μ =0.16 (-0.17 0.48)**	U=640, p=0.011, d=0.45, E=3, μ =0.54 (0.25 0.89)	**U=599, p=0.053, d=0.37, E=0, μ =0.32 (0.1 0.6)**	**U=573, p=0.136, d=0.31, E=0, μ =0.18 (0.03 0.38)**
γ	FZ–CZ	**U=475, p=0.982, d=0.11, E=0, μ =0.04 (-0.09 0.17)**	**U=511, p=0.894, d=0.19, E=0, μ =0.13 (-0.05 0.34)**	U=584, p=0.043, d=0.34, E=3, μ =0.29 (0.05 0.56)	**U=589, p=0.053, d=0.35, E=0, μ =0.22 (0.04 0.47)**	**U=545, p=0.198, d=0.26, E=0, μ =0.08 (0 0.19)**
γ	F3–FZ	**U=472, p=0.982, d=0.11, E=0, μ =0.05 (-0.11 0.2)**	**U=513, p=0.894, d=0.19, E=0, μ =0.2 (-0.06 0.45)**	U=620, p=0.018, d=0.41, E=3, μ =0.5 (0.22 0.81)	**U=594, p=0.053, d=0.36, E=0, μ =0.35 (0.08 0.65)**	**U=566, p=0.136, d=0.3, E=0, μ =0.17 (0.03 0.37)**
γ	T4–C4	**U=471, p=0.982, d=0.1, E=0, μ =0.08 (-0.13 0.26)**	**U=469, p=0.894, d=0.1, E=0, μ =0.09 (-0.23 0.44)**	U=582, p=0.043, d=0.33, E=3, μ =0.4 (0.11 0.73)	**U=543, p=0.084, d=0.25, E=0, μ =0.22 (-0.01 0.59)**	**U=514, p=0.248, d=0.19, E=0, μ =0.11 (-0.05 0.3)**
γ	T3–C3	**U=454, p=0.982, d=0.07, E=0, μ =0.04 (-0.15 0.21)**	**U=499, p=0.894, d=0.16, E=0, μ =0.15 (-0.12 0.44)**	**U=540, p=0.086, d=0.25, E=0, μ =0.27 (-0.02 0.6)**	**U=544, p=0.084, d=0.25, E=0, μ =0.25 (0 0.53)**	**U=525, p=0.226, d=0.21, E=0, μ =0.14 (-0.03 0.34)**
γ	C4–CZ	**U=415, p=0.982, d=0.01, E=0, μ =-0.01 (-0.17 0.15)**	**U=414, p=0.974, d=0.01, E=0, μ =-0.01 (-0.27 0.22)**	**U=456, p=0.583, d=0.07, E=0, μ =0.06 (-0.18 0.33)**	**U=520, p=0.128, d=0.2, E=0, μ =0.18 (-0.06 0.47)**	**U=504, p=0.28, d=0.17, E=0, μ =0.07 (-0.05 0.21)**

γ	C3–CZ	U=474, p=0.982, d=0.11, E=0, μ =0.06 (-0.09 0.23)	U=466, p=0.894, d=0.09, E=0, μ =0.09 (-0.16 0.32)	U=539, p=0.086, d=0.24, E=0, μ =0.25 (-0.03 0.55)	U=565, p=0.064, d=0.3, E=0, μ =0.25 (0.03 0.63)	U=551, p=0.192, d=0.27, E=0, μ =0.12 (0 0.42)
γ	CZ–PZ	U=422, p=0.982, d=0, E=0, μ =0 (-0.16 0.22)	U=471, p=0.894, d=0.1, E=0, μ =0.09 (-0.14 0.34)	U=566, p=0.069, d=0.3, E=0, μ =0.29 (0.03 0.57)	U=579, p=0.056, d=0.32, E=0, μ =0.21 (0.03 0.51)	U=517, p=0.248, d=0.2, E=0, μ =0.06 (-0.02 0.16)
γ	C4–P4	U=414, p=0.982, d=0.01, E=0, μ =-0.01 (-0.15 0.14)	U=428, p=0.974, d=0.02, E=0, μ =0.02 (-0.25 0.24)	U=534, p=0.094, d=0.23, E=0, μ =0.23 (-0.03 0.49)	U=535, p=0.09, d=0.23, E=0, μ =0.16 (-0.03 0.48)	U=473, p=0.457, d=0.11, E=0, μ =0.05 (-0.1 0.2)
γ	C3–P3	U=434, p=0.982, d=0.03, E=0, μ =0.01 (-0.21 0.18)	U=447, p=0.923, d=0.06, E=0, μ =0.03 (-0.2 0.27)	U=552, p=0.074, d=0.27, E=0, μ =0.23 (0.01 0.52)	U=561, p=0.064, d=0.29, E=0, μ =0.21 (0.02 0.54)	U=513, p=0.248, d=0.19, E=0, μ =0.09 (-0.04 0.24)
γ	T4–T6	U=451, p=0.982, d=0.06, E=0, μ =0.04 (-0.14 0.21)	U=456, p=0.894, d=0.07, E=0, μ =0.08 (-0.22 0.36)	U=557, p=0.072, d=0.28, E=0, μ =0.32 (0.02 0.64)	U=518, p=0.13, d=0.2, E=0, μ =0.17 (-0.06 0.47)	U=498, p=0.311, d=0.16, E=0, μ =0.08 (-0.08 0.25)
γ	T3–T5	U=439, p=0.982, d=0.04, E=0, μ =0.02 (-0.17 0.22)	U=462, p=0.894, d=0.09, E=0, μ =0.09 (-0.24 0.44)	U=539, p=0.086, d=0.24, E=0, μ =0.31 (-0.01 0.71)	U=538, p=0.086, d=0.24, E=0, μ =0.27 (-0.03 0.57)	U=534, p=0.222, d=0.23, E=0, μ =0.15 (-0.02 0.41)
γ	P4–PZ	U=431, p=0.982, d=0.02, E=0, μ =0.01 (-0.11 0.18)	U=449, p=0.923, d=0.06, E=0, μ =0.04 (-0.21 0.36)	U=510, p=0.173, d=0.18, E=0, μ =0.26 (-0.11 0.7)	U=546, p=0.084, d=0.26, E=0, μ =0.3 (0 0.71)	U=506, p=0.28, d=0.18, E=0, μ =0.1 (-0.05 0.27)
γ	P3–PZ	U=463, p=0.982, d=0.09, E=0, μ =0.04 (-0.09 0.25)	U=474, p=0.894, d=0.11, E=0, μ =0.12 (-0.16 0.43)	U=562, p=0.069, d=0.29, E=0, μ =0.3 (0.04 0.71)	U=570, p=0.063, d=0.31, E=0, μ =0.31 (0.06 0.65)	U=524, p=0.226, d=0.21, E=0, μ =0.1 (-0.03 0.27)
γ	T6–O2	U=406, p=0.982, d=0.03, E=0, μ =-0.01 (-0.22 0.09)	U=382, p=0.894, d=0.08, E=0, μ =-0.05 (-0.3 0.13)	U=525, p=0.12, d=0.21, E=0, μ =0.17 (-0.02 0.4)	U=523, p=0.126, d=0.21, E=0, μ =0.1 (-0.02 0.31)	U=466, p=0.504, d=0.09, E=0, μ =0.02 (-0.06 0.1)
γ	T5–O1	U=398, p=0.982, d=0.04, E=0, μ =-0.02 (-0.16 0.13)	U=403, p=0.967, d=0.03, E=0, μ =-0.02 (-0.3 0.25)	U=549, p=0.074, d=0.26, E=0, μ =0.21 (0.01 0.5)	U=539, p=0.086, d=0.24, E=0, μ =0.17 (-0.01 0.42)	U=483, p=0.403, d=0.13, E=0, μ =0.05 (-0.06 0.19)
γ	P4–O2	U=398, p=0.982, d=0.04, E=0, μ =-0.02 (-0.14 0.09)	U=403, p=0.967, d=0.03, E=0, μ =-0.02 (-0.24 0.15)	U=564, p=0.069, d=0.29, E=0, μ =0.25 (0.03 0.5)	U=548, p=0.084, d=0.26, E=0, μ =0.14 (0 0.38)	U=495, p=0.317, d=0.15, E=0, μ =0.04 (-0.04 0.15)
γ	P3–O1	U=388, p=0.982, d=0.07, E=0, μ =-0.01 (-0.16 0.1)	U=433, p=0.974, d=0.03, E=0, μ =0.02 (-0.19 0.24)	U=550, p=0.074, d=0.27, E=0, μ =0.21 (0 0.45)	U=550, p=0.084, d=0.27, E=0, μ =0.16 (0 0.43)	U=474, p=0.457, d=0.11, E=0, μ =0.03 (-0.06 0.13)
γ	O1–O2	U=392, p=0.982, d=0.06, E=0, μ =-0.02 (-0.18 0.11)	U=374, p=0.894, d=0.09, E=0, μ =-0.06 (-0.42 0.14)	U=538, p=0.086, d=0.24, E=0, μ =0.24 (-0.02 0.7)	U=522, p=0.126, d=0.21, E=0, μ =0.12 (-0.03 0.35)	U=439, p=0.775, d=0.04, E=0, μ =0.01 (-0.07 0.11)

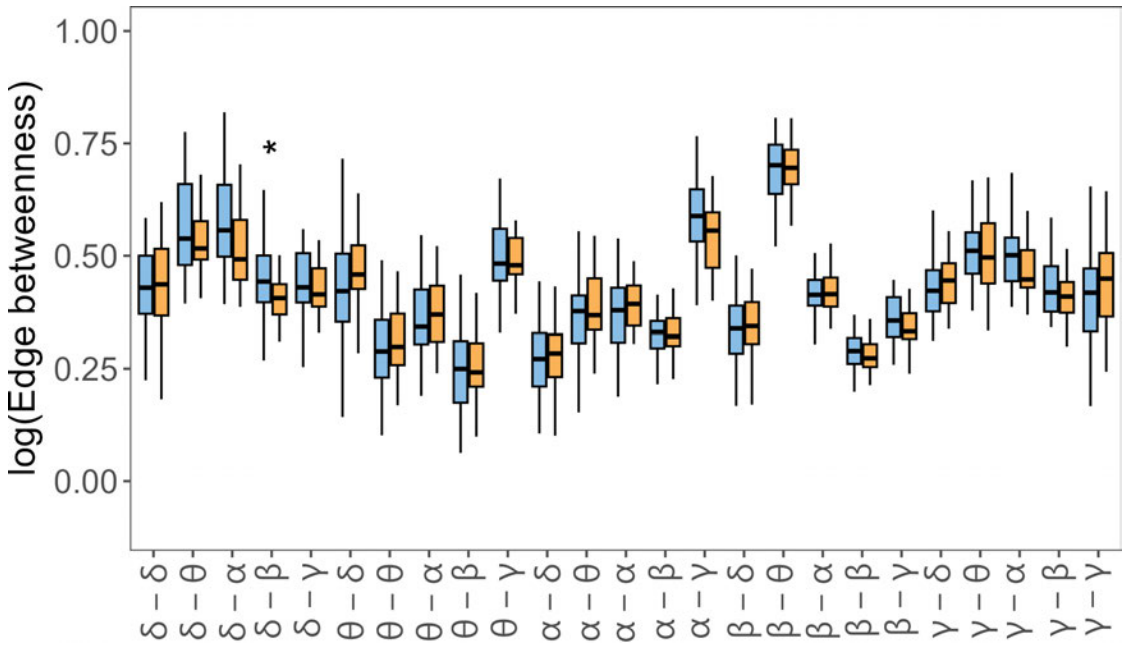

Figure A.16: Importance of each type of frequency coupling of HC (blue) and AD (orange) measured by edge betweenness in epoch 3. Significant differences ($p \leq 0.05$) observed in at least ten thresholded networks are encoded by asterisks. The number of asterisks corresponds to the p-value (FDR corrected), i.e. $p \leq 0.0001$ "****", $p \leq 0.001$ "***", $p \leq 0.01$ "**", and $p \leq 0.05$ "*".

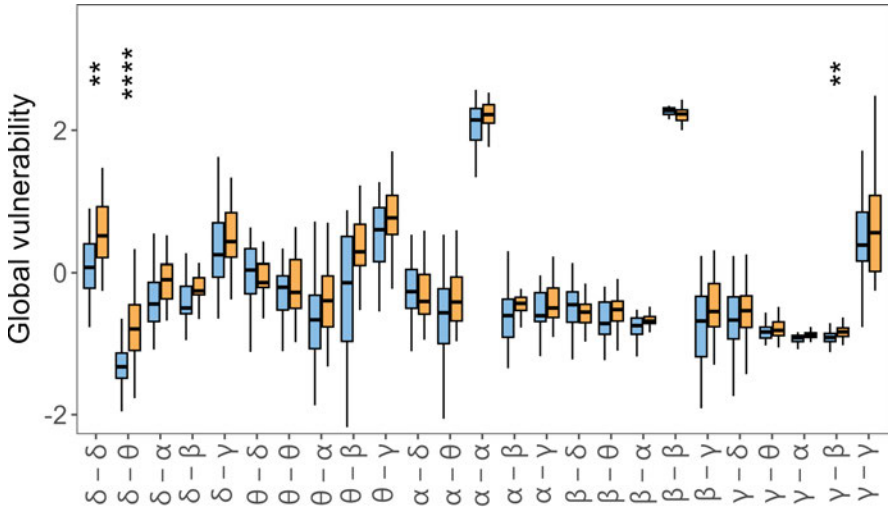

Figure A.17: Global vulnerability of HC (blue) and AD (orange) in epoch 3. Significant differences ($p \leq 0.05$) observed in at least ten thresholded networks are encoded by asterisks. The number of asterisks corresponds to the p-value (FDR corrected), i.e. $p \leq 0.0001$ "****", $p \leq 0.001$ "***", $p \leq 0.01$ "**", and $p \leq 0.05$ "*".

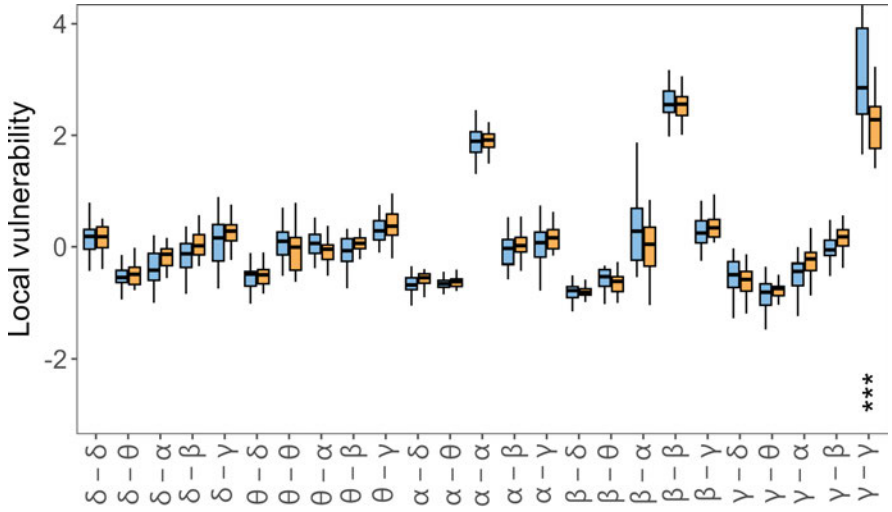

Figure A.18: Local vulnerability of HC (blue) and AD (orange) in epoch 3. Significant differences ($p \leq 0.05$) observed in at least ten thresholded networks are encoded by asterisks. The number of asterisks corresponds to the p-value (FDR corrected), i.e. $p \leq 0.0001$ "****", $p \leq 0.001$ "***", $p \leq 0.01$ "**", and $p \leq 0.05$ "*".

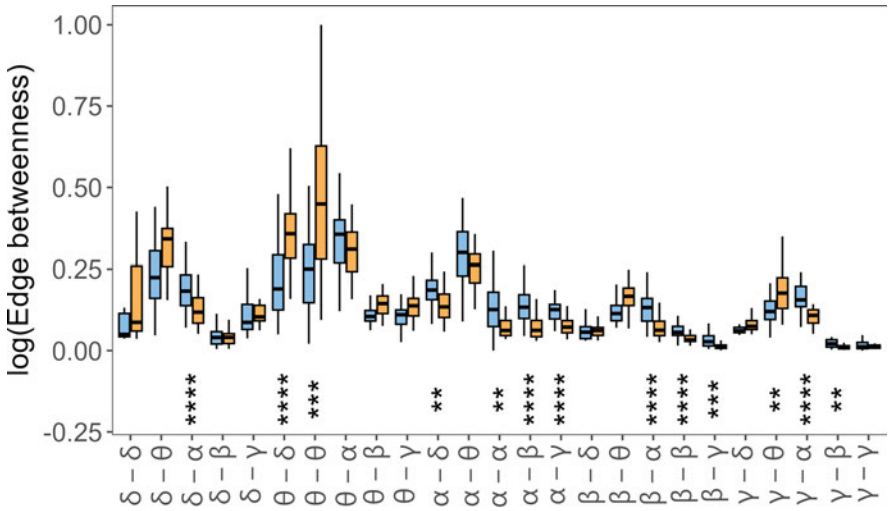

Figure A.19: Importance of each type of frequency coupling of HC (blue) and AD (orange) measured by weighted edge betweenness in epoch 3. Significant differences ($p \leq 0.05$) observed in at least ten thresholded networks are encoded by asterisks. The number of asterisks corresponds to the p-value (FDR corrected), i.e. $p \leq 0.0001$ "****", $p \leq 0.001$ "***", $p \leq 0.01$ "**", and $p \leq 0.05$ "*".

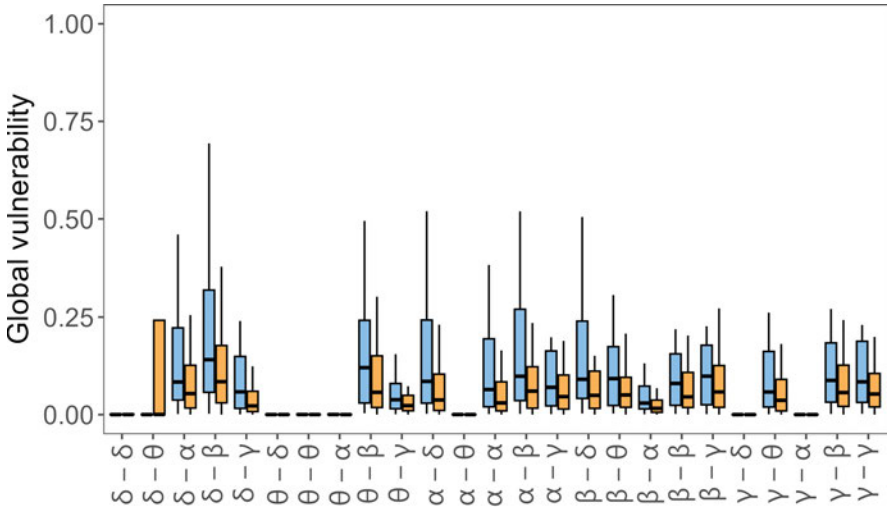

Figure A.20: Weighted global vulnerability of HC (blue) and AD (orange) in epoch 3. Significant differences ($p \leq 0.05$) observed in at least ten thresholded networks are encoded by asterisks.
The number of asterisks corresponds to the p-value (FDR corrected), i.e. $p \leq 0.0001$ "****", $p \leq 0.001$ "***", $p \leq 0.01$ "**", and $p \leq 0.05$ "*".

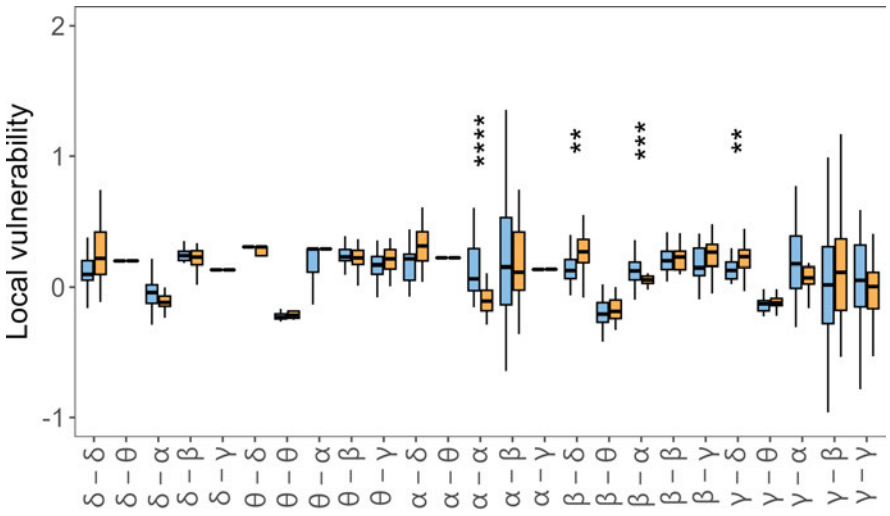

Figure A.21: Weighted local vulnerability of HC (blue) and AD (orange) in epoch 3. Significant differences ($p \leq 0.05$) observed in at least ten thresholded networks are encoded by asterisks. The number of asterisks corresponds to the p-value (FDR corrected), i.e. $p \leq 0.0001$ "****", $p \leq 0.001$ "***", $p \leq 0.01$ "**", and $p \leq 0.05$ "*".

Table A.25: Results from epoch 3 comparing unweighted edge betweenness. The results are reported as follows: statistics value (degrees of freedom), p-value of the test, Cohen's d effect size or nonparameteric alternative, number of thresholds where significant differences were observed (T), number of epochs where significant differences were observed (E), group difference estimate (95% CI). Reliable differences (significant in all three epochs) are highlighted with bold text.

	δ	θ	α	β	γ
δ	t(32.85)=-0.35, p=0.726, d=-0.09, T=0, E=0, μ = −0.09 (-0.62 0.43)	U=464, p=0.501, d=0.09, T=0, E=0, μ = 0.13 (-0.28 0.58)	U=539, p=0.065, d=0.24, T=2, E=0, μ = 0.44 (-0.05 0.87)	**U=565, p=0.024, d=0.3, T=15, E=3,** μ = 0.49 **(0.07 0.99)**	U=479, p=0.365, d=0.12, T=2, E=0, μ = 0.16 (-0.22 0.5)
θ	t(31.84)=-0.92, p=0.364, d=-0.24, T=0, E=0, μ = −0.24 (-0.76 0.28)	t(37)=-1.13, p=0.262, d=-0.3, T=0, E=0, μ = −0.3 (-0.82 0.23)	t(36.82)=-0.81, p=0.423, d=-0.21, T=0, E=0, μ = −0.21 (-0.74 0.31)	t(36.9)=-0.34, p=0.735, d=-0.09, T=0, E=0, μ = −0.09 (-0.62 0.44)	U=436, p=0.811, d=0.03, T=0, E=0, μ = 0.05 (-0.35 0.44)
α	t(36.51)=-0.56, p=0.579, d=-0.15, T=0, E=0, μ = −0.15 (-0.67 0.38)	t(36.91)=-1.2, p=0.235, d=-0.32, T=0, E=0, μ = −0.31 (-0.84 0.21)	t(32.72)=-0.93, p=0.356, d=-0.24, T=0, E=0, μ = −0.24 (-0.76 0.28)	t(33.58)=0.46, p=0.651, d=0.12, T=0, E=0, μ = 0.12 (-0.41 0.64)	t(36.14)=1.75, p=0.087, d=0.46, T=9, E=0, μ = 0.45 (-0.07 0.96)
β	t(35.71)=-0.42, p=0.674, d=-0.11, T=0, E=0, μ = −0.11 (-0.64 0.42)	t(34.17)=-0.95, p=0.345, d=-0.25, T=0, E=0, μ = −0.25 (-0.77 0.27)	t(33.59)=-0.12, p=0.903, d=-0.03, T=0, E=0, μ = −0.03 (-0.56 0.49)	U=469, p=0.453, d=0.1, T=0, E=0, μ = 0.14 (-0.22 0.53)	U=516, p=0.138, d=0.2, T=7, E=0, μ = 0.22 (-0.05 0.55)
γ	U=360, p=0.357, d=0.12, T=0, E=0, μ = −0.14 (-0.46 0.19)	U=449, p=0.66, d=0.06, T=0, E=0, μ = 0.1 (-0.35 0.5)	U=530, p=0.088, d=0.22, T=8, E=0, μ = 0.29 (-0.06 0.65)	U=473, p=0.417, d=0.11, T=0, E=0, μ = 0.17 (-0.18 0.56)	t(36.95)=-1.15, p=0.255, d=-0.3, T=5, E=0, μ = −0.3 (-0.82 0.22)

Table A.26: Results from epoch 3 comparing unweighted global vulnerability. The results are reported as follows: statistics value (degrees of freedom), p-value of the test, Cohen's d effect size or nonparameteric alternative, number of thresholds where significant differences were observed (T), number of epochs where significant differences were observed (E), group difference estimate (95% CI). Reliable differences (significant in all three epochs) are highlighted with bold text.

	δ	θ	α	β	γ
δ	**t(33.04)=-3.27, p=0.002, d=-0.86, T=16, E=3,** μ = −0.8**(-1.29 -0.31)**	**U=169, p¡0.001, d=0.51, T=17, E=3,** μ = −0.92**(-1.38 -0.49)**	t(35.18)=-3.15, p=0.003, d=-0.82, T=14, E=1, μ = −0.76(-1.25 -0.28)	U=264, p=0.015, d=0.32, T=13, E=1, μ = −0.65(-0.97 -0.18)	U=321, p=0.126, d=0.2, T=6, E=0, μ = −0.3(-0.82 0.09)
θ	t(35.29)=1.13, p=0.263, d=0.3, T=3, E=0, μ = 0.29(-0.23 0.82)	U=411, p=0.896, d=0.02, T=0, E=0, μ = −0.05(-0.59 0.41)	t(34.97)=-2.11, p=0.04, d=-0.55, T=11, E=1, μ = −0.53(-1.04 -0.03)	U=272, p=0.021, d=0.3, T=12, E=1, μ = −0.63(-1.2 -0.1)	U=316, p=0.108, d=0.21, T=0, E=0, μ = −0.32(-0.77 0.07)
α	t(31.62)=1.23, p=0.224, d=0.32, T=6, E=0, μ = 0.32(-0.2 0.84)	U=319, p=0.118, d=0.21, T=1, E=0, μ = −0.35(-0.87 0.11)	U=314, p=0.101, d=0.22, T=7, E=0, μ = −0.31(-0.71 0.07)	U=268, p=0.018, d=0.31, T=15, E=1, μ = −0.55(-1.01 -0.09)	U=323, p=0.134, d=0.2, T=5, E=0, μ = −0.31(-0.79 0.1)
β	U=512, p=0.156, d=0.19, T=6, E=0, μ = 0.32(-0.09 0.8)	t(35.23)=-1.92, p=0.06, d=-0.5, T=9, E=0, μ = −0.49(-1 0.02)	U=282, p=0.032, d=0.28, T=11, E=1, μ = −0.33(-0.7 -0.06)	U=532, p=0.083, d=0.23, T=8, E=0, μ = 0.38(-0.04 0.87)	t(36.84)=-2.19, p=0.033, d=-0.57, T=11, E=2, μ = −0.55(-1.06 -0.05)
γ	t(36.99)=-0.6, p=0.549, d=-0.16, T=0, E=0, μ = −0.16(-0.69 0.37)	t(36.84)=-1.12, p=0.265, d=-0.29, T=0, E=0, μ = −0.29(-0.82 0.23)	U=272, p=0.021, d=0.3, T=13, E=1, μ = −0.36(-0.76 -0.05)	**t(33.74)=-3.15, p=0.003, d=-0.82, T=10, E=3,** μ = −0.76**(-1.25 -0.28)**	U=360, p=0.357, d=0.12, T=1, E=0, μ = −0.2(-0.58 0.24)

Table A.27: Results from epoch 3 comparing unweighted local vulnerability. The results are reported as follows: statistics value (degrees of freedom), p-value of the test, Cohen's d effect size or nonparameteric alternative, number of thresholds where significant differences were observed (T), number of epochs where significant differences were observed (E), group difference estimate (95% CI). Reliable differences (significant in all three epochs) are highlighted with bold text.

	δ	θ	α	β	γ
δ	t(32.88)=0.57, p=0.569, d=0.15, T=0, E=0, μ = 0.15 (-0.37 0.67)	t(33.67)=-1.38, p=0.174, d=-0.36, T=2, E=0, μ = −0.36 (-0.89 0.16)	t(35.06)=-2.72, p=0.009, d=-0.71, T=12, E=1, μ = −0.67 (-1.17 -0.18)	t(34.69)=-2.65, p=0.01, d=-0.69, T=14, E=1, μ = −0.66 (-1.15 -0.16)	U=336, p=0.195, d=0.17, T=2, E=0, μ = −0.26 (-0.81 0.1)
θ	t(36.88)=-0.99, p=0.327, d=-0.26, T=4, E=0, μ = −0.26 (-0.78 0.27)	t(33.16)=1.79, p=0.08, d=0.47, T=4, E=0, μ = 0.46 (-0.06 0.98)	t(36.64)=1.78, p=0.081, d=0.47, T=6, E=0, μ = 0.46 (-0.06 0.98)	U=299, p=0.06, d=0.25, T=9, E=0, μ = −0.53 (-1.05 0.03)	t(36.96)=-1.43, p=0.157, d=-0.38, T=4, E=0, μ = −0.37 (-0.89 0.15)
α	t(34.25)=-2.05, p=0.045, d=-0.54, T=10, E=1, μ = −0.52 (-1.03 -0.01)	t(37)=-1.27, p=0.209, d=-0.33, T=0, E=0, μ = −0.33 (-0.85 0.19)	t(33.04)=-1.19, p=0.24, d=-0.31, T=6, E=0, μ = −0.31 (-0.83 0.21)	t(36.81)=-1.33, p=0.189, d=-0.35, T=3, E=0, μ = −0.35 (-0.87 0.17)	U=301, p=0.065, d=0.24, T=8, E=0, μ = −0.43 (-0.94 0.03)
β	U=447, p=0.682, d=0.06, T=0, E=0, μ = 0.11 (-0.4 0.46)	t(35.31)=1.78, p=0.08, d=0.47, T=7, E=0, μ = 0.46 (-0.06 0.98)	U=527, p=0.098, d=0.22, T=4, E=0, μ = 0.41 (-0.07 0.97)	t(36.58)=0.26, p=0.795, d=0.07, T=1, E=0, μ = 0.07 (-0.46 0.6)	t(36.81)=-1.76, p=0.083, d=-0.46, T=9, E=0, μ = −0.45 (-0.97 0.06)
γ	t(36.34)=1.21, p=0.233, d=0.32, T=0, E=0, μ = 0.31 (-0.21 0.84)	t(35.53)=-0.95, p=0.345, d=-0.25, T=0, E=0, μ = −0.25 (-0.77 0.27)	U=264, p=0.015, d=0.32, T=12, E=1, μ = −0.6 (-1 -0.11)	t(32.6)=-1.98, p=0.053, d=-0.52, T=8, E=0, μ = −0.5 (-1.01 0.01)	**U=630, p=0.001, d=0.43, T=12, E=3,** μ = 0.28 **(0.11 0.49)**

Table A.28: Results from epoch 3 comparing weighted edge betweenness. The results are reported as follows: statistics value (degrees of freedom), p-value of the test, Cohen's d effect size or nonparameteric alternative, number of thresholds where significant differences were observed (T), number of epochs where significant differences were observed (E), group difference estimate (95% CI). Reliable differences (significant in all three epochs) are highlighted with bold text.

	δ	θ	α	β	γ
δ	**U=595, p=0.005, d=0.37, T=13, E=3,** μ = 0.13 **(0 0.31)**	**U=651, p¡0.001, d=0.5, T=13, E=3,** μ = 0.33 **(0.02 0.46)**	**U=677, p¡0.001, d=0.53, T=13, E=3,** μ = 0.6 **(0.2 1.16)**	**U=697.5, p¡0.001, d=0.57, T=19, E=3,** μ = 0.3 **(0.15 0.61)**	**t(24.74)=3.38, p=0.002, d=0.88, T=16, E=3,** μ = 0.8 **(0.32 1.28)**
θ	**U=658, p¡0.001, d=0.49, T=12, E=3,** μ = 0.82 **(0.35 1.3)**	**U=570, p=0.019, d=0.31, T=11, E=3,** μ = 0.62 **(0.11 1.24)**	U=477.5, p=0.093, d=0.22, T=4, E=0, μ = 0 (0 0)	U=396, p=0.579, d=0.07, T=2, E=0, μ = 0 (0 0)	t(36.87)=-0.96, p=0.341, d=-0.25, T=0, E=0, μ = −0.25 (-0.78 0.27)
α	U=520, p=0.076, d=0.23, T=7, E=0, μ = 0 (0 0.01)	U=344, p=0.159, d=0.19, T=6, E=0, μ = 0 (-0.04 0)	U=437, p=0.75, d=0.04, T=2, E=0, μ = 0 (0 0)	U=397.5, p=0.664, d=0.06, T=0, E=0, μ = 0 (0 0)	U=333, p=0.18, d=0.18, T=4, E=0, μ = −0.05 (-0.16 0.03)
β	**U=675, p¡0.001, d=0.52, T=19, E=3,** μ = 0.54 **(0.29 0.98)**	U=456, p=0.583, d=0.07, T=0, E=0, μ = 0.09 (-0.35 0.38)	U=350, p=0.179, d=0.18, T=3, E=0, μ = 0 (0 0)	U=381, p=0.548, d=0.08, T=0, E=0, μ = −0.01 (-0.05 0.01)	**U=176, p¡0.001, d=0.5, T=19, E=3,** μ = −0.75 **(-1.12 -0.34)**
γ	**U=613, p=0.002, d=0.39, T=14, E=3,** μ = 0.9 **(0.4 1.42)**	U=336, p=0.195, d=0.17, T=5, E=0, μ = −0.23 (-0.59 0.1)	U=350, p=0.282, d=0.14, T=2, E=0, μ = −0.08 (-0.26 0.06)	**U=171, p¡0.001, d=0.51, T=18, E=3,** μ = −0.74 **(-1.36 -0.35)**	**t(36.92)=-3.88, p¡0.001, d=-1.02, T=19, E=3,** μ = −0.91 **(-1.38 -0.44)**

Table A.29: Results from epoch 3 comparing weighted global vulnerability. The results are reported as follows: statistics value (degrees of freedom), p-value of the test, Cohen's d effect size or nonparameteric alternative, number of thresholds where significant differences were observed (T), number of epochs where significant differences were observed (E), group difference estimate (95% CI). Reliable differences (significant in all three epochs) are highlighted with bold text.

	δ	θ	α	β	γ
δ	U=466, p=0.482, d=0.09, T=1, E=0, μ = 0 (0 0)	U=451, p=0.638, d=0.06, T=2, E=0, μ = 0 (0 0)	U=514, p=0.147, d=0.19, T=4, E=0, μ = 0 (0 0)	**U=626, p=0.001, d=0.42, T=17, E=3,** μ = 0.23 **(0.02 0.95)**	U=581, p=0.012, d=0.33, T=15, E=2, μ = 0.68 (0.2 1.12)
θ	U=453, p=0.616, d=0.07, T=2, E=0, μ = 0 (0 0)	U=441, p=0.752, d=0.04, T=0, E=0, μ = 0 (0 0)	U=399, p=0.752, d=0.04, T=0, E=0, μ = 0 (0 0)	U=440, p=0.763, d=0.04, T=0, E=0, μ = 0 (0 0)	t(32.07)=0.4, p=0.69, d=0.1, T=0, E=0, μ = 0.1 (-0.42 0.63)
α	U=517, p=0.134, d=0.2, T=2, E=0, μ = 0 (0 0)	U=404, p=0.811, d=0.03, T=0, E=0, μ = 0 (0 0)	U=389, p=0.638, d=0.06, T=0, E=0, μ = 0 (-0.12 0.01)	U=404, p=0.811, d=0.03, T=0, E=0, μ = 0 (0 0)	t(30.11)=-1.11, p=0.275, d=-0.29, T=2, E=0, μ = −0.29 (-0.8 0.23)
β	**U=659, p¡0.001, d=0.49, T=10, E=3,** μ = 0.65 **(0.03 1.1)**	U=390, p=0.649, d=0.06, T=0, E=0, μ = 0 (0 0)	U=451, p=0.638, d=0.06, T=0, E=0, μ = 0 (0 0)	U=365, p=0.399, d=0.11, T=0, E=0, μ = 0 (0 0)	**U=135, p¡0.001, d=0.58, T=20, E=3,** μ = −0.95 **(-1.32 -0.55)**
γ	U=453, p=0.616, d=0.07, T=1, E=0, μ = 0.15 (-0.41 0.7)	U=442, p=0.74, d=0.04, T=0, E=0, μ = 0.02 (-0.26 0.27)	U=388, p=0.627, d=0.07, T=0, E=0, μ = −0.14 (-0.62 0.4)	**t(36.03)=-4.75, p¡0.001, d=-1.24, T=16, E=3,** μ = −1.06 **(-1.5 -0.61)**	**U=176, p¡0.001, d=0.5, T=18, E=3,** μ = −0.99 **(-1.4 -0.51)**

Table A.30: Results from epoch 3 comparing weighted local vulnerability. The results are reported as follows: statistics value (degrees of freedom), p-value of the test, Cohen's d effect size or nonparameteric alternative, number of thresholds where significant differences were observed (T), number of epochs where significant differences were observed (E), group difference estimate (95% CI). Reliable differences (significant in all three epochs) are highlighted with bold text.

	δ	θ	α	β	γ
δ	U=651, p¡0.001, d=0.47, T=20, E=0, μ = 0.85 (0.43 1.22)	U=591, p=0.007, d=0.35, T=14, E=1, μ = 0.71 (0.19 1.19)	U=281, p=0.03, d=0.28, T=11, E=0, μ = −0.47 (-0.92 -0.07)	**t(36.97)=-5.04, p¡0.001, d=-1.32, T=15, E=3,** μ = −1.11 **(-1.55 -0.67)**	U=470, p=0.444, d=0.1, T=0, E=0, μ = 0.19 (-0.33 0.6)
θ	t(25.91)=4, p¡0.001, d=1.04, T=19, E=0, μ = 0.92 (0.46 1.38)	t(31.29)=2.94, p=0.005, d=0.78, T=14, E=1, μ = 0.73 (0.23 1.23)	U=270, p=0.019, d=0.31, T=12, E=0, μ = −0.6 (-0.99 -0.1)	t(33.76)=-3.42, p=0.001, d=-0.89, T=16, E=0, μ = −0.82 (-1.3 -0.34)	U=378, p=0.521, d=0.09, T=0, E=0, μ = −0.13 (-0.49 0.26)
α	t(28.9)=3.6, p=0.001, d=0.94, T=19, E=0, μ = 0.85 (0.37 1.32)	t(36.71)=2.34, p=0.023, d=0.61, T=13, E=0, μ = 0.59 (0.08 1.1)	U=280, p=0.029, d=0.29, T=11, E=0, μ = −0.5 (-0.94 -0.04)	U=215, p=0.001, d=0.42, T=15, E=0, μ = −0.68 (-1.03 -0.29)	U=361, p=0.365, d=0.12, T=5, E=0, μ = −0.16 (-0.67 0.22)
β	**t(34.02)=4.25, p¡0.001, d=1.11, T=18, E=3,** μ = 0.97 **(0.51 1.43)**	t(34.1)=2.65, p=0.011, d=0.7, T=14, E=0, μ = 0.67 (0.16 1.17)	U=320, p=0.122, d=0.2, T=6, E=0, μ = −0.42 (-0.89 0.11)	U=223, p=0.002, d=0.4, T=14, E=0, μ = −0.55 (-0.85 -0.21)	U=311, p=0.092, d=0.22, T=9, E=0, μ = −0.32 (-0.77 0.05)
γ	t(32.21)=1.26, p=0.213, d=0.33, T=0, E=0, μ = 0.33 (-0.19 0.84)	t(35.92)=1.07, p=0.29, d=0.28, T=2, E=0, μ = 0.28 (-0.25 0.81)	U=493, p=0.261, d=0.15, T=0, E=0, μ = 0.19 (-0.19 0.44)	**t(37)=-2.64, p=0.011, d=-0.69, T=12, E=3,** μ = −0.66 **(-1.16 -0.16)**	**t(36.16)=-3.28, p=0.002, d=-0.86, T=13, E=3,** μ = −0.79 **(-1.28 -0.31)**

Appendix B

Additional results from EEG-based Graph Neural Network Classification: An Empirical Evaluation of Functional Connectivity Methods (Chapter 5)

B.1 Comparison of node features - power spectral density

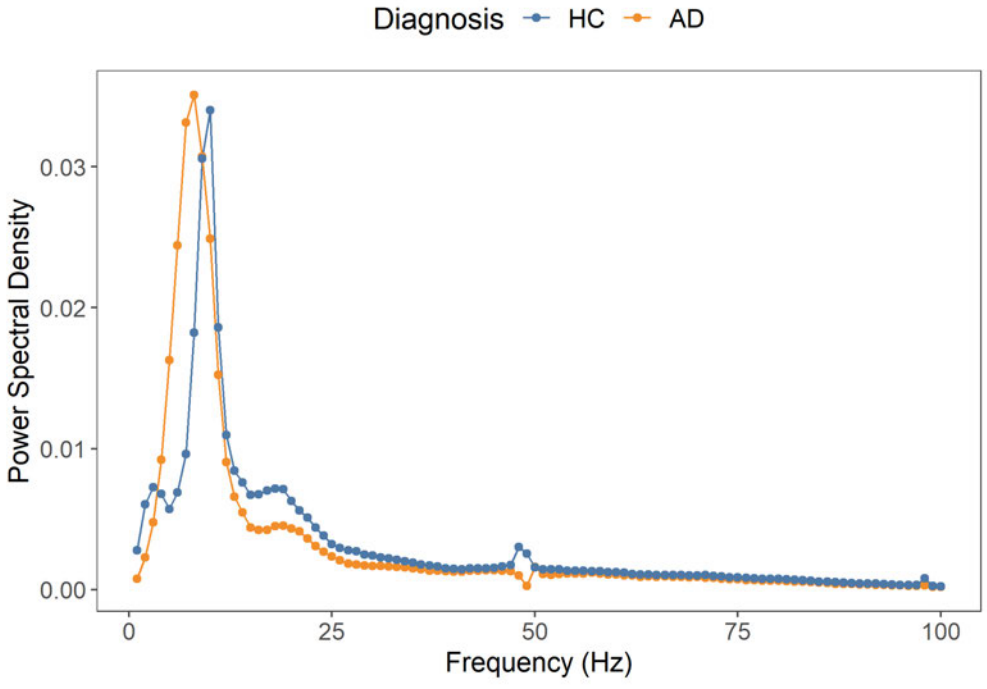

Figure B.1: Averaged node features

B.2 Comparison of functional connectivity measures

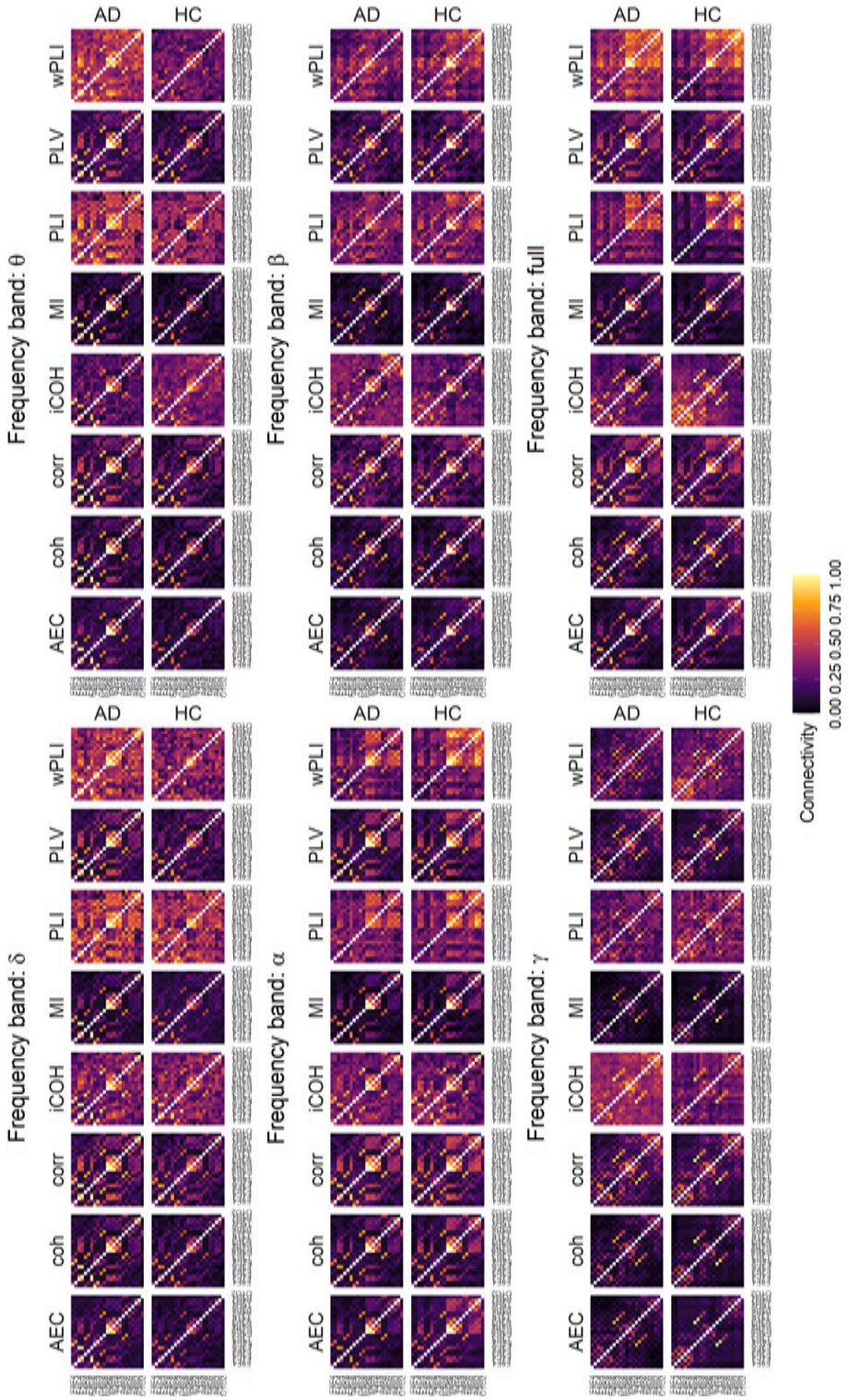

Figure B.2: Averaged adjacency matrices of AD and HC cases measured with various functional connectivity measures

B.3 Effect of frequency bands on model performance

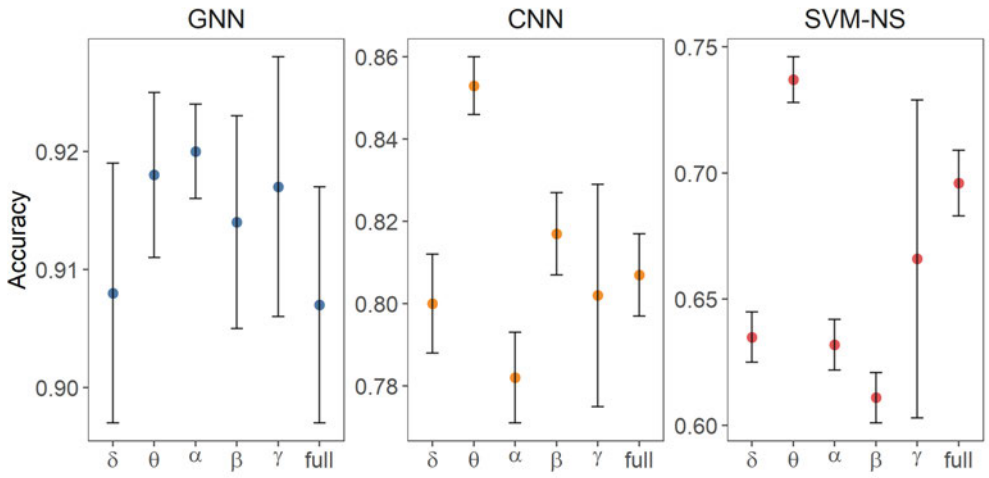

Figure B.3: Effect of frequency band

Table B.1: Performance of the GNN model across five frequency bands and the full frequency range. Values are based on 20-times repeated 20-fold cross-validation. Differences might occur between the main-text results and the supplementary results as the main-text results are based on 50-times repeated 20-fold cross-validation.

Band	area under curve (AUC)	Accuracy	Sensitivity	Specificity
delta	0.98 ± 0.003	90.59% ± 0.77	93.43% ± 1.65	87.79% ± 2.08
theta	0.983 ± 0.003	90.59% ± 0.77	93.43% ± 1.65	87.79% ± 2.08
alpha	0.984 ± 0.002	90.59% ± 0.77	93.43% ± 1.65	87.79% ± 2.08
beta	0.984 ± 0.003	90.59% ± 0.77	93.43% ± 1.65	87.79% ± 2.08
gamma	0.984 ± 0.003	90.59% ± 0.77	93.43% ± 1.65	87.79% ± 2.08
full	0.983 ± 0.002	90.59% ± 0.77	93.43% ± 1.65	87.79% ± 2.08

Table B.2: Performance of the CNN model across five frequency bands and the full frequency range. Values are based on 20-times repeated 20-fold cross-validation. Differences might occur between the main-text results and the supplementary results as the main-text results are based on 50-times repeated 20-fold cross-validation.

Band-	AUC-	Accuracy-	Sensitivity-	Specificity-
theta-	0.937- 0.004-	85.51%-±0.6-	82.77%-±1.24-	88.22%-±1.45-
beta-	0.904- 0.009-	85.51%-±0.6-	82.77%-±1.24-	88.22%-±1.45-
full-	0.902- 0.005-	85.51%-±0.6-	82.77%-±1.24-	88.22%-±1.45-
delta-	0.898- 0.005-	85.51%-±0.6-	82.77%-±1.24-	88.22%-±1.45-
gamma-	0.873- 0.019-	85.51%-±0.6-	82.77%-±1.24-	88.22%-±1.45-
alpha-	0.867- 0.01-	85.51%-±0.6-	82.77%-±1.24-	88.22%-±1.45-

Table B.3: Performance of the SVM-NS model across five frequency bands and the full frequency range. Values are based on 20-times repeated 20-fold cross-validation. Differences might occur between the main-text results and the supplementary results as the main-text results are based on 50-times repeated 20-fold cross-validation.

Band-	AUC-	Accuracy-	Sensitivity-	Specificity-
delta-	0.67- 0.017-	63.54%-±1.05-	62.91%-±1.19-	64.22%-±1.02-
theta-	0.801- 0.013-	63.54%-±1.05-	62.91%-±1.19-	64.22%-±1.02-
alpha-	0.69- 0.042-	63.54%-±1.05-	62.91%-±1.19-	64.22%-±1.02-
beta-	0.725- 0.068-	63.54%-±1.05-	62.91%-±1.19-	64.22%-±1.02-
gamma-	0.761- 0.056-	63.54%-±1.05-	62.91%-±1.19-	64.22%-±1.02-
full-	0.752- 0.037-	63.54%-±1.05-	62.91%-±1.19-	64.22%-±1.02-

B.4 Effect of edge filters on model performance

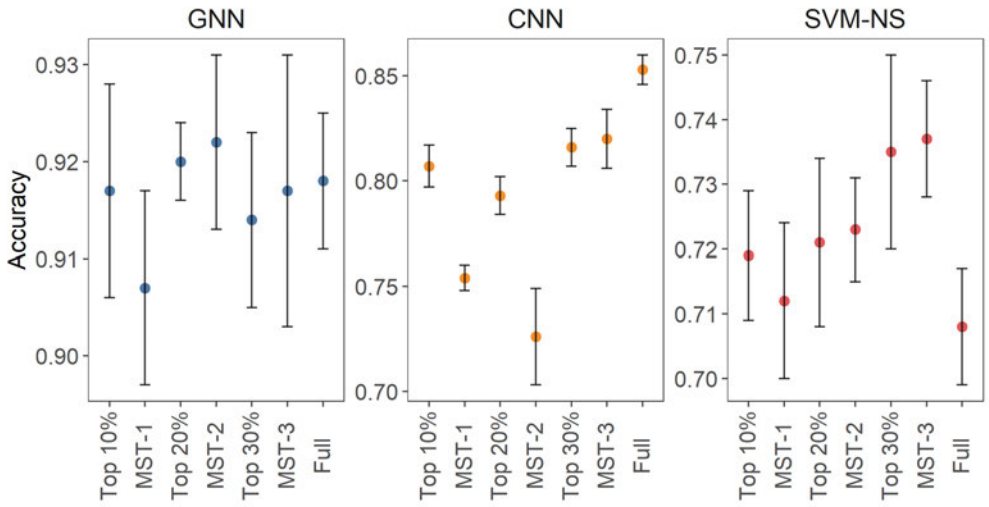

Figure B.4: Effect of edge filters

Table B.4: Performance of the GNN model across the graph filters used. Values are based on 20-times repeated 20-fold cross-validation. Differences might occur between the main-text results and the supplementary results as the main-text results are based on 50-times repeated 20-fold cross-validation.

Edge-Filter	AUC	Accuracy	Sensitivity	Specificity
Top-10%	0.984 - 0.003	91.74% ±1.1	95.13% ±1.31	88.4% ±2.02
MST-1	0.983 - 0.002	91.74% ±1.1	95.13% ±1.31	88.4% ±2.02
Top-20%	0.984 - 0.002	91.74% ±1.1	95.13% ±1.31	88.4% ±2.02
MST-2	0.981 - 0.004	91.74% ±1.1	95.13% ±1.31	88.4% ±2.02
Top-30%	0.984 - 0.003	91.74% ±1.1	95.13% ±1.31	88.4% ±2.02
MST-3	0.981 - 0.003	91.74% ±1.1	95.13% ±1.31	88.4% ±2.02
Full	0.983 - 0.003	91.74% ±1.1	95.13% ±1.31	88.4% ±2.02

Table B.5: Performance of the CNN model across the edge filters used. Values are based on 20-times repeated 20-fold cross-validation. Differences might occur between the main-text results and the supplementary results as the main-text results are based on 50-times repeated 20-fold cross-validation.

Edge-Filter	AUC	Accuracy	Sensitivity	Specificity
Full	0.937 - 0.004	85.51% ±0.6	82.77% ±1.24	88.22% ±1.45
MST-3	0.911 - 0.004	85.51% ±0.6	82.77% ±1.24	88.22% ±1.45
Top-10%	0.902 - 0.005	85.51% ±0.6	82.77% ±1.24	88.22% ±1.45
Top-30%	0.896 - 0.005	85.51% ±0.6	82.77% ±1.24	88.22% ±1.45
MST-2	0.887 - 0.004	85.51% ±0.6	82.77% ±1.24	88.22% ±1.45
MST-1	0.88 - 0.004	85.51% ±0.6	82.77% ±1.24	88.22% ±1.45
Top-20%	0.872 - 0.006	85.51% ±0.6	82.77% ±1.24	88.22% ±1.45

Table B.6: Performance of the SVM-NS model across the edge filters used. Values are based on 20-times repeated 20-fold cross-validation. Differences might occur between the main-text results and the supplementary results as the main-text results are based on 50-times repeated 20-fold cross-validation.

Edge-Filter	AUC	Accuracy	Sensitivity	Specificity
Top-10%	0.77 - 0.011	71.86% ±1.05	72.21% ±1.06	71.55% ±1.22
MST-1	0.772 - 0.013	71.86% ±1.05	72.21% ±1.06	71.55% ±1.22
Top-20%	0.772 - 0.03	71.86% ±1.05	72.21% ±1.06	71.55% ±1.22
MST-2	0.785 - 0.014	71.86% ±1.05	72.21% ±1.06	71.55% ±1.22
Top-30%	0.779 - 0.014	71.86% ±1.05	72.21% ±1.06	71.55% ±1.22
MST-3	0.801 - 0.013	71.86% ±1.05	72.21% ±1.06	71.55% ±1.22
Full	0.759 - 0.008	71.86% ±1.05	72.21% ±1.06	71.55% ±1.22

Appendix C

Additional results from Adaptive Gated Graph Convolutional Network for Explainable Diagnosis (Chapter 6)

C.1 Hyperparameters of proposed model

The optimised and allowed values of the various hyperparameters of the proposed AGGCN are reported in Tables C.1 and C.2, respectively.

Table C.1: Hyper-parameter values of the optimised model

L_{CNN}	kernel size	CNN filters	h_{CNN}	$drop_{CNN}$	k_{KNN}
1	4	84	403	0.024	16
R	h_{GNN}	activation	aggregation	$drop_{GNN}$	
4	372	Tanh	mean	0.9	
k_{pool}	$drop_{pool}$	negative slope	L_{MLP}	h_{MLP}	$drop_{MLP}$
3	0.75	0.085	3	16	0
learning rate	momentum	weight decay	γ	σ	p_{noise}
0.063	0.859	0.076	0.896	0.346	0.1

Table C.2: Hyper-parameter value ranges allowed during optimisation

Hyperparameter	Values
L_{CNN}	$[1, \ldots, 4]$
kernel-size	$[2, \ldots, 4]$
CNN-filters	$[16, \ldots, 100]$
h_{CNN}	$[16, \ldots, 1024]$
$drop_{CNN}$	$[0, 0.9]$
k_{KNN}	$[1, \ldots, 23]$
R	$[1, \ldots, 10]$
h_{GNN}	$[16, \ldots, 1024]$
activation	$ReLU, Tanh, ELU, LeakyReLU$
aggregation	$add, mean, max$
$drop_{GNN}$	$[0, 0.9]$
k_{pool}	$[1, \ldots, 23]$
$drop_{pool}$	$[0, 0.9]$
negative-slope	$[0, 0.5]$
L_{MLP}	$[1, \ldots, 5]$
h_{MLP}	$[16, \ldots, 2048]$
$drop_{MLP}$	$[0, 0.9]$
learning-rate	$[0.001, 0.1]$
momentum	$[0, 0.9]$
weight-decay	$[0, 0.1]$
γ	$[0.8, 0.95]$
σ	$[0, 0.5]$
p_{noise}	$[0, 0.6]$

C.2 Parameter sensitivity experiments

Multiple parameter sensitivity experiments were performed to test the influence of the selected crucial hyperparameters of AGGCN. The results of these experiments are reported in Figures C.1, C.2, C.3 and C.4 for the number of GGCN iterations, K-nearest neighbour edges kept in the sparse learned graph structure, size of the coarsened (pooled) graph and aggregation function, respectively.

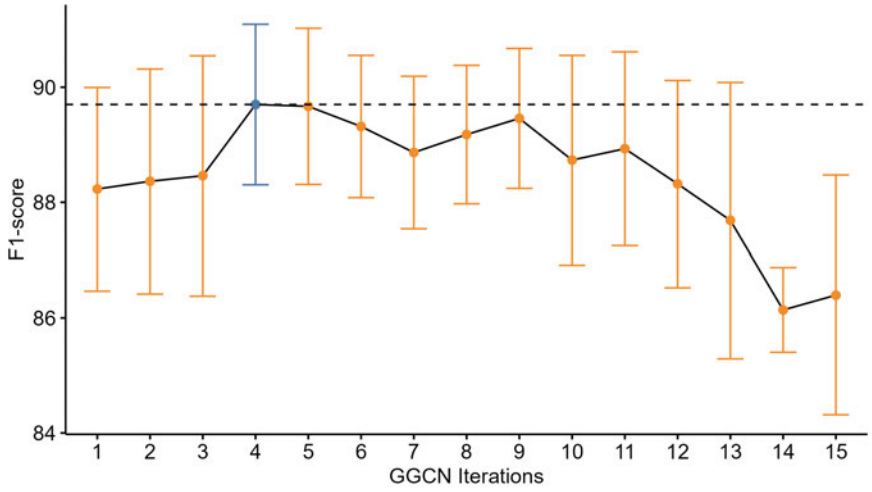

Figure C.1: Sensitivity of the proposed model to the number of iterations of the GGCN encoder. The error bars show the standard deviation of accuracies measured across ten repetitions. The optimal value is shown in blue.

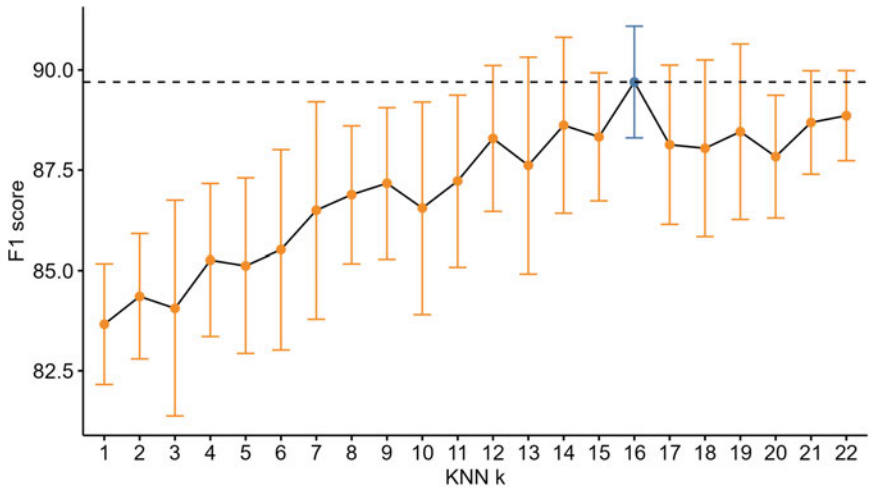

Figure C.2: Sensitivity of the proposed model to the k-nearest-neighbour edges kept in the learned graph structure. The error bars show the standard deviation of accuracies measured across ten repetitions. The optimal value is shown in blue.

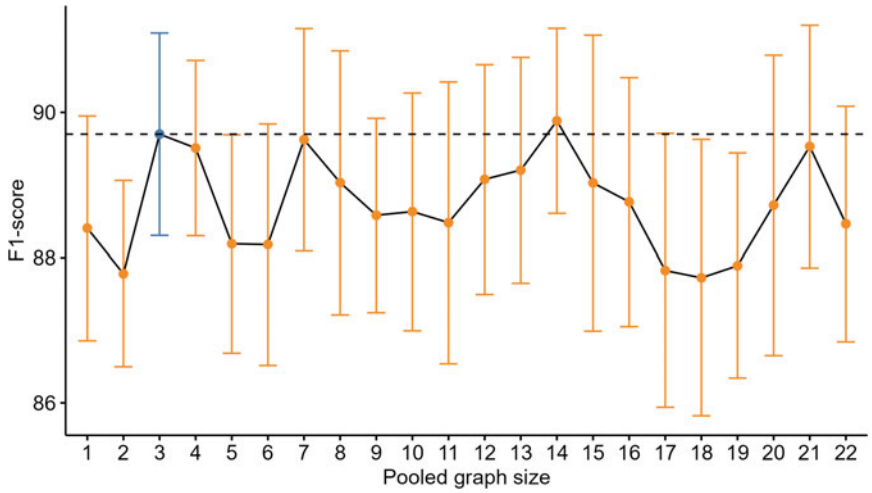

Figure C.3: Sensitivity of the proposed model to the size of the pooled graph. The error bars show the standard deviation of accuracies measured across ten repetitions. The optimal value is shown in blue.

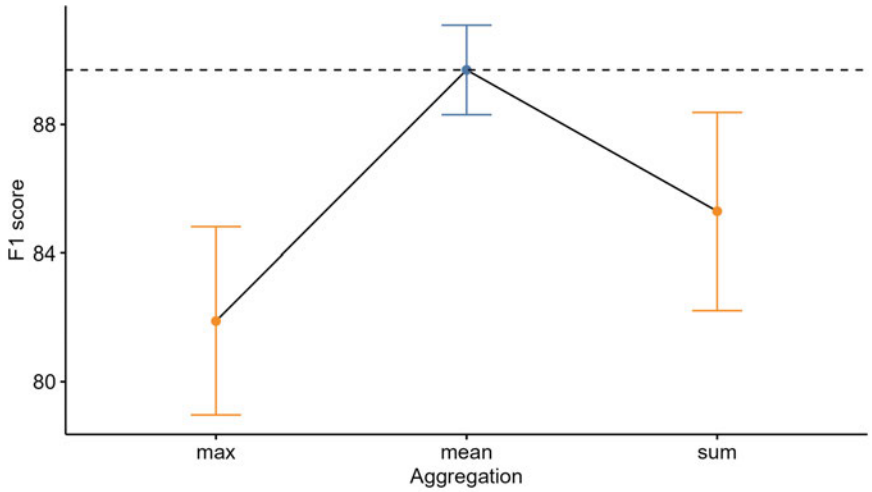

Figure C.4: Sensitivity of the proposed model to the choice of the aggregation function. The error bars show the standard deviation of accuracies measured across ten repetitions. The optimal value is shown in blue.

C.3 Explainability of AGGCN: Adjacency-based visualisations

The main manuscript shows the AGGCN-learned graphs and the node pooling patterns as a graph. In order to facilitate a different view of the same results, we report the averaged adjacency matrices in Figure C.5 that correspond to Figure 6.3 in the main text. Similarly, we report the differences between the learned graphs together with effect sizes (Wilcox permutation effect size) to quantify the strength of these differences (Figure C.6, corresponding to Figure 6.4 in the main text). Finally, we report an adjacency-like view of the node pooling attention scores (Figure C.7) corresponding to Figure 6.8 in the main text.

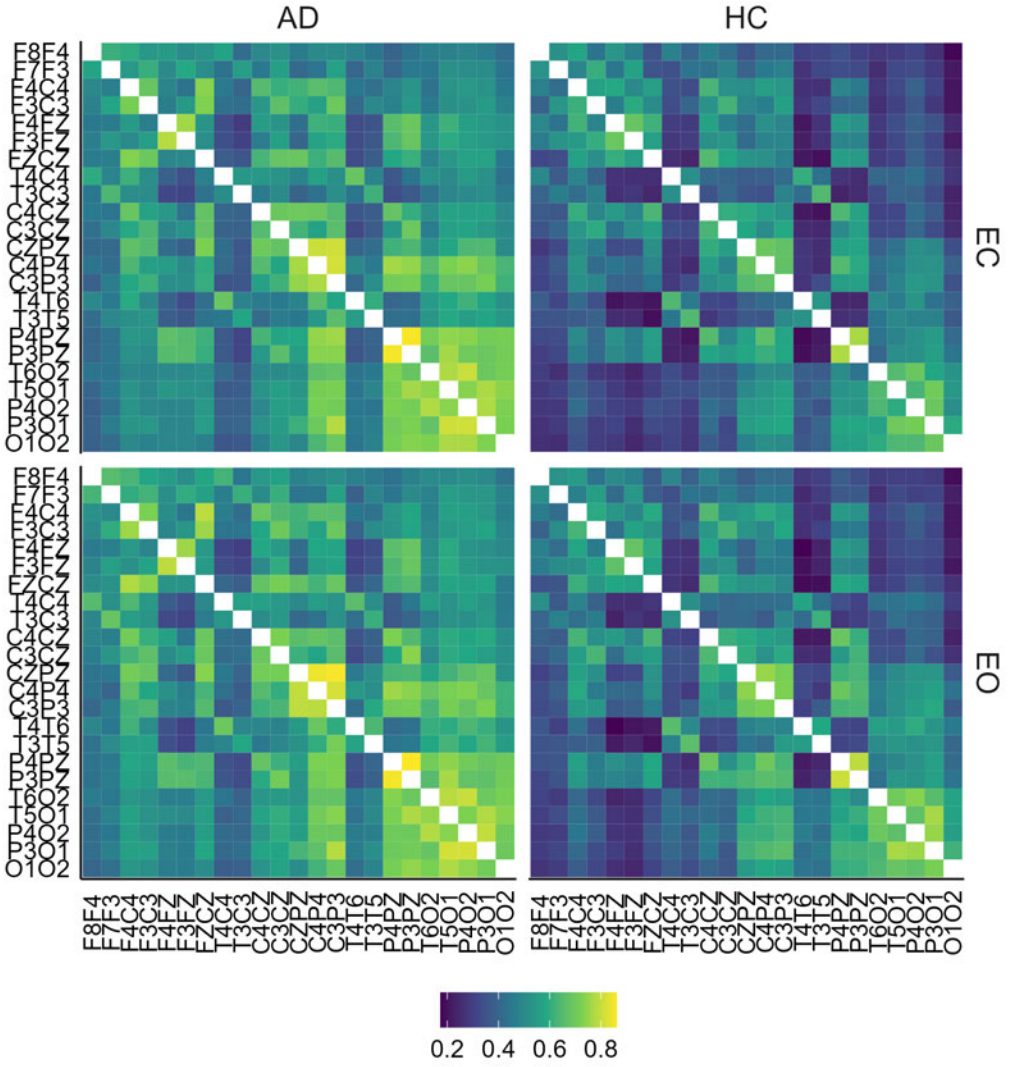

Figure C.5: Average adjacency matrix of learned graphs of AD and HC cases in EC and EO conditions.

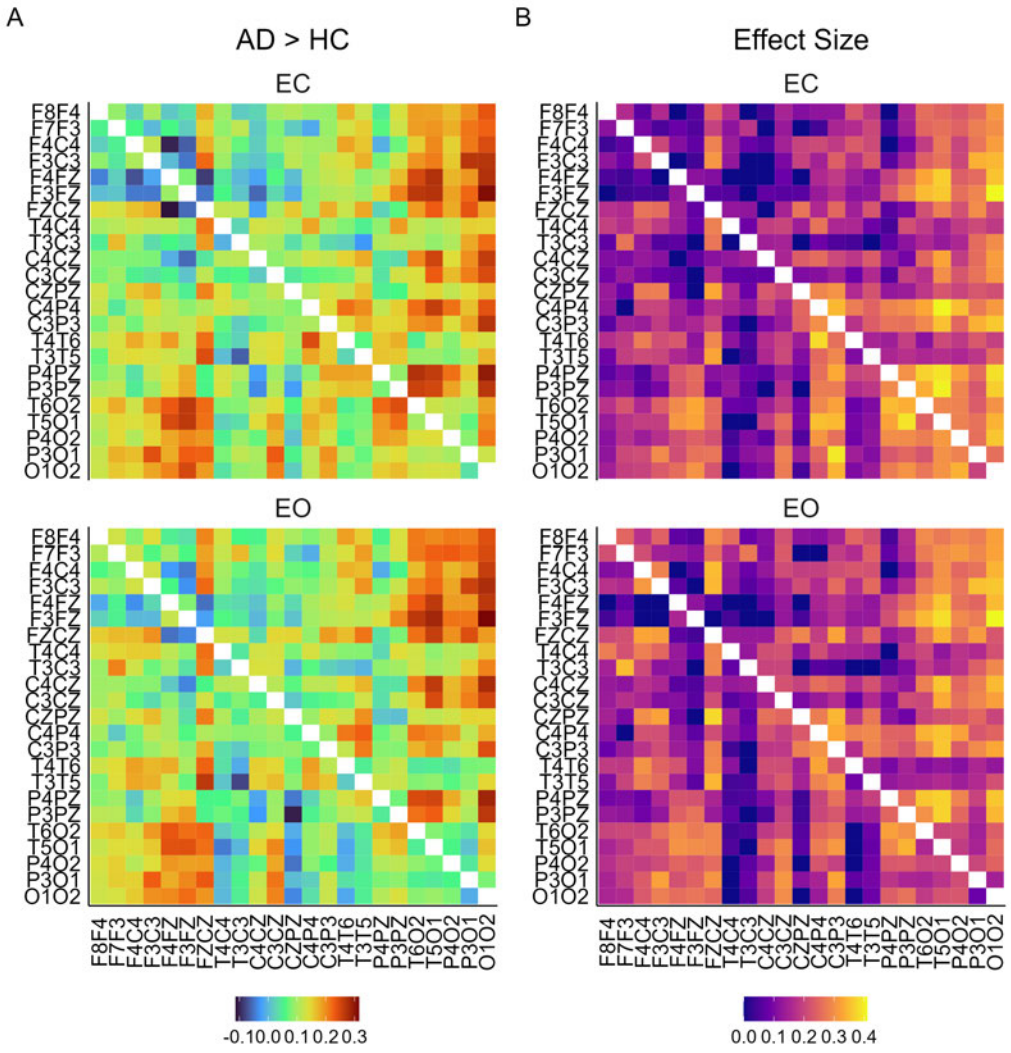

Figure C.6: Difference of averaged adjacency matrices of learned graphs of AD and HC cases (AD − HC) in EC and EO conditions (A). (B)-The-effect-size-for-the-non-parametric-Mann-Whitney-U-tests-comparing-AD-and-HC-with-values-set-to-0-where-p-value-> 0.05,-

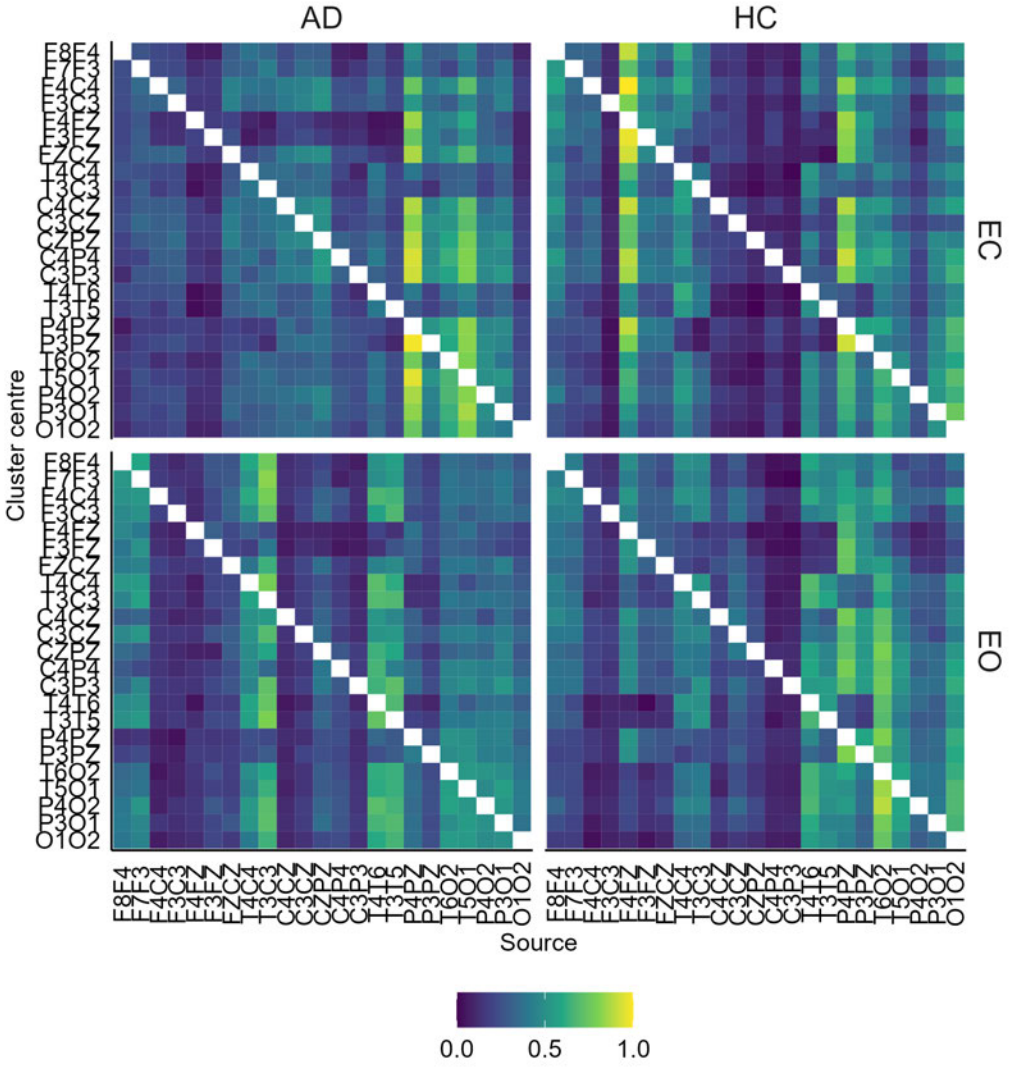

Figure C.7: Average adjacency matrix of attention scores obtained by the node pooling module for AD and HC cases across EC and EO conditions.